SAN-1485-2

HIGH-TEMPERATURE FUEL CELL RESEARCH AND DEVELOPMENT

Final Technical Status Report for June 1977—September 1978

By
J. J. Rasmussen
R. Guidotti
P. Lessing

October 15, 1978

Work Performed Under Contract No. EC-77-C-03-1485

Montana Energy and MHD Research & Development Institute
Butte, Montana

U. S. DEPARTMENT OF ENERGY

DISCLAIMER

NOTICE

SAN-1485-2
Distribution Categories UC-90g and UC-93

4DOE-FC-N2

FINAL
TECHNICAL STATUS REPORT

October 15, 1978

Period Covered: June 1977 - September 1978

HIGH-TEMPERATURE FUEL CELL RESEARCH AND DEVELOPMENT

Contract No. EC-77-C-03-1485

Prepared by

J. J. Rasmussen, R. Guidotti, P. Lessing

Montana Energy and MHD Research and
Development Institute

Submitted to

U. S. Department of Energy
Office of Fossil Energy
Division of Power Systems

ABSTRACT

An initial survey of the literature produced a list of ceramic materials (other than lithium aluminate) with properties which made them potential candidates for use in molten-carbonate fuel cell tiles or electrodes. Seven of the materials in the original list were dropped from consideration because of unfavorable thermodynamic properties; four materials were set aside because of high cost, lack of availability, or fabrication difficulties. Thirteen compositions were tested statically at 1000 K in a Li_2CO_3-K_2CO_3 bath under a dry CO_2 atmosphere. Only four of the materials tested showed severe degradation reactions in the molten carbonate.

A low-temperature process for forming small diameter, high-aspect ratio ceramic fibers for fuel cell use has been developed. A patent application currently is being filed by DOE.

A short-term program to initiate a computer study on the thermodynamic analysis of fuel cell materials was initiated at Montana State University. The report on this program is included as Appendix B.

The MHD and high-temperature fuel cell literature was surveyed, and material properties were evaluated to identify MHD materials with potential use for fuel cell applications. A technology transfer report of these findings was prepared. This report is included as Appendix A. Laboratory facilities were established to conduct research on interfacial diffusion processes which could be detrimental to successful long-term operation of the solid-electrolyte fuel cell. A variety of physical and chemical techniques were examined for the preparation of high-density substituted $LaCrO_3$ which was to be one component of a diffusion couple with Y_2O_3-stabilized ZrO_2. Hydrolysis of a mixed metal-nitrate solution with urea produced the most reactive powder. A final theoretical density of almost 98% was attained in cold-pressed sintered discs of this material.

TABLE OF CONTENTS

LIST OF TABLES

LIST OF FIGURES

LIST OF FIGURES (Continued)

I. OBJECTIVE AND SCOPE OF WORK

The objective of the program was to define and demonstrate components for improved, fuel-versatile medium- and high-temperature fuel cells with potential application to large-scale utility power generation. Two tasks were carried out to obtain the data required to meet this objective:

1. Survey and develop materials and material systems with microstructural properties suitable for the containment of molten-carbonate electrolytes in a fuel cell environment. Emphasis was placed on developing improved tile fabrication techniques and improved tile and container materials.

2. Identify materials developed for MHD energy conversion that may have applicability as high-temperature fuel cell components such as electrodes, solid-electrolytes, electrode interconnectors or support materials; conduct a preliminary experimental program on the most promising materials to evaluate their applicability in fuel cells; and prepare a report on these findings.

II. SUMMARY OF PROGRESS TO DATE

A. Molten-Carbonate Fuel Cell

An initial search of the literature was made to identify ceramics known to be corrosion resistant at elevated temperatures. Both electronically conducting (electrode) and non-conducting (tile) materials were considered. Thermodynamic functions were collected, and calculations were performed for postulated materials interactions. Of the materials selected in the literature search, seven were found to be unsuitable because of unfavorable thermodynamic properties. Four materials were set aside because of high materials cost, lack of availability, and/or fabrication difficulties. Thirteen compositions were tested statically at 1000 K in a Li_2CO_3-K_2CO_3 bath under a dry CO_2 atmosphere. Only four of the materials tested showed severe degradation in the molten-carbonate bath.

Toward the end of the contract period, the literature survey and calculations performed under Task B to evaluate MHD materials suitable for use in fuel cells was completed. The conclusion of that report (Appendix A) indicates several materials which could be added to the initial list of

candidates for use in the molten-carbonate fuel cell. Perovskites such as rare-earth nickelates, cobaltates, and manganates should be corrosion-tested for use as air electrodes. The most promising materials for the electrolyte support include the alkaline-earth hafnates and zirconates, lithium and alkaline-earth tantalates, and rare-earth aluminates.

A low-temperature process for forming small diameter (1 μm), high aspect ratio ceramic fibers for reinforcement of fuel cell tiles has been developed. The details of this process are described in a DOE patent application which will be filed in the near future. The fiber diameter is limited on the low side by the size of the powder particles which are utilized.

B. Solid-Electrolyte Fuel Cell

The MHD and high-temperature fuel cell literature was surveyed for data pertaining to materials properties to identify materials used in MHD power generation which also might be suitable for use in high-temperature fuel cells. The classes of MHD materials evaluated include the carbides, nitrides, silicides, borides, composites, and oxides. Y_2O_3-stabilized ZrO_2 was used as a reference point to evaluate materials for use in the solid-oxide fuel cell. Physical and chemical properties such as electrical resistivity, coefficient of thermal expansion, and thermodynamic stability toward oxidation were used to screen candidate materials. This report is included in its entirety as Appendix A.

Laboratory facilities were established to carry out research on interfacial diffusion processes which could be detrimental to the successful long-term operation of the solid-electrolyte fuel cell. A variety of physical and chemical techniques was examined for the preparation of high-density substituted $LaCrO_3$ which was planned to be one component of a diffusion couple with Y_2O_3-stabilized ZrO_2. Hydrolysis of a mixed metal-nitrate solution with urea produced the most reactive powder. A final theoretical density of almost 98 percent was attained in sintered, cold-pressed discs of this material.

III. DETAILED DESCRIPTION OF TECHNICAL PROGRESS

A. Molten-Carbonate Fuel Cell

At the onset of the MERDI fuel cell materials research program, literature was searched to identify ceramics known to be corrosion resistant.

Both electronically conducting (electrode) and non-conducting (tile) materials were considered. Thermodynamic functions were assembled, and calculations were performed for postulated cation substitution, cation exchange, and oxidation chemical reactions. Because of incomplete values in the literature for various compounds of interest, not all of the reactions were treated thermodynamically. The results indicated that the reactivity of the lithium and potassium carbonates would make materials selection difficult. The possibility of kinetic barriers, protective coatings, and nonstoichiometric alloying tempered this pessimism. Of the materials selected in the literature search, seven were found to be unsuitable due to unfavorable results of the thermodynamic calculation, and four materials were set aside due to high cost, lack of availability, or fabrication considerations. Thirteen ceramic compositions were tested statically at 1000 K under a dry carbon dioxide atmosphere using 62 mol % Li_2CO_3--38 mol % K_2CO_3 as the electrolyte. The disposition of the various ceramics considered is listed in Table 1.

Toward the end of FY 78, the literature survey and appropriate calculations were completed for MHD materials that might have application for fuel cells. The conclusion of that report (Appendix A) indicates more candidate materials could be added to Table 1. For the air electrode in the molten-carbonate fuel cell, perovskites such as the rare-earth nickelates, cobaltates, and manganates should be corrosion-tested. The most promising MHD materials for the electrolyte support (tile) are alkaline-earth hafnates and zirconates, lithium and alkaline-earth tantalates, and rare-earth aluminates.

Short-term corrosion tests were completed on the ceramic materials in Table 1 that are listed as "tested". Tests were conducted from 112 to 162 hours. Samples were tested in dense, crucible form and were dimensioned and weighed before and after testing. The carbonate was leached from the crucibles using glacial acetic acid and acetic anhydride (70/30 vol %). Analytical tests (atomic absorption--AA, electron microprobe) were used to determine impurity concentrations in the carbonate and potassium disposition in the ceramic. An X-ray diffractometer was used to identify second-phase compounds that were present in the ceramics. Arrangements were made for the use of a scanning Auger microprobe to analyze the ceramics for lithium and carbon content. This would allow quantitative determination of

TABLE 1.--Predicted Corrosion Resistance

Material	Results of Free Energy Calculations	Disposition
Magnesium Aluminate Spinel ($MgAl_2O_4$)	Favorable (Slightly positive ΔG's)	Tested
Magnesia-Rich Spinel ($Mg_{1+x}Al_2O_4$)	Favorable	Tested
Alumina-Rich Spinel ($MgAl_{2+x}O_4$)	Inadequate Information	Tested
Berylium Oxide (BeO)	Inadequate Information	Dropped due to hazardous fabrication and availability
Lithium Chromate ($LiCrO_2$)	Inadequate Information (known to passivate on Type 300 stainless steel)	Sidelined - Hot pressing necessary; poisonous; Purchased powders
Calcium Oxide (CaO)	Unfavorable (Dissolution Predicted)	Tested
Chromium Oxide (Cr_2O_3)	Unfavorable (Lithium chromate formation)	Dropped
Hafnium Oxide (HfO_2)	Inadequate Information	Dropped due to cost.
Thorium Oxide (ThO_2)	Inadequate Information	Tested - Hazardous fabrication
Lithium Aluminum Silicate (Rosolite)	Inadequate Information	Tested
Mullite ($3Al_2O_3 \cdot 2SiO_2$)	Unfavorable ($LiSiO_3$ and $LiAlO_2$ formation)	Dropped
Titanium Carbide (TiC)	Unfavorable (oxidation)	Dropped

Table 1.--Predicted Corrision Resistance (Continued)

Material	Results of Free Energy Calculations	Disposition
Titanium Oxide (TiO_2)	Unfavorable ($LiTiO_3$ formation)	Dropped
Titanium Boride (TiB_2)	Inadequate Information	Tested
Zirconium Oxide (ZrO_2 + CaO)	Inadequate Information	Tested
Aluminum Oxide (Impurity doped)	Inadequate Information	Tested
ELECTRODE MATERIALS		
Stannic Oxide (SnO_2)	Inadequate Information	Tested
Tantalum-doped Rutile (TiO_2 + Ta)	Unfavorable ($LiTiO_3$ formation)	Dropped
Calcium Titanate ($CaTiO_3$)	Unfavorable	Dropped
Calcium Doped Manganese Oxide (MnO_2 + Ca)	Inadequate Information	Purchased powders Needs hotpressing

lithium distribution and differentiate between elemental lithium and lithium carbonate. Due to the length of time needed to set up this new instrument, the lithium analysis work will be started in FY 79, if the necessary funding is received. A partial summary of the short-term corrosion work on crucibles is tabulated in Table 2.

Lithium aluminum silicate, calcium oxide, stannic oxide, and titanium boride reacted sufficiently with the carbonate to make them unusable in fuel cell applications under the test conditions. The high-purity MgO gained over 6 wt. % which seems contrary to the predicted dissolution mechanism. However, microstructural analysis indicated that the crucible was 92 percent of theoretical density and that the pores had filled with carbonate. This was verified by electron microprobe analysis for potassium and X-ray diffraction patterns of the crucible. The carbonate contained high levels of magnesium, supporting the conclusion that a dissolution mechanism had been active.

Of the spinels, stoichiometric spinel (50/50) had an intermediate weight change. Based on weight change/area exposed, spinels rich in aluminum (35/65) had the lowest weight change. Both the carbonate and microprobe analyses (see Figures 1 and 2) indicate that aluminum-rich spinel is more corrosion resistant than other spinels; that is, less aluminum and magnesium were found in the leached carbonate and less potassium found its way into the ceramic. This is significant because spinel has a wide solid solution phase field. Spinel rich in Al^{+3} ions should have lattice defects. If Li^{+1} or K^{+1} enters the spinel lattice, it can be expected that a partial annihilation of defects can take place and the ceramic will be stabilized with respect to corrosion. There is microstructural evidence verified by X-ray diffraction that some α-alumina second phase is present in the 35/65 spinel. In the future longer firing times and higher temperatures will be used to move into the single-phase field. If this approach is unsuccessful, the composition will be adjusted to 40/60.

The AA results on the leached carbonate indicate that potassium and perhaps lithium replaced Mg^{+2} ion in the spinel lattice more readily than the Al^{+3} ion. The low level of K found in the alumina samples supports this concept. This information also would indicate the alpha alumina could be doped with cation or anion impurities in such a way as to reduce corrosion

TABLE 2.--Results of Corrosion Tests in 62 mol % Li_2CO_3-38 mol % K_2CO_3 at 1000 K

Sample	Test Time	Weight Change %	Weight Change/Area Exposed	Carbonate Analysis	Crucible Analysis
Spinel ($MgAl_2O_4$) (50/50)	162 hrs	+00.468	$+1.8 \times 10^{-3}$ gm/cm^2	00.00465 wt % Al 00.27898 wt % Mg 5.00×10^{-6} gm Al/cm^2 (exposed) 3.00×10^{-4} gm Mg/cm^2 (exposed	0.2 to 0.9 wt % K_2O
Spinel (65/35)	112 hrs	+00.311	$+3.2 \times 10^{-3}$ gm/cm^2	00.00250 wt % Al 00.22250 wt % Mg 5.55×10^{-6} gm Al/cm^2 (exposed) 4.94×10^{-4} gm Mg/cm^2	0.06 to 0.18 wt % K_2O
Spinel (35/65)	112 hrs	+00.023	$+2.6 \times 10^{-4}$ gm/cm^2	00.00088 wt % Al 00.05063 wt % Mg 1.33×10^{-6} gm Al/cm^2 7.56×10^{-5} gm Mg/cm^2	0.01 to 0.19 wt % K_2O
MgO (99.99% pure)	112 hrs	+06.198	$+2.0 \times 10^{-2}$ gm/cm^2	00.00376 wt % Al 01.53192 wt % Mg 1.46×10^{-6} gm Al/cm^2 (exposed) 5.97×10^{-4} gm Mg/cm^2 (exposed)	4.40 to 11.70 wt % K_2O
ThO_2	120 hrs	-00.187	Estimate (Maximum) -2.3×10^{-3} gm/cm^2		

TABLE 2.--Results of Corrosion Tests in 62 mol % Li_2CO_3-38 mol % K_2CO_3 at 1000 K (Cont.)

Sample	Test Time	Weight Change%	Weight Change/Area Exposed	Carbonate Analysis	Crucible Analysis
Lithium Aluminum Silicate (Rosolite	120 hrs	--	---	---	Warped, Broken, Swollen
Calcium Oxide (CaO)	120 hrs	--	---	Indication of high Ca solution	Slumped and dissolved
Stannic Oxide (SnO_2)	120 hrs	+08.331	---	---	Swollen and cracked
Titanium Boride (TiB_2)	120 hrs	--	---	Dark color in carbonate	Severe reaction. Bubbled Surface. No longer structurally stable.
α-Alumina (Al_2O_3)	121 hrs	-00.016	-1.4×10^{-4} gm/cm^2	$\leq$ 00.00040 wt% Al $\leq 4.76 \times 10^{-7}$ gm Al/cm^2(exposed)	$\leq$ 0.01 wt % K_2O
α-Alumina 10% Cr doped	121 hrs	-00.008	-2.4×10^{-4} gm/cm^2	$\leq$ 00.00030 wt % Al $\leq 1.71 \times 10^{-5}$ gm Al/cm^2(exposed) $\leq 5.69 \times 10^{-6}$ gm Cr/cm^2(exposed)	

TABLE 2.--Results of Corrosion Tests in 62 mol % Li_2CO_3-38 mol % K_2CO_3 at 1000 K (Cont.)

Sample	Test Time	Weight Change%	Weight Change/Area Exposed	Carbonate Analysis	Crucible Analysis
α-Alumina Carbon doped	121 hrs.	-00.018	-2.4×10^{-4} gm/cm^2	$\leq$ 00.00040 wt % Al $\leq 4.76 \times 10^{-7}$ gm Al/cm^2 (exposed)	
Zirconia (calcia stabilized)	121 hrs.	+00.013	$+3.9 \times 10^{-5}$ gm/cm^2	* 00.56804 wt % Zr 4.15×10^{-4} gm Zr/cm^2 (exposed)	

* Flame emission technique; not detected by flameless AA.

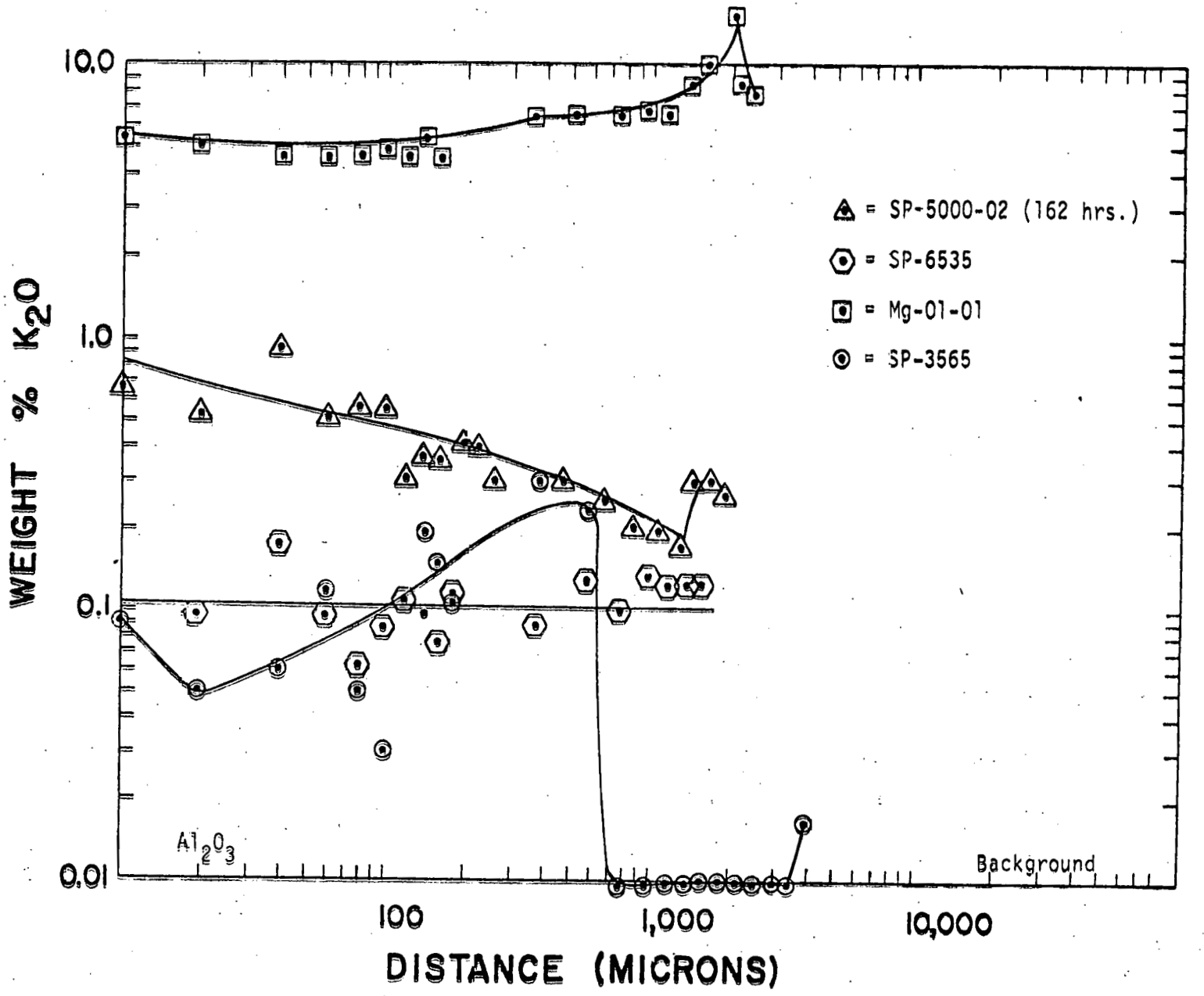

Figure 1.--Electron Microprobe Analysis of Crucibles

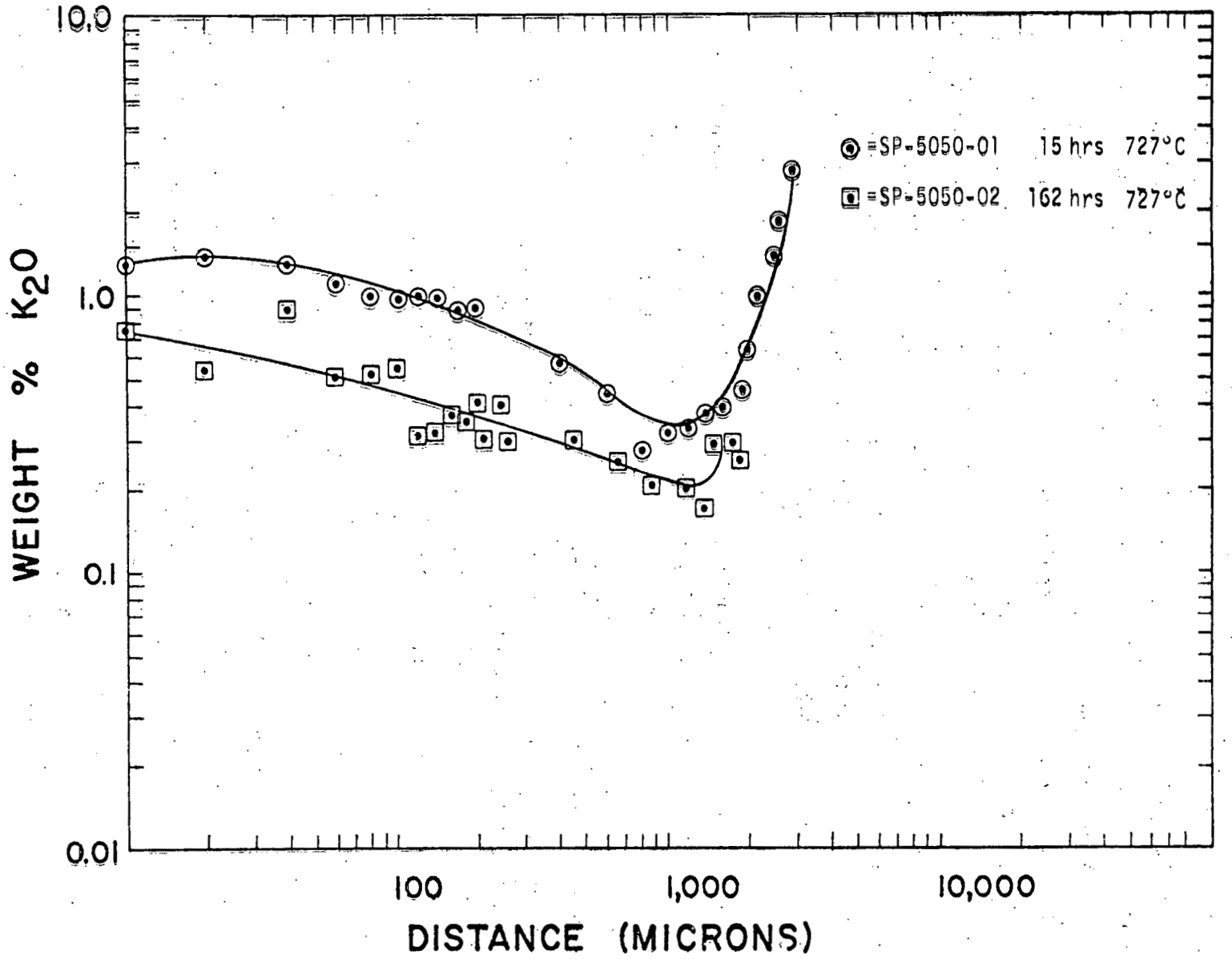

Figure 2.--Electron Microprobe Analysis of Stoichiometric Spinel Crucibles

or compensate for the presence of a +1 valence impurity (Li^{+1}, K^{+1}). At this time, the most corrosion resistant ceramics are stabilized zirconia, impurity-doped alpha alumina, thoria, 65/35 spinel, and 35/65 spinel.

The goal of the corrosion tests on ceramic crucibles was to identify materials suitable for fabrication into a form useful in a fuel cell. In support of this goal MERDI has developed a low-temperature process to form small diameter, high aspect ratio ceramic fibers. This process is unique, and a United States patent has been applied for with the Department of Energy as holder of the rights (DOE Case No. S-49, 753 [RL-7146]).

A wide range of experiments has been directed toward producing a variety of fiber types to cover many possible applications. These applications are not limited strictly to high-temperature fuel cells and may include low-temperature fuel cells, batteries, and other energy conversion devices. Fibers of the smallest possible diameter have been made. The size was governed by the particle size of the powder used. When viewed under a microscope, these fibers show individual particles sintered to each other in a single line to form a fiber. Experimental grinding shows that the fired fibers of Al_2O_3 can be ground in a mortar and pestle to produce fibers with a short length and an 8:1 aspect ratio (eight microns in length and one micron in diameter). Sizing of fibers has been accomplished by using a hydro-classification process. It appears that sintered fibers can be made from any ceramic that has a reasonable sintering rate at high temperature. In addition to the Al_2O_3, fibers have been formed from 50/50 spinel, 35/65 spinel and 65/35 spinel.

Corrosion tests were conducted at 1000 K in 62 mol % Li_2CO_3-38 mol % K_2CO_3 for 120 hours on bundles of longer length, small diameter fibers. Compositions which were tested included alpha alumina (Al_2O_3) and 50/50 and 35/65 spinel. After testing, the carbonate was leached from the fibers using acids. Weight changes indicated that the carbonate was leached from the alumina in 24 hours, but carbonate still remained in the spinel fiber bundles after 72 hours. After leaching, the solutions were filtered, washed, and dried. It is apparent that quantitative weight change measurements will be impossible using ordinary filtration techniques. Accurate determinations of corrosion rates will be difficult compared to crucible analysis. The primary tests used to determine the extent of reaction will be scanning electron and auger microscopy and X-ray diffraction.

Visual observation indicated that the alpha alumina suffered from breakage of the fibers while the spinels did not.

B. Solid-Electrolyte Fuel Cell

A major objective of the fuel cell program was to scrutinize the formal and informal MHD literature for performance characteristics of materials used in MHD generators with the intent of identifying materials which might be suitable for use as components in the solid-electrolyte and molten-carbonate fuel cell. The components in the solid-electrolyte fuel cell include the anode, cathode, electrolyte, and cell interconnector. The components in the molten-carbonate fuel cell include the anode, cathode, and electrolyte support (tile). The general physical and chemical requirements for materials for MHD and fuel cell applications are similar for certain components.

Classes of MHD materials which were evaluated include the carbides, nitrides, silicides, borides, oxides, and composites. An electrolyte of Y_2O_3-stabilized ZrO_2 was chosen as a reference point for evaluation of materials for the solid-oxide fuel cell. Physical and chemical properties such as electrical resistivity, coefficient of thermal expansion, and thermodynamic stability toward oxidation were used for screening of candidate materials.

A report on the findings of the study was prepared in which promising materials and areas for additional research were delineated. A copy of this technology transfer report is included herein as Appendix A.

A second major area of activity during the contract period involved the establishment of the necessary laboratory facilities to conduct research in potential problem areas detrimental to the successful long-term operation of the solid-electrolyte fuel cell. A number of these problem areas were outlined by Westinghouse in a letter to the Department of Energy[1] on August 2, 1977. Cationic diffusion across the component interfaces of the cell was rated highest on the Westinghouse scale of importance. The study of the rate and extent of the interfacial diffusion processes, both with and without current flow, is an area which merits study and one in which MERDI felt it could make an important contribution. MERDI, therefore, chose to undertake this area of study, with initial emphasis on cation diffusion across the interconnector-electrolyte interface. Examination of diffusion processes at the electrolyte-anode, electrolyte-cathode, interconnector-cathode, and

interconnector-anode interfaces was envisioned as part of a subsequent (follow-on) research effort.

The electrical resistivity of the diffusion couple was to be measured temperature to monitor the interfacial diffusion process. These data were to be corroborated with quantitative diffusion profiles on sectioned samples after testing. Initially, simple a-c and d-c resistivities were to be measured. Ultimately, however, the complex admittance technique was felt necessary to sort out interfacial contributions from grain, bulk, and electrode effects.

The possibility of undertaking a study of interfacial diffusion processes in the solid-electrolyte fuel cell did not occur until approximately a third of the contract period had elapsed. At that point, considerable time and effort was spent in determining relevant equipment, electrical power, and supply needs. A large part of the remaining contract period was required for setting up and establishing the necessary facilities for carrying out this anticipated research effort.

For conducting long-term testing of diffusion couples at a typical fuel cell operating temperature of 1273 K, wirewound tube furnaces were constructed with heating elements rated at 1475 K. Commercial tube furnaces with silicon carbide heating elements were procured for accelerated testing at temperatures of 1473 K to 1773 K. For sintering test samples, a $MoSi_2$-type box furnace rated at 1973 K was acquired (Figure 3).

Millivolt shunts and potentioneter and a precision d-c power supply were obtained for measurement of the d-c resistivities of test specimens. A surplus impedance bridge was renovated and combined with an a-c null detector and function generator for a-c impedance measurements. X-Y and stripchart recorders were purchased for recording data.

A gas-manifold system necessary for control of the test atmosphere (P_{O_2}) was assembled and leak-checked, and the flowmeters were calibrated. A schematic of the system is shown in Figure 4. Figure 5 shows the manifold assembly and ancillary equipment to be used for electrical conductivity measurements for temperatures up to 1773 K.

Once the apparatus for interfacial diffusion tests had been assembled and checked, attention then was focused on the actual preparation of the test specimens. A number of techniques were considered for preparation of the diffusion

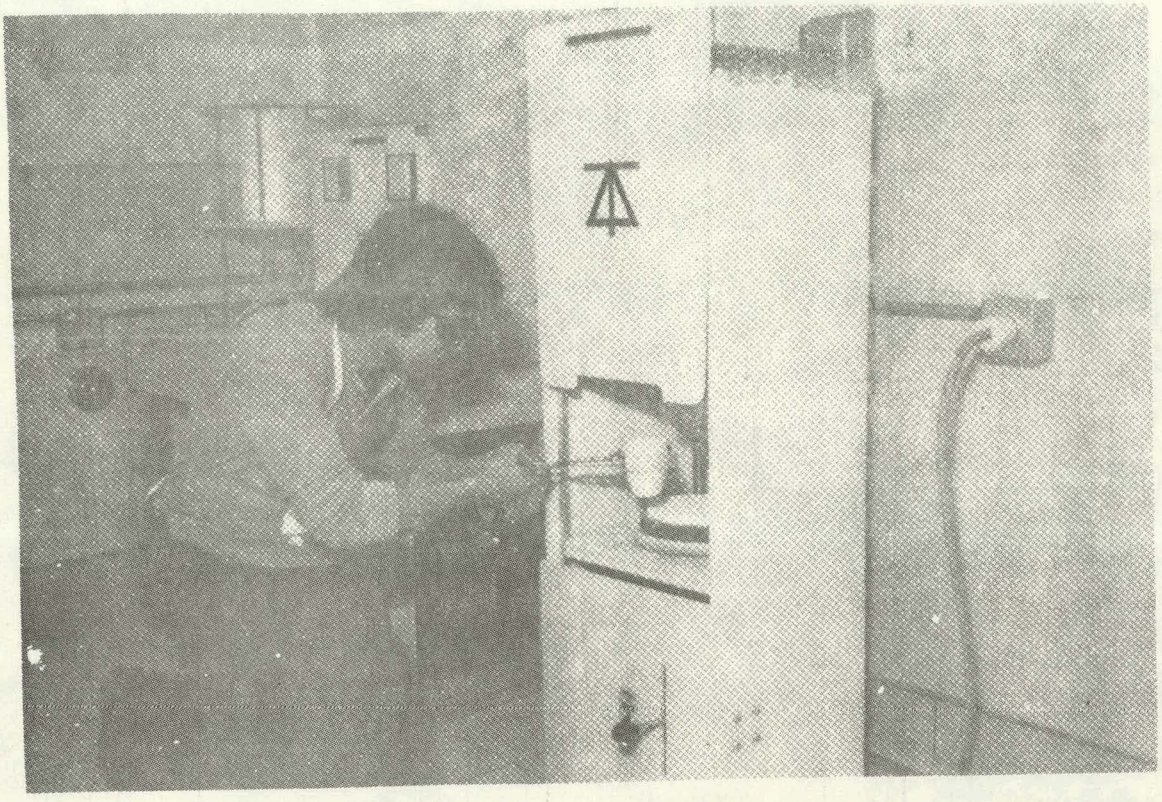

Figure 3.--Sample Being Loaded into $MoSi_2$ Furnace for Sintering

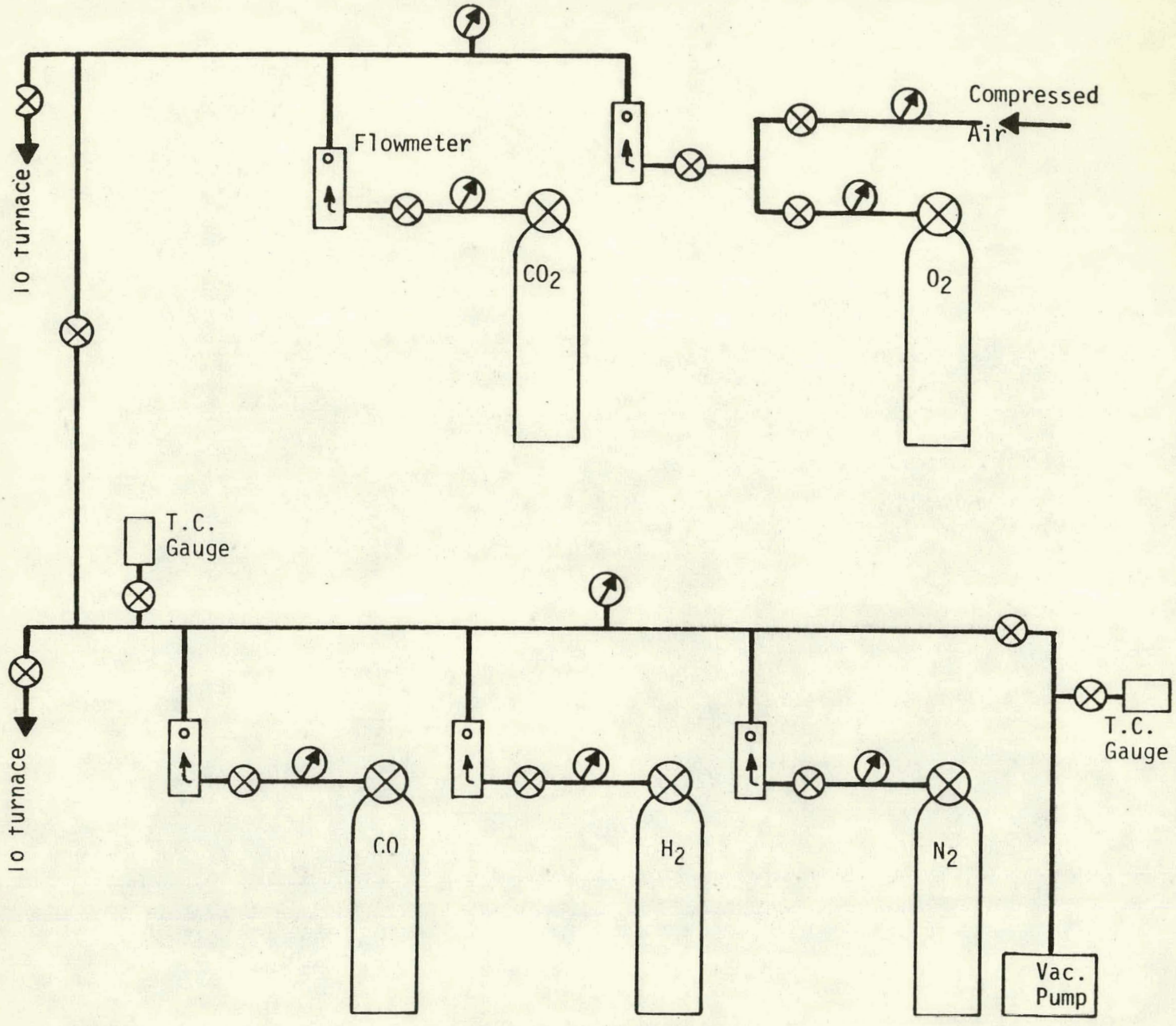

Figure 4.--Gas-Manifold System for Atmosphere Control During Electrical Conductivity Measurements

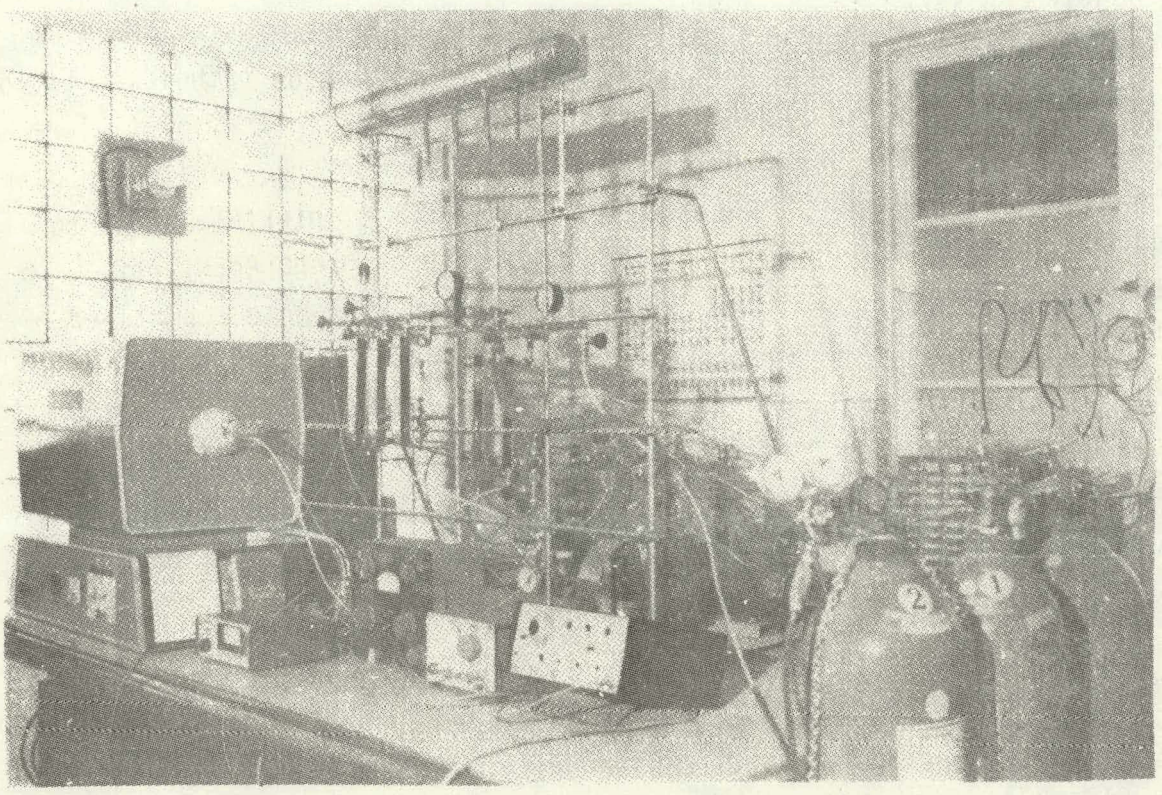

Figure 5.--Experimental Setup for Interfacial Diffusion Measurements

couples. One technique involves the use of a disc of one material (A) sintered to a high theoretical density in contact with a second material (B) in the form of a powder or as a film coating using various organic binders and solvents. A second method involves cold-pressing powder B around a sintered disc of material A in a die or isostatic press, followed by firing. In the third method, pressing or slipcasting multiple-layer discs is followed by sintering to prepare the diffusion couple. A fourth method involves heating high-density polished discs of materials A and B together under a small applied pressure. The fifth approach utilizes hot-pressing techniques to form test discs from powders of materials A and B or from a sintered disc of material A with powder B. Platinum-wire markers would be incorporated into the test samples to define the location of the initial A-B interface prior to diffusion. The diffusion couples ultimately would be prepared by r-f sputtering or chemical vapor deposition of one component onto a sintered sample of the second component (probably the substituted $LaCrO_3$) to simulate the conditions expected in the fabrication of the thin-film, solid-electrolyte fuel cell.

It was decided that substituted $LaCrO_3$ would be used for material A because of volatilization of chromium at elevated temperatures. By "sandwiching" or coating it with material B (the ZrO_2 electrolyte), a BAB diffusion couple would be formed, which would reduce the tendency for vaporization of chromium during testing.

Of the five methods considered, the third method appeared least desirable. Different rates of sintering for the two materials could result in an interface which is not as well-defined as in the other methods. The fourth method would make the use of platinum-wire markers somewhat impractical (extremely low rates of diffusion, however, could make the platinum markers unnecessary). Thus, methods one, two, and five appeared to be the most feasible.

Hot pressing (as in method five) would require the least time. In one experiment, a three-layered disc was hot-pressed from $La_{0.95}Mg_{0.05}Cr_{0.75}Al_{0.25}O_{3-x}$ and ZrO_2- 10 wt % Y_2O_3, with the substituted $LaCrO_3$ in the center. The powdered samples were cold-pressed successively in a graphite die before final hot-pressing at 1623 K and 5000 psi for 20 minutes. An extremely dense composite resulted which was almost black in color because the reducing conditions present (vacuum and graphite die) caused some loss of the O_2 from the

ZrO_2 and substituted $LaCrO_3$. (The sample readily oxidized, however, by heating to 1273 K in air.)

As can be seen in Figure 6, the interface between the substituted $LaCrO_3$ and the stabilized ZrO_2 was not as well-defined as needed for critical diffusion tests. This was the result of using powdered materials for the three layers. Replacement of the powdered, substituted-$LaCrO_3$ with a high-density, polished disc undoubtedly would resolve this problem.

While method five would be the preferred technique for preparation of the diffusion couples, the current lack of in-house facilities and the long distance to the nearest hot-pressing establishment precluded the use of this technique, except on a limited basis. As a result, methods one and two were chosen for fabrication of the diffusion samples.

Before suitable diffusion couples can be prepared, the component-mixed oxides first must be synthesized in suitable purity, chemical composition, and homogeneity (i.e., with little or no second-phase formation). A prerequisite for utilizing techniques one and two for interdiffusion tests is the preparation of homogeneous discs of substituted $LaCrO_3$ of high density. This requires a combination of reactive oxides as well as very high temperatures because this material is difficult to sinter.

While Y_2O_3-ZrO_2 solid solution can be prepared readily from the oxides, substituted $LaCrO_3$ is not prepared as easily by this method as a single-phase material. Alternate techniques which were examined for preparing substituted $LaCrO_3$ are listed in Table 3; the mixed-oxide technique is included as a reference point. Pyrolysis of mixed alkoxides[2] was not considered because it is expensive and time-consuming. According to published results,[3] $LaCrO_3$ can be prepared at temperatures as low as 873 K using technique three of Table 3. To determine the suitability of this as well as the other methods of Table 3 for preparation of substituted $LaCrO_3$, powdered samples of composition $La_{0.95}Mg_{0.05}Cr_{0.75}Al_{0.25}O_{3-x}$ were prepared by each technique.

Since there are indications that Mg^{+2} substitutes for Cr^{+3} and not La^{+3} in the pseudo-perovskite lattice,[4] the formula is written more properly as $La_{0.9}(Mg_{0.05}Cr_{0.71}Al_{0.24})O_{2.82}$. It is important that the A:B ratio be less than stoichiometric (i.e., slightly La^{+3} deficient) to avoid the possibility of any uncombined La_2O_3 which will react with atmospheric moisture to form the hydroxide:

Figure 6.--Cross-section of Hot-Pressed Substituted-$LaCrO_3$ Sample, (50X magnification)

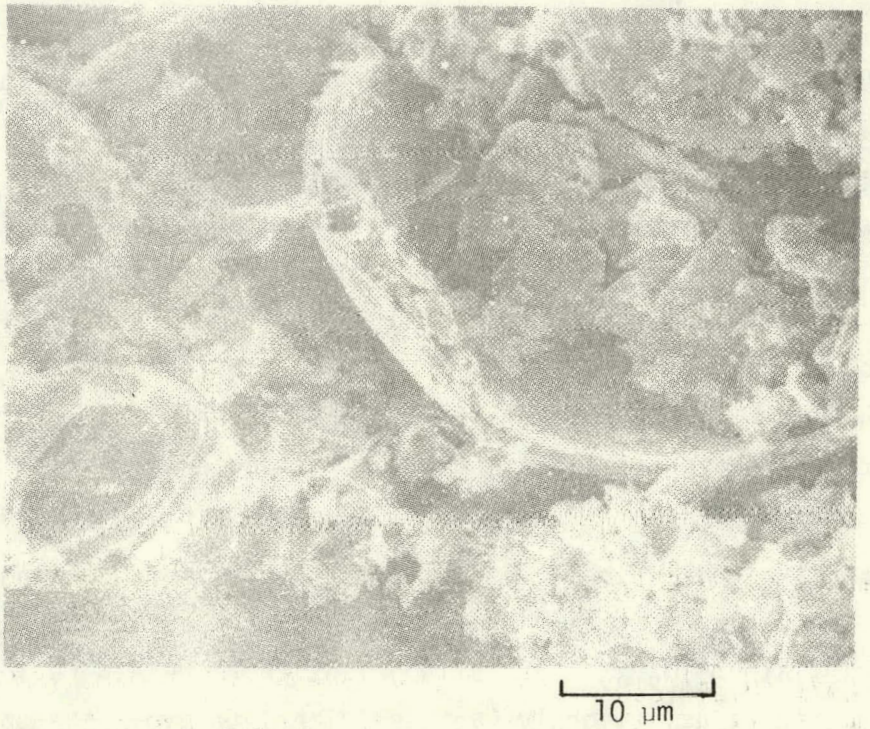

Figure 7.--$LaCrO_3$ Prepared from Citric Acid Precursor Heated at 923 K for 4 Hours, (2000X magnification)

TABLE 3.--Techniques Utilized for Fabrication of Substituted $LaCrO_3$

No.	Technique
1.	Milling of mixed oxides, followed by calcining, further grinding, and recalcining.
2.	Coprecipitation of mixed hydroxides/oxides from nitrate solution with gaseous NH_3, followed by calcining.
3.	Evaporation of a mixed-nitrate solution containing citric acid to produce a homogeneous multi-component solid solution or finely divided oxide mixture contained in a resin matrix. Subsequent calcination removes the organic binder producing a reactive oxide powder.
4.	Similar to method three but using ethylene glycol as well as citric acid to form the resin.
5.	Similar to method three but using an inexpensive polymer-forming organic polyhydroxy compound.
6.	Similar to method five but with ethylene glycol added.
7.	Homogeneous precipitation of a mixed hydroxide/oxide from a mixed nitrate solution using urea to destroy the nitrate, resulting in metal hydrolysis.
8.	Modification of methods three, four or five using urea for nitrate removal.

$$La_2O_3(free) + 3H_2O(\ell,g) \rightarrow 2La(OH)_3 \quad (1)$$

Even hot-pressed samples of $LaCrO_3$ compounds with excess La_2O_3 have been found to react in this manner, albeit very slowly.[4] The above composition has an effective A:B ratio of 0.9:1.0, where ABO_3 is the general formula for perovskites.

Powders of substituted $LaCrO_3$ synthesized by the different techniques presented in Table 3 were heated at 923 K for four hours to decompose the organic precursor and remove water and excess nitrate and were examined by X-ray diffraction and SEM techniques. Similar testing was carried out after calcining the samples at 1673 K for nine hours. The test results obtained are presented in Table 4.

Only tests two, five, and nine yielded multi-colored nonhomogeneous materials after heating at 923 K for four hours. This was confirmed by X-ray diffraction analysis. Further heating to 1673 K, however, resulted in single-phase $LaCrO_3$ in all cases. Monitoring of the solution temperature during tests two and five confirmed earlier suspicions of an exothermic reaction between citrate and nitrate during heating to 423 K. A peak temperature in excess of 723 K was observed in one test. Addition of ethylene glycol (test four), however, prevented this reaction from occurring. The ethylene glycol acts to raise the boiling point of the solution sufficiently to allow nitrate decomposition to occur over a longer time during heating, thus avoiding the sudden oxidation of citrate which occurs when the water (in the absence of glycol) is removed too rapidly.

Sample morphology of the substituted $LaCrO_3$ varied greatly among the preparative techniques. The reaction of citrate with nitrate (method three in Table 3) caused rapid formation of large gas bubbles (Figure 7). Similar morphology resulted when citric acid was replaced by the organic polyhydroxy material (method five). The finer sample porosity which resulted when ethylene glycol was present (method four) can be seen in Figure 8; the uniformity of the pores is evident in Figure 9.

Figure 10 shows the conchoidal fracture surfaces which result from the use of the organic polyhydroxy precursor with the mixed nitrates solution (method six); the particles appeared dense, as seen in Figure 11.

TABLE 4.--Properties of $La_{0.9}(Mg_{0.05}Cr_{0.71}Al_{0.21})_{1.0}O_{2.82}$, Prepared by Various Techniques*

Test No.	Preparation Technique	After Heating at 923 K/4h		After Heating at 1673 K/9h	
		Color	Phase	Color	Phase
1.	Mixed oxides	-	-	+Choc. bn.	+M=$LaCrO_3$
2.	Coprecipitation with NH_3	Green	M=La_2O_3 + unid.; m=$LaCrO_3$	Choc. bn.	M=$LaCrO_3$
3.	Citric acid precursor	Brown	M=$LaCrO_3$	Choc. bn.	M=$LaCrO_3$
4.	Citric acid + ethylene glycol	Brown	M=$LaCrO_3$	Choc. bn.	M=$LaCrO_3$
5.	Organic polyhydroxy precursor	Brown, with green second phase	M=$LaCrO_3$; m=unid.	Choc. bn.	M=$LaCrO_3$
6.	Organic polyhydroxy + ethylene glycol	Black	-	Choc. bn.	M=$LaCrO_3$
7.	Urea hydrolysis	Brown	M=$LaCrO_3$	Light bn.	M=$LaCrO_3$
8.	Citric acid + urea	Brown	M=$LaCrO_3$	Choc. bn.	M=$LaCrO_3$
9.	Evapn. of NO_3 soln.	Green	M=La_2O_3 + unid.; m=$LaCrO_3$	Choc. bn.	M=$LaCrO_3$

* Starting solution equivalent to 0.46 M $La_{0.9}(Mg_{0.05}Cr_{0.71}Al_{0.21})_{1.0}O_{2.82}$ in HNO_3.

+ After heating at 1923 K for 19 h.

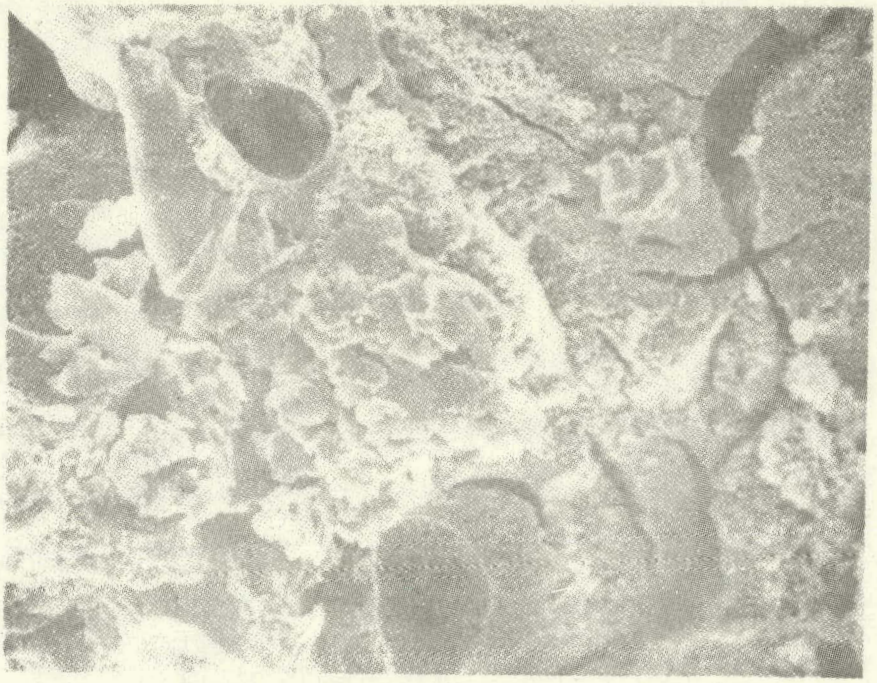

Figure 8.--$LaCrO_3$ Prepared from Citric Acid Precursor with Ethylene Glycol Present, Heated at 923 K for 4 Hours; (1000X magnification)

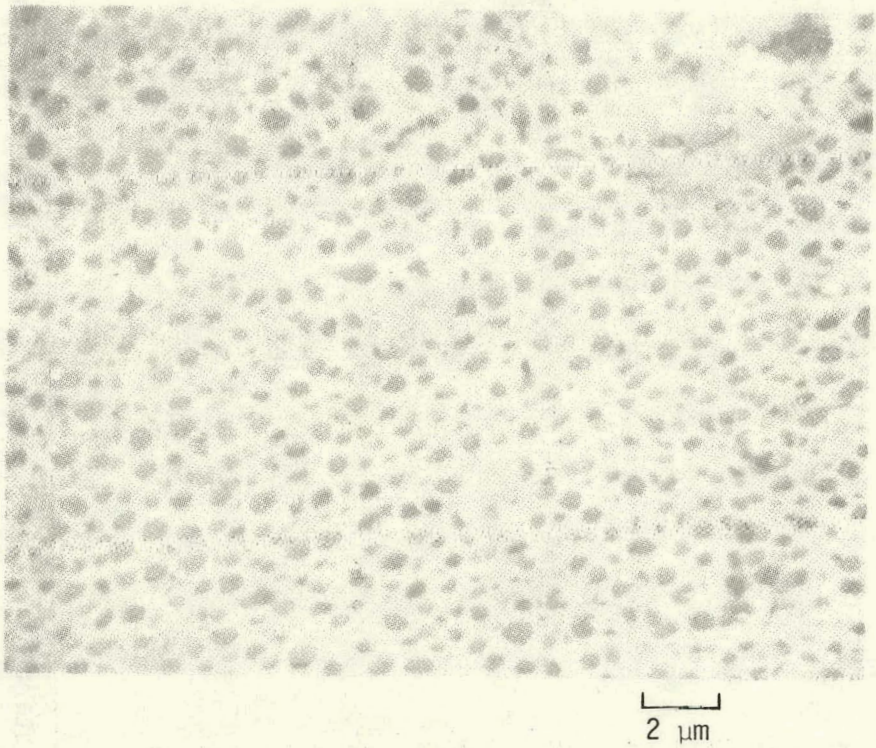

Figure 9.--$LaCrO_3$ Prepared from Citric Acid Precursor with Ethylene Glycol Present, Heated at 923 K for 4 Hours; (5000X magnification)

Figure 10.--$LaCrO_3$ Prepared from Polyhydroxy-Resin Precursor with Ethylene Glycol Present, Heated at 923 K for 4 Hours; (100X magnification)

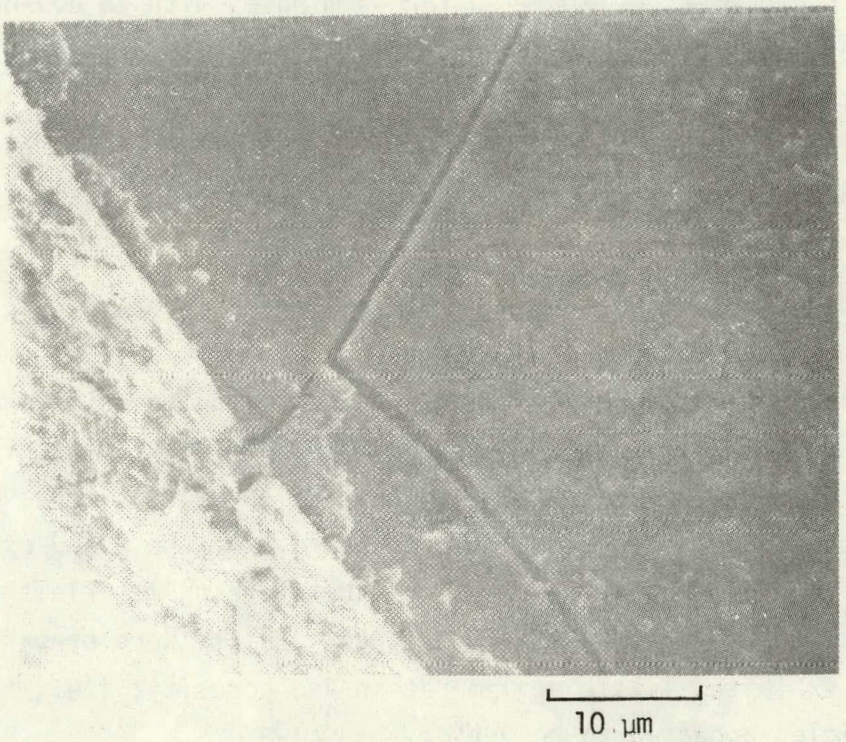

Figure 11.--$LaCrO_3$ Prepared from Polyhydroxy-Resin Precursor with Ethylene Glycol Present, Heated at 923 K for 4 Hours; (2000X magnification)

Coprecipitation of the mixed oxides using gaseous NH_3 (method two) produced porous granules when the material was heated to 923 K for four hours (Figure 12). Closer examination revealed the presence of submicron agglomerates (Figure 13).

Evaporation of the mixed-nitrate solution to dryness produced a hard cake which became porous when heated to 923 K (Figure 14). The cratered surface (Figure 15) probably resulted from the rapid dehydration of the mixed oxides or from gas evolution during nitrate decomposition. Additions of urea to the mixed nitrate solution produce material with a flakey, plate-like morphology (Figure 16).

Sintering tests conducted at 1673 K with substituted $LaCrO_3$ prepared from the citric acid precursor showed evidence of some sintering after nine hours (Figure 17). Because of the wide difference in sample morphologies, noticeable differences in density might be expected in test discs prepared by the various techniques after firing at 1923 K. This was confirmed in subsequent sintering tests with cold-pressed pellets formed from materials calcined at 923 K and 1673 K.

The calcined powders were milled for 30 minutes with an aqueous solution of 1 to 2 wt % binders and lubricant and 2 to 3 wt % surfactant. After evaporation of the water, the crushed powders (-80 mesh) were cold-pressed in a double-acting die at 10,000 psi. The pellets were bisqued and heated to 1273 K before final sintering at 1923 K for 24 hours. The final test results are shown in Table 5.

Of the powders calcined at 923 K, the highest theoretical density was observed in the sample prepared by homogeneous hydrolysis of the mixed-nitrate solution. Similar results were obtained with the polyhydroxy resin-precursor. The chemically prepared sample with the lowest density was powder from the evaporation of the mixed-nitrate solution; it was essentially identical in density to the disc prepared from the mixed oxide. Examination of the SEM photomicrographs of the starting materials revealed that the two sintered samples with the highest density were prepared from powders which exhibited little agglomeration and porosity, i.e., the individual particles appeared to be dense.

TABLE 5.--Densities of Substituted-$LaCrO_3$ Discs Prepared by Various Chemical Techniques and Sintered at 1923 K for 24 Hours

*Preparation Method	+Theoretical Density (Percent) Calcined at 923 K/4h	Calcined at 1673 K/19h
Citric acid resin-precursor	95.7	95.9
Citric acid resin-precursor + ethylene glycol	93.8	94.2
Citric acid + urea, homogeneous coprecipitation	94.7	96.7
Polyhydroxy resin-precursor	97.0	96.2
Polyhydroxy resin-precursor + ethylene glycol	88.7	94.9
Urea homogeneous hydrolysis	97.6	96.5
Coprecipitation with gaseous NH_3	94.7	--
Evaporation of mixed-nitrate solution	91.4	96.4
Mixed oxides	--	^{x}91.3 --

* Mixed nitrate solution of equivalent concentration of 0.46 M $La_{0.9}(Mg_{0.05}Cr_{0.71}Al_{0.21})_{1.0}O_{2.82}$ in HNO_3.

+ Measured by liquid displacement; theoretical density for this composition = 6.53 g/cc, by X-ray measurements.[3]

x Ground twice and heated at 1923 K for 19 hours.

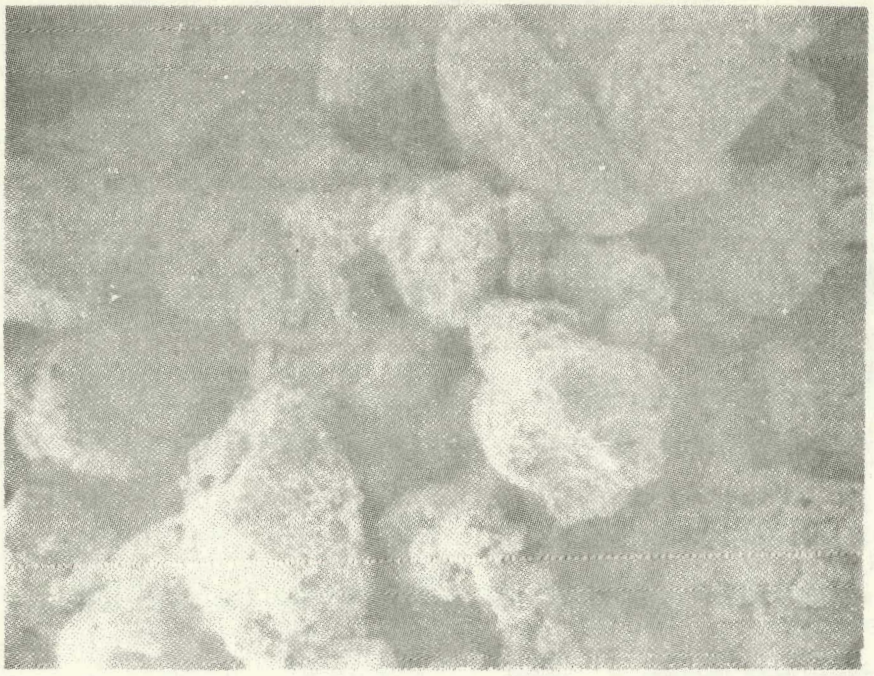

Figure 12.--$LaCrO_3$ Prepared by Coprecipitation with NH_3, Heated at 923 K for 4 Hours; (100X magnification)

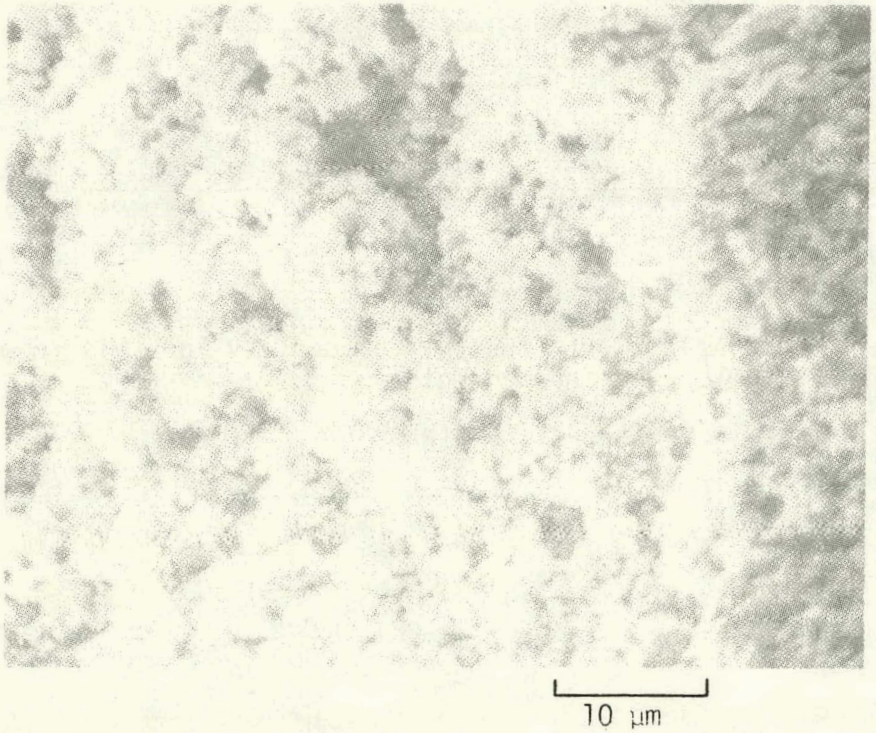

Figure 13.--$LaCrO_3$ Prepared by Coprecipitation with NH_3, Heated at 923 K for 4 Hours; (2000X magnification)

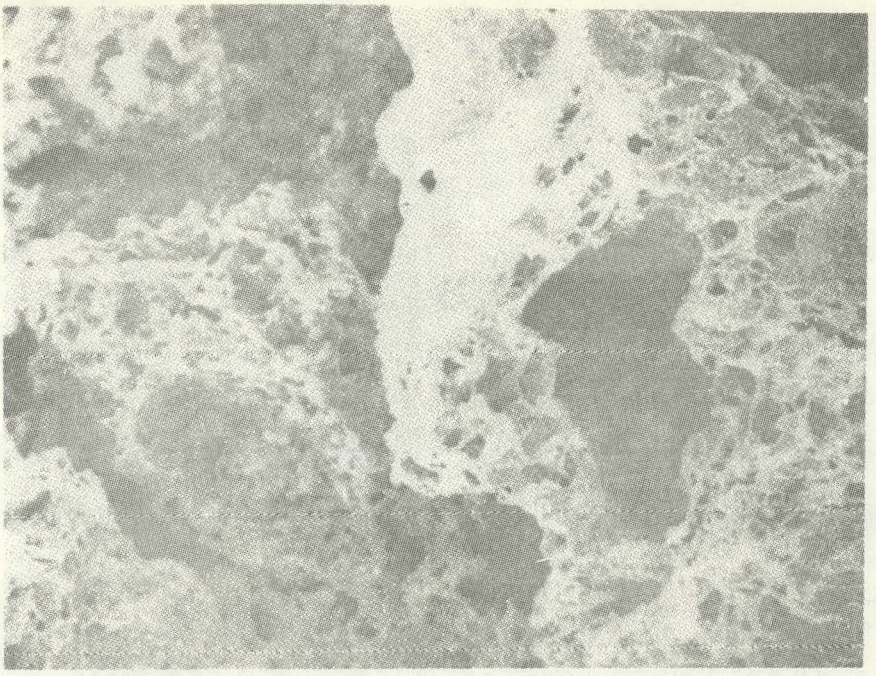

Figure 14.--$LaCrO_3$ Prepared by Evaporation of Mixed Nitrate Solution to Dryness, Heated at 923 K for 4 Hours; (100X magnification)

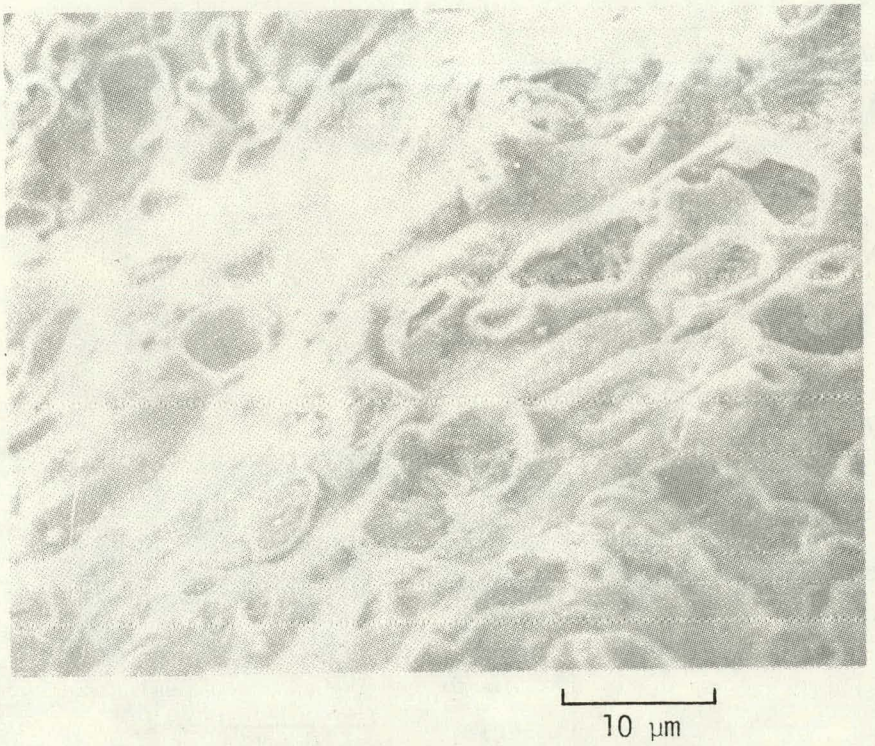

Figure 15.--$LaCrO_3$ Prepared by Evaporation of Mixed Nitrate Solution to Dryness, Heated at 923 K for 4 Hours; (2000X magnification)

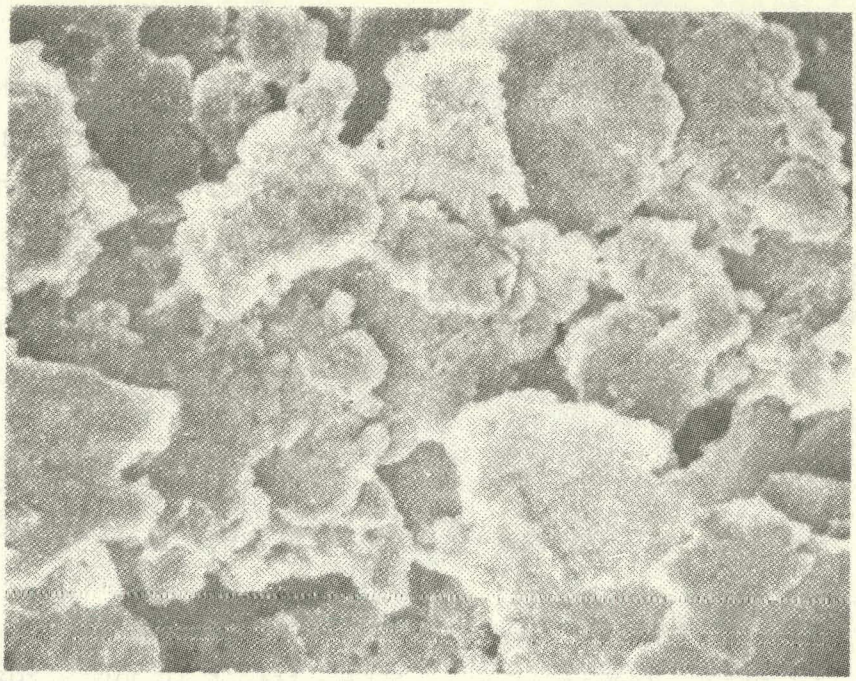

Figure 16.--$LaCrO_3$ Prepared from Evaporation of Mixed Nitrate Solution with Urea Added, Heated at 923 K for 4 Hours; (2000X magnification)

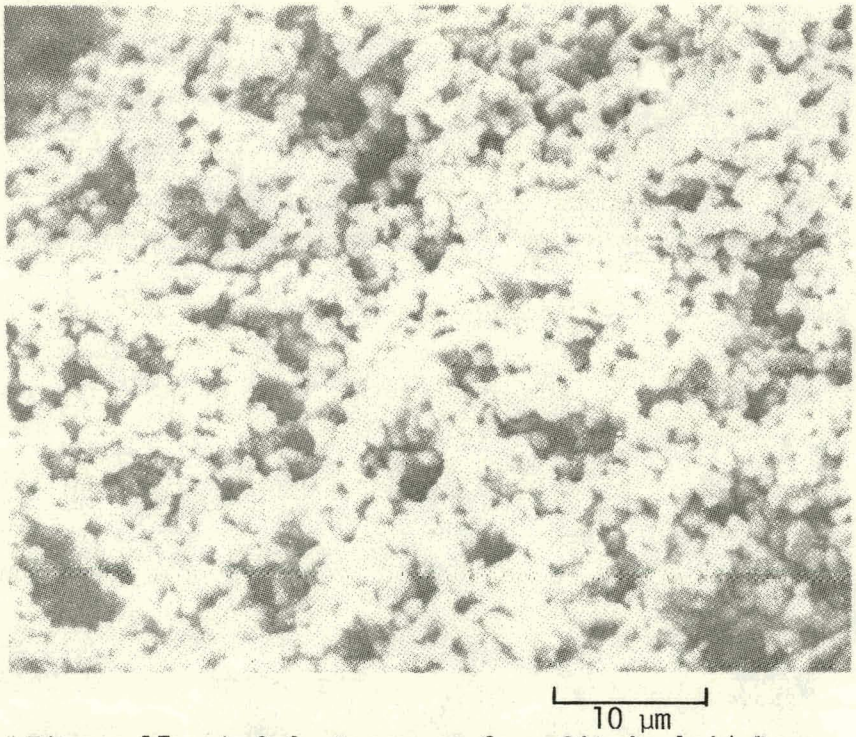

Figure 17.--$LaCrO_3$ Prepared from Citric Acid Precursor, Heated at 1673 K for 9 hours; (2000X magnification)

Calcination of the substituted-$LaCrO_3$ powders at 1673 K for 19 hours caused a substantial increase in theoretical density (relative to the powders calcined at 923 K for four hours) of test discs prepared via the polyhydroxy-resin precursor plus ethylene glycol. Some improvement in theoretical density also was noted for the disc prepared via evaporation of the mixed nitrate solution. The remaining chemically prepared samples showed little or no improvement in theoretical density for powders calcined at 1673 K relative to calcination at 923 K.

Parallel sintering tests were attempted with discs prepared by slip-casting. Severe contamination problems were encountered, however, from the plastic content of the container used for grinding the powders. There was difficulty, as well, in obtaining sufficiently stable slips of substituted $LaCrO_3$. The resultant slipcast discs tended to crack readily during drying and were not suitable for further testing. For these reasons, a sintering study of slipcast substituted-$LaCrO_3$ specimens was not carried out.

The microstructure of the two sintered samples in Table 5 with the highest theoretical density is shown in Figures 18 and 19. The samples were polished to 6 μm with diamond powder and then were "etched" thermally at 1873 K for one-half hour. The average grain size and morphology of the urea-mixed nitrate sample (Figure 18) was similar to that for the polyhydroxy resin-precursor sample (Figure 19).

With the successful preparation of high-density substituted-$LaCrO_3$ discs, subsequent combination with Y_2O_3-stabilized ZrO_2 to form test specimens for interfacial-diffusion measurements appears to pose no difficulties.

IV. CONCLUSIONS

Lithium aluminum silicate, calcium oxide, stannic oxide, and titanium boride reacted sufficiently in a 62 mol % Li_2CO_3-38 mole % K_2O_3 solution at 1000 K to eliminate them from consideration for use in molten-carbonate fuel cells.

Techniques were developed for the production of 98 percent theoretical density substituted $LaCrO_3$ for use in solid-electrolyte fuel cells.

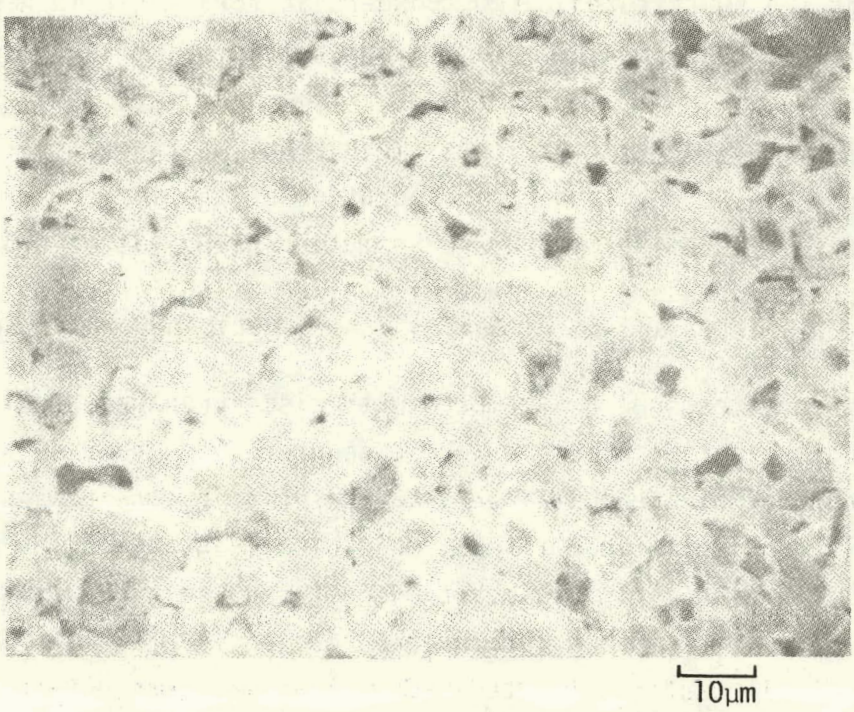

Figure 18.--Microstructure of Polished Section of Sintered, Substituted $LaCrO_3$ Prepared from Urea Hydrolysis of Mixed Nitrate Solution.

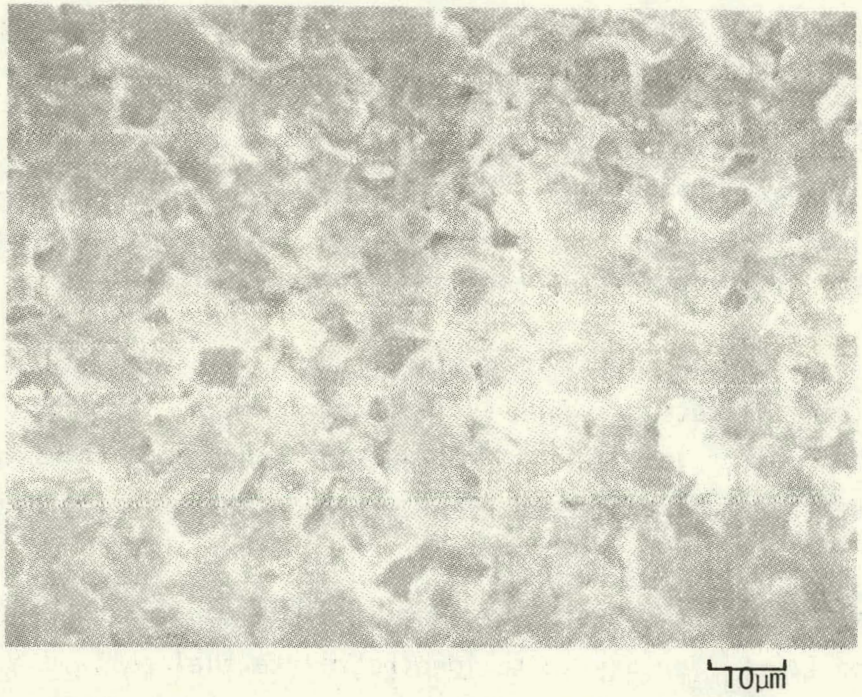

Figure 19.--Microstructure of Polished Section of Sintered, Substituted $LaCrO_3$ Prepared from Polyhydroxy Resin-Precursor.

REFERENCES

1. W. Feduska and A. Isenberg, Westinghouse Electric Corporation, Pittsburgh, Pennsylvania, personal correspondence to Mr. L. Harry, DOE, Washington, D.C., August 2, 1977.

2. C. T. Lynch, K. S. Magdiyasni, and J. S. Smith, Special Ceramics, Volume IV, P. Popper, ed., The British Ceramics Research Association, p. 83, 1968.

3. C. Marcilly, P. Courty, and B. Dalman, Journal American Ceramic Society, 53 (1), pp. 56-7, 1970.

4. H. Anderson, University of Missouri, Rolla, Missouri, private communication, August 10, 1978.

THIS PAGE

WAS INTENTIONALLY

LEFT BLANK

APPENDIX A

EVALUATION OF MHD MATERIALS FOR USE IN HIGH-TEMPERATURE FUEL CELLS

by

Ronald Guidotti

June 15, 1978

Topical Report

Contract No. EC-77-C-03-1485

Montana Energy and MHD Research and
Development Institute

Submitted to

U. S. Department of Energy
Office of Fossil Energy
Division of Power Systems

ABSTRACT

The MHD and high-temperature fuel cell literature was surveyed for data pertaining to materials properties in order to identify materials used in MHD power generation which also might be suitable for component use in high-temperature fuel cells. Classes of MHD-electrode materials evaluated include carbides, nitrides, silicides, borides, composites, and oxides. Y_2O_3-stabilized ZrO_2 used as a reference point to evaluate materials for use in the solid-oxide fuel cell. Physical and chemical properties such as electrical resistivity, coefficient of thermal expansion, and thermodynamic stability toward oxidation were used to screen candidate materials.

A number of the non-oxide ceramic MHD-electrode materials appear promising for use in the solid-electrolyte and molten-carbonate fuel cell as anodes or anode constituents. The MHD-insulator materials appear suitable candidates for electrolyte-support tiles in the molten-carbonate fuel cells. The merits and possible problem areas for these applications are discussed and additional needed areas of research are delineated.

TABLE OF CONTENTS

LIST OF TABLES

LIST OF FIGURES

INTRODUCTION

This technology-transfer report is prepared as a part of the requirements of Contract No. EC-77-C-03-1485, "High Temperature Fuel Cell Research and Development," to identify materials developed for magnetohydrodynamic (MHD) energy conversion that may have applicability as high-temperature fuel cell components.

Generation of electrical power by MHD using a coal-fired combination creates an extremely hostile environment for the electrodes and insulation in the channel. The high temperatures and erosive and corrosive effects of the coal slag-seed mixture presents formidible materials requirements which can be met by only a limited class of compounds. The chemical and physical requirements of materials for use in the MHD generator are listed in Table 1; comparable data for the high-temperature solid-electrolyte fuel cell are presented in Table 2.

As indicated in these tables, the general materials requirements are similar for certain components. Operating conditions for the solid-electrolyte fuel cell, however, are less severe--lower current density, temperature, and pressure. The requirements for the electrical properties of the fuel cell components, on the other hand, are more stringent because of the manner of fabrication of the multi-cell stack. (See Figure 1 for a cross sectional view of Westinghouse's thin-film fuel cell stack). The electrodes, electrolyte, and interconnector used to connect individual cells together

TABLE 1.--Materials requirements for an MHD generator[1,2]

Parameter	Electrode	Interelectrode Insulator
Electrical Resistivity*	ρ < 10 ohm-cm, electronic	ρ > 100 ohm-om; dielectric breakdown > 4KV/m
Current density*	> 1 A/cm^2	---
	General Requirements	
Channel wall temp.		
a) Cold	< 1200°C	
b) Intermediate	1200° to 1700°C	
c) Hot	> 1700°C	
Thermionic emission*	Good electron transfer between plasma & electrodes.	
Chemical stability*	Stable at P_{O_2} = 10^{-2} to 10^{-3} atm, low vapor pressure and high melting point.	
Pressure*	Maximum of 10 atm.	
Thermal conductivity*	Able to maintain wall temperature below melting point.	
Thermal shock	Good shock resistance during start-up and cool-down; must tolerate thermal stresses due to large temperature gradients.	
Erosion resistance*	Minimum material loss under slagging conditions and when exposed to high-velocity gases and particulates.	
Corrosion resistance*	Resistant to coal slag, K_2SO_4, K_2CO_3, and mixtures thereof.	
Compatibility*	Must be chemically and mechanically compatible with other components; especially important for graded materials.	
Mechanical stability*	Creep resistant; no destructive phase changes from ambient to operating temperatures.	
Life*	> 10,000 hr.	
Fabrication	Economical and easy to fabricate.	
Porosity	Minimum porosity (dense).	

* At temperature

TABLE 2.--Materials requirements for a solid-electrolyte fuel cell[3,4]

Parameter	Interconnector	Cathode (Air) Electrode	Anode (Fuel) Electrode	Electrolyte
Electrical Resistivity*	ρ<50 ohm-cm, ~100% electronic	ρ/δ < 1 ohm, electronic +	ρ/δ < 1 ohm, electronic+	ρ= 25-50 ohm-cm, ionic
Porosity	Gas-tight	Moderate; gas permeable	Moderate; gas permeable	Gas-tight
Current Density*	0.4 to 0.8 A/cm^2			
Temperature	700^o to 1000^{o}C			
Pressure*	Atmospheric			
Chemical Stability*	Stable under oxidizing and reducing atmosphere; low vapor pressure	Stable in air; low vapor pressure	Stable with reducing atmos. (Po_2 = 10^{-16} atm); low vapor pressure	Same as for interconnector.
Compatibility*	Must be chemically and mechanically compatible; coefficient of thermal expansion of 10 x $10^{-6}/^oC$.			
Mechanical Stability	Creep resistant, with no destructive phase changes from ambient to 1000^{o}C			
Life*	> 30,000 hrs			
Fabrication	Moderate in cost and easy to fabricate			

*At temperature

+ δ= thickness, generally 20 to 50 μm

electrically are successively applied to a porous-tube substrate in the form of films 20 to 50 μm thick. The very thin layers require an electrical conductivity as high as possible to minimize power losses during operation of the fuel cell.

The MHD electrodes and interelectrode insulators are exposed to the same mildly oxidizing atmosphere ($P_{O_2} \simeq 0.10$ atm, typically). The electrolyte and interconnector of the solid-electrolyte fuel cell, however, are exposed to dual atmospheres simultaneously. On the air-electrode (cathode) side, the atmosphere is quite oxidizing ($P_{O_2} \simeq 0.2$ atm), while extremely reducing conditions (P_{O_2} as low as 10^{-18} atm) are found on the fuel-electrode (anode) side. Thus, while some materials may possess properties compatible under either oxidizing or reducing conditions, imposing both criteria at once severely restricts material options available.

The corrosive action of molten mixtures of coal slag, K_2SO_4, and K_2CO_3 upon the MHD interelectrode insulator has an analogy in the molten-carbonate fuel cell. Even though the operating temperature of the fuel cell (580° to 730°C) is considerably lower than that for the typical MHD channel (1200° to 1700°C), the molten electrolyte--binary and ternary mixtures of Na_2CO_3, K_2CO_3, and Li_2CO_3--is still quite corrosive. Thus, the ceramic matrix (tile) used to contain the electrolyte must be quite resistant to attack if a 40,000-hour cell life is to be realized. Candidate materials for the tile, however, do not need the extremely high melting point required of MHD interelectrode

insulators.

The general similarity of the chemical and physical properties of materials used for MHD and high-temperature fuel cells suggests the possibility, where appropriate, of transferring materials technology from one area to another. A good electricity-conducting ceramic found to be suitable for MHD electrode use could be an appropriate candidate for the interconnector in the solid-electrolyte fuel cell. Similarly, a material which is resistant to corrosion by coal slag as an inter-electrode insulator in the MHD channel may show promise as a tile in the molten-carbonate fuel cell. As a result of the generally less stringent component requirements, materials examined for MHD use as electrodes or insulators and found to be deficient in performance may prove more than adequate for use in the solid-electrolyte or molten-carbonate fuel cells.

The purpose of this report, therefore is to examine and evaluate the published data in the MHD and fuel cell fields as related to materials properties and to identify materials used or considered for MHD power generation which also might prove suitable candidates for components in the high-temperature fuel cells.

DISCUSSION

I. SOLID-ELECTROLYTE DESIGN CONSIDERATIONS

The heart of the solid-electrolyte fuel cell is the oxide electrolyte. It is important that the oxide system chosen for use as the electrolyte have the proper electrochemical characteristics (i.e., high ionic conductivity) as well as stability from destructuve phase transformations upon thermal cycling. Once an appropriate oxide has been chosen for the electrolyte, materials for the remaining cell components--air and fuel electrodes and cell interconnector--can be selected for physical and chemical compatibility with the electrolyte and each other. The physical property of prime concern is the coefficient of thermal expansion. The reason for this becomes clear after examining the current Westinghouse design for a thin-film cell shown in Figure 1.[3] A substantial mismatch in thermal expansion of the electrolyte and interconnector could cause cracking of the impervious films, resulting in severe degradation or failure of the fuel cell upon thermal cycling. In order to evaluate MHD materials properly for potential use in solid-electrolyte fuel cells, it is first necessary to examine those materials which can possibly be used as oxide-conducting electrolytes. Auxiliary materials then can be screened for the remaining cell components to ensure the thermal expansion behavior is compatible with that of the chosen electrolytes.

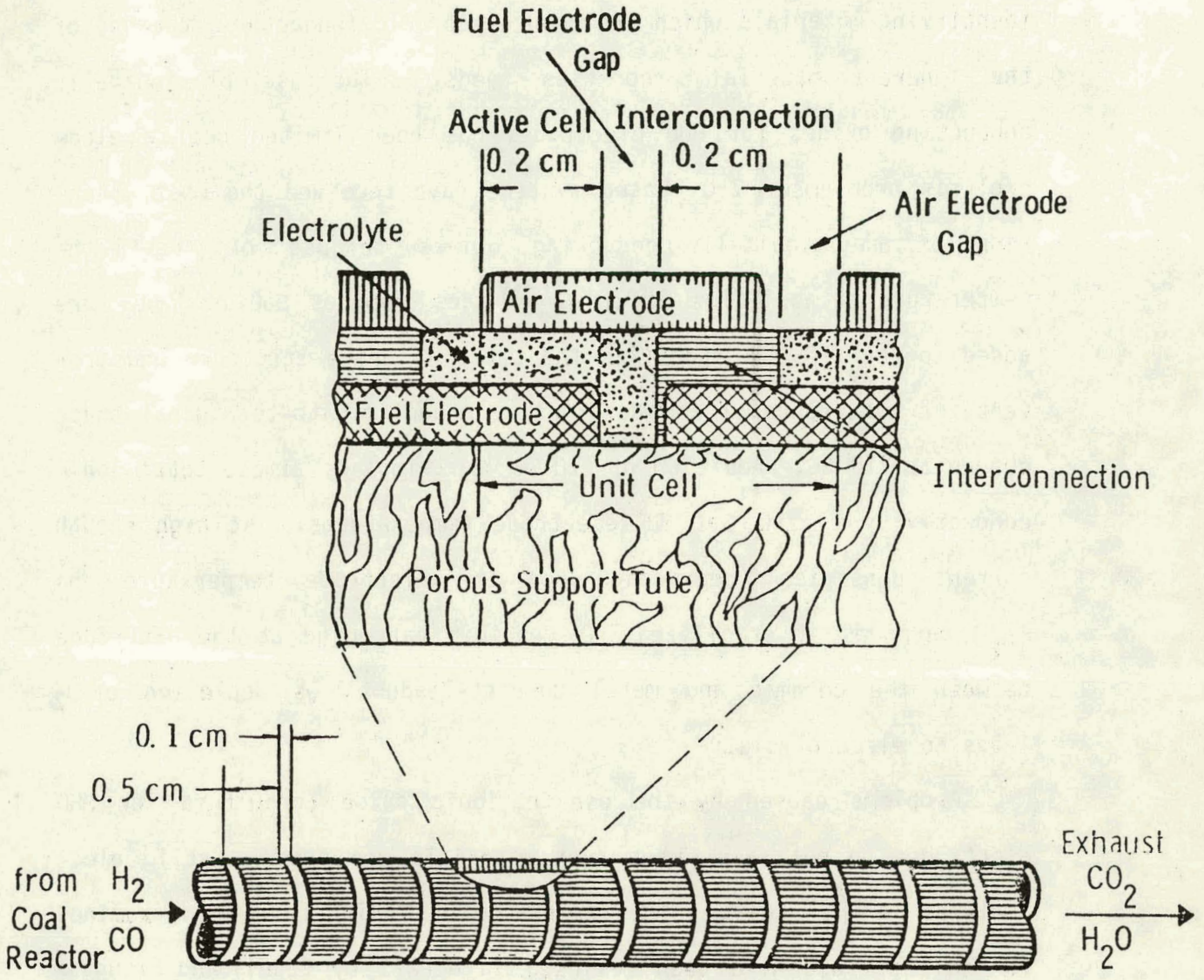

Figure 1.--Westinghouse high-temperature fuel cell structure (from ref. 3.)

A. Ionically Conducting Oxides

The bulk of research on MHD electrodes has been oriented toward identifying materials which are good electronic conductors, because of the inherent material properties needs. The use of ionically conducting oxides for MHD electrodes has been limited due to electrolysis problems. ZrO_2-based systems have received the most attention of the ionically conducting oxides because of the high-temperature capabilities of ZrO_2.[2,5,6] Oxides such as CaO or Y_2O_3 are added to the ZrO_2 to stabilize the cubic flourite structure and prevent the occurrence of the destructive monoclinic-to-tetragonal phase change at 1100°C. Addition of CaO or Y_2O_3 imparts almost total ionic conductivity to ZrO_2 at MHD-electrode temperatures. At high enough current densities (depending upon the electrode temperature and P_{O_2}), cathodes of stabilized ZrO_2 exhibit darkening at the interface between the ceramic and metal current-leadout, as depletion of O_2 leads to electrolysis.

Problems caused by the use of ionic oxide conductors for MHD electrodes do not exist when such materials are used as solid electrolytes in fuel cells. The various oxides which have been examined for this purpose have been reviewed in detail by Etsell and Flengas.[7] The results of their review are summarized below to justify the selection of the most promising systems as solid electrolytes for high-temperature fuel cells; evaluation of MHD materials for potential use for the remaining cell components is discussed separately.

Oxide systems based upon ZrO_2, HfO_2, ThO_2, and CeO_2 have been studied extensively as solid electrolytes. Divalent (e.g., alkaline earth) and trivalent (e.g., rare earth) oxides are added to stabilize the desired cubic flourite structure or to increase the electrical conductivity. In addition to being a good conductor, a potential solid-electrolyte should have an ionic transference number (t_i) as close to unity as possible, over the range P_{O_2} expected during fuel cell operation--$\sim$0.2 atm at the cathode and $\sim 10^{-16}$ at the anode. The electrolyte also should exhibit a resistance to ordering and destabilization of the cubic solid solution after prolonged periods (10,000 hr.) at operating temperature.

1. ZrO_2 Systems

The electrical properties of typical ZrO_2-based electrolytes are summarized in Table 3 for compositions where the conductivity is greatest. The three oxide stabilizers which best meet the desired electrical requirements are Sc_2O_3, Y_2O_3, and CaO. Unfortunately, the cost of Sc_2O_3 is too prohibitive to warrant serious consideration for commercial application. While Y_2O_3 is more expensive that CaO, the additional cost is justified because of the increased conductivity and greater stability of Y_2O_3-ZrO_2 solid solutions.[7-10]

2. HfO_2 Systems

The electrical transport properties of HfO_2-based systems are, as might be expected, similar to their ZrO_2 counterparts. For ex-

TABLE 3.--Electrical properties of ZrO_2-based solid electrolytes at 1000°C and in air

Oxide Additive	Conc., m/o	ρ, Ω-cm	Transport Properties: Avg. t_i	Transport Properties: -Log P_{O_2}, atm	References
Sc_2O_3	8-10	4	est.>0.99	-	11,12
Y_2O_3	10	10	>0.99	0 to 17	13-15
Gd_2O_3	8-10	9	-	-	16
Yb_2O_3	10	9	0.99	? to 10	16
CaO	12-13	17-24	>0.99	0 to 20	4,11,17-19
*MgO	20	26	-	-	10,20
Pr_6O_{11}	25	37	0.95	?	21
Nd_2O_3	15	59-71	0.93	0	22,23
La_2O_3	5	227	-	-	24,25
	15	330-910	0.08-0.17	0	12,22

*Cubic solid solution is unstable below 1300° to 1400°C

ample, HfO_2-Y_2O_3 and HfO_2-CaO solid solutions are good ionic conductors at 1000°C. The electrical conductivities, however, are only a fraction as great as the ZrO_2 solid solutions at the 10 to 12 m/o additive level, where conductivity is greatest.[7] The use of HfO_2 solid solutions as solid electrolytes in fuel cells does not appear warranted because of lower conductivities and higher costs relative to the ZrO_2 systems.

3. ThO_2 Systems

Lower-valent oxides are added to ThO_2 solely to increase the electrical conductivity, as ThO_2 already has a cubic flourite structure. The electrical properties of ThO_2-based solid-electrolytes are summarized in Table 4 for a number of the more common systems. The ThO_2-based electrolytes are characterized as being ionically conducting to a much lower P_{O_2} than the corresponding ZrO_2 systems. Unfortunately, the magnitude of the electrical conductivity is one or two orders of magnitude less for the ThO_2 solid electrolytes. More importantly, at a P_{O_2} greater than 10^{-16} atm electronic (p-type) conduction becomes significant. Thus, a fuel cell solid electrolyte based on ThO_2 is not feasible because of the incompatible electrolytic domain.

4. CeO_2 Systems

CeO_2 is similar to ThO_2 in that both have the flourite structure. A considerable amount of research has been carried out with CeO_2-based electrolytes because of the promise of el-

TABLE 4.--Electrical Properties of ThO_2-Based Solid Electrolytes at 1000°C and in air

Oxide Additive	Conc., m/o	ρ,Ω-cm	-Log P_{O_2},atm	Transport Properties		References
				Avg. t_i	-Log P_{O_2},atm	
Y_2O_3	8.1	139 to 435	> 8	>0.99	7 to 24	26,27
CaO	5	2,120	15	0.89	1(=$\bar{P}_{O_2}$)*	26
La_2O_3	14	312	0.7	0.87	1(=$\bar{P}_{O_2}$)*	28,29

*$\bar{P}_{O_2}$ = avg. P_{O_2} = $\frac{1}{2}$ [$P_{O_2\ cathode}$ + $P_{O_2\ (anode)}$]

ectrical conductivities comparable to some of the better stabilized-ZrO_2 systems at 1000°C, but at much lower temperatures--typically 700°C. The electrical properties of a number of CeO_2 -based solid-electrolytes are presented in Table 5.

Doping of CeO_2 with alkaline-earth and rare-earth oxides results in good ionic conductivities at temperatures below 1000°C and high oxygen pressures (e.g., $P_{O_2} > 10^{-5}$ atm), in many cases.[7] However, at temperatures near 1000°C or at low oxygen pressures (e.g., $P_{O_2} < 10^{-10}$ atm), Ce^{+4} is reduced to Ce^{+3}, which gives rise to unacceptable levels of electronic (n-type) conduction. The large increase in electrical conductivity for CaO-doped CeO_2 under strongly reducing conditions, relative to air, indicates the presence of electronic conduction. Similarly, while good ionic conductivity results when CeO_2 is doped with a number of rare-earth oxides at a P_{O_2} of 0.2-1.0 atm, the ionic transference number is strongly dependent upon P_{O_2} and drops markedly under reducing conditions. Thus, the best solid-electrolyte developed to date based upon CeO_2 would appear marginally acceptable at best. This conclusion is supported in recent work by Ross and Benjamin,[36] who analyzed the thermal efficiency (η_T) which could be expected for a H_2 -air fuel cell utilizing various solid electrolytes.

The thermal efficiencies of cells using various CeO_2 -based

TABLE 5.--Electrical properties of CeO_2-based solid electrolytes

Oxide Additive	Conc., m/o	Temp., °C	ρ, Ω-cm	-Log P_{O_2}, atm	Transport Properties: Avg. t_i	Transport Properties: -Log P_{O_2}, atm	References
Y_2O_3	5	700	50	0	1.0	$\leq$ 5.5	30
		1,000	6	0	1.0	$\leq$ 3.5	30
CaO	10	700	27	0	-	-	31
		700	4	20	-	-	31
		1,000	5	0	-	-	31
		1,000	0.5	14	-	-	31
Nd_2O_3	15	727	21	0.7	1.0	0.7 to 0	32
Sm_2O_3	15	727	25	0.7	0.96	0.7 to 0	32
Gd_2O_3	15	727	22	0.7	1.0	0.7 to 0	32
Dy_2O_3	15	727	26	0.7	1.0	0.7 to 0	32
Er_2O_3	15	727	30	0.7	1.0	0.7 to 0	32
La_2O_3	11	1,000	14	0.7	0.18	15	33-35

electrolytes are shown in Table 6. The Electric Power Research Institute goal for a solid-oxide fuel cell is an overall thermal efficiency of 45.5 percent. None of the CeO_2-based systems approach the efficiency goal at 700°C, except CeO_2-La_2O_3; unfortunately, this combination has a power density that is too low to be of practical use in thin-film fuel cells.

5. Other Oxides

Takahaski and coworkers have conducted extensive research on development of solid-oxide electrolytes with ionic conductivities comparable to stabilized-ZrO_2 at 1000°C, but at temperatures as low as 700°C. Doped Bi_2O_3 was reported to be a good oxide conductor at a relatively high P_{O_2} at temperatures as low as 800°C.[37] Substituted perovskites studied included $La_{1-x}Ca_xAlO_{3-\alpha}$, $La_{1-x}Ba_xAlO_{3-\alpha}$, $CaTi_{1-x}Mg_xO_{3-\alpha}$, $CaTi_{1-x}Al_xO_{3-\alpha}$, $SrTi_{1-x}Al_xO_{3-\alpha}$, $BaTh_{0.95}La_{0.05}O_{3-\alpha}$, $BaZr_{0.9}Bi_{0.1}O_{3-\alpha}$, and $BaCe_{0.9}Bi_{0.1}O_{3-\alpha}$. The electrolyte of composition $CaTi_{0.7}Al_{0.3}O_{3-\alpha}$ showed the most promise.

The electrolytes listed above are not purely ionic conductors and exhibit changes in conductivity and ionic transference number as a function of P_{O_2}. This mixed conduction generally has been considered undesirable for fuel cell purposes. Takahashi[43] has considered the ramifications of mixed conduction in solid-oxide, high-temperature fuel cells. According to his calculations, a purely ionic electrolyte with a $t_i=1$ in a solid-electrolyte fuel

TABLE 6.--Maximum thermal efficiencies of H_2-air fuel cells with various solid electrolytes[36]

Electrolyte	Ionic Conductivity, $10^{-2}\Omega^{-1}cm^{-1}$	P_θ, atm*	Power Density, 10^{-3} W/cm	η_t,%
ZrO_2-7 m/o Y_2O_3	1.27	1.00×10^{-44}	1.5	50.2
CeO_2-18 m/o Gd_2O_3	3.3	3.16×10^{-19}	4.8	40.0
CeO_2-5 m/o CaO	1.4	1.00×10^{-17}	2.1	35.7
CeO_2-5 m/o Y_2O_3	1.03	5.31×10^{-18}	1.7	36.6
CeO_2-33 m/o La_2O_3	0.14	1.34×10^{-26}	0.17	49.5

* $P_e = P_{O_2}$ where ionic σ = electronic σ (i.e., $t_i = 0.5$)

cell would be comparable in energy conversion efficiency (η=0.6) to a mixed-conductor electrolyte with t_i =0.94, if the conductivity were 50 percent greater.[43]

A similar theoretical study has been published recently by Tannhauser [44] and applied to doped-CeO_2 electrolytes. The equivalent circuit used for modeling was not found to represent the system very well in practice. Still, it was felt that doped CeO_2 should be considered more suitable as a solid electrolyte in high-temperature fuel cells than believed previously.

While a number of the above substituted perovskites appear promising for use as solid electrolytes in high-temperature fuel cells, there are still areas of deficiency which must be resolved before they can be considered competitive with other, more suitable electrolyte materials.

B. Choosing a Solid-Oxide Electrolyte

As mentioned earlier, mechanical stability under thermal-cycling conditions is very important for long-term integrity of fuel cell operation. The thermal-stress problems can be approached in several ways. One involves carefully matching the coefficient of thermal expansion of the cell interconnector to that of the electrolyte. Alternatively, the interconnector can be plastic and have a low modulus of elasticity at operating temperature to minimize thermal stresses. Generally, this involves the use of a glassy matrix containing the interconnector material.[45] This approach, while possibly solving one

problem, presents additional problems of long-term chemical stability in contact with the electrolyte. In addition, incorporation of a glassy phase inherently lowers the overall conductivity of the interconnecting layers. Thus, this latter approach does not appear practical. For the purposes of this report, potential interconnector materials should have an average linear coefficient of thermal expansion (α) compatible with that of ZrO_2-10 m/o Y_2O_3, which is 10×10^{-6} /°C up to 1000°C.[4]

At this time, none of the solid-oxide electrolytes for which published information is available appears to satisfy all the electrochemical requirements for efficient operation of high-temperature fuel cells at temperatures as low as 700°C. Doped-CeO systems have unacceptable electronic conduction (low t_i) resulting in low fuel cell efficiencies, while doped-ZrO_2 systems have ionic conductivities which are insufficient (at 700°C) for the desired power-density levels. In addition, little is known about the long-term behavior of the CeO_2-based electrolytes and substituted perovskites under fuel cell conditions, although work currently is underway at the National Bureau of Standards to study long-term degradation mechanisms in CeO_2-Gd_2O_3 and -Y_2O_3 solid solutions.[46,47]

Of all the solid-oxide electrolytes discussed above, only the ZrO_2-CaO and ZrO_2-Y_2O_3 solid solutions meet the requirements necessary for efficient electrochemical conversion at 1000°C of fuels such as H_2 and CO at a reasonable material cost. The ZrO_2-Y_2O_3 system is the preferred choice for use as a solid

electrolyte in high-temperature fuel cells because of higher conductivity greater stability against long-term structural ordering. Rohr [48] has reported a significant increase in the electrical conductivity of ZrO_2-Y_2O_3 solid solutions in which part of the Y_2O_3 has been replaced by Yb_2O_3 (e.g., ZrO_2-4 m/o Y_2O_3 - 4 m/o Yb_2O_3). Even though the conductivity may be lower for ZrO_2-10 m/o Y_2O_3--the composition with the highest conductivity in the ZrO_2-Y_2O_3 system--this composition was chosen as a reference point or basis for evaluating and screening various MHD materials for possible use as ancillary components in the solid-electrolyte fuel cell because it has been studied more extensively for this purpose. Physical and chemical properties data also are more readily available for comparison.

II. MHD ELECTRODE MATERIALS

Materials examined for use as MHD electrodes can be classified into three general categories: metals, non-oxide ceramics, and oxide ceramics.

A. Metals

A variety of metals has been examined for use as MHD electrodes, with the choice of materials based upon properties such as chemical inertness, electrical and thermal conductivity, and low vapor pressure at elevated temperatures. Classes of metals which have been tested include noble metals (e.g., Pt, Rh, Pd, Au, and Ag), refractory metals (e.g., W, Mo, Ta, Nb, Hf, and Zr), and base metals (e.g.,

Fe, Ni, and Cu) and their alloys. The use of noble metals in the solid-electrolyte fuel cell would be prohibitively expensive and, therefore, will not be considered further. A number of the base and refractory metals suitable for MHD electrodes at temperatures of 200° to 700°C would be limited to use as fuel electrodes in the solid-electrolyte fuel cell by P_{O_2} constraints. The equilibrium P_{O_2}s at 1000°C for a number of these metal-metal oxide systems are tabulated in Table 7.

In comparison to the P_{O_2} of 10^{-16} to 10^{-18} atm expected for the fuel, copper is stable over a wider range of P_{O_2} than any of the other base metals, i.e., CuO formation would not be expected until the P_{O_2} had reached a value of 5.75×10^{-7} atm. Unfortunately, copper has a melting point of only 1083°C, which is very close to the operating temperature of the solid-electrolyte fuel cell, thus making it unsuitable for anode use. Currently, nickel is the preferred choice for the anode in both the solid-electrolyte and molten-carbonate fuel cells. As indicated in Table 7, it has a greater stability range than either cobalt or iron, with respect to oxidation by the fuel mixture.

The present technique employed for the fabrication of the nickel anode in the solid-electrolyte fuel cell is relatively simple and straightforward. The Ni-ZrO_2 cermet electrode is prepared by first sintering (at 1600°C) a coating of NiO and CaO-stabilized ZrO_2 on a porous support tube, and reducing the mixture at 1350°C in hydrogen.[50] The result is a porous, mechanically sound structure consisting of continuous interlocking phases of ZrO_2 and nickel. The nickel anode

TABLE 7.--Equilibrium P_{O_2} for select metal-metal oxide systems at 1000°C

Metal-Metal Oxide System	-Log P_{O_2} (atm)	Reference
Cu-CuO	6.24	49
Ni-NiO	10.3	49
Co-CoO	11.9	49
Fe-$Fe_{0.95}O$	14.8	7
Mo-MoO_2	15.0	7
W-WO_2	15.8	7
Cr-Cr_2O_3	21.6	7
Mn-MnO	24.0	7
Ta-Ta_2O_5	24.6	7
Nb-NbO	25.1	7

produced in this manner also provides a good surface for bonding to the other cell components, such as the porous support tube, electrolyte, and interconnector films, which reduces the tendency for cracking due to thermal stresses.

There are no apparent advantages of substituting a more exotic or costlier alloy or metal for pure nickel, unless perhaps a significant resistance to sulfur poisioning was realized and the life of the fuel cell substantially increased. A number of nickel alloys, such as the Inculoy alloys and stainless steels, have increased resistance to sulfur (as H_2S), relative to pure nickel. Unfortunately, these alloys also have electrical resistivities which are an order of magnitude higher.[51] With today's desulfurization technology, no serious problems are envisioned in lowering the sulfur content of the fuel to acceptable levels (< 0.05 ppm) for satisfactory long-term performance of nickel anodes in fuel cells.[52]

B. Non-Oxide Ceramics

Materials used for MHD electrodes in the non-oxide ceramic category include carbides, nitrides, silicides, and borides and their mixtures.

1. Carbides

Only a limited number of elements form carbides of potential interest for MHD electrodes, i.e., good electronic (metallic) conductors. These are generally the transition elements of Groups IVA to VIA (Ti, V, and Cr families). Elements to the left of these groups in the Periodic Table form reactive, ionic (salt-

like) carbides which are hydrolyzed by water to the hydroxide and acetylene, methane, ethylene, or mixtures thereof, depending upon the oxidation state of the metal.[53] The rare-earth carbides are similarly reactive to moisture. Of the elements to the right of the transition metals in the Periodic Table, only Al, B, and Si form carbides of any thermal stability. Al_4C_3, however, is like the alkaline-earth carbides in that it hydrolyzes readily.

Physical properties for transition-metal carbides which have been studied or considered for MHD electrodes are listed in Table 8; data for several non-transition metal carbides, B_4C and SiC, are included for comparison. The transition metal carbides are characterized by high melting points and, in general, a high metallic conductivity, so that the values reported here for room temperature would be considerably higher at the solid-electrolyte fuel cell operating temperature of 1000 °C. The resistivities of ZrC, HfC, and TaC, however, are reported to decrease with temperature. Carbon-deficient (metal-rich) phases show higher resistivities than the stoichiometric phases.[54,55]

Electrical conductivity data at elevated temperatures were not readily available for most of the carbides. Sources of additional physical properties information for transition metal carbides--including the above type resistivity data--are listed in Appendix A. These references predominantly are Russian journals to which the author did not have ready access during the

TABLE 8.--Physical properties of metal carbides

Material	Melting Point, °C	Coefficient of Thermal Expansion (α), 10^{-6}/°C	Electrical Resistivity at 25°C, μΩ-cm	References
B_4C	2,450	4.3 (25°-871°C)	0.3-0.8Ω-cm	56,57
β-SiC	2,700	4.4 (25°-1,400°C)	2.1Ω-cm	57,58
TiC	3,250	8.3 (0°-1,400°C)	60-250	57-59
ZrC	3,550	7.5 (25°-1,350°C)	57-75	57-60
HfC	3,890	7.2 (25°-2,030°C)	109	57,59,60
VC	2,830	6.6 (25°-1,930°C)	150	57,59,60
NbC	3,500	7.3 (25°-1,450°C)	60-150	57-60
TaC	3,880	6.5 (25°-1,000°C)	30	57,59,60
MoC	2,690	-	49	58,59
Mo_2C	2,687	7.3 (25°-1,930°C)	71-97	57-59
WC	>2,755 (dec.)	5.2 (25°-2,200°C)	25-53	58-60
W_2C	2,800	-	80	59,60
Cr_3C_2	1,915	10.3 (25°-1,100°C)	75-84	57-60

allotted time. Only infrequently did the published English abstract contain numerical data for the desired physical properties. Acquisition of copies of these journal articles also was hampered seriously by recently enacted federal copyright legislation which limits the number of articles which any one organization can obtain, through interlibrarly loan, from a given journal in a particular calendar year. Under the new law, only five copies of articles from the previous five years of publication of a journal are allowed per organization per year.

While the conductivities of most of the carbides are compatible with the electrical requirements for the interconnector and fuel electrodes (Table 2), none of the carbides, except for perhaps Cr_3C_2, possess thermal-expansion properties that would be suitable for use with the ZrO_2-Y_2O_3 solid electrolyte. Perhaps this deficiency, however, can be mitigated by suitable materials engineering.

The requirement of stability to partial pressures of oxygen as high as 0.2 atm is prohibitively stringent and does not allow the carbides to be used as interconnector material. At 1300K, all the carbides are thermodynamically unstable in air with respect to the oxides, i.e., the free energy of oxidation is extremely negative, as indicated in Table 9. Data are included in Table 9 for oxidation at 900K, also, for evaluating carbides for possible use in the molten-carbonate fuel cell.

In spite of thermodynamic predictions, however, kinetic factors can be overriding to prevent the reactions from occurring at

TABLE 9.--Free energy of oxidation of metal carbides

Reaction	-ΔG° for Reaction, kcal/g-at C T = 1300K	T = 900K	References
$B_4C + 4O_2 \rightarrow 2B_2O_3$ (ℓ) + CO_2	542.4	583.3	61
α-SiC + $2O_2 \rightarrow SiO_2$ (quartz) + CO_2	242.2	258.0	61
TiC + $2O_2 \rightarrow TiO_2$ (rutile) + CO_2	223.9	239.4	61
ZrC + $2O_2 \rightarrow ZrO_2$ + CO_2	254.2	270.9	61
VC + $2.25O_2 \rightarrow 0.5V_2O_5$ (ℓ) + CO_2	191.6	206.8	62,63
$1.02\ NbC_{0.98}$ + $2.28O_2 \rightarrow 0.51Nb_2O_5$ + CO_2	225.4	245.3	63
TaC + $2.25O_2 \rightarrow 0.5Ta_2O_5$ + CO_2	238.1	257.8	63
$0.5\ Cr_3C_2$ + $2.12O_2 \rightarrow 0.75Cr_2O_3$ + CO_2	224.9	243.8	63
WC + $2.5O_2 \rightarrow WO_3$ + CO_2	210.0	232.3	62,63

a significant rate. For example, a protective, impervious oxide layer can form to prevent further oxidation from taking place. (The formation of a SiO_2 layer on SiC, for example, allows its use as a heating element in air at temperatures as high as 1500°C).

Even if some of the carbides in Table 8 were to form a protective oxide layer upon heating in air at 1000°C, they still would not be practical for interconnector use in the solid-electrolyte fuel cell for a number of reasons. Loss of the initially impervious interconnector film would very likely occur as the side in contact with air began oxidizing. While the transition metals in Table 8 form a continuous series of solid solutions with many of the interstitial elements, formation of a separate oxide phase would eventually occur once the oxide-solubility limit was exceeded. This would very likely result in separation at the interconnector-air electrode interface, causing rapid deterioration in cell performance and ultimately resulting in failure. Even if mechanical separation did not take place immediately, a substantial increase in the interfacial resistivity would occur during oxidation, since the oxides of the transition metals in Table 8 are poor conductors. There also is the question of the long-term chemical compatibility with the other cell components of any oxide which might form. Thus, transition metal carbides would appear suitable for high-temperature fuel cell use only under reducing conditions, i.e., as fuel electrodes.

To determine the thermodynamic stability of the carbides under typical anode conditions during fuel cell operation, values of P_{O_2} for the reactions in Table 9 were calculated for equilibrium partial pressures of CO_2 expected for fuel mixtures derived from the gasification of coal. The Lurgi Medium-Btu gasification was chosen to be representative of a process with a low conversion efficiency (37 percent) for $CO+H_2$ production, while the Combustion Engineering Medium-Btu gasification was chosen to be representative of a process with a high conversion efficiency (79 percent).

The compositions of the gas streams exiting the gasifiers are listed in Table 10, along with the equilibrium compositions at 1300K and 900K for the water-gas shift reaction:

(1) $CO_2 + H_2 \leftrightharpoons CO + H_2O(g)$

(The higher temperature is representative of the solid-electrolyte fuel cell, while the lower temperature is applicable to the molten-carbonate fuel cell). The compositions were calculated from the relationship:

(2) $K_p = \exp\left(-\Delta G^{o}_{(1)}/RT\right) = \dfrac{P_{CO} \cdot P_{H_2O}}{P_{CO_2} \cdot P_{H_2}}$

At 1300K, $\Delta G^{o}_{(1)}$ is -1444 cal, which translates into a K of 1.75. The corresponding values at 900K are 1,500 cal and 0.432, respectively. The data in Table 10 indicate that the gases are very close to the equilibrium composition with regard to reaction (1) at 1300K. The equilibrium composition of the Lurgi gas, however, was substantially changed at 900K.

TABLE 10.--Gas Composition from low- and high-efficiency coal gasifiers[64]

Gasification Process	Exit Gas Composition, m/o							Condition
	H_2	CO	CH_4	H_2O	CO_2	N_2	P_{O_2}, atm*	
Lurgi Medium-Btu	21	8	5	50	15	0.2	-	From gasifier at 1088K
	20	9	5	51	14	0.2	5.0×10^{-14}	Calculated for equilibrium at 1300K.
	25	4	5	46	19	0.2	3.5×10^{-23}	Calculated for equilibrium at 900K.
Combustion Engineering	30	63	0.05	2	2	1	-	From gasifier at 1000K
	30	63	0.05	2	2	1	2.7×10^{-17}	Calculated for equilibrium at 1300K.
	31	62	0.05	<1	3	-	5.3×10^{-27}	Calculated for equilibrium at 900K.

*For the reaction: $CO_2 + H_2 \rightleftarrows CO + H_2O(g)$.

The equivalent P_{O_2} values for the two gas mixtures are determined by the equilibrium:

(3) $CO + 1/2O_2 \leftrightharpoons CO_2$

The equilibrium P_{CO_2}/P_{CO} values determined for the gas mixtures were used to calculate P_{O_2} from the equilibrium expression for reaction (3):

(4) $$P_{O_2} = \left[\frac{P_{CO_2}}{P_{CO}}\right]^2 \left[\frac{1}{K^2_{p(3)}}\right]$$

The P_{O_2} values for the reactions of Table 9 are listed in Table 11 for a temperature of 1300K and in Table 12 for a temperature of 900K. At 1300K, the P_{O_2} for the high-CO_2 gas (Table 10) is higher than the P_{O_2} for oxidation of the carbides in all cases; i.e., the carbides would not be thermodynamically stable against oxidation by the fuel from the Lurgi gasifier at this temperature, according to the reactions of Table 9. The low-CO_2 gas from the Combustion Engineering gasifier, on the other hand, would be reducing enough to prevent oxidation of two carbides--WC and VC. At 900K, the difference between the P_{O_2} of the gas mixture and that for the oxidation reactions is much less than at 1300K. WC and VC are almost stable against oxidation by the high-CO_2 gas. As at 1300K, VC and WC are thermodynamically stable against formation of the higher oxides in the low-CO_2 gas from the Combustion Engineering gasifier at 900K; $NbC_{0.98}$ is almost stable under the same conditions. Thus, from the viewpoint of thermodynamic stability against oxidation, the carbides would be suited better for use in a fuel cell operating at 900K (e.g., the molten-carbonate fuel cell) on fuel from a gasifier of the Combustion Engineering type.

TABLE 11.--Calculated P_{O_2} for oxidation of metal carbides at 1300K at equilibrium P_{CO_2} of fuel gases*

Carbide/Oxide	K_p for Oxidation	P_{O_2} for Oxidation for P_{CO_2} = 0.14 atm+	P_{O_2} for Oxidation for P_{CO_2} = 0.02 atm†
$B_4C/B_2O_3(\ell)$	$P_{CO_2}/P_{O_2}^4 = 1.56 \times 10^{91}$	9.73×10^{-24}	5.98×10^{-24}
α-SiC/SiO_2(q)	$P_{CO_2}/P_{O_2}^2 = 5.20 \times 10^{40}$	1.64×10^{-21}	6.20×10^{-22}
TiC/TiO_2(rutile)	$P_{CO_2}/P_{O_2}^2 = 4.37 \times 10^{37}$	5.66×10^{-20}	2.14×10^{-20}
ZrC/ZrO_2	$P_{CO_2}/P_{O_2}^2 = 5.48 \times 10^{42}$	1.60×10^{-22}	6.04×10^{-23}
VC/$V_2O_5(\ell)$	$P_{CO_2}/P_{O_2}^{2.25} = 1.64 \times 10^{32}$	2.01×10^{-15}	8.46×10^{-16}
$NbC_{0.98}/Nb_2O_5$	$P_{CO_2}/P_{O_2}^{2.28} = 7.76 \times 10^{37}$	1.02×10^{-17}	4.33×10^{-18}
TaC/Ta_2O_5	$P_{CO_2}/P_{O_2}^{2.25} = 1.09 \times 10^{40}$	6.70×10^{-19}	2.82×10^{-19}
Cr_3C_2/Cr_2O_3	$P_{CO_2}/P_{O_2}^{2.12} = 6.37 \times 10^{37}$	5.82×10^{-19}	2.33×10^{-19}
WC/WO_3	$P_{CO_2}/P_{O_2}^{2.5} = 2.05 \times 10^{35}$	3.42×10^{-15}	1.57×10^{-15}

*Refer to Table 9.
+Lurgi gasifier (Table 10); $P_{O_2} = 5.0 \times 10^{-14}$ atm.
†Combustion engineering gasifier (Table 10); $P_{O_2} = 2.7 \times 10^{-17}$ atm.

TABLE 12.--Calculated P_{O_2} for oxidation of metal carbides at 900K at equilibrium P_{CO_2} of fuel gases*

Carbide/Oxide	K_p for Oxidation	P_{O_2} for Oxidation at P_{CO_2} = 0.19 atm+	P_{O_2} for Oxidation at P_{O_2} = 0.03 atm†
$B_4C/B_2O_3(\ell)$	4.04×10^{141}	2.61×10^{-36}	1.65×10^{-36}
α-SiC/SiO_2(q)	4.53×10^{62}	2.05×10^{-32}	8.14×10^{-33}
TiC/TiO_2(rutile)	1.38×10^{58}	3.71×10^{-30}	1.47×10^{-30}
ZrC/ZrO_2	6.15×10^{65}	5.56×10^{-34}	2.21×10^{-34}
VC/$V_2O_5(\ell)$	1.67×10^{50}	2.28×10^{-23}	1.00×10^{-23}
$NbC_{0.98}Nb_2O_5$	3.73×10^{59}	3.59×10^{-27}	1.60×10^{-27}
TaC/Ta_2O_5	4.05×10^{62}	7.14×10^{-29}	3.14×10^{-29}
Cr_3C_2/Cr_2O_3	1.61×10^{59}	5.39×10^{-29}	2.26×10^{-29}
WC/WO_3	2.60×10^{56}	1.40×10^{-23}	6.68×10^{-24}

*Refer to Table 9.
+Lurgi gasifier (Table 10); $P_{O_2} = 3.5 \times 10^{-23}$ atm.
†Combustion engineering gasifier (Table 10); $P_{O_2} = 5.3 \times 10^{-27}$ atm.

However, thermodynamic predictions (such as above) are not realized in practice in many cases because of extremely limiting kinetic factors; i.e., the rate of oxidation may be so low that the reactions do not occur to any measurable extent. Experimental data would be needed to ascertain this, however.

In addition, the oxidation of the carbides may not proceed as written for the reactions of Table 9, and lower-oxide phases may instead be formed. The equilibrium P_{O_2} values may be more favorable from a thermodynamic-stability viewpoint under these conditions. Since solid solutions of oxygen and carbon are quite stable for many of the transition metals, formation of such solutions (i.e., oxycarbides) could be expected during the early stages of the oxidation process. Of the carbides of Table 8, MO-MC solid solutions are possible for Ti, V, and Nb, since only these elements form a crystalline metal monoxide which is stable at fuel cell temperatures. Tungsten, on the other hand, forms WO_2 as its lowest oxide.

The oxidation of TiC, VC, NbC, and WC to the lowest stable oxide was calculated at 900K and 1300K, but with CO as the preferred gaseous product. The corresponding P_{O_2} for the reaction was determined from the K_p expression and Equation (4) using, as before, values for P_{CO_2} from Table 10. These data are summarized in Table 13.

As can be seen, none of the carbides would be thermodynamically stable in the high-CO_2 fuel gas at either 900K or 1300K, while $NbC_{0.98}$ and WC would be compatible with the low-CO_2 fuel gas

TABLE 13.--Calculated P_{O_2} for oxidation of metal carbides to lower oxides at 900 and 1300K at equilibrium P_{CO_2} of fuel gases

Reaction*	K_p** at 1300K	P_{O_2} for Oxidation for P_{CO_2} = 0.14 atm+	P_{O_2} for Oxidation for P_{CO_2} = 0.02 atm†
$TiC + O_2 \rightarrow$ β-TiO + CO	$P_{CO_2}/K_{p(3)}P_{O_2}^{1.5} = 1.39 \times 10^{19}$	1.32×10^{-18}	3.61×10^{-19}
$VC + O_2 \rightarrow$ VO + CO	" $= 4.00 \times 10^{17}$	1.41×10^{-17}	3.84×10^{-18}
$1.02NbC_{0.98} + 1.01O_2 \rightarrow 1.02NbO + CO$	$P_{CO_2}/K_{p(3)}P_{O_2}^{1.51} = 1.07 \times 10^{16}$	2.00×10^{-16}	5.50×10^{-17}
$WC + 1.5O_2 \rightarrow WO_2 + CO$	$P_{CO_2}/K_{p(3)}P_{O_2}^{2} = 1.46 \times 10^{22}$	1.20×10^{-15}	4.55×10^{-16}
	K_p at 900K	P_{O_2} for Oxidation for P_{CO_2} = 0.19 atm+	P_{O_2} for Oxidation for P_{CO_2} = 0.03 atm†
$TiC + O_2 \rightarrow$ α-TiO + CO	8.70×10^{26}	4.47×10^{-27}	1.30×10^{-27}
$VC + O_2 \rightarrow VO + CO$	1.23×10^{25}	7.63×10^{-26}	2.23×10^{-26}
$1.02NbC_{0.98} + 1.01O_2 \rightarrow 1.02NbO + CO$	1.38×10^{23}	2.19×10^{-24}	6.46×10^{-25}
$WC + 1.5O_2 \rightarrow WO_2 + CO$	5.99×10^{33}	6.59×10^{-24}	2.62×10^{-24}

*ΔG_f° for metal oxides from Reference 63.

**$K_p(3) = K_p$ for equation 3 = $P_{CO_2}/P_{CO}P_{O_2}0.5 = 6.64 \times 10^6$ at 1300 K and 7.31×10^{11} at 900K.

+Lurgi gasifier (Table 10).

†Combustion engineering gasifier (Table 10).

at 1300K. At 900K, all of the carbides except TiC--and it is borderline--would be stable against metal-monoxide formation in the low-CO_2 gas mixture. The data of Table 13 are only approximate, as they do not reflect the interaction of the MO and MC phases to form the solid solution or oxycarbide. Still, the above information points out that thermodynamic calculations are only a starting point in predicting materials compatibility, unless the exact reaction path is known with certainty. Even so, laboratory testing under the expected experimental conditions must ultimately be conducted to determine if the kinetics of a thermodynamically possible reaction are favorable or not.

The current design being used for fabrication of the anode in the thin-film solid-electrolyte fuel cell involves applying a porous Ni-ZrO_2 cermet to a ZrO_2 support tube which also is porous. The ZrO in the cermet acts as a separator to maintain the desired electrode porosity and to prevent shrinkage and excessive sintering which would result in the absence of this dispersed oxide phase. Because ZrO_2 is a poor electronic conductor, there is some problem in obtaining a Ni-ZrO_2 cermet of high enough conductivity. Westinghouse has overcome this problem to a large extent by electroplating additional nickel into the pores of the cermet.[65]

Modification of the present anode-fabrication technique by substituting a powdered carbide phase for the ZrO_2 would be difficult, as carbides do not sinter except under extreme conditions (e.g., as in hot pressing or in the presence of a sintering

aid). Any overall increase in electrical conductivity could be at the expense of structural integrity. A compromise might be realized by substitution of only a portion of the oxide phase, retaining sufficient ZrO_2 to form an interlocking matrix during the initial sintering step of the fabrication process. For best results, however, the carbide should have an average linear coefficient of expansion that is within ten percent (preferably less) of that for the ZrO_2-Y_2O_3 electrolyte of 10×10^{-6} /°C, to minimize possible thermal stresses.

Values of 9.0 to 11.7 x 10^{-6}/°C and 10.8 to 12.6 x 10^{-6}/°C have been reported for thermal expansion of TiC-Ni or -Co and Cr_3C_2-Ni composites, for example, over a temperature range of 25 to 980°C. These materials also showed good oxidation resistance at elevated temperatures.[57] There is the possibility, however, of reactions between the nickel matrix and carbide phase of a composite anode taking place over a long period of time to form intermetallic compounds. A number of the nickel-transition metal intermetallics have substantial heats and free energies of formation.[66] Carbides of uranium, for example, react with nickel between 900° and 1300°C to form a number of Ni-U and Ni-U-C compounds, depending on the carbide and temperature.[67] Such reactions could be detrimental to the performance of composite electrodes.

In theory, the fuel-electrode film could be solely constituted of the carbide phase, accomplished by a modified chemical vapor-deposition technique such as is currently done for the electrolyte layer of the fuel cell.[4] This approach is not as likely to be successful, however. Even if suitable porous carbide film could be deposited with thermal-expansion properties

engineered so as to be compatible with the ZrO_2-Y_2O_3 electrolyte, it appears unlikely that the conductivity can be increased sufficiently to equal that of nickel. At room temperature, for example, the electrical resistivity of nickel is only 6.87 μΩ-cm, which is about a fourth of that for the better-conducting carbides of Table 8.[68]

In spite of the shortcomings of carbide materials, the possible incorporation of a carbide or carbide-based material into the anode structure of the solid-electrolyte fuel cell to increase the overall conductivity of the fuel electrode merits further attention. It may be possible to increase the coefficient of thermal expansion and maintain adequate electrical conductivity by doping the carbide phase with transition metals--many of the transition-metal carbides form a continuous series of solid solution with each other[59]--or with other interstitials (e.g., Si or B). Any research effort in this area should examine critically both the short-term as well as the long-term stability of any newly developed anode material and its chemical compatibility with other cell components under typical fuel cell operating conditions.

Additionally, potential exists for using such materials as anodes in the molten-carbonate fuel cell. In this case, preparation of a thin-film (20 to 50 μm) electrode would not be necessary. Typically, the electrode plaque is made by sintering or cold pressing nickel powder onto a support grid.[69] This obviates many strict requirements for thermal-expansion properties

inherent in the possible use of new materials in the solid-electrolyte fuel cell. If deemed desirable, it should not be difficult to incorporate a carbide phase into the electrode structure since nickel acts as a good binder and is used commonly to form cemented carbides for cutting bits. There may be some difficulty, however, in achieving the desired porosity, pore-size distribution, and tortuosity with such a composite electrode.

Even though the molten-carbonate fuel cell operates at a much lower temperature (an average of 660°C) than the solid-electrolyte fuel cell, the electrical conductivity of a composite electrode will, in all probability, be substantially less than that of an all nickel one. Still, if the composite anode exhibits a significantly improved resistance to sulfur relative to nickel, the net results may be beneficial enough for long-term fuel cell operation to warrant its use.

Some of the transition-metal carbides may be resistant to the molten-carbonate electrolyte. For example, Mo_2C has been electrodeposited from a high-temperature molten-salt bath containing carbonate.[70] It has also been reported, however, that TiC, ZrC, TaC, Mo_2C, and WC dissolve in molten Na_2CO_3 (and NaOH) at 900°C under vacuum to form TiO_2, ZrO_2, $NaTaO_3$, Na_2MoO_4, and Na_2WO_4, respectively.[71] (The fact that Mo_2C can be prepared electrolytically from a carbonate-containing bath results from the potential applied across the sample during electrolysis, which counteracts any tendancy for chemical dissolution.) SiC has been reported to have

good long-term corrosion resistance to basic coal slags at maximum temperatures of 1250°C.[72] Little is known, however, of the long-term chemical compatibility of carbides or carbide composites under actual operating conditions of the molten-carbonate fuel cell. Additional study is necessary before the suitability of such materials for fuel cell use can be evaluated properly.

In many cases, there is a large discrepancy between the electrical resistivities reported for many of the transition-metal carbides, as well as other interstitial alloys. This discrepancy is caused by a number of factors, such as differences in the method of preparation and impurity levels, inadequate analytical characterization, and the wide range of homogeneity demonstrated by a number of systems. If serious consideration is given to the possibility of using transition-metal carbides in high-temperature fuel cells, it first will be necessary to resolve these discrepancies and to obtain reliable electrical resistivity data at elevated temperatures.

2. Nitrides

The elements whose nitrides are good metallic conductors are generally the same ones that form conducting carbides: elements of the Ti, V, and Cr families. Similarly, elements that form ionic carbides also form ionic nitrides. Thus, nitrides of the alkali, alkaline-earth, and rare-earth metals hydrolyze readily:

$$(5)\quad M_3^{}N + 3H_2O(\ell,g) \leftrightharpoons \frac{3}{2} M(OH)_x(s) + NH_3(g)$$

where M is a metallic cation and x is the oxidation state of the

metal.[73] Like the carbides, the nitrides of B, Al, and Si also have considerable thermal stability. BN, AlN, and Si_3N_4 are electrical insulators, even at elevated temperatures. (The electrical resistivity of hexagonal BN, for example, is 1900 Ω-cm at 2000 C.)[74]

Only a limited number of nitrides have been tested as MHD electrodes. The physical properties of the more stable transition-metal nitrides are listed in Table 14. Melting points are not included because of the questionalbe literature values in many cases. The melting point is a function of nitrogen pressure over the sample and this is not specified for most of the reported values. The melting points reported for some mononitrides (e.g., NbN), in all probability pertain to metal-nitrogen solid solutions.

In general, the transition-metal nitrides of Table 14 are much better electronic conductors and have higher coefficients of thermal expansion than the corresponding carbides. Four of the nitrides (TiN, VN, NbN, and Cr_2N) have coefficients of thermal expansion which approximate that for Y_2O_3-stabilized ZrO_2.

The nitrides are not as thermally stable as the carbides, in that they dissociate at high temperatures. The theoretical equilibrium partial pressure of nitrogen (P_{N_2}) for the dissociation of the mononitride, according to the reaction

(6) $M_xN(s) \rightarrow xM(s) + 1/2N_2(g)$,

can be calculated from the relationship

(7) $\Delta G_f^{\circ} = -RT \ln K_p = -RT \ln P_{N2}^{1/2}$

Values of P_{N_2} obtained in this manner are listed in Table 15 for a

TABLE 14.--Select physical properties of transition metal nitrides[75]

Material	Coefficient of Thermal Expansion(α), 10^{-6}/°C		Electrical Resistivity at 25°C, μΩ-cm
$TiN_{0.98}$	9.5	(20°-1100°C)	26
$ZrN_{0.98}$	7.24	(20°-1100°C)	28
$HfN_{0.86}$	6.9	(20°-1100°C)	33
$VN_{0.93}$	9.2	(20°-1100°C)	85
$VN_{0.34}$	8.1	(20°-1100°C)	123
$NbN_{1.0}$	10.1	(20°-1100°C)	78
$NbN_{0.5}$	3.26	(20°-1100°C)	142
$TaN_{1.0}$	3.6	(20°-700°C)	128
$TaN_{0.45}$	5.2	(20°-1000°C)	263
$CrN_{0.93}$	2.3	(20°-800°C)	640
$CrN_{0.50}$	9.41	(20°-1000°C)	79
$MoN_{0.5}$	6.2	(20°-1100°C)	20

temperature of 1300K. Data for the dissociation to a lower nitride are also included. The results indicate that the titanium-family members (Ti, Zr, Hf) form the most stable nitrides. As one moves to the right of the Periodic Table across the transition-metal series, the thermal stability of the mononitrides rapidly decreases and P_{N_2} similarly increases.

However, the calculated P_{N_2} values for MN materials are not observed in practice if lower nitride phases form during decomposition of MN, i.e., if MN does not dissociate according to reaction (6); this is the case for VN, NbN, and TaN. The P_{N_2} over NbN, for example, is an order of magnitude larger when Nb_2N, rather than Nb, is taken as the phase in equilibrium with NbN. Conversely, the P_{N_2} for the Nb_2N-Nb system is several orders of magnitude smaller than for the NbN-Nb_2N system. [By using a vacuum to drive the reaction, nitrogen can be successively removed at elevated temperatures from both NbN and TaN (e.g., by arc melting) to form lower nitrides and, eventually, pure Nb and Ta metals.[76] The nitrogen in VN, in comparison, can be taken to only the solid-solution level under comparable conditions.].

While a number of the transition-metal nitrides have a low thermal stability, all have one major shortcoming: poor resistance to oxidation. Like the carbides, the nitrides are thermodynamically unstable in air at 1300K with respect to their most stable oxides, as shown in Table 16. Oxidation to lower oxides is included for nitrides of Ti, V, Nb, and Mo, for comparison. Experimentally, the nitrides have been noted to oxidize more

TABLE 15.--Calculated equilibrium dissociation pressures of N_2 at 1300K for various transition-metal nitrides

Nitride	Dissociation P_{N_2}, atm	References
TiN	5.27×10^{-18}	61
ZrN	3.02×10^{-20}	61
HfN	2×10^{-20} (est.)	62
VN	2.51×10^{-9}*	63
NbN	7.01×10^{-11}*	77
TaN	2.09×10^{-12}*	77
CrN	3.44×10^{-2}*	63
$VN \rightarrow VN_{0.465}$	6.33×10^{-6}	63
$NbN \rightarrow Nb_2N$	6.76×10^{-10}	77
$TaN \rightarrow Ta_2N$	5.20×10^{-18}	78
$CrN \rightarrow Cr_2N$	0.413	63
$VN_{0.465}$	3.02×10^{-13}	63
Nb_2N	7.28×10^{-12}	77
Ta_2N	8.33×10^{-7}	78
Cr_2N	2.86×10^{-3}	63
Mo_2N	3.94×10^{-3}**	62

*Calculated for hyopthetical reaction: $MN \rightarrow M + 1/2\ N_2$.
**Value for 800K.

readily than the corresponding carbides.[59] Thus, their possible use in the solid-electrolyte fuel cell is limited to the fuel electrode, as in the case of the carbides.

Calculated values of P_{O_2} are listed in Table 17 for the oxidation reactions at 1300K for P_{N_2} equal to the equilibrium pressure over the nitride phases. (Oxidation of TaN and Ta_2N does not exhibit a P_{N_2} dependency in the K_p expression). Thus, at an equilibrium P_{N_2} for VN-V_2N of 2.74×10^{-6} atm (Table 15), a P_{O_2} of 4.88×10^{-16} atm is calculated for the oxidation of VN to V_2O_5 at 1300K. This is in the range of P_{O_2} expected at the fuel electrode of the solid-electrolyte fuel cell. Only the VN oxidation has a P_{O_2} that falls into the same range.

In all cases, the P_{O_2} for oxidation of nitrides to lower oxides is considerably smaller than that for the corresponding highest, stable oxide. If reaction kinetics were to favor formation of the suboxide over the highest oxide, then none of the nitrides in Table 16 would be thermodynamically stable as fuel electrodes. Even though P_{O_2} calculations indicate a number of the transition-metal nitrides would be unstable with respect to oxide formation in a fuel-gas environment, unfavorable reaction kinetics for the oxidation could permit most, if not all, of the nitrides to be used indefinitely (in this respect) under anode conditions. In other words, equilibrium may never be achieved in practical-time terms for the reactions of Table 16. To determine if kinetic factors are limiting would require actual experimental

TABLE 16.--Oxidation of transition-metal nitrides at 1300K

Reaction	-ΔG° for Reaction, kcal/g-at N	References
$TiN + O_2 \rightarrow TiO_2(rutile) + 0.5N_2$	118.2	61
$TiN + 0.5O_2 \rightarrow TiO + 0.5N_2$	48.7	61
$ZrN + O_2 \rightarrow ZrO_2 + 0.5N_2$	145.4	61
$HfN + O_2 \rightarrow HfO_2 + 0.5N_2$	148 (est.)	62
$VN + 1.25O_2 \rightarrow 0.5V_2O_5(\ell) + 0.5N_2$	97.3	63
$VN + 0.5O_2 \rightarrow VO + 0.5N_2$	50.9	63
$NbN + 1.25O_2 \rightarrow 0.5Nb_2O_5 + 0.5N_2$	129.8	63,77
$NbN + 0.5O_2 \rightarrow NbO + 0.5N_2$	42.1	63,77
$TaN + 1.25O_2 \rightarrow 0.5Ta_2O_5 + 0.5N_2$	142.3	63,77
$TaN + 0.5O_2 \rightarrow TaON$	55.9+	77,79
$CrN + 0.75O_2 \rightarrow 0.5Cr_2O_3 + 0.5N_2$	90.5	63
$2.15VN_{0.465} + 2.69O_2 \rightarrow 1.08V_2O_5(\ell) + 0.5N_2$	228.1	63
$2.15VN_{0.465} + 1.08O_2 \rightarrow 2.15VO + 0.5N_2$	127.3	63
$Nb_2N + 2.5O_2 \rightarrow Nb_2O_5 + 0.5N_2$	286.9	63,77
$Nb_2N + O_2 \rightarrow 2NbO + 0.5N_2$	111.5	63
$Ta_2N + 2.5O_2 \rightarrow Ta_2O_5 + 0.5N_2$	336	63,78
$Ta_2N + 3.5O_2 \rightarrow TaON + 0.5Ta_2O_5$	255+	78,79
$Cr_2N + 1.5O_2 \rightarrow Cr_2O_3 + 5N_2$	182.2	63
$Mo_2N + 3O_2 \rightarrow 2MoO_3 + 0.5N_2$	263.6*	61,62
$Mo_2N + 2O_2 \rightarrow 2MoO_2 + 0.5N_2$	207.5*	61,62

+Value for 1100K.
*Value for 800K.

TABLE 17.--Calculated P_{O_2} for the oxidation of transition-metal nitrides at 1300K for equilibrium nitride P_{N_2}*

Nitride/Oxide	K_p for Oxidation	P_{O_2} at Equilibrium P_{N_2}, atm+
TiN/TiO_2(rutile)	$P_{N_2}^{0.5}/P_{O_2} = 7.51 \times 10^{19}$	3.07×10^{-29}
TiN/TiO	$P_{N_2}^{0.5}/P_{O_2}^{0.5} = 1.57 \times 10^{8}$	2.14×10^{-34}
ZrN/ZrO_2	$P_{N_2}^{0.5}/P_{O_2}^{0.5} = 2.79 \times 10^{24}$	6.23×10^{-35}
HfN/HfO_2	" $= 7.64 \times 10^{24}$	1.85×10^{-35}
VN/V_2O_5(ℓ)	$P_{N_0}^{0.5}/P_{O_2}^{1.25} = 2.28 \times 10^{16}$	4.88×10^{-16}
VN/VO	$P_{N_2}^{0.5}/P_{O_2}^{0.5} = 3.67 \times 10^{8}$	4.71×10^{-23}
NbN/Nb_2O_5	$P_{N_2}^{0.5}/P_{O_2}^{1.25} = 6.66 \times 10^{21}$	7.46×10^{-22}
NbN/NbO	$P_{N_2}^{0.5}/P_{O_2}^{0.5} = 1.21 \times 10^{7}$	4.62×10^{-24}
TaN/Ta_2O_5	$P_{N_2}^{0.5}/P_{O_2}^{1.25} = 8.41 \times 10^{23}$	8.84×10^{-27}
TaN/TaON	$P_{O_2}^{-0.5} = 1.28 \times 10^{11}$ x	6.10×10^{-23} x
CrN/Cr_2O_3	$P_{N_2}^{0.5}/P_{O_2}^{0.75} = 1.64 \times 10^{15}$	3.01×10^{-21}
$VN_{0.465}/V_2O_5$(ℓ)	$P_{N_2}^{0.5}/P_{O_2}^{2.69} = 2.24 \times 10^{38}$	2.62×10^{-17}
$VN_{0.465}/VO$	$P_{N_2}^{0.5}/P_{O_2}^{1.08} = 2.53 \times 10^{21}$	2.44×10^{-26}

TABLE 17.--Calculated P_{O_2} for the oxidation of transition-metal nitrides at 1300K for equilibrium nitride P_{N_2}* (Cont.)

Nitride/Oxide	K_p for Oxidation	P_{O_2} at Equilibrium P_{N_2}, atm+
Nb_2N/Nb_2O_5	$P_{N_2}^{0.5}/P_{O_2}^{2.5} = 1.72 \times 10^{48}$	3.01×10^{-22}
Nb_2N/NbO	$P_{N_2}^{0.5}/P_{O_2} = 5.64 \times 10^{18}$	4.78×10^{-25}
Ta_2N/Ta_2O_5	$P_{N_2}^{0.5}/P_{O_2}^{2.5} = 3.10 \times 10^{56}$	1.54×10^{-24}
$Ta_2N/(TaON + Ta_2O_5)$	$P_{O_2}^{-3.5} = 4.96 \times 10^{50}$ x	3.28×10^{-15} x
Cr_2N/Cr_2O_3	$P_{N_2}^{0.5}/P_{O_2}^{1.5} = 4.30 \times 10^{30}$	5.40×10^{-22}
Mo_2N/MoO_3	$P_{N_2}^{0.5}/P_{O_2}^{3} = 1.04 \times 10^{72}$ †	3.87×10^{-25} †
Mo_2N/MoO_2	$P_{N_2}^{0.5}/P_{O_2}^{2} = 5.00 \times 10^{56}$ †	1.12×10^{-29} †

*Refer to Table 15.

+P_{N_2} = equilibrium pressure of N_2 over nitride phase, or over nitride-subnitride mixture (for V, Nb, Ta, Cr, and Mo).

†Value for 800K.

xValue for 1100K.

testing. Until then, nitrides should still be considered potentially usable as node material.

The data in Table 17 calculated for formation of suboxides (e.g., TiO) should be considered as only approximations, as oxynitride formation would almost certainly occur in actual practice, which could change the equilibrium P_{O_2} considerably. The effect of oxynitride formation upon P_{O_2} is evident in the oxidation of Ta_2N. At 1100K, P_{O_2} for formation of TaON + 0.5 Ta_2O_5 is 3.28×10^{-15} (Table 17); formation of only Ta_2O_5 results in a calculated P_{O_2} of 1.96×10^{-30} atm (at the equilibrium dissociation pressure for Ta_2N of 5.34×10^{-11} atm).

The greater thermal stability of TiN, ZrN, and HfN makes them the preferred choice of the transition-metal nitrides for consideration as possible anode material for the solid-electrolyte fuel cell. However, of these, only TiN has a coefficient of thermal expansion suitable for use with the solid electrolyte. Even though VN, NbN, and Cr_2N also have compatible thermal expansion properties, they lack the thermal stability of TiN.

Maintaining long-term stability of a nitride-based fuel electrode is important from an electrical standpoint, as the resistivity can vary substantially with nitrogen content for some materials, as shown in Figure 2 for the Ti-N and Zr-N systems.[75] (Note that the mononitrides are better conductors than the parent metals.) The compositional effect upon electrical resistivity is pronounced for both systems. Loss of one-fourth of the nitrogen

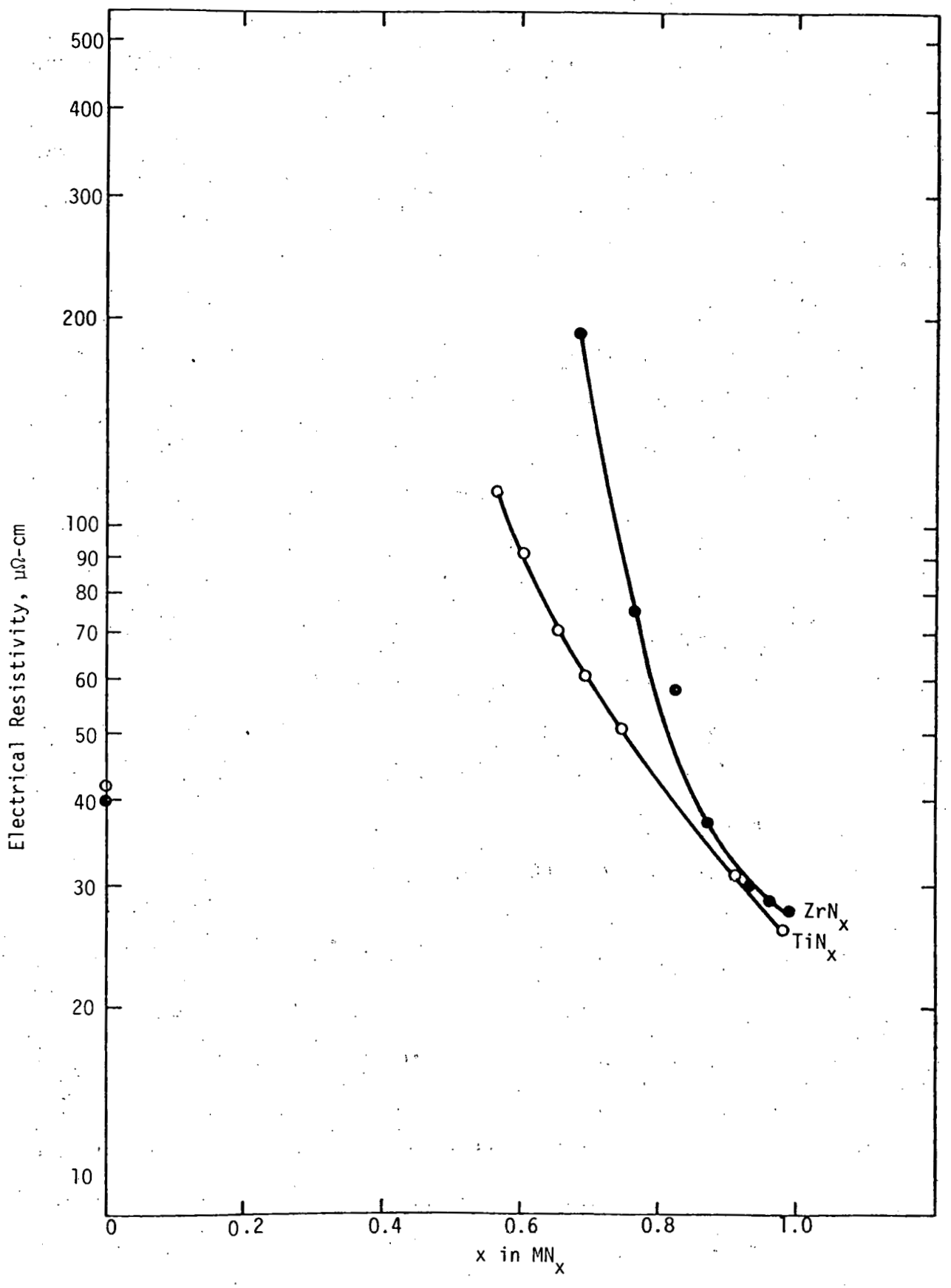

Figure 2.--Electrical Resistivity of Zr-N and Ti-N Systems at 25°C

9-11-78 8-000-040-A

from TiN, for example, causes a doubling of the resistivity. (TiN has a very large homogeneity range--from $TiN_{0.46}$ to $TiN_{1.16}$).[74] The data in Figure 2 thus refer to single-phase material. Titanium (as well as the other Group IVA elements) does not form lower nitrides; the only confirmed, stable phases are the mononitride (TiN) and the Ti-N (interstitial) solid solution.[74]

The confirmation of the long-term stability under fuel cell operating conditions of any nitride material considered for anode use (e.g., TiN) is an item of prime concern in evaluating overall stability. The potential for compositional changes with time is inherently greater for nitrides than for the corresponding carbides because of the increased tendency for dissociation at elevated temperatures. If the equilibrium P_{N_2} is low enough at 1000°C, however, it should be possible to maintain the nitrogen pressure above this value in the fuel atmosphere and thus prevent loss of nitrogen from a nitride-based anode. Excessive dilution of the fuel mixture with nitrogen, however, would adversely effect fuel cell efficiency.

A nitride-based anode for the solid-electrolyte fuel cell could be fabricated in the form of a Ni-nitride cermet or thin nitride films, much in the same manner described earlier for a hypothetical carbide-based electrode. It would be necessary, however, to maintain a sufficiently high partial pressure of nitrogen above the nitride material to prevent dissociation during sintering and reduction. As an alternative, chemical vapor deposition of a TiN-electrode film from $TiCl_4$ and H_2-N_2 or-NH_3 gases

could be considered (facilitated by the fact that the $TiCl_4$ is a liquid at room temperature).

Composites of transition-metal nitrides with metals, such as nickel, are potential candidates for anodes in high-temperature fuel cells. By appropriate manipulation of composition and choice of materials, the desired thermal expansion and electrical properties can most probably be achieved. Consideration should be given to the possible formation of intermetallic compounds or solid solutions which could cause decomposition of the nitride phase over an extended period of time. This decomposition, in turn, could result in performance degradation of fuel cells using such anodes.

Like the transition-metal carbides, the nitrides, in many instances, form a continuous series of solid solution with each other (e.g., ZrN-TiN) and with other interstitials (e.g., carbon and oxygen, during carbonitride and oxynitride formation, respectively). This capability can be used to advantage for appropriate modification of the electrical and thermal expansion properties of a system to meet material requirements necessary for possible utilization in the high-temperature fuel cells.

While the thermal expansion properties of TiN (Table 14) match closely those for the ZrO_2 electrolyte, an increase in the electrical conductivity would be desirable. Addition of oxygen (as TiO) has an appreciable effect upon the electrical resistivity of TiN,[75] as seen in Figure 3. The resistivity drops to a minimum of 11.3 $\mu\Omega$-cm at about 30 m/o TiO in TiN. Similar studies with other

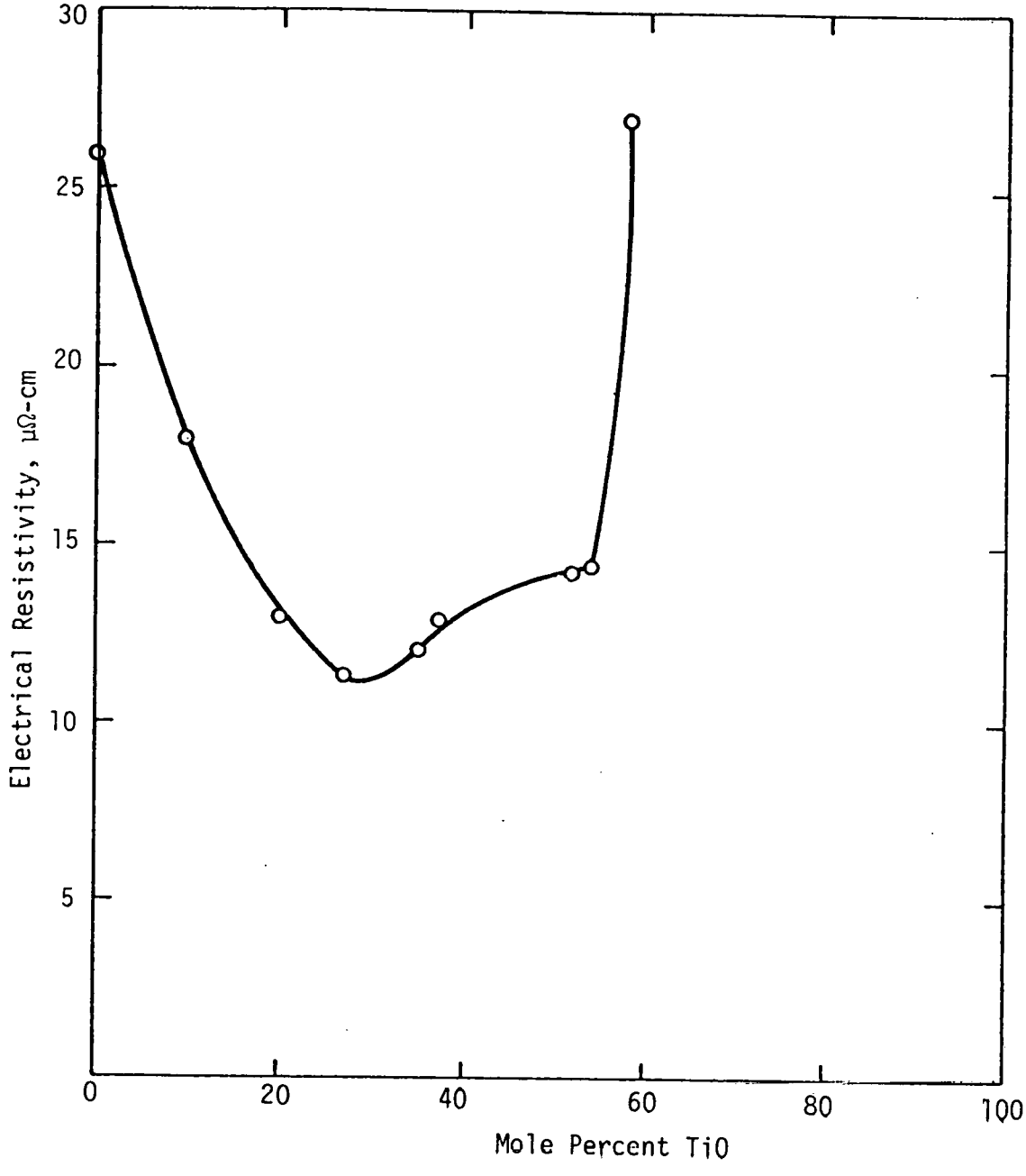

Figure 3.--Electrical Resistivity of TiN-TiO Solid Solutions at 25°C

interstitials or transition metals could lead to further improvements in the electrical properties. All the resistivity data reported here are for room temperature; there is a need for similar data at elevated temperature for a more valid comparison with nickel for anode use (Appendix B lists other physical properties references for transition-metal nitrides).

Nitrides or nitride-based materials may be suited for use as anodes in the molten-carbonate fuel cell if significant amounts of hydroxide are not present. Thermodynamic calculations indicate that the nitrides should be compatible with molten carbonates. However, the presence of hydroxide could lead to extensive nitride corrosion, since TiN and ZrN, for example, are reportedly decomposed by molten alkali, with the evolution of NH_3.[74]

The formation of hydroxide occurs in the presence of water according to the reaction

(8) $M_2CO_3(soln.) + H_2O(g) \rightarrow 2MOH(soln.) + CO_2(g)$

where M is a metallic cation. The equilibrium constant for this reaction is

(9) $$K_h = \frac{a^2_{MOH}}{a_{M_2CO_3}} \cdot \frac{P_{CO_2}}{P_{H_2O}}$$

For the ternary eutectic 43.5 m/o Li_2CO_3-31.5 m/o Na_2CO_3-25.0 m/o K_2CO_3, K_h is approximately 4.06×10^{-4} at 1000K.[69] The activity (concentration, for practical purposes) of the hydroxide in the carbonate solution thus will be influenced by the P_{CO_2}/P_{H_2O} ratio in the gas atmosphere over the melt. Because of the high P_{CO_2} normally present, however, the hydroxide composition is not expected to exceed several mole percent.

Another process which produces a molten-carbonate impurity reactive to nitrides is the decomposition of carbonate by the reaction

(10) $M_2CO_3(soln.) \rightarrow M_2O(soln.) + CO_2(g)$

The equilibrium constant, K_d, for the decomposition reaction is much smaller than for the hydrolysis reaction. A K_d of 1.66×10^{-7} has been reported for the above ternary-carbonate eutectic at 1000K. [69] However, a clear understanding of the various reactions which can take place during operation of the molten-carbonate fuel cell, and the disposition of the various moieties which can form, is still lacking. Relevant oxide-carbonate phase diagrams, for example, are available only for Li_2CO_3 and Na_2O-Na_2CO_3.[64] Workers at Montana State University, however, currently are involved in evaluation and computation of phase diagrams pertinent to the molten-carbonate fuel cell, using a sophisticated computer program.[80]

Since the operating temperature of the molten-carbonate fuel cell is significantly lower than that of the solid-electrolyte fuel cell, there will be a substantial reduction in the equilibrium dissociation pressure of nitrogen (P_{N_2}) over the nitrides. The ΔG° for the oxidation reaction will be affected similarly, which in turn will change the K_p and the P_{O_2} for oxidation. The effect of temperature upon these parameters was examined at 900 K for the oxidation of VN and $VN_{0.465}$ to V_2O_5 (ℓ). These nitrides were chosen as they would be expected to be thermodynamically stable

with respect to V_2O_5 in the fuel-gas environment.

For the VN-V_2O_5 reaction, the P_{O_2} of 4.88×10^{-16} atm calculated at 1300K was reduced to 1.69×10^{-25} atm at 900K Similarly, the P_{O_2} for the $VN_{0.465}$-V_2O_5 reaction decreased from 2.62×10^{-17} atm at 1300K to only 8.78×10^{-28} atm at the lower temperature. Thus, by lowering the temperature 400K , the vandium nitrides are no longer thermodynamically stable in the anode environment. Similar large changes in P_{O_2} occur for the other nitrides under comparable conditions.

By strictly thermodynamic considerations, then, the nitrides would not appear, at first glance, to be as suited for use in the lower-temperature, molten-carbonate fuel cell as in the solid-electrolyte fuel cell. At the lower temperature, on the other hand, the oxidation kinetics may be less favorable, so that increased resistance to oxidation could result. This resistance will be offset, however, by an accelerating effect caused by the fluxing action of the carbonate melt. Dissolution of oxidation products in the molten carbonate as rapidly as they form will act to drive the reaction to completion. It is exceedingly difficult--impossible at times--to predict a priori which factors will be controlling. There is a definite need for experimental data in this area to resolve these questions.

3. Silicides

A third category of non-oxide ceramics which has been studied for use as MHD electrodes is the silicide. A larger number of

elements form stable silicides than carbides or nitrides. For a given element, silicon also forms a larger number of compounds than do carbon or nitrogen. In addition to the transition metals, the alkali, alkaline-earth, and rare-earth metals all form stable silicides. Aluminum does not form a silicide, although it is miscible with silicon in the liquid state.

The silicides are more closely related to the intermetallic than the typical interstitial compounds and possess many of the properties associated with metals, such as metallic luster and high electrical and thermal conductivity. Many of the silicides are metallic conductors, i.e., they have a positive temperature coefficient of resistivity. The higher silicides, however, show semiconducting behavior in many cases, much as silicon itself. The silicides also exhibit an absence of homogeneity ranges, except for VSi_2, in marked contrast to the corresponding carbides and nitrides.[59]

For high-temperature applications (up to 1500°C), the silicides of primary interest are those of Group IVA to VIA transition metals, the actinide metals, the rare-earth metals, the platinum metals, and rhenium. Since the precious-metal silicides are prohibitively expensive and the actinide silicides are radioactive, they will not be considered further in this report. While the rare-earth silicides are not as reactive to water vapor as the corresponding carbides and nitrides, they are still insufficiently inert to be considered practical for fuel cell use. As a result,

this section will concentrate on the stable silicides of the Group IVA to VIA transition metals.

The key physical properties of select transition-metal silicides are presented in Table 18. Compared to the carbides and nitrides, a larger number of the silicides have thermal expansion properties which are compatible with the Y_2O_3-stabilized ZrO_2 for possible fuel cell use. Unfortunately, the resistivity and thermal-expansion data are either not available for many of the silicides of Table 18 or have been published in a number of foreign (mostly Russian) journals to which the author did not have ready access (these references are listed in Appendix C). Still, sufficient data are available to make resonable value judgments regarding the possibility of utilizing such materials in high-temperature fuel cells.

The data in Table 18 show that the disilicides $TiSi_2$, $NbSi_2$, and $TaSi_2$ have the lowest resistivities as well as the most suitable thermal-expansion properties for possible use in the solid-electrolyte fuel cell. At room temperature, the reported electrical resistivity of $NbSi_2$ is actually lower than that of nickel. The temperature coefficient is probably less than that or nickel for $NbSi_2$ as well as a number of the other higher silicides, as a result of their semi-conducting nature ($TiSi_2$, however, is reported to be a metallic conductor[82]). If this is so, the electrical conductivity of $NbSi_2$ at 1000°C would be superior to that of nickel. The coefficient of thermal expansion for $NbSi_2$, however, exhibits a larger change over the temperature range of 20°

TABLE 18.--Select physical properties of transition-metal silicides

Silicide	Melting Point, °C	Coefficient of Thermal Expansion (α), 10^{-6}/°C	Electrical Resistivity at 20°C, μΩ-cm	References
Ti_5Si_3	2120	11.0 (70°-1070°C)	350	57,81
TiSi	1760(p)†	10.4 (370°-1070°C)	36.4-39.3	81,82
$TiSi_2$	1540	10.4 (20°-1070°C)	11.6-16.7	81,82
Zr_2Si	2220(dec.)	-	-	81
Zr_5Si_3	2250	-	-	81
ZrSi	2150(dec.)	-	49.4	81
$ZrSi_2$	1680(dec.)	-	106-161	81
Hf_5Si_3	2300	-	-	57
HfSi	2100	-	-	57
$HfSi_2$	1700	-	-	57
V_3Si	1730(p)	7.92-14.0 (20°-1070°C)*	-	57,81
V_5Si_3	2150	9.54-11-2 (20°-1070°C)*	-	57,81
VSi_2	1670	11. 2-14.8 (20°-1070°C)*	9.5-13.3	57,81
Nb_4Si	1950(p)	-	-	81
Nb_5Si_3	2480	-	-	81
$NbSi_2$	1930	8.5-11.7 (20°-1070°C)	6.3	57,81
$Ta_{4.5}Si$	2510	-	-	81
Ta_2Si	2460	-	-	81
Ta_5Si_3	2500	-	-	81
$TaSi_2$	2200	9.54-10.8 (20°-1070°C)*	8.5-38	57,81

Table 18.--Select physical properties of transition-metal silicides (Cont.)

Silicide	Melting Point, °C	Coefficient of Thermal Expansion (∝),	Electrical Resistivity at 20°C, μΩ-cm	References
Cr_3Si	1710	10.5 (20°-1070°C)	45.5	57,81
Cr_5Si_3	1560(dec.)	5.9-14.2 (20°-1000°C)*	114	57,81,83
CrSi	1545	11.3 (20°-770°C)	143	57,81
$CrSi_2$	1550	-	>250-1420	81,83
Mo_3Si	2050(dec.)	7.11 (20°-1130°C)	-	57,81
Mo_5Si_3	2100	4.3 -7.4 (20°-1070°C)*	-	57,81
$MoSi_2$	2030	8.10 (20°-1000°C)	21.8	57,81
W_5Si	2320	-	38.2	81
WSi_2	2165	8.28 (20°-1000°C)	33.4	57,81
Co_3Si	1210	-	-	81
Co_2Si	1332	-	-	81
CoSi	1460	12.0 (25°-1000°C)	150	81,84
$CoSi_2$	1326	-	64.8	81
Ni_3Si	1165(p)	-	-	81
Ni_5Si_2	1282	-	-	81
Ni_2Si	1318	-	-	81
Ni_3Si_2	845(p)	-	-	81
NiSi	992	-	-	81
$NiSi_2$	993(p)	-	-	81

TABLE 18.--Select physical properties of transition-metal silicides (Cont.)

Silicide	Melting Point, °C	Coefficient of Thermal Expansion (∞), 10^{-6}/°C	Electrical Resistivity at 20°C. μΩ-cm	References
Fe_3Si	-	-	55	81
Fe_5Si_3	-	-	170	81
FeSi	1415	-	240	81
$FeSi_{2+x}$	1220	-	350	81
Mn_3Si	-	-	-	81
Mn_5Si_3	-	-	-	81
MnSi	1280	-	-	81
$MnSi_2$	-	-	-	81

† Peritectic = (p).

* Range given for α, due to change in slope of $\Delta\ell/\ell_o$-T plot over indicated temperature range.

to 1070°C than do $TiSi_2$ and $TaSi_2$.

The stoichiometry of the silicide has a profound effect upon its electrical properties. The electrical resistivity data of Table 18 are plotted in Figure 4 as a function of the atomic ratio of silicon to metal. The $FeSi_x$, $CrSi_x$, and $ZrSi_x$ systems show a rapid increase in resistivity with increase in x. $CoSi_x$, on the other hand, exhibits a maximum in resistivity near x = 1. Due to the lack of data points, it is not clear whether WSi_x shows a lack of compositional dependence in resistivity or exhibits a maximum between x = 0.2 and 2.

The behavior of the $TiSi_x$ system, however, differs drastically from the other silicides in that the resistivity rapidly decreases after a very sharp maximum near x = 0.5 (this same behavior is evident for the nitrides of titanium, as well, as indicated in Figure 2). From x = 1 to 2, the resistivity of $TiSi_x$ is lower than that of pure titanium. In addition to $TiSi_2$, the disilicides of the vanadium family also have electrical resistivities of the parent metals.

Of the three types of interstitial compounds considered thus far, the silicides have the best resistance to high-temperature oxidation and increased resistance at higher silicon contents. The formation of a nonporous, adherent oxide film protects the silicide from further oxidation. Use of silicides at elevated temperatures under reducing conditions, however, can lead to destruction of the protective SiO_2 film. For $MoSi_2$, for example,

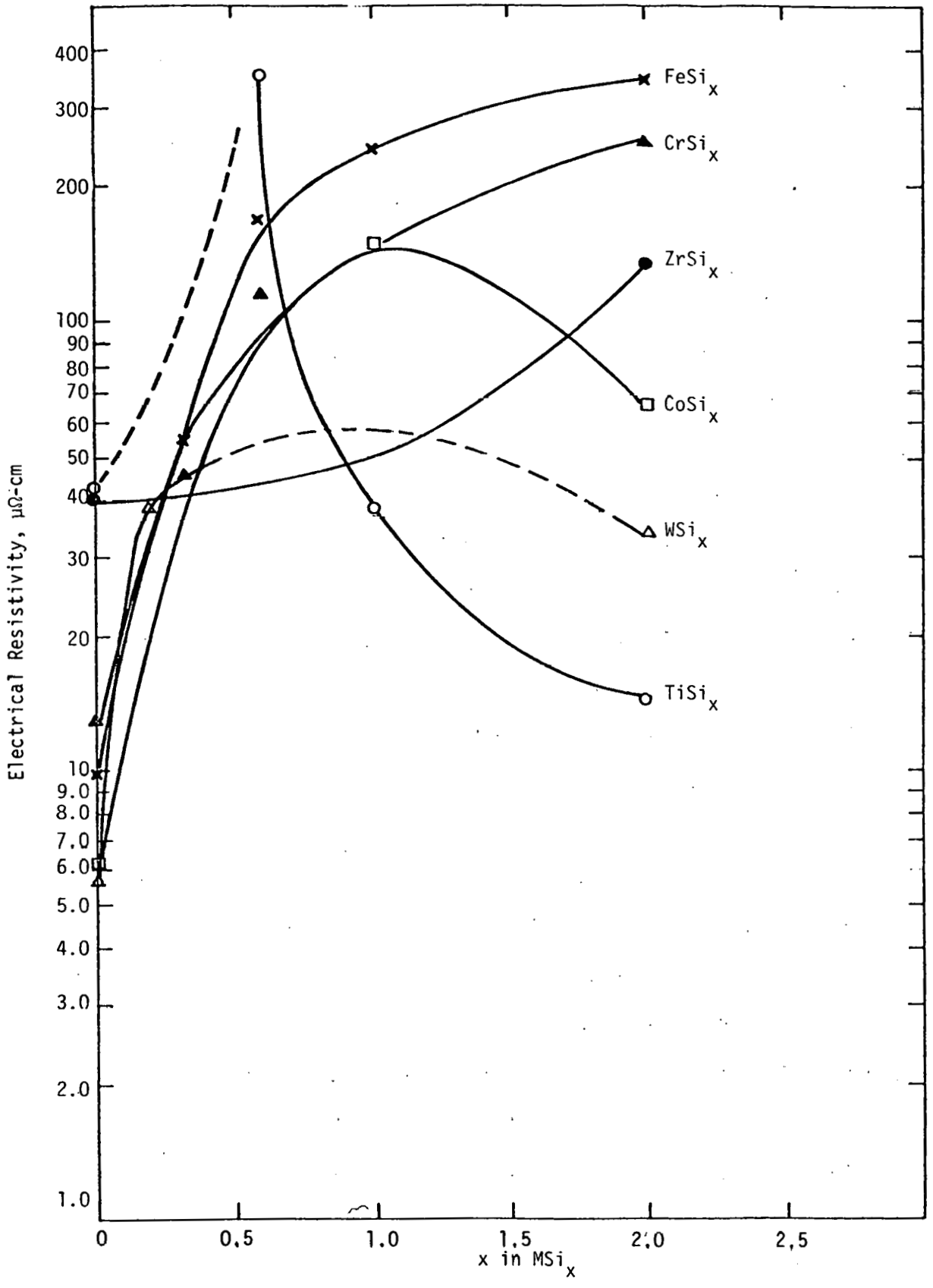

Figure 4.--Electrical Resistivities of Transition-Metal Silicides at 25°C as a Function of Composition

this occurs readily above 1350°C in hydrogen:[85]

(11) SiO_2 (on $MoSi_2$)(s,ℓ) + H_2(g) → SiO (g) + H_2O(g)

$MoSi_2$ is perhaps the most well-known silicide employed for high-temperature applications. It has received extensive use as electrical heating elements at temperatures up to 1700°C in air. The generally recommended operating range, however, is between 1000° and 1700°C, as in this temperature interval the oxide film is dense and adherent. At temperatures between 300° and 800°C, for example, the SiO_2 which forms is porous and spalls from the element, allowing further oxidation.[85]

Besides silicides of molybdenum, those of tungsten and titanium also exhibit good resistance to oxidation at high temperatures. In the case of the Ti-Si system, the protective layer is thought to be a silicate phase, rather than SiO_2.[57] The rest of the silicides in Table 18 generally form porous, nonadherent coatings which are not protective against oxidation.

The formation of a silicate or SiO_2 film under oxidizing conditions precludes the use of transition metal silicides for interconnector materials for the solid-electrolyte fuel cell, even though the thermal and electrical properties may be acceptable. The chemical-compatibility and interfacial problems discussed earlier for similar films for the carbides apply to the silicides as well. Thus, the possible use of silicides for high-temperature fuel cells should be restricted to the fuel electrode.

It would be desirable to know the P_{O_2} for the oxidation of the transition-metal silicides at 1300K in order to ascertain the

thermodynamic stability under anode conditions, as was done with the carbides and nitrides. This can be determined readily for the general reaction

$$(12)\quad M_xSi + \frac{xz+2}{2} O_2 \rightarrow xMO_z + SiO_2$$

once the ΔG^o_{Rxn} is known at the desired temperature. The P_{O_2} can then be calculated from the relationship

$$(13)\quad P_{O_2} = (K_p)\ \exp[-2/(xz+2)] = \exp\left[\frac{\Delta G^o_{(12)}}{RT}\right] \cdot \left[\frac{2}{xz+2}\right]$$

Unfortunately, limited thermodynamic data are available in the literature for many of the silicides, espceially at elevated temperatures. The bulk of the published data pertains to enthalpies of formation (ΔH^o_f) at 298 K and heat capacities; little information was readily evident for the free energies of formation for many of the silicides as a function of temperature.

Values of ΔH^o_f at 1300 K were calculated for silicides from ΔH^o_f at 298 K and heat capacities according to[86]

$$(14)\quad \Delta H^o_{f,1300}(M_xSi) = \Delta H_{f,298}(M_xSi) + \int_{298}^{1300} \Delta C_p(M_xSi)dT$$

where ΔC_p is the difference in heat capacities of the silicide and the component elements, i.e.,

$$(15)\quad \Delta C_p(M_xSi) = C_p(M_xSi) - xC_p(M) - C_p(Si)$$

Where heat capacities were not available for the silicides, additivity of the heat capacities of the metal and silicon was assumed

$$(16)\quad C_p(M_xSi) = xC_p(M) + C_p(Si)$$

Combining equations 15 and 16 results in a ΔC_p of essentially zero under these conditions. Or, in other words, ΔH^o_f is not temperature dependent. This was found to be the case for a number of

the silicides. Values of ΔH_f^o at 298 and 1300K (calculated using reported C_p data), for example, differed by less than one percent for Nb_5Si_3 and W_5Si_3.[81,87,88]

Values of ΔS_f^o were obtained from reported C_p data for the silicides as a function of temperature from the relationship

$$(17)\quad \Delta S^o_{f,1300}(M_xSi) = \Delta S_{f,298}(M_xSi) + \int_{298}^{1300} \frac{\Delta C_p(M_xSi)dT}{T}$$

To calculate $\Delta S^o_{f,298}$ the value of $S^o_{298}(M_xSi)$ must first be known

$$(18)\quad \Delta S^o_{f,298}(M_xSi) = S^o_{298}(M_xSi) - xS^o_{298}(M) - S^o_{298}(Si)$$

This is usually obtained by heat-capacity measurements down to absolute zero

$$(19)\quad S^o_{f,298}(M_xSi) = S^o_0(M_xSi) + \int_0^{298} C_p(M_xSi)dT \simeq \int_0^{298} C_p(M_xSi)dT$$

Generally, S^o_{298} for the silicide was not reported, so that assumption of additivity of entropies was necessary. This results in a value for ΔS^o_{298} of zero for the silicide, using equation 18. The error introduced into subsequent calculations as a result of this assumption is quite acceptable for the purposes of this report, as available data generally indicate low values of $\Delta S^o_{f,298}$ for silicides. Silicides of chromium, for example, have reported ΔS^o_f values ranging from -0.9 to 0.3 gibbs/g-at Si at 298K.[89]

The free energy of formation, ΔG^o_f, was then calculated for the silicide at 1300K from

$$(20)\quad \Delta G^o_{f,1300}(M_xSi) = \Delta H^o_{f,1300}(M_xSi) - T\Delta S^o_{f,1300}(M_xSi)$$

Where heat-capacity data as a function of temperature or entropy data were missing for silicides, $\Delta S^o_{f,1300}$ was set equal to zero,

so that the following resulted

(21) $\Delta H^{o}_{f,298} = \Delta H^{o}_{f,1300} \simeq \Delta G^{o}_{f,1300}$ (for M_xSi)

The estimated thermodynamic data for a number of the silicides at 1300K (or experimental values, where obtainable) are presented in Table 19. The values of ΔG^{o}_{f} for the silicides were used with other thermodynamic data to calculate the free energies of oxidation listed in Table 20. The corresponding K_p and equilibrium P_{O_2} values for these reactions are presented in Table 21 for formulation of the highest, stable oxide and, where applicable, the most stable suboxide. The data indicate that none of the silicides would be thermodynamically stable relative to both the highest oxide and suboxide at a fuel-gas P_{O_2} of 10^{-16} atm. At a P_{O_2} of 10^{-18} atm, only Ni_2Si and Ni_3Si would be stable against oxide formation.

At the average operating temperature of the molten-carbonate fuel cell of 900K cursory calculations indicate that none of the silicides would be thermodynamically stable with respect to oxidation. This large P_{O_2} dependency as a function of temperature was noted earlier for the nitrides and carbides.

In a number of cases, the calculated P_{O_2} data are derived from extrapolated or estimated values for ΔG^{o}_{f} for the silicides. The true equilibrium P_{O_2} could be higher than calculated, therefore, with a resultant greater chance for silicide compatibility with the fuel gas. The formation of compound oxides or silicates in-

TABLE 19.--Thermodynamic data for transition-metal silicides

Silicide	$-\Delta H^{\circ}_{f,298}$, kcal/g-at Si	$-\Delta H^{\circ}_{f,1300}$, kcal/g-at Si	$\Delta S^{\circ}_{f,1300}$, gibbs/g-at Si*	$-\Delta G^{\circ}_{f,1300}$, kcal/g-at Si	References
Ti_5Si_3	46.2	(46.2)†	(∿0)	(46.2)	81
TiSi	31.0	(31.0)	(∿0)	(31.0)	81
$TiSi_2$	16.1	13.8	1.96	16.8	81,90
Zr_2Si	26.6	(26.6)	(∿0)	(26.6)	91
Zr_5Si_3	26.6	(26.6)	(∿0)	(26.6)	91
$ZrSi_{1.17}$	29.4	(29.4)	(∿0)	(29.4)	91
$ZrSi_2$	15.0	(15.0)	(∿0)	(15.0)	91
V_2Si	36.9	(36.9)	(∿0)	(36.9)	81
$NbSi_{0.55}$	21	(21)	(∿0)	(21)	81
Nb_5Si_3	21	21.1	0.42	21.4	81,87
$NbSi_2$	15	15.1	1.64	17.2	81,92
$TaSi_{0.22}$	32.2	-	-	37.3	81,93
Ta_2Si	30.7	-	-	27.2	81,93
Ta_5Si_3	28.8	-	-	24.0	81,93
$TaSi_2$	13.1	-	-	8.1	81,92,93
Cr_3Si	8.22	(8.22)	(-0.90)x	(7.95)	81
Cr_5Si_3	8.23	(8.23)	(-0.27)x	(8.15)	81
CrSi	7.12	7.15+	0.28+	7.44+	81,89,94
$CrSi_2$	6.36	6.20+	0.39+	6.60+	81,89,94

TABLE 19.--Thermodynamic data for transition-metal silicides (Cont.)

Silicide	$-\Delta H^{\circ}_{f,298}$, kcal/g-at Si	$-\Delta H^{\circ}_{f,1300}$, kcal/g-at Si	$\Delta S^{\circ}_{f,1300}$, gibbs/g-at Si*	$-\Delta G^{\circ}_{f,1300}$, kcal/g-at Si	References
Mo_3Si	21	(21)	(∿0)	(21)	59
Mo_5Si_3	22	(22)	(∿0)	(22)	59
$MoSi_2$	13.6	(13.6)	(∿0)	(13.6)	59
W_5Si_3	15.0	14.8	2.16	16.7	81,88,95
WSi_2	11.2	11.4	0.37	11.9	81,88,95
Mn_5Si_3	30	(30)	(∿0)	(30)	59
Fe_3Si	9.2	(9.2)	(∿0)	(9.2)	59
Fe_5Si_3	4.6	(4.6)	(∿0)	(4.6)	59
FeSi	9.6	(9.6)	(∿0)	(9.6)	59
$FeSi_2$	5.6	(5.6)	(∿0)	(5.6)	59
Co_2Si	9.2	(9.2)	(∿0)	(9.2)	59
CoSi	12.0	(12.0)	(∿0)	(12.0)	59
$CoSi_2$	8.2	(8.2)	(∿0)	(8.2)	59
Ni_3Si	5.3	(5.3)	(∿0)	(5.3)	59
Ni_2Si	10.5	(10.5)	(∿0)	(10.5)	59
Ni_3Si_2	10.7	(10.7)	(∿0)	(10.7)	59
NiSi	10.3	(10.3)	(∿0)	(10.3)	59

*$\Delta S^{\circ}_{f,298} \sim 0$ gibbs/g-at Si, unless noted otherwise.
†Estimated values are in parentheses.
xValues are for 298 K.
+Values are for 1023 K.

TABLE 20.--Oxidation of transition-metal silicides at 1300K

Reaction	-ΔG° for Reaction, kcal/g-at Si*
$0.33Ti_5Si_3 + 2.67O_2 \rightarrow 1.67TiO_2(rutile) + SiO_2(q)$ †	399.2
$0.33Ti_5Si_3 + 1.83O_2 \rightarrow 1.67TiO + SiO_2(q)$	283.1
$TiSi + 2O_2 \rightarrow TiO_2(rutile) + SiO_2(q)$	300.7
$TiSi + 1.5O_2 \rightarrow TiO + SiO_2(q)$	231.2
$0.5\ TiSi_2 + 1.5O_2 \rightarrow 0.5TiO_2(rutile) + SiO_2(q)$	230.1
$0.5\ TiSi_2 + 1.25O_2 \rightarrow 0.5TiO + SiO_2(q)$	195.4
$Zr_2Si + 3O_2 \rightarrow 2ZrO_2 + SiO_2(q)$	542.5
$0.33Zr_5Si_3 + 2.67O_2 \rightarrow 1.67ZrO_2 + SiO_2(q)$	475.3
$0.85ZrSi_{1.17} + 1.85O_2 \rightarrow 0.85ZrO_2 + SiO_2(q)$	306.6
$0.5ZrSi_2 + 1.5O_2 \rightarrow 0.5ZrO_2 + SiO_2(q)$	248.9
$V_2Si + 3.5O_2 \rightarrow V_2O_5(\ell) + SiO_2(q)$	370.9
$V_2Si + 2O_2 \rightarrow 2VO + SiO_2(q)$	278.2
$1.82NbSi_{0.55} + 3.28O_2 \rightarrow 0.91Nb_2O_5 + SiO_2(q)$	432.3
$1.82NbSi_{0.55} + 1.91O_2 \rightarrow 1.82NbO + SiO_2(q)$	272.7
$0.33Nb_5Si_3 + 3.08O_2 \rightarrow 0.83Nb_2O_5 + SiO_2(q)$	406.3
$0.33Nb_5Si_3 + 1.83O_2 \rightarrow 1.67NbO + SiO_2(q)$	261.5
$0.5\ NbSi_2 + 1.62O_2 \rightarrow 0.25Nb_2O_5 + SiO_2(q)$	224.9
$0.5\ NbSi_2 + 1.25O_2 \rightarrow 0.5NbO + SiO_2(q)$	181.1

TABLE 20.--Continued

Reaction	-ΔG° for Reaction, kcal/g-at Si*
$4.54TaSi_{0.22} + 6.68O_2 \rightarrow 2.27Ta_2O_5 + SiO_2(q)$	928.6
$Ta_2Si + 3.5O_2 \rightarrow Ta_2O_5 + SiO_2(q)$	489.0
$0.33Ta_5Si_3 + 3.08O_2 \rightarrow 0.83Ta_2O_5 + SiO_2(q)$	432.0
$0.5TaSi_2 + 1.52O_2 \rightarrow 0.25Ta_2O_5 + SiO_2(q)$	331.0
$Cr_3Si + 3.25O_2 \rightarrow 1.5Cr_2O_3 + SiO_2(q)$	438.8
$0.33Cr_5Si_3 + 2.25O_2 \rightarrow 0.83Cr_2O_3 + SiO_2(q)$	312.1
$CrSi + 1.75O_2 \rightarrow 0.50Cr_2O_3 + SiO_2(q)$	271.1+
$0.5CrSi_2 + 1.38O_2 \rightarrow 0.25Cr_2O_3 + SiO_2(q)$	223.2+
$Mo_3Si + 5.5O_2 \rightarrow 3MoO_3 + SiO_2(q)$	529.8
$Mo_3Si + 4O_2 \rightarrow 3MoO_2 + SiO_2(q)$	459.0
$0.33Mo_5Si_3 + 3.5O_2 \rightarrow 1.67MoO_3 + SiO_2(q)$	356.5
$0.33Mo_5Si_3 + 2.67O_2 \rightarrow 1.67MoO_2 + SiO_2(q)$	317.1
$0.5MoSi_2 + 1.75O_2 \rightarrow 0.5MoO_3 + SiO_2(q)$	339.7
$0.5MoSi_2 + 1.5O_2 \rightarrow 0.5MoO_2 + SiO_2(q)$	201.5
$0.33W_5Si_3 + 3.5O_2 \rightarrow 1.67WO_3 + SiO_2(q)$	350.4
$0.33W_5Si_3 + 2.67O_2 \rightarrow 1.67WO_2 + SiO_2(q)$	287.5
$0.5WSi_2 + 1.75O_2 \rightarrow 0.5WO_3 + SiO_2(q)$	211.6
$0.5WSi_2 + 1.5O_2 \rightarrow 0.5WO_2 + SiO_2(q)$	192.8
$0.33Mn_5Si_3 + 2.11O_2 \rightarrow 0.56Mn_3O_4 + SiO_2(q)$	255.5
$0.33Mn_5Si_3 + 1.83O_2 \rightarrow 1.67MnO + SiO_2(q)$	247.5

TABLE 20.--Continued

Reaction	-ΔG° for Reaction, kcal/g-at Si*
$Fe_3Si + 3.25O \rightarrow 1.5Fe_2O_3 + SiO_2(q)$	327.8
$Fe_3Si + 2.58O_2 \rightarrow 3.16Fe_{0.95}O + SiO_2(q)$	245.5
$0.33Fe_5Si_3 + 2.25O_2 \rightarrow 0.83Fe_2O_3 + SiO_2(q)$	254.3
$0.33Fe_5Si_3 + 1.88O_2 \rightarrow 1.75Fe_{0.95}O + SiO_2(q)$	236.4
$FeSi + 1.75O_2 \rightarrow 0.5Fe_2O_3 + SiO_2(q)$	210.8
$FeSi + 1.53O_2 \rightarrow 1.05Fe_{0.95}O + SiO_2(q)$	199.8
$0.5FeSi_2 + 1.38O_2 \rightarrow 0.25Fe_2O_3 + SiO_2(q)$	185.7
$0.5FeSi_2 + 1.26O_2 \rightarrow 0.53Fe_{0.95}O + SiO_2(q)$	180.2
$Co_2Si + 2O_2 \rightarrow 2CoO + SiO_2(q)$	221.0
$CoSi + 1.5O_2 \rightarrow CoO + SiO_2(q)$	184.2
$0.5CoSi_2 + 1.25O_2 \rightarrow 0.5CoO + SiO_2(q)$	170.9
$Ni_3Si + 2.5O_2 \rightarrow 3NiO + SiO_2(q)$	245.5
$Ni_2Si + 2O_2 \rightarrow 2NiO + SiO_2(q)$	210.7
$0.5Ni_2Si_3 + 1.75O_2 \rightarrow 1.5NiO + SiO_2(q)$	195.7
$NiSi + 1.5O_2 \rightarrow NiO + SiO_2(q)$	181.4

*ΔG_f° for silicides from Table 18; ΔG_f° for oxides from References 61-63.

†Quartz = (q).

+Values are for 1000K.

Table 21:--Calculatec P_{C_2} for oxidation of transition-metal silicides at 1300K *

Silicide/Oxide	K_p for Oxidation	Equilibrium P_{O_2}, atm
Ti_5Si_3/TiO_2 (rutile)	1.29×10^{67}	7.34×10^{-26}
Ti_5Si_3/TiO	4.01×10^{47}	9.71×10^{-27}
$TiSi/TiO_2$ (rutile)	3.62×10^{50}	5.26×10^{-26}
$TiSi/TiO$	7.57×10^{38}	1.20×10^{-26}
$TiSi_2/TiO_2$ (rutile)	4.88×10^{38}	1.61×10^{-26}
$TiSi_2/TiO$	7.05×10^{32}	5.27×10^{-27}
Zr_2Si/ZrO_2	1.62×10^{91}	3.95×10^{-31}
Zr_5Si/ZrO_2	8.30×10^{79}	1.17×10^{-30}
$ZrSi_{1.17}/ZrO_2$	3.58×10^{51}	1.36×10^{-28}
$ZrSi_2/ZrO_2$	6.91×10^{41}	1.28×10^{-28}
$V_2Si/V_2O_5(\ell)$	2.29×10^{42}	1.52×10^{-18}
V_2Si/VO	6.04×10^{46}	4.07×10^{-24}
$NbSi_{0.55}/Nb_2O_5$	4.86×10^{72}	6.91×10^{-23}
$NbSi_{0.55}/NbO$	7.18×10^{45}	9.81×10^{-25}
Nb_5Si_3/Nb_2O_5	2.06×10^{68}	6.61×10^{-23}
Nb_5Si_3/NbO	9.22×10^{43}	9.45×10^{-25}
$NbSi_2/Nb_2O_5$	6.52×10^{37}	4.55×10^{-24}
$NbSi_2/NbO$	2.77×10^{30}	4.42×10^{-25}

Table 21:--Continued

Silicide/Oxide	K_p for Oxidation[+]	Equilibrium P_{O_2}, atm
$TaSi_{0.22}/Ta_2O_5$	1.23×10^{156}	4.25×10^{-24}
Ta_2Si/Ta_2O_5	1.63×10^{82}	3.24×10^{-24}
Ta_5Si_3/Ta_2O_5	4.27×10^{72}	2.62×10^{-24}
$TaSi_2/Ta_2O_5$	4.56×10^{55}	5.60×10^{-35}
Cr_3Si_2/Cr_2O_3	6.03×10^{73}	1.99×10^{-23}
Cr_5Si_3/Cr_2O_3	2.98×10^{52}	4.76×10^{-24}
$CrSi/Cr_2O_3$	$^{+}1.77 \times 10^{59}$	$^{+}1.40 \times 10^{-34}$
$CrSi_2/Cr_2O_3$	$^{+}6.19 \times 10^{48}$	$^{+}3.27 \times 10^{-36}$
Mo_3Si/MoO_3	1.21×10^{89}	6.36×10^{-17}
Mo_3Si/MoO_2	1.48×10^{77}	5.10×10^{-20}
Mo_5Si_3/MoO_3	8.67×10^{59}	7.50×10^{-18}
Mo_5Si_3/MoO_2	2.03×10^{53}	1.08×10^{-20}
$MoSi_2/MoO_3$	7.26×10^{35}	3.22×10^{-21}
$MoSi_2/MoO_2$	7.52×10^{33}	2.61×10^{-23}
W_5Si_3/WO_3	8.03×10^{58}	1.48×10^{-17}
W_5Si_3/WO_2	2.19×10^{48}	7.86×10^{-19}
WSi_2/WO_3	3.72×10^{35}	4.72×10^{-21}
WSi_2/WO_2	2.56×10^{32}	2.48×10^{-22}
Mn_5Si_3/Mn_3O_4	9.09×10^{42}	4.37×10^{-21}
Mn_5Si_3/MnO	4.10×10^{41}	1.82×10^{-23}

Table 21.--Continued

Silicide/Oxide	K_p for Oxidation[†]	Equilibrium P_{O_2}, atm
Fe_3Si/Fe_2O_3	1.31×10^{55}	1.10×10^{-17}
$Fe_3Si/Fe_{0.95}O$	3.77×10^{49}	5.98×10^{-20}
Fe_5Si_3/Fe_2O_3	5.69×10^{42}	9.95×10^{-20}
$Fe_5Si_3/Fe_{0.95}O$	5.48×10^{39}	6.74×10^{-22}
$FeSi/Fe_2O_3$	2.78×10^{35}	5.58×10^{-21}
$FeSi/Fe_{0.95}O$	3.95×10^{33}	9.63×10^{-23}
$FeSi_2/Fe_2O_3$	1.64×10^{31}	2.40×10^{-23}
$FeSi_2/Fe_{0.95}O$	1.96×10^{30}	1.04×10^{-24}
Co_2Si/CoO	1.45×10^{37}	2.63×10^{-19}
$CoSi/CoO$	9.19×10^{30}	2.28×10^{-21}
$CoSi_2/CoO$	5.48×10^{28}	1.02×10^{-23}
Ni_3Si/NiO	1.85×10^{41}	3.11×10^{-17}
Ni_2Si/NiO	2.67×10^{35}	1.99×10^{-18}
Ni_3Si_2/NiO	8.09×10^{32}	1.57×10^{-19}
$NiSi_2/NiO$	3.10×10^{30}	4.70×10^{-21}

---

* Refer to Table 19.

† $K_p = P_{O_2}^{-n}$, where n = number of moles O_2 reacting (Table 19).

+ Values are for 1000K.

stead of simple oxide mixtures will also affect the equilibrium P_{O_2} for oxidation. Oxidation of $ZrSi_{1.17}$ to form $ZrSiO_4$ + $0.17SiO_2(q)$ for example, results in a calculated P_{O_2} of 5.65×10^{-29} atm at 1300K, compared to 1.36×10^{-28} atm for formation of the mixed oxides. The use of a number of transition-metal silicides as anodes may still be possible in the face of unfavorable P_{O_2} indications, if kinetic factors (e.g., negligible oxidation rates) are more important and overriding.

Of the silicides of Table 19, V_2Si, Mo_3Si, Mo_5Si_3, W_5Si_3, Ni_3Si, and Ni_2Si offer the greatest potential for use as anode material in high-temperature fuel cells, based on approximate thermodynamic stabilities against oxidation. Unfortunately, no single silicide possesses this stability as well as a high electrical conductivity and thermal-expansion properties compatible with requirements of the solid-electrolyte fuel cell. Thus, some compromise will be necessary to satisfy all fuel cell needs.

The silicides are the most attractive, in terms of their overall physical properties, of the interstitial (non-oxide ceramics) compounds discussed so far for use as anode materials in high-temperature fuel cells. The stoichiometry of the silicides can be readily altered to engineer changes in the electrical as well as the thermal-expansion properties. Doping with other transition metals or interstitials is also possible to effect the desired change in physical properties.

Preparation of a thin-film silicide anode by chemical vapor deposition can be accomplished readily if this technique is seri-

ously considered for fabrication purposes and if the resultant film has the proper chemical and physical properties for use in the solid-electrolyte fuel cell.

The incorporation of silicides into the anode structure also can be accomplished, as was described earlier with the carbides and nitrides, by replacing a portion of the ZrO_2 in the ZrO_2-Ni cermet. The silicides, though, sinter more readily and should bond better with nickel than the carbides and nitrides. The one area of concern is the possibility of the formation of nickel silicides (or silicides of other metals used for cementing) over prolonged periods of time at temperatures of 700° to 1000°C. Thermodynamic estimates indicate that the reaction of silicides with nickel to form Ni_2Si, Ni_3Si_2, and Ni_3Si, for example, should not be favorable at 1300 K, except for several silicides of iron and cobalt. There is a possibility that ternary-system (M-M'-Si) compounds or solid solutions will form, as indicated by published data for the various binary-silicide systems.[59]

At very high temperatures, it has been reported that the disilicides $TiSi_2$, $ZrSi_2$, $ThSi_2$, $TaSi_2$, WSi_2, and $MoSi_2$ are soluble in liquid nickel. The lower silicides Ti_5Si_3 and ZrSi, on the other hand, were not attacked.[81] This suggests that the lower silicides would be better suited for preparing composite electrodes using transition-metal binders, such as nickel. Kinetic data on the extent of possible interactions at temperatures of 700° to 1000°C would be invaluable for such materials for engineering and evaluation purposes.

The possible use of silicides as anode material in the molten-carbonate fuel cell may be limited, as was indicated earlier for the nitrides, by the presence of hydroxide in the melt. Silicides of the Group IVA to VIA elements are reportedly soluble in molten alkali hydroxides;[81] this is a function of the atmosphere used and may occur only under oxidizing conditions. Chemical compatibility data are needed under reducing conditions for silicides in contact with molten-carbonate melts containing varying amounts of impurities (e.g., hydroxides, oxides, etc.) which can be considered as representative of melt conditions during operation of the molten-carbonate fuel cell.

In addition to the lack of chemical-compatibility data for the transition-metal silicides, there is little known about the electrical and thermal-expansion properties of binary and ternary silicon-based systems. Until additional experimental data for such parameters are available--especially at the higher temperatures (700 ^{o} to 1000^{o}C)--comprehensive evaluation of the use of silicides for potential anode use in high-temperature fuel cells is not possible.

4. Borides

The last category of the non-ceramic materials to be discussed in this report is the borides. Transition-metal borides of Groups IVA to VIA have received the most attention for consideration as MHD electrodes because of their high melting points (1900^{o} to 3000^{o}C), low volatility and high stability at elevated temperatures, high hardness, and good electrical conductivity. The only

other class of interstitial compound with similar properties is the transition-metal carbide. The borides have the widest range of compositions for compound formation--M_3B to MB_{12}--of all the interstitial compounds because of the chains and network configurations assumed by the boron atoms in these compounds.[59] The borides of the alkaline-earth and rare-earth metals are not reactive to water as are their corresponding carbides, nitrides, and silicides; this is indicative of the high chemical stability of borides.

The key physical properties of a number of borides are listed in Table 22. As is readily evident, data for many of the borides are missing. Data of this type, however, may be contained in a number of references listed in Appendix D which were not readily accessible during the course of this study. Thus, some of the lower borides may have thermal expansion and electrical properties which are better suited to high-temperature fuel cell needs than is indicated in Table 22.

Compared to the silicides, the transition-metal borides generally have lower electrical resistivities (the silicides of the vanadium family being the exceptions) and lower coefficients of thermal expansion. The borides are metallic conductors, i.e., they have a positive temperature-coefficient of resistivity. The resistivity of TiB_2 at 1000°C, for example, is two to four times as great as at room temperature (Table 22).

The electrical resistivity data of Table 22 are plotted in Figure 5 as a function of composition. The TaB_x, VB_x, and CrB_x

TABLE 22.--Select physical properties of metal borides

Boride	Melting Poirt,°C	Coefficient of Thermal Expansion (α), 10^{-6}/°C	Electrical Resistivity, μΩ-cm	Temp., °C	Reference
Ti_2B	2,250 (dec.)	--	--	--	57,95
TiB	2,060 (dec.)	--	40	25	57,95
TiB_2	2,871	7.3 - 9.1 (25°-2041°C)[X]	15-28	25	57,59,95-99
"	"	--	60	1000	59
"	"	9.7 (200°-1800°C)	78	1200	100
Ti_2B_5	2,093 (dec.)	--	--	--	57
ZrB	1,250 (?)(dec.)	--	9-16	25	56,59
ZrB_2	3,040	6.7 - 8.3 (25°-1800°C)[X]	9-39	25	57,59,95,96,98,99
"	"	"	87.6	1600	95
ZrB_{12}	2,680	--	--	--	95
HfB	2,900 (pl)[†]	--	8-14	25	56,57,59
HfB_2	3,250	6.5 - 8.2 (25°-2041°C)[*]	10-17	25	56,59,98
V_3B_2	2,070	--	--	--	57
VB	2,250	--	35-40	25	57,59,95
V_3B_4	2,280	--	--	--	57
VB_2	2,430	7.56 (25°-800°C)	16	25	57,95,98
Nb_3B_2	1,815	--	--	--	57
NbB	2,260	--	64.5	25	57,95
Nb_3B_4	2,195	--	--	--	57
NbB_2	3,000	6.7 - 9.1 (25°-1700°C)[*]	28-66	--	57,95,96,98

TABLE 22.--Select physical properties of metal borides (Continued)

Boride	Melting Point, °C	Coefficient of Thermal Expansion (α) 10^{-6}/°C	Electrical Resistivity μΩ-cm	Temp., °C	Reference
Ta_2B	1,900	--	--	--	57
Ta_3B_2	2,040	--	--	--	57
TaB	2,430	--	100	25	57,95
Ta_3B_4	2,650	--	--	--	57
TaB_2	3,095	6.3 - 8.0 (25°-1700°C)[x]	68-86	25	57,95,95-98
Cr_4B	1,650	--	--	--	57
Cr_2B	1,815	--	--	--	57
Cr_5B_3	1,900	--	--	--	57
CrB	2,045	--	64	25	57,95
Cr_3B_4	1,930	--	--	--	57
CrB_2	2,150	10.5,11.1(25°-1200°C)	22-45	25	57,95,98
Cr_2B_5	2,000	--	--	--	57
Mo_2B	2,280 (p)	7.74 (25°-335°C)	--	--	57
α-MoB	2,180 (p)	--	45-50	25	57,95
β-MoB	2,665	--	25	25	57,95
MoB_2	2,475 (dec.)	--	22-45	25	57,95
Mo_2B_5	2,140 (p)	5.00 (25°-500°C)	25	25	57,95
W_2B	2,670	--	--	--	57
α-WB	2,170 (dec.)	--	--	--	57
β-WB	2,665 (dec.)	--	--	--	57
W_2B_5	2,365	7.37 (10°-2210°C)[+]	21	25	57,95

TABLE 22.--Select physical properties of metal borides (Continued)

Boride	Melting Point,°C	Coefficient of Thermal Expansion (α) 10^{-6}/°C	Electrical Resistivity μΩ-cm	Temp., °C	Reference
LaB_6	2,150	6.30 (25°-800°C)	27	--	57,95
CeB_6	2,190	7.20 (" ")	--	--	57
PrB_6	--	7.56 (" ")	--	--	57
NdB_6	2,540	7.20 (" ")	--	--	57
YB_4	2,750 (est.)	7.68 (20°-1000°C)	--	--	57,101
YB_6	2,300	6.12 (25 - 800°C)	--	--	57
ScB_2	2,250	9.47 (" ")	--	--	57
GdB_4	3,030 est.)	7.00 (20°-1000°C)	--	--	57,101
CaB_6	2,230	6.49 (25°-800°C)	--	--	57
SrB_6	2,230	6.67 (" ")	--	--	57
BaB_6	2,265	6.85 (" ")	--	--	57
Ni_3B	1,170	--	--	--	95
Ni_2B	1,230	--	--	--	95
NiB	---	--	--	--	95

x α_L calculated from X-ray data using $\alpha_L = \frac{1}{3}\alpha_c + \frac{2}{3}\alpha_a$; range of values given due to changes in slope of $\Delta l/l_o$-T plot over indicated temperature range.

† Peritectic = (p).

+ Estimated value.

systems exhibit maxima near x = 1, while the CrB_x system has a maximum resistivity at x = 2. With the exception of the VB_x system, the resistivities of the borides are greater than that of the parent metals.

The resistivity behavior of the CrB_x system contrasts with that of $CrSi_x$ alloys, which did not show maximum values as a function of x (Figure 4). Conversely, the borides of titanium show a general decrease in resistivity with increasing boron content, while the corresponding resistivity-composition curve for the silicides is characterized by a pronounced maxima. The resistivity-composition curves for HfB_x and ZrB_x are similar to that of the titanium borides, except with a reversed curvature (the large scatter in resistivity data for ZrB_2 makes the apparent minimum in the curve for ZrB_x inconclusive).

Four of the borides--ZrB, ZrB_2, HfB, and HfB_2--have electrical resistivities of 10 $\mu\Omega$-cm or less at 25 C. However, none of them has a coefficient of thermal expansion of $\sim 10 \times 10^{-6}/^{o}C$ necessary for compatibility with the ZrO_2-Y_2O_3 solid-electrolyte. Of the borides in Table 22, only ScB_2, CrB_2, and possibly TiB_2 have thermal expansion properties which would make them potentially usable in the solid-electrolyte fuel cell. The prohibitive cost of scandium compounds, however, essentially eliminate ScB_2 from further consideration.

The borides of the Group IV elements are the most resistant to oxidation. Like the silicides, they depend upon the formation of an impervious oxide film for protection against destructive oxi-

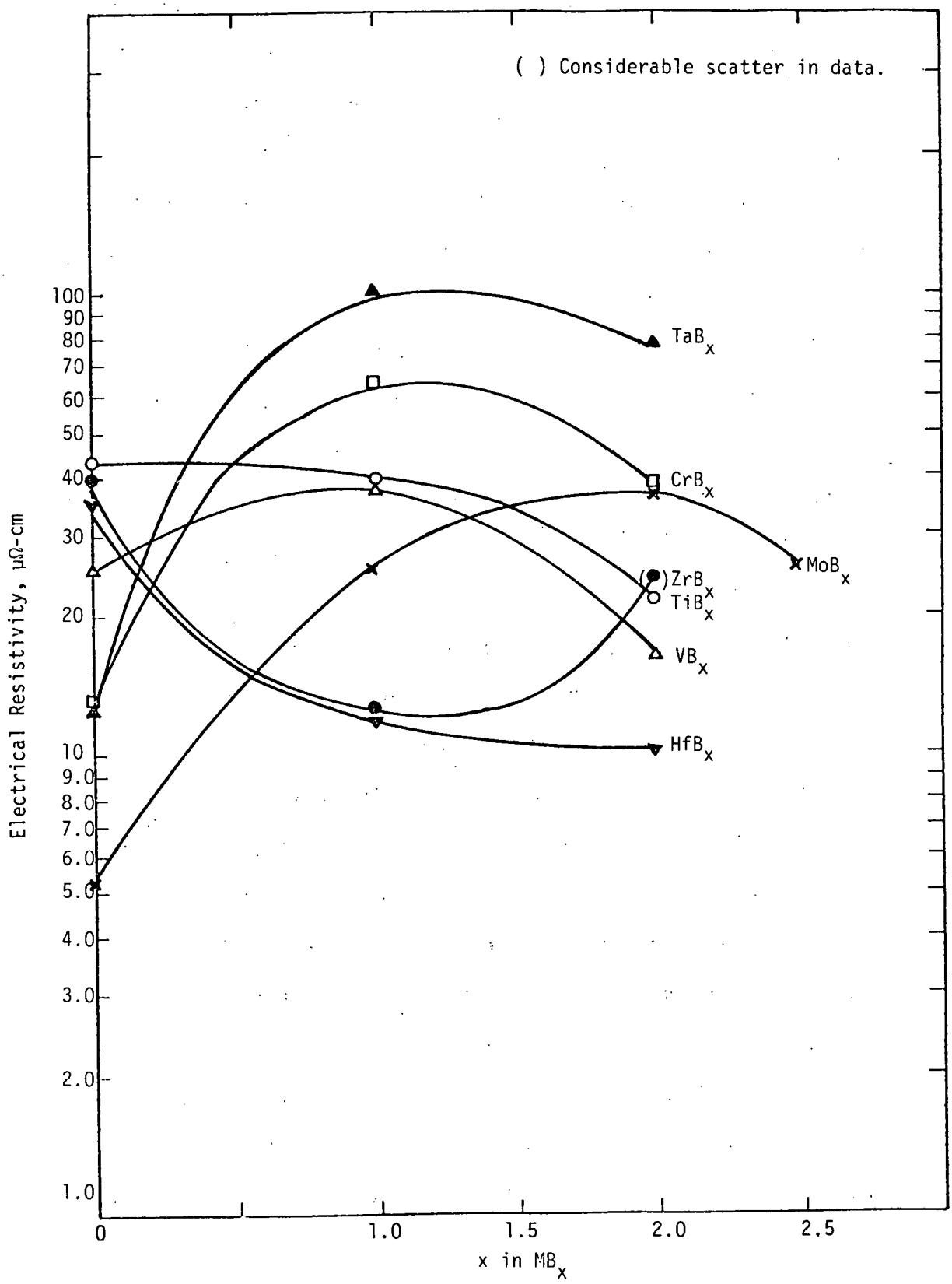

Figure 5.--Electrical Resistivities of Transition-Metal Borides at 25°C as a Function of Composition

dation. Titanium boride, for example, is reported to be stable up to 1500°C. In contrast, borides of Mo, W, V. Nb, and Ta oxidize readily at 1000°C.[95] The formation of a borate or oxide film under oxidizing conditions limits the use of metal borides in high-temperature fuel cells to the fuel electrode. Such films would result in chemical compatibility and interfacial problems with other cell components over prolonged periods of time at operating temperatures.

The thermodynamic stability of the metal borides under the reducing conditions at the anode in high-temperature fuel cells can be estimated from ΔG_f^o data for the borides at elevated temperatures, using a simplified reaction for oxidation

(22) $$M_xB + \left[\frac{2xz+3}{4}\right] O_2 \rightarrow xMO_z + 1/2\ B_2O_3(\ell)$$

The equilibrium P_{O_2} for oxidation then can be calculated from

(23) $$P_{O_2} = (K_p)\exp[-4/(2xz+3)] = \exp\ \frac{\Delta G^o_{(22)}}{RT} \cdot \frac{4}{(2xz+3)}$$

ΔG_f^o information for many of the borides is even less evident than that for the silicides--even at lower temperatures.

Thermodynamic data which was readily available are presented in Table 23. For some borides, only ΔH_f^o at 298K was found. In these cases, ΔG_f^o at 1300K was set equal to ΔH_f^o at 298K, as was done with the silicides (Table 19). Examination of $\Delta H^o_{f,298}$ and $\Delta G^o_{f,1300}$ data for TiB., TiB_2, and ZrB_2 in Table 23 show less than ten percent difference in these values. Thus, this would appear to be adequate, as a first approximation, for purposes of calculating the thermodynamic stabilities of the borides toward oxidation. The free energy changes for oxidation

TABLE 23.--Thermodynamic data for select metal borides

Boride	$-\Delta H^\circ_{f,298}$ kcal/g-at B	$-\Delta H^\circ_{f,3000}$ kcal/g-at B	References
TiB	38.3	37.1	61
TiB_2	33.4	30.8	61
ZrB_2	38.6	35.8	61
HfB_2	39.0	(39.0)*	102
TaB_2	23.2	(23.2)	103
Mo_2B	22.6	27.9	104
W_2B	20.8	23.5	104
WB	14.1	(14.1)	105
Co_3B	-	-30.9+	106
Co_2B	-	64.3+	106
LaB_6	5.12	(5.12)	107

* Estimated values are in parentheses.

+ Values are for 1200K.

of a select number of metal borides are presented in Table 24 (additional data may be contained in a number of the references of Appendix D, which then would permit later up-dating of the information in Table 24). The corresponding values of K_p and P_{O_2} for the oxidation reactions at 1300K are listed in Table 25.

Only M_2B and W_2B are thermodynamically stable toward oxidation under P_{O_2} conditions of 10^{-16} to 10^{-18} atm expected at the fuel electrode in the solid-electrolyte fuel cell. Tungsten boride would be stable only at a P_{O_2} of 10^{-18} atm. This is true for formation of the higher as well as the lower oxides. None of the borides are thermodynamically stable with respect to their oxides at 900K , under conditions expected at the fuel electrode in the molten-carbonate fuel cell. This parallels similar behavior for the other interstitial compounds under comparable conditions. Kinetic factors, of course, could still permit the use of borides which are not predicted to be stable in the fuel gas environment. The formation of borates rather than mixed oxides, as indicated in Table 20, will influence the equilibrium P_{O_2} for oxidation, analogous to the previously noted effect of silicate formation during oxidation of silicides.

None of the borides possess the desired resistance to oxidation, high electrical conductivity, and compatible thermal expansion properties which would make it ideally suited for use in the solid-electrolyte fuel cell. Thus, some modification or compositional changes in the borides will be necessary in order to meet all the fuel cell requirements.

TABLE 24.--Oxidation of select metal borides at 1300K

Reaction	-ΔG° for Reaction kcal/g-at B	References
$TiB + 1.75O_2 \rightarrow TiO_2(rutile) + 0.5B_2O_3(\ell)$	246.6	61,108
$TiB + 1.25O_2 \rightarrow \beta TiO + 0.5B_2O_3(\ell)$	177.1	61,63,108
$0.5TiB_2 + 1.25O_2 \rightarrow 0.5TiO_2$ (rutile) $+ 0.5B_2O_3(\ell)$	168.0	61,108
$0.5TiB_2 + O_2 \rightarrow 0.5\beta TiO + 0.5B_2O_3(\ell)$	133.3	61,63,108
$0.5HfB_2 + 1.25O_2 \rightarrow 0.5HfO_2 + 0.5B_2O_3(\ell)$	178.5	62,102,108
$0.5ZrB_2 + 1.25O_2 \rightarrow 0.5ZrO_2 + 0.5B_2O_3(\ell)$	180.0	61,108
$0.5TaB_2 + 1.38O_2 \rightarrow 0.25Ta_2O_5 + 0.5B_2O_3(\ell)$	179.4	63,103,108
$Mo_2B + 3.75O_2 \rightarrow 2MoO_3(\ell) + 0.5B_2O_3(\ell)$	293.7	61,104,108
$Mo_2B + 2.75O_2 \rightarrow 2MoO_2 + 0.5B_2O_3(\ell)$	257.6	61,104,108
$W_2B + 3.75O_2 \rightarrow 2WO_3 + 0.5B_2O_3(\ell)$	336.0	61,104
$W_2B + 2.75O_2 \rightarrow 2WO_2 + 0.5B_2O_3(\ell)$	260.7	61,104
$WB + 2.25O_2 \rightarrow WO_3 + 0.5B_2O_3(\ell)$	222.7	61,105,108
$WB + 1.75O_2 \rightarrow WO_3 + 0.5B_2O_3(\ell)$	185.0	61,105,108
$Co_3B + 2.25O_2 \rightarrow 3CoO + 0.5B_2O_3(\ell)$	254.7*	106,108
$Co_2B + 1.75O_2 \rightarrow 2CoO + 0.5B_2O_3(\ell)$	252.4*	106,108
$0.17LaB_6 + 0.88O_2 \rightarrow 0.083La_2O_3(\ell) + 0.5B_2O_3(\ell)$	138.7*	62,107,108

*Values for 1200K.

TABLE 25.--Calculated P_{O_2} for oxidation of metal borides at 1300K

Boride/Oxide	K_p for Oxidation	P_{O_2} for Oxidation atm
TiB/TiO_2 (rutile)	$P_{O_2}^{-1.75} = 2.85 \times 10^{41}$	2.05×10^{-24}
TiB/TiO	$P_{O_2}^{-1.25} = 5.96 \times 10^{29}$	1.51×10^{-24}
TiB_2/TiO(rutile)	$P_{O_2}^{-1.25} = 1.80 \times 10^{28}$	2.49×10^{-23}
TiB_2/TiO	$P_{O_2}^{-1} = 2.60 \times 10^{22}$	3.85×10^{-23}
HfB_2/HfO_2	$P_{O_2}^{-1.25} = 1.02 \times 10^{30}$	9.80×10^{-25}
ZrB_2/ZrO_2	$P_{O_2}^{-1.25} = 1.84 \times 10^{30}$	6.14×10^{-25}
TaB_2/Ta_2O_5	$P_{O_2}^{-1.38} = 1.45 \times 10^{30}$	1.16×10^{-22}
$Mo_2B/MoO_3(\ell)$	$P_{O_2}^{-3.75} = 2.36 \times 10^{49}$	6.82×10^{-14}
Mo_2B/MoO_2	$P_{O_2}^{-2.75} = 2.05 \times 10^{43}$	1.78×10^{-16}
W_2B/WO_3	$P_{O_2}^{-3.75} = 3.06 \times 10^{56}$	8.65×10^{-16}
W_2B/WO_2	$P_{O_2}^{-2.75} = 6.81 \times 10^{43}$	1.15×10^{-16}
WB/WO_3	$P_{O_2}^{-2.25} = 2.77 \times 10^{37}$	2.28×10^{-17}
WB/WO_2	$P_{O_2}^{-1.75} = 1.27 \times 10^{31}$	1.68×10^{-18}
Co_3B/CoO	$P_{O_2}^{-2.25} = 2.46 \times 10^{46}$*	2.41×10^{-21}*

TABLE 25.--Calculated P_{O_2} for oxidation of metal borides at 1300K (Continued)

Boride/Oxide	K_p for Oxidation	P_{O_2} for Oxidation, atm
Co_2B/CoO	$P_{O_2}^{-1.75} = 9.19 \times 10^{45}$*	5.43×10^{-27}*
LaB_6/La_2O_3	$P_{O_2}^{-0.875} = 1.8 \times 10^{25}$*	1.4×10^{-29}*

* Values are for 1200K.

Metal borides can be incorporated into the fuel electrode of the solid-electrolyte fuel cell by several techniques. A thin-film anode could be fabricated solely from the boride by chemical vapor exposition. Zirconium boride films have been prepared in this manner using metal halide mixtures[109], as well as borane mixtures.[110] The film could be applied by plasma spraying,[111,112] although this generally does not produce as coherent a film as does CVD. R-F sputtering also can be used for the preparation of thin films. The sputtering process is generally much slower than CVD, however. For fuel cell applications, the morphology and physical properties of the film are equally as important as the chemical composition. All of these factors will require evaluation in any of the above techniques and are considered for thin-film fabrication of the solid-electrolyte fuel cell.

An alternate anode-fabrication technique involves the use of metal binders to form a cermet. Thus, part of the ZrO_2 in the ZrO_2-Ni cermet currently used for the solid-electrolyte fuel cell could be replaced by a metal boride or boride-based material. Unfortunately, nickel forms a number of stable borides (see Table 22). At 1000°C, the metal boride could begin to react with the nickel to form intermetallic compounds, eutectic solutions, or solid solutions after prolonged periods. The resulting change in the electrical and thermal expansion properties could be detrimental to a fuel cell utilizing such a cermet electrode.

There are indications that a number of the metal borides react with nickel at temperatures expected in the solid-electrolyte fuel

cell. The system TaB_2-Ni, for example, forms an eutectic at 1090°C at 17 a/o TaB_2.[59] Similar behavior has been indicated for TaB_2-Fe and -Co systems, and between Fe, Co, or Ni and TiB_2 or ZrB_2.[59] Tungsten boride is reported to form a liquid phase with nickel at 1300K which indicates boride dissolution occurs to form a eutectic.[113] In the V-B-Ni system, a phase of composition $Ni_{20.4}V_{2.6}B_6$ has been observed at a temperature as low as 800°C.[114] Extreme caution must be exercized, therefore, in choosing suitable boride-transition metal combinations for anode use in high-temperature fuel cells to avoid the reactivity problems outlined above. These potential compatibility problems do not occur when nickel is used to bond transition-metal nitrides and carbides under similar conditions because of the instability of carbides and nitrides of nickel and the low solubility of carbon and nitrogen in nickel at 1000°C.

The borides are reported to be soluble in molten alkali,[95] which would appear to preclude their use as anodes in the molten-carbonate fuel cell. However, without oxygen present, no feasible chemical reactions can be written to describe possible dissolution mechanisms. It appears likely, therefore, that borides would be compatible with the molten-carbonate eutectic in the absence of substantial amounts of hydroxide and water vapor and under suitable reducing conditions, as would exist at the fuel electrode. Compatibility studies should be conducted under such conditions if serious consideration is given to the use of boride materials as anodes.

5. Composite, Non-Oxide Ceramics

A number of composite, non-oxide ceramics have been examined for use as MHD electrodes. Addition of SiC to ZrB_2 was found to increase the oxidation resistance of this material by the formation of a protective SiO_2 film at high temperatures.[115] $MoSi_2$ also has been used with ZrB_2 for this purpose.[116] LaB_6 has been added to ZrB_2 to increase its thermionic emission for MHD use.[117] The properties of such materials also makes them candidates for possible use in high-temperature fuel cells.

While many of the carbides, nitrides, silicides, and borides have certain materials properties which would make them potentially suitable for anode use in the solid-electrolyte fuel cell, invariably no one material appears to satisfy all of the fuel cell needs. Thus, modification of the chemical composition of a promising material or combining it with a second or third material would appear to be necessary to effect the desired change(s) in physical properties (e.g., thermal coefficient of expansion, electrical resistivity, melting point, etc.). Such effects are not as critical for anode use in the molten-carbonate fuel cell, although chemical compatibility with the carbonate then becomes a primary prerequisite.

The effect of various interstitials upon the properties of a given metal is typified for the case of titanium in Table 26. Addition of $TiSi_2$ to TiB_2 would be expected to increase the coefficient of thermal expansion and the electrical conductivity, but lower the P_{O_2} for oxidation, if the effects were additive. This

TABLE 26.--Comparison of select physical properties of interstitial compounds of titanium

Compound	Melting Point, °C	Coefficient of Thermal Expansion, 10^{-6}/°C	Electrical Resistivity at 25°C, μΩ-cm	P_{O_2} for oxidation to TiO_2 (rutile) at 1300K, atm
TiC	3,250	8.3 (0°-1,400°C)	60-250	1.39×10^{-21}*
TiN	(func. of P_{N_2})	9.5 (20°-1,100°C)	26	3.07×10^{-29}+
TiSi	1,760 (dec.)	10.4 (370°-1,070°C)	39	5.26×10^{-26}
TiB	2,060 (dec.)	?	40	2.05×10^{-24}
TiO	[61] 1,750	[118] 6.6 (25°C)	[59] 300	[59] 4.37×10^{-24}
$TiSi_2$	1,540	10.4 (20°-1,070°C)	11.6-16.7	1.61×10^{-26}
TiB_2	2,871	7.3-9.1 (25°-2,040°C)	15 - 28	2.49×10^{-23}
TiO_2(rutile)	[61] 1,838	[57] 8.82 (25-1,500°C)	$>10^{10}$	0

*For P_{CO_2} = 0.1 atm.

+For P_{N_2} = equilibrium dissociation pressure of 5.27×10^{-18} atm.

may not always be the case, however, as evidenced by the minimum in the electrical resistivity of TiN-TiO solid solutions as a function of composition (Figure 3).

In general, silicides have higher thermal coefficients of electrical resistivity (TCOER) than carbides and nitrides. The TCOER for mixed interstitial compounds varies, depending upon the material and composition. HfC and TaC, for example, have low TCOERs compared to TiC and ZrC. Chromium carbide (Cr_3C_2) also has a low TCOER. The TCOER increases with WC content for solid solutions with TiC, ZrC, and VC.[119]

The coefficient of thermal expansion for interstitial alloys is similarly affected by composition, as indicated in Table 27 by data for Zr and Hf. Substitution of oxygen for carbon and nitrogen raises the coefficient of thermal expansion. Similarly, for $TiCO_y$, α increases with increasing y at constant $(x+y)$ or x.[121]

Thus, by appropriate choice of materials, composites may be engineered to have the desired physical properties such as increased oxidation resistance, higher electrical conductivity, or compatible coefficient of thermal expansion for the particular use envisioned. In certain cases, it will not always be possible to determine a priori the value of a specific physical property for a composite material based on the values of the individual components. A CrB_2-TiB_2 composite, for example, has a higher electrical resistivity at high temperatures than each of the individual component borides.[59] This may result from the formation of a compound between the borides rather than a simple solid so-

TABLE 27.--Effect of composition upon the thermal expansion properties of interstitial alloys of zirconium and hafnium [120]

Composition	Coefficient of Thermal Expansion (α), 10^{-6}/°C*
$ZrC_{0.957}$	6.86
$ZrC_{0.83}O_{0.18}$	7.14
$ZrN_{0.76}O_{0.19}$	7.60
$HfC_{0.95}$	6.75
$HfC_{0.66}O_{0.21}$	6.80
$HfC_{0.57}O_{0.13}$	7.30
$HfN_{1.1}$	7.88
$HfN_{0.74}O_{0.16}$	8.08

* Assumed temperature range of 25° to 1000°C.

lution. The nature of the interaction between components of a potential composite must be known before effects upon the properties of the resultant material can be predicted.

Knowledge of the intersolubilities of refractory phases is important when the preparation of composite materials is being considered. In some cases, the component compounds may be completely mutually soluble (e.g., TaC-TiC or ZrB_2-TiB_2).[122] In other instances, one material may be only partially soluble in a second or third material (e.g., TiB_2 in $TaSi_2$, $MoSi_2$, or TiC).[122] Compound formation may result in still a third possibility (e.g., TaC or MoB_2 with $TaSi_2$, Nb_5Si_3, or $MoSi_2$).[122] Solubility limitations can therefore place constraints on the range of concentrations which can be considered in composites for potential use in the high-temperature fuel cells.

Considerable research has been conducted in the development, for a variety of purposes, of composite materials based on interstitial alloys. In some cases, the goal was to develop a hard, refractory material for use in cutting tools and dies. Composites also have been examined as a means of reducing corrosion in situations where a particular material alone did not satisfy the necessary requirements. Addition of BN to TiB_2, TiC, or ZrB_2, for example, resulted in a container material suitable for vaporization of molten aluminum.[123] Because BN is an insulator, however, the electrical resistivity of the composite was considerably higher than the interstitial alloys without BN. At 25°C,

the resistivity of a 70 w/o TiB_2-30 w/o BN composite was 180 $\mu\Omega$-cm,[123] compared to only 15-28 $\mu\Omega$-cm for TiB_2 alone (Table 22). While the desired goal of corrosion resistance may have been attained, the considerable increase in elelctrical resistivity of the composite, as a result of the presence of BN, makes its use as a heater to vaporize aluminum impractical. In addition, the addition of BN resulted in reduced resistance to moisture. The moisture resistance was improved, however, when TiN was incorporated into the composite.[124]

As indicated in the example for the TiB_2-BN composite, improvement or change in one property of a material by composite formation can also result in undesired changes in other properties. In the case of the solid-electrolyte fuel cell, design of a composite to have suitable thermal-expansion properties may cause an unacceptable increase in the electrical resistivity or a reduced stability toward oxidation; it may be impractical to fabricate, by conventional techniques, a thin-film fuel cell using such a composite material. These factors all must be considered when such materials are considered for potential use in the solid-electrolyte fuel cell.

Perhaps the most promising area of use of composite and cermet refractories is for the anode in the molten-carbonate fuel cell. A number of the individual interstitial compounds of transition metals are being examined already for use as electrocatalysts in low-temperature aqueous fuel cell systems.[46,47] Similar work with boride and silicide

composites as anodes also has been reported. Cermets of noble and transition metals with carbides, oxides, and nitrides have shown promise as cathode materials.[126]

Refractory composites also have been used for electrolytic applications at high temperatures. Composites of 80 w/o TiB_2-20 w/o TiC and 95 w/o ZrB_2-5 w/o Mo were tested as cathodes in the electrolysis of cryolite melts for aluminum production.[127] (Electrical resistivities of TiB_2-TiC composites ranged from 62 to 125 $\mu\Omega$-cm at 1000°C.)[128] Composite cathodes of ZrB_2 and TiB_2 also were used in aluminum-reduction cells at 990° to 1010°C.[129] The corrosive nature of the melt in the aluminum cell parallels that of the molten-carbonate cell.

There is a vast number of possible combinations of interstitial alloys with each other and with suitable transition metals to form multicomponent systems with considerable promise in high-temperature fuel cells, especially the molten-carbonate fuel cell. Published research relative to this specific application, however, has been rather limited. There is a definite need to evaluate critically the most promising candidate materials for this application, in order to determine whether additional in-depth research in this area is warranted.

It is interesting to note that work of this nature has been reported just recently by the Institute of Gas Technology. Tungsten carbide is being explored (along with other materials) as a sintering inhibitor for the porous nickel or cobalt anodes of the molten-carbonate fuel cell.[130] Initial tests indicate

that ten w/o WC added to a cobalt anode results in an increase in the measured surface area. Electrochemical tests have not yet been conducted, however.

C. Oxide Ceramics

The oxide ceramics have received the most attention for use as MHD electrodes because of their inherent stability in an oxidizing environment at high temperatures. For discussion purposes, the oxides in this section of the report will be grouped into the following general categories: perovskites and pseudoperovskites, spinels, ZrO_2-based oxides, and other metal oxides.

1. Perovskites

The physical properties of perovskites used for MHD electrodes are listed in Table 28. Melting point data were not always available for many of the complex, multicomponent systems. However, since most of these materials were being used or tested at temperatures of 1500°C or higher, their metling points are at least greater than this. The rare-earth nickelates and cobaltates are exceptions, however, in that they are not stable at MHD-electrode temperatures. ($La_{0.5}Sr_{0.5}CoO_3$, for example, begins to decompose in air at 1200°C.)[144] The bulk of the electrical (d-c) conductivity data are reported for temperatures of 1000° and 727°C, to be representative of operating temperatures of the solid-electrolyte and molten-carbonate fuel cells, respectively.

The chromite-type oxides have received the most attention, with the major emphasis on $LaCrO_3$-based systems. Pure $LaCrO_3$ is not suitable for use at electrode use at MHD temperatures because

TABLE 28.--Select physical properties of perovskites and pseudo-perovskites

Oxide	Coefficient of Thermal Expansion (α), 10^{-6}/°C*	Electrical (d-c) Resistivity, Ω-cm	Temp., °C	-Log P_{O_2} (atm)	References
$LaCrO_3$	8.92 (25°-1,000°C)	1.4-10;1.1-8	727; 1,000	0	131-133
		16;15	727; 1,000	3	132
		27;10	727; 1,000	4	131
$LaCr_{0.5}Al_{0.5}O_3$	-	4	1,000	0.7+	4
$LaCr_{0.8}Co_{0.2}O_3$	11.5 (25°-1,000°C)	-	-	-	134
$LaCr_{0.5}Co_{0.5}O_3$	19.0 (25°-1,000°C)	-	-	-	4
$LaCr_{0.8}Ni_{0.2}O_3$	9.2 (25°-1,000°C)	-	-	-	4
$SmCrO_3$	-	10	1,000	0.7	4
$YCrO_3$	8.0 (25°-1,000°C)	0.36	1,000	0.7	133,135
		0.79	727	0.7	135
		1.8	1,000	est 5 (Ar)	135
		6.7	727	est 5 (Ar)	135
$NdCrO_3$	8.3 (25°-1,000°C)	4	1,000	0.7	4,133
$NdCrO_3$-CaO	-	0.25	1,300	0.7(?)	136
$La_{0.99}Sr_{0.01}CrO_3$	-	1.0	727- 1,000	0.7	132
$La_{0.98}Sr_{0.02}CrO_3$	-	0.25;0.28	727- 1,000	0	131
$La_{0.97}Sr_{0.03}CrO_3$	-	0.33	727- 1,000	0.7	132,137
$La_{0.94}Sr_{0.06}CrO_3$	-	0.22	727- 1,000	0.7	132
$La_{0.90}Sr_{0.10}CrO_3$	9.2 (50°-287°C)	0.32	727	2	132,137

TABLE 28.--Select physical properties of perovskites and pseudo-perovskites (Cont.)

Oxide	Coefficient of Thermal Expansion (α), 10^{-5}/°C*	Electrical (d-c) Resistivity, Ω-cm	Temp., °C	-Log P_{O_2} (atm)	Reference
$La_{0.87}Sr_{0.13}CrO_3$	-	0.12	727-1,000	0.7	131,134
$La_{0.84}Sr_{0.16}CrO_3$	10.9 (25°-1,000°C)	0.031;0.029	727;1,000	0	131,134
		0.10	727-1,000	0.7	132
$La_{0.80}Sr_{0.20}CrO_3$	-	0.06	727-1,000	0.7	132
$La_{0.84}Sr_{0.16}Cr_{0.75}Al_{0.25}O_3$	10.0 (25°-1,000°C)	-	-	-	134
$LaCrO_3$-8 m/o CaO	-	0.27	1,000	0.7	138
		0.39	727	0.7	138
$LaCrO_3$-24 m/o CaO	-	0.31	1,000	0.7	138
		0.26	727	0.7	138
$LaCrO_3$-32 m/o CaO	-	0.26	1,000	0.7	138
		0.30	727	0.7	138
$La_{1-x}Ca_xCrO_3$	-	0.32	727	2	137
$La_{0.92}Ba_{0.08}CrO_3$	10.3 (25°-1,000°C)	-	-	-	134
$La_{0.95}Mg_{.05}CrO_2$	8.8 (100°-1,400°C)	0.1 -0.27	1,000	0.7-5.2	139,140,4
		0.36 -0.40	600	0.7-5.2	140
		0.16 -0.13	1.000; 727	0.7-5.2	141
$La_{0.95}Mg_{0.05}Cr_{0.75}Al_{0.25}O_3$	9.9 (25°-1,000°C)	0.3 -0.42	1,000	0.7	4,142
	9.8 (25°-1,000°C)	0.46	727	0.7	142

TABLE 28.--Select physical properties of perovskites and pseudo-perovskites (Cont.)

Oxide	Coefficient of Thermal Expansion (α), 10^{-6}/°C*	Electrical (d-c) Resistivity, Ω-cm	Temp., °C	-Log P_{O_2} (atm)	References
$La_{0.95}Mg_{0.05}Cr_{0.5}Al_{0.5}O_3$	10.8 (25°-1,000°C)	1.0	1,000	0.7	4,142
	10.7 (25°-1,000°C)	1.5	727	0.7	142
$La_{0.95}Mg_{0.05}Cr_{0.25}Al_{0.75}O_3$	-	3.2	1,000	0.7	142
		5.6	727	0.7	142
$La_{0.95}Mg_{0.05}Cr_{0.75}Co_{0.25}O_3$	16.7 (25°-1,000°C)	-	-	-	143
$La_{0.95}Mg_{0.05}Cr_{0.5}Co_{0.5}O_3$	19.9 (25°-1,000°C)	-	-	-	143
$La_{0.95}Mg_{0.05}Cr_{0.25}Co_{0.75}O_3$	20.6 (25°-1,000°C)	-	-	-	143
$LaCr_{0.5}Co_{0.5}O_3$	19.0 (25°-1,000°C)	-	-	-	134
$LaCr_{0.95}Mg_{0.05}O_3$	-	0.13-0.14	1,000	0.7-5.2	140,141
		0.15-0.16	727	0.7-5.2	140
$LaCr_{0.85}Mg_{0.15}O_3$	9.3 (25°-1,000°C)	-	-	-	134
$LaCoO_3$	23 (25°-1,000°C)	0.001	750	0.7	143,144
$La_{0.5}Sr_{0.5}CoO_3$		0.001	1,000	0	4
		0.01	1,000	Vacuum	4
$LaNiO_3$	14.1 (25°-1,000°C)	-	-		4

TABLE 28.--Select physical properties of perovskites and pseudo-perovskites (Cont.)

Oxide	Coefficient of Thermal Expansion (α), 10^{-6}/°C*	Electrical (d-c) Resistivity, Ω-cm	Temp., °C	-Log P_{O_2} (atm)^2	References
$LaNi_{0.9}Co_{0.1}O_3$	14.9 (25°-1,000°C)	-	-	-	4
$La_{0.9}Co_{0.1}NiO_3$	14.5 (25°-1,000°C)	-	-	-	4
$La_{0.7}Sr_{0.3}MnO_3$	-	0.02	1,000	0.7	4
$YFeO_3$	11.0 (25°-1,000°C)	-	-		133
$LaFeO_3$	10.6 (25°-1,000°C)	-	-	-	133
$La_{0.9}Sr_{0.1}FeO_3$	-	0.017	727- 977	0.7	145
$La_{0.8}Sr_{0.2}FeO_3$	-	0.055	727- 977	0.7	145
$La_{0.5}Sr_{0.5}FeO_3$	-	0.0055	900	0.7	144
$La_{0.25}Sr_{0.75}FeO_3$	-	0.014	800-1,000	0.7	146
$(La_{0.75}Sr_{0.25})Fe_{0.5}Cr_{0.5}O_3$	-	0.0046	1,027	0.7	146
$Y_{0.95}Ca_{0.05}FeO_{3-y}$	10.7-11.8 (25°-1,1100°C)	0.074	1,000	0.7-5.2	147
	3 ranges)	0.086	727	0.7-5.2	147
$Y_{0.90}Ca_{0.10}FeO_{3-y}$	-	0.064	1,000	0.7	147
		0.084	727	0.7	147
		0.14;0.11	727;1,000	3.0-5.2	147
$Y_{0.85}Ca_{0.15}FeO_{3-y}$	10.8-12.0 (20°-1,100°C; 3 ranges)	0.074	727-1,000	0.7-5.2	147

TABLE 28.--Select physical properties of perovskites and pseudo-perovskites (Cont.)

Oxide	Coefficient of Thermal Expansion (α) 10^{-6}/°C*	Electrical (d-c) Resistivity, Ω-cm	Temp., °C	-Log P_{O_2} (atm)	References
$Y_{0.70}Ca_{0.24}Fe_{0.90}Zr_{0.10}O_{3-y}$	- -	0.26;0.20	727;1,000	0.7	147
		0.44;0.30	727;1,000	3	147
		0.44;0.47	727;1,000	5.2	147
$Y_{0.68}Ca_{0.32}Fe_{0.80}Zr_{0.20}O_{3-y}$	10.6-12.1(20°-1,100°C; 3 ranges)	0.066;0.046	727;1,000	0.7	147
		1.3;0.09	727;1,000	3	147
		1.5;1.0	727;1,000	5.2	147

* In air.

+ Air.

of volatilization of chromium oxides [e.g., CrO_3, CrO_2, and $CrO_2(OH)$]. While the electrical conductivity is essentially wholly electronic ($t_i > 0.995$ at 980°C),[132] it also shows a strong P_{O_2} dependency. The increase in resistivity under reducing conditions is thought to result from the formation of triply-ionized chromium vacancies.[132] The substitution of La^{+3} by divalent cations such as Mg^{+2}, Ca^{+2}, Sr^{+2}, and Ba^{+2}, however, leads to a substantial increase in the electrical conductivity (p-type) by the formation of Cr^{+4} for charge compensation.[131] The electrical resistivities of alkaline-earth-doped $LaCrO_3$ show only a slight P_{O_2} and temperature dependency, as can be seen by the data in Table 28.

When a portion of the Cr^{+3} in $LaCrO_3$ is replaced by Al^{+3}, the desired reduction of the volatilization of chromium oxides is obtained;[142,143] unfortunately, it also causes an increase in the electrical resistivity. However, the resistivity remains more than adequate to meet MHD-electrode requirements of less than ten Ω-cm. The Al^{+3} substitution has a second effect upon the physical properties of doped-$LaCrO_3$ in that the coefficient of thermal expansion is increased. In addition, the destructive rhombohedral-to-orthorhombic phase transformation is eliminated in the 25° to 1000°C temperature range.[4]

In evaluation of the oxides of Table 28 for possible use in the high-temperature solid-electrolyte fuel cell, it can be seen that virtually all the materials have electrical resistivities which are compatible with the requirement of 50 Ω-cm for the

interconnector (Table 2). However, potential interconnector candidates must be primarily electronic conductors and simultaneously must be stable under both severe reducing conditions (P_{O_2} = 10^{-16} to 10^{-18} atm) as well as an air environment at 1000°C. Not all of the oxides of Table 28 have been examined at such low values of P_{O_2}, nor have transference measurements been carried out for many of them. The P_{O_2} dependence of conductivity for a number of the perovskites, however, suggests the presence of an undesirable ionic contribution. In addition, the candidate oxide must have a coefficient of thermal expansion which closely matches that of the Y_2O_3-stabilized ZrO_2 electrolyte of 10 x 10^{-6}/°C.

With these needs in mind, researchers at Westinghouse evaluated many perovskites for possible interconnector use. The most promising candidate was doped, substituted-$LaCrO_3$. By adjusting the Al^{+3} content, a very close thermal expansion match was obtained with adequate electrical conductivity at a composition of $La_{0.95}Mg_{0.05}Cr_{0.75}Al_{0.25}O$. The physical and chemical properties of this material have subsequently been studied extensively by Westinghouse. It now appears that the Mg^{+2} substitutes for Cr^{+3} rather than the La^{+3} and that only about half the Mg^{+2} added in the above compsosition actually goes into solid solution.[149] In other words, there appears to be evidence for second-phase formation, where excessive MgO exsolves.

At a low P_{O_2}, loss of O_2 from $La_{0.95}Mg_{0.05}Cr_{0.75}Al_{0.25}O_3$ become pronounced at 10^{-18} atm. Under these conditions, oxygen

vacancies are formed and the electrical resistivity increases. There is concern that oxygen transport (leakage) then could occur as a result of ionic conduction during operation of the solid-electrolyte fuel cell, which would affect the performance adversly. This process is under study by R. Ruka at Westinghouse in relation to possible deleterious long-term effects upon the performance of their thin-film solid-electrolyte battery.[134]

In their overall physical properties, the Mg^{+2}- and Sr^{+2}-doped $LaCrO_3$s have the most promise of the perovskites of Table 28 for use as interconnector material for the high-temperature solid-electrolyte fuel cell. The rare-earth colbaltates and nickelates are not expected to be stable under the reducing conditions of the anode side of the fuel cell. The equilibrium P_{O_2} for CoO and NiO, for example, is greater than that of the fuel (Table 7), so that formation of elemental Co and Ni would probably result at 1000°C for $LaCoO_3$ and $LaNiO_3$, according to the reaction:

(24) $2LaMO_3 + 3H_2 \rightarrow La_2O_3 + 2M + 3H_2O(g)$,

where M is a metal cation. This is an approximation, of course, as the free energy of formation of $LaCoO_3$ will be more negative than the sum of the component oxides as a result of compound formation. The equilibrium P_{O_2}, under these conditions, would be less than that indicated in Table 7. Lacking ΔG^o_f data for $LaCoO_3$ and $LaNiO_3$ at 1000°C, the P_{O_2} for reaction 24 was not calculated for fuel cell conditions.

Similar arguments apply for the case of the stability of fer-

rites in a strongly reducing environment, although the rare-earth ferrites have a much greater thermal stability than the corresponding nickelates and colbaltates.[145]

In comparison to the non-oxide ceramics previously discussed, the electrical resistivities of the conducting perovskites are orders of magnitude greater. Their lower conductivities makes the perovskites unattractive for possible use as anode materials in the solid-electrolyte fuel cell. This is aggravated, as discussed above, by the instability problems of certain perovskites under extremely reducing conditions. Of course, these materials could be reduced deliberately to form a metal cermet, much as is now done by Westinghouse with a sintered $NiO-ZrO_2$ mixture to form the fuel cell anode. In the case of $LaCoO_3$ or $LaNiO_3$, for example, a Co- or $Ni-La_2O_3$ cermet would form (see equation 24). This offers no advantages, however--indeed, it profers disadvantages--and would be more costly than the technique presently used.

The potential for using the conducting perovskites as anodes or cathodes in the molten-carbonate fuel cell is more limited than in the solid-electrolyte fuel cell by the high probability for chemical reaction. As the molten carbonate is basic, basic and amphoteric metal oxides offer the best chance for compatibility. An alternate possibility is to use the oxide in the form of the final reaction-product, so that the likelihood of further reaction is reduced substantially. This is the rationale by which $LiAlO_2$--the product of reaction of Al_2O_3 and the carbonate

melt--was chosen as the preferred tile matrix in the current molten-carbonate fuel cell program.

While a number of the conducting perovskites have been subjected to corrosion tests in the molten coal slag (as would be experienced by the electrodes in the MHD channel), there has been only a limited amount of compatibility testing with molten-carbonate melts. In one test, a doped chromite of composition $La_{0.84}Ca_{0.16}CrO_3$ was found to react with molten K_2CO_3 at 925°C.[150] The apparent reaction was between the carbonate and the chromite portion of the oxide (La_2O_3 and CaO do not form stable oxyanion compounds)

$$(25)\quad 2La_{0.84}Ca_{0.16}CrO_3 + 2K_2CO_3(\ell) + 1.42O_2 \rightarrow 2K_2CrO_4(\text{soln.}) + 0.84La_2O_3 + 0.32CaO + 2CO_2(g).$$

Thus, perovskite chromites do not appear to be compatible with the molten-carbonate melt. Even if corrosion is not a problem, the higher electrical resistivity of the conducting perovskites makes them uncompetitive with the nickel and cobalt anodes (and alloys thereof) currently used.

In addition to selective doping of $LaCrO_3$ to improve its properties for MHD-electrode use, formation of $LaCrO_3$ cermets has also been explored. Addition of chromium to $LaCrO_3$ increases the electrical conductivity and the resulting cermet has a high resistance to oxidation. Representative electrical resistivity data for Cr-$LaCrO_3$ cermets are shown in Table 29. Cermets of this type would offer no advantage over the less expensive and more easily fabricated Ni-ZrO_2 cermet for anode use in the solid-

TABLE 29.--Electrical resistivities of $LaCrO_3$-Cr cermets at 1027°C [138]

Cr Content of Cr-$LaCrO_3$ Cermet, w/o	Electrical (d-c.) Resistivity, Ω-cm
0	1.0
20	1.5×10^{-2}
30	4.1×10^{-4}
40	1.3×10^{-4}
50	1.0×10^{-4}
60	2.8×10^{-5}
70	1.9×10^{-5}
80	1.6×10^{-5}

electrolyte fuel cell, or over the nickel or cobalt plaques in the molten-carbonate fuel cell.

The rare-earth nickelates and cobaltates of Table 28 which do not appear suitable for use as anodes in the solid-oxide fuel cell perform quite well as cathodes. Brown, Boveri, and Cie have reported success in using plasma-sprayed cathodes of Bi-doped $LaNiO_3$ in cells operating at 1000°C for over four years.[48] Plasma-sprayed Sr-doped $LaMnO_3$ and $LaCoO_3$ also are efective air electrodes. While $PrCoO_3$ shows a nigh electronic conductivity, it tends to scale from the electrolyte surface, most likely because of the incompatibility in the coefficients of thermal expansion of the two materials.

Even though the rare-earth colbaltates, nickelates, and manganates have adequate electrical conductivity for use as cathode materials, their thermal expansion characteristics are not compatible with that of the Y_2O_3-stabilized ZrO_2 electrolyte, which has a lower α. These materials would appear promising candidates for the cathode in the molten-carbonate fuel cell (where thermal expansion properties are not as critical), provided they are not reactive with the melt. Increasing the electronic component of conductivity of these materials would make them even more attractive as cathode materials. This area of research merits further attention.

The Sr-doped, Cr-substituted $YFeO_3$ (Table 28) has electrical and thermal expansion properties which make it promising as a possible cathode material for the solid-oxide fuel cell using a

ZrO_2 electrolyte. No tests of this nature have been reported yet, however. One area of concern is the long-term chemical compatibility of the ZrO_2 and ferrite. The high mobility of Fe^{+3} could result in degradation of cell performance as a result of increased interfacial resistance caused by Fe^{+3} diffusion. A diffusion coefficient of iron, D_{Fe}, in Fe_3O_4 of 8.3×10^{-11} cm^2/sec ast 1027^oC has been reported at a P_{O_2} of 10^{-10} atm, increasing to $3.6 \times 10^{-9} cm^2/sec$ at a P_{O_2} of 10^{-6} atm.[151]

The two oxides (non-perovskites) which have received the most attention at Westinghouse for cathodes in the solid-oxide fuel cell are Sb-doped SnO_2 and Sn-doped In_2O_3.[152] The electrical and thermal expansion properties of these oxides are compared in Table 30. The severe thermal expansion mismatch of the Sb-doped SnO_2 made its use as cathode material impractical, even though it has a high electrical conductivity. Sn-doped In_2O_3 has a higher conductivity and a value of α which is more compatible with the ZrO_2 electrolyte. It has been successfully tested as a cathode in the solid-oxide fuel cells at 1000^oC for 1100 hours.[152]

While the Sn-doped In_2O_3 is a better conductor than the rare-earth nickelates, colbaltates, and manganates and has much better thermal expansion properties, problems can result when it is used alone as the cathode. Because it is an almost purely electronic conductor, it must be porous to allow rapid mass transfer at the three-phase interface (air, cathode, and electrolyte).[154,155] At high current densities, oxygen diffusion through the porous film can become the rate-limiting step in the electrochemical process,

TABLE 30.--Electrical conductivity and thermal-expansion properties of Doped SnO_2 and In_2O_3 at 1000°C

Oxide	Form	Coefficient of Thermal Expansion (α), $10^{-6}/°C$	Electrical (d-c) Resistivity, Ω-cm	References
SnO_2-3w/o Sb_2O_5*	CVD Film	5.0	1.3×10^{-3}	4,65
In_2O_3-2.4w/o SnO_2	Sintered bar	8.95	1.5×10^{-3}	65
(In_2O_3-2.4w/o SnO_2) + 2w/o kaolin+	Sintered bar	9.23	-	65
In_2O_3-2.4w/o SnO_2	CVD film	-	0.6×10^{-3}	65

* Sb_2O_4 is the actual stable SbO_x phase under firing conditions.[153]

\+ Kaolin added as a sintering aid.

resulting in severe electrode polarization. By incorporation of a highly-conducting perovskite (e.g., $LaNiO_3$, $PrCoO_3$, etc.) into the In_2O_3 cathode structure, however, the electrochemical reduction of oxygen can take place at the two-phase interface between the air and the cathode, because the mixed conductivity of the perovskite phase now permits oxide-ion mobility.

The development of a better, mixed-conducting cathode material based on perovskite-type oxides merits further research for improving the electron and mass-transfer processes during oxygen reduction, thereby reducing polarization losses.

2. Spinels

A number of the spinel oxides have been studied for use as MHD electrodes. The physical properties of these materials are presented in Table 31. In general, the spinels have considerably lower electrical resistivities and coefficients of thermal expansion than perovskites.[133]

A number of the spinels have electrical conductivities high enough for use as interconnector material in the high-temperature solid-oxide fuel cell. The bulk of the spinels, however, are mixed conductors, which would predicate against their use for this purpose. The coefficients of thermal expansion also are less than that for the ZrO_2 electrolyte. Only $CoCr_2O_4$ of the spinels of Table 31 has been studied as a possible interconnector, and that was years ago before the improved perovskites were developed.[156] As might be expected, the results were not encouraging.

TABLE 31.--Select physical properties of spinels

Oxide	Coefficient of Thermal Expansion (α), $10^{-6}/°C$*	Electrical (d-c) Resistivity, Ω-cm	Temp., °C	-Log P_{O_2} (atm)	References
$CoCr_2O_4$ (48% T.D.)†	7.28 (25°-1,000°C)	22	1,000	0.7+	133,156
		0.002	1,000	14	156
$CoCr_2O_4$-1 m/o V(64% T.D.)	-	15	1,000	0.7	156
$CoCr_2O_4$-2 m/o V(70% T.D.)	-	10	1,000	0.7	156
$CoCr_2O_4$-2 m/o Mn	-	6	1,000	0.7	156
		50	1,000	14	156
$NiAl_2O_4$-15 m/o Fe_3O_4 (87% T.D.)	-	17;7.7	727;1,000	0.7	157
		12;3.2	727;1,000	3-5.3	157
Fe_3O_4	-	0.0054	727-1,000	?	158
		0.004	1,227	4	159
Fe_3O_4-29.5 m/o Co_3O_4		2.6;0.14	727;1,000	3-5.3	160
$MgCr_2O_4$	7.08 (25°-1,000°C)	5.0;3.0	727;1,000	0.7-5.2	133,161,162
$MgCr_2O_4$- 20 m/o Fe_3O_4	-	24 ;4.3	727;1,000	3-5.2	160
$MgCr_2O_4$- 33 m/o Fe_3O_4	-	13 ;1.0	727;1,000	3-5.2	160
$MgAl_2O_4$-10 m/o Fe_3O_4 (82.7% T.D.)	-	555 ;143	727,1,000	0.7	163
		400 ;115	727;1,000	3	163
		263 ;103	727;1,000	5.3	163
$MgAl_2O_4$- 15 m/o Fe_3O_4 (80.[illegible] T.D.)		204 ;50	727;1,000	0.7-3	163
		250 ;71	727;1,000	5.3	163
$MgAl_2O_4$-20 m/o Fe_3O_4	-	19	1,000	3-5.2	160
$MgAl_2O_4$-25 m/o Fe_3O_4	9.7 (100°-1400°C)	26	1,000	2-5.2	160
		5.6;1.7	600;1,000	0.7	141
		1.6	1,000	3-5.2	141

TABLE 31.--Select physical properties of spinels (Cont.)

Oxide	Coefficient of Thermal Expansion (α), 10^{-6}/°C*	Electrical (d-c) Resistivity, Ω-cm	Temp., °C	-Log P_{O_2} (atm)	References
($MgAl_2O_4$-25 m/o Fe_3O_4) + 40 w/o Cr	-	0.0032	727-1,000	0.7 (?)	164
$FeAl_2O_4$-8.3 m/o $MnAl_2O_4$	-	19 ;3.1	727;1,000	0.7	163
		4.3 ;1.4	727;1,000	5.3	163
$FeAl_2O_4$-25 m/o Fe_3O_4	9.0 (100°-1400°C)	1.0 ;0.22	600;1,000	0.7	141
		0.24;0.05	600;1,000	3-5.2	141
$FeAl_2O_4$- 27 m/o Fe_3O_4	-	0.081	1,227	8	145
$FeAl_2O_4$-75.5 m/o Fe_3O_4	-	0.0081	1,227	8	145

* In air.

‡ T.D = theoretical density.

+ Air.

The hercynite ($FeAl_2O_4$) spinels have the lowest electrical resistivities, but are limited in their stability under varying reducing conditions. The resistivities of these materials show a strong P_{O_2} dependency. At low values of P_{O_2}, reduction of Fe^{+3} to Fe^{+2} increases the concentration of current carriers via electron "hopping" between the two oxidation states of iron. The equilibrium P_{O_2} for the various oxides of iron are listed in Table 32 for temperatures of 1300 and 900K.

At a P_{O_2} of 10^{-16} to 10^{-18} atm at the anode of a fuel cell operating at 1300K Fe_3O_4 would not be stable toward reduction to Fe. This would rule out the use of Fe_3O_4-containing mixtures as possible fuel electrodes in the solid-electrolyte fuel cell. In comparison at 900K Fe_3O_4 would be the thermodynamically stable phase which, in theory, would allow hercynite-Fe_3O_4 mixtures to be used as anodes in the molten-carbonate fuel cell. Even if there were no chemical compatibility problems, it does not appear likely that such materials would be considered seriously for use as fuel electrodes in such cells, as the electrical resistivities are at least two orders of magnitude greater than the nickel and cobalt anodes currently used.

While several of the Fe_3O_4-containing oxides have low electrical resistivities under reducing conditions, their much higher values under more oxidizing conditions precludes their consideration as possible air electrodes for high-temperature fuel cells. The thermodynamically-stable oxide of iron in air at 900 and 1300K is Fe_2O_3, which is a poor electronic conductor.

TABLE 32.--Equilibrium P_{O_2} for iron oxide mixtures*

	Temp., K	-Log P_{O_2} (atm)
$Fe-Fe_{0.95}O$	1300	15.1
	900	23.9
$Fe_{0.95}O-Fe_3O_4$	1300	13.1
	900	23.6
$Fe_3O_4-Fe_2O_3$	1300	1.48
	900	13.3

*Thermodynamic data from Reference 61 used for calculation purposes.

In short, none of the spinels of Table 31 appear to offer any promise for possible use in the solid-electrolyte or molten-carbonate fuel cell when compared to more suitable, alternate materials.

3. ZrO_2-Based Oxides

In addition to the perovskites, ZrO_2-based oxides also have received considerable attention for use as MHD electrodes because of high-temperature stability of ZrO_2. However, since it is an ionic conductor, doping with various rare-earth oxides (mainly CeO_2) is necessary to impart the desired electronic conductivity and to avoid electrolysis problems. The physical properties of ZrO_2-based oxide systems examined for MHD electrodes are presented in Table 33.

Compared to the perovskites and spinels, the ZrO_2-based oxides have electrical resistivities which are considerably higher. These materials also exhibit mixed conduction, which is dependent upon the P_{O_2} of the surrounding atmosphere. In many cases, the ionic transport numbers vary considerably with temperature.[162] Except for Y_2O_3-doped ZrO_2--the preferred solid electrolyte for high-temperature fuel cell use--the oxides of Table 33 do not appear to have suitable application in either the solid-electrolyte or the molten-carbonate fuel cell The electrical and thermal expansion properties are not compatible with the requirements of the electrode or interconnector.

III. MHD INSULATOR MATERIALS

A number of materials have been examined for use as interelectrode insulators in the MHD channel. Generally, they have been the refractory oxides or oxide composites. Because they are insula-

TABLE 33.--Select physical properties of ZrO_2-based oxide systems

Oxide	Coefficient of Thermal Expansion (α), 10^{-6}/°C*	Electrical (d-c) Resistivity, Ω-cm	Temp., °C	-Log P_{O_2} (atm)	References
ZrO_2-12 m/o Y_2O_3	10.9 (25°-1,000°C)	17	1,000	0.7+	4,165
		185	727	0.7	165
		17	1,000	6	165
		161	727	6	165
ZrO_2-42 m/o $PrO_{1.83}$	-	~ 1	1,400	0.7	166
ZrO_2-68 m/o $PrO_{1.83}$	-	~ 1	1,400	0.7	166
ZrO_2-18 m/o CeO_2	11.5 (100°-1,400°C)	670	1,000	0.7	165,167
		$5.3x10^3$	727	0.7	165,167
		330	1,000	6	165,167
		$2.5x10^3$	727	6	165,167
ZrO_2-30 m/o CeO_2	-	100	1,000	0.7	166
ZrO_2-50 m/o CeO_2	12.2 (100°-1,400°C)	143	1,000	0.7	165,167
		10^4	727	0.7	165,167
		42	1,000	6	165,167
		910	727	6	165,167
ZrO_2-75 m/o CeO_2	13.2 (100°-1,400°C)	26	1,000	0.7	165,167
		10^3	727	0.7	165,167
		5	1,000	6	165,167
		110	727	6	165,167
ZrO_2-78 m/o CeO_2-2 m/o Ta_2O_5	13.6 (100°-1,400°C)	7	1,000	0.7	165,167

TABLE 33.--Select physical properties of ZrO_2-based oxide systems (Continued)

Oxide	Coefficient of Thermal Expansion (α), 10-6/°C*	Electrical (d-c) Resistivity, Ω-cm	Temp., °C	-Log P_{O_2} (atm)	References
	-	450	727	0.7	165,167
		12	1,000	6	165,167
		77	727	6	165,167
ZrO_2-12 m/o CeO_2-3 m/o Y_2O_3	-	23	1,000	0.7	166
		250	727	0.7	166
ZrO_2-10 m/o La_2O_3-10 m/o CeO_2	-	320	1,027	0.7	138
ZrO_2-20 m/o La_2O_3-10 m/o CeO_2	-	320	1,027	0.7	138
ZrO_2-10 m/o La_2O_3-20 m/o CeO_2	-	100	1,027	0.7	138
ZrO_2- 5 m/o La_2O_3-15 m/o CeO_2	-	79	1,027	0.7	138
ZrO_2-10 m/o Nd_2O_3-10 m/o CeO_2		28	1,027	0.7	138
ZrO_2-10 m/o Nd_2O_3-20 m/o CeO_2	-	48	1,027	0.7	138
ZrO_2-20 m/o Nd_2O_3-20 m/o CeO_2	-	63	1,027	0.7	138

* In air

+ Air

tors, these materials would have no application as active components in the solid-electrolyte fuel cell. They would have potential use, however, as tile candidates in the molten-carbonate fuel cell. A listing of materials used for considered as MHD electrode insulators is presented in Table 34.

All these materials have melting points (or dissociation temperatures, for the nitrides) above 1500°C; therefore, no problems are anticipated in their potential use as tiles in the molten-carbonate fuel cell at 600° to 750°C. The electrical resistivities at 1000°C are more than adequate for tile use, also being generally greater than $10^3\ \Omega$-cm. The primary area of concern regarding the suitability of the materials of Table 34 for tile use is their chemical and electrochemical compatibility with the carbonate melt.

Both BN and Si_3N_4 suffer from low resistance to moisture, which would reduce their usefulness as tiles at the fuel electrode side. Over long periods of cell operation, oxidation of Si_3N_4 could occur slowly at the cathode side of the fuel cell. This oxidation would be accelerated by the fluxing action of the basic carbonate solution. These potential problems appear to rule out the use of BN and Si_3N_4 as tiles. SiO_2-containing materials such as SiAlON, $3Al_2O_3 \cdot 2SiO_2$, and $2MgO.2SiO_2$ do not appear suitable for the use, as well, because of the reactivity of the SiO_2 portion of these ceramics with the molten carbonate to form silicate :

(26) $SiO_2(s) + M_2CO_3(\ell) \rightarrow M_2SiO_3(soln.) + CO_2(g)$

MgO has been used in the past in sintered form as tile material and in powdered form to form a paste for containment of the carbon-

TABLE 34.--Materials used or considered for MHD electrode insulators

Material	Reference
Nitrides	
BN	2,168,169
Si_3N_4	2,138
SiAlON	1,162
Perovskites	
$SrZrO_3$	170
$CaZrO_3$	2
$Sr_{0.97}La_{0.02}ZrO_3$	170
$SrHfO_3$	2
$CaHfO_3$	2
$LaAlO_3$	171
$SrZrO_3$-14 m/o CeO_2	137
$SrZrO_3$- 6 m/o $SrTiO_3$-1.5 m/o Ta_2O_5	137
Spinels	
$MgAl_2O_4$	172,173
Other Oxides	
Al_2O_3	2
MgO	2,165
ZrO_2	?
ThO_2	2
$3Al_2O_3 \cdot 2SiO_2$	1
$2MgO \cdot 2SiO_2$	1
CeO_2-82 m/o HfO_2	174

ate electrolyte.[69] The MgO was not sufficiently inert, however, for long cell lifetimes. Work at the National Bureau of Standards has shown that MgO forms a eutectic with K_2CO_3 at 2 m/o and 896°C.[137]

$MgAl_2O_4$ spinel (MgO combined with Al_2O_3) has shown good resistance to molten coal slag-seed mixtures.[175] $MgAl_2O_4$ recently was examined by General Electric Company as a possible tile material in part of its molten-carbonate research program. Powdered $MgAl_2O_4$ appeared to react with a melt of 62 m/o Li_2CO_3-K_2CO_3 at 640°C in a CO_2-enriched air atmosphere after two hours. The following reaction was presumed to occur:

(27) $MgAl_2O_4(s) + Li_2CO_3(\ell) \rightarrow MgO(s) + 2\ LiAlO_2(s) + CO_2(g)$

This was confirmed by X-ray diffraction analysis of the sample afterward, which showed the presence of $LiAlO_2$ and the absence of $MgAl_2O_4$.

These results are somewhat surprising, as the calculated free energy of reaction for equation 27 is +21,608 cal/mole $MgAl_2O_4$ at 900K.[61] This corresponds to an equilibrium constant of only 5.65×10^{-6}, which approximated the P_{O_2} (in atm) for this reaction. The P_{O_2} was not specified for the test, but was certainly greater than the above value, which should have prevented reaction (26) from taking place. As no lines of MgO were reported in the diffraction pattern, perhaps the reaction which actually occurred was not the one written in equation (27); this could explain the apparent discrepancy between the observed and predicted behavior of $MgAl_2O_4$ with the carbonate melt. Other alkaline-earth spinels of Al_2O_3 may be more corrosion resistant to the carbonate melt.

Similar corrosion tests in the Li_2CO_3-K_2CO_3 eutectic are currently underway at MERDI, with nonstoichiometric $MgAl_2O_4$ spinels as well as other candidate tile materials as part of the current fuel cell contract. In the MERDI tests, however, high-density crucibles of the test materials are being used initially in an atmosphere of CO_2 at a temperature of 727°C. (Subsequent tests with powdered samples are planned also.) Preliminary tests with crucibles of pure MgO, 65 m/o MgO-Al_2O_3, 35 m/o MgO-Al_2O_3, and $MgAl_2O_4$, indicate that the corrosion rate is lowest when nonstoichiometric $MgAl_2O_4$ spinels are employed; i.e., when either excess Al_2O_3 or MgO is present.[80] The disagreement between test results by General Electric and MERDI on the corrosion behavior of $MgAl_2O_4$ is probably a result of the high-density samples used in the latter case. Finely divided Al_2O_3, for example, is quite reactive to molten carbonate while high-density Al_2O_3 is relatively inert.

ZrO_2 has been examined as a support material for the molten-carbonate fuel cell, but was found to exhibit a chemical stability which was dependent upon the P_{O_2}. This could cause problems during actual fuel cell operation.[69]

While data for the chemical compatibility of ThO_2 with molten carbonates do not appear to have been published, its radioactivity would make it less than desirable for tile use.

No corrosion data on molten carbonates was found for the remaining oxides of Table 34. The hafnates and zirconates, however, would appear to be promising test candidates for electrolyte-support materials, as they would be the final products of reaction between

the parent oxides (HfO_2 and ZrO_2) and the carbonate melt. This is analogous to the present use of $LiAlO_2$ for tiles in the molten-carbonate cell by reaction of Al_2O_3 and Li_2CO_3.[64] Once the $LiAlO_2$ has formed, further reaction does not occur. Thus, molten-carbonate corrosion studies of the alkaline-earth zirconates and hafnates appear merited.

The preferred molten-carbonate electrolyte is an eutectic mixture of 62 m/o Li_2CO_3 and 38 m/o K_2CO_3, with a melting point of 491°C.[64] There is the possibility of metathesis reactions taking place between zirconates, for example, and the components of the molten-carbonate melt:

(28) $MZrO_3(s) + Li_2CO_3(\ell) \rightarrow Li_2ZrO_3(s) + MCO_3(s)$

where M is an alkaline-earth metal. At fuel cell temperatures of 670°C, the alkaline-earth carbonate would begin to decompose

(29) $MCO_3(s) \rightarrow MO(s) + CO_2(g)$,

so that a mixture of alkaline-earth oxide and alkali zirconate would result. There is considerable question, however, as to the stability and solubility of alkali zirconates in the molten carbonate environment. If stable, solid reaction products are formed, the rate of corrosion may slow or stop after a short period of time, so that even slightly reactive oxides may be suitable for electrolyte-support use.

TiO_2, like the other dioxides of the titanium family, formes oxy-anion complexes with basic oxides. The titanates differ from the zirconates and hafnates, however, in the ease in which lower-valent titanium is formed. ZrO_2 and HfO_2 do not form stable lower oxides under normal circumstances. Formation of Ti^{+3} under reducing con-

ditions would introduce unwanted electronic conductivity into the oxide by electron exchange between Ti^{+3} and Ti^{+4} in the crystal lattice. Reduced $SrTiO_3$, for example, is semiconducting.[176]

Thus, for good insulating properties under the P_{O_2} gradient to which the tile is exposed during normal fuel cell operation, oxides which readily assume multivalent oxidation states should be avoided. This would include oxides of Ti, V, Nb, Cr, Mo, W, Mn, and Sn--all of which form oxyanion compounds. Except for the titanates, niobates, and some stannates, these oxyanion compounds have limited thermal stability as well.

Calculation of the equilibrium P_{O_2} for the Ti_2O_3-TiO_2 couple yields a value of 2.1×10^{-34} atm at 900K.[61] Similarly, P_{O_2} for the NbO_2-Nb_2O_5 couple is found to be 3.4×10^{-29} atm. This would indicate that the lower oxides of titanium and niobium would not be stable at the P_{O_2} of 10^{-16} atm expected at the fuel electrode. However, the probability of the formation of oxygen vacancies under reducing conditions is high, and this likewise would reduce the insulating qualities of these materials and make them less suitable as cndidates for tiles in the molten carbonate fuel cell.

In comparison, tantalum does not form lower oxides, even under severely reducing conditions. Thus, alkaline-earth and possibly alkali tantalates may insulate sufficiently to merit consideration as electrolyte-containment material.

Other perovskites potentially suitable for tile use are the rare-earth aluminates. As with the zirconates and hafnates, there is the possibility of metathesis reactions occurring

(30) $2LaAlO_3(s) + Li_2CO_3(\ell) \rightarrow 2LiAlO_2(s) + La_2O_3(s) + CO_2(g)$

Lacking thermodynamic data for $LaAlO_3$, however, it is not possible to calculate if the ΔG_f^o of reaction is favorable or not. Thus, direct experimental testing of these materials is necessary to determine compatibility with molten carbonates.

It is important to note that the rate of corrosion of ceramics by molten carbonates can be accelerated greatly in the presence of an applied d-c field. A material which may be apparently inert to the molten carbonate under emf-free conditions can experience catastrophic failure in the presence of an imposed emf.[177] The corrosion rate of MgO in molten K_2SO_4, for example, is increased by two orders of magnitude in the presence of an applied d-c field.[178] Thus, any realistic screening program for material compatibility with the molten-carbonate electrolyte should incorporate testing in the presence of an applied emf of magnitude comparable to that expected under typical fuel cell operating conditions.

SUMMARY AND CONCLUSIONS

I. SOLID-ELECTROLYTE FUEL CELL

A. Electrolyte

A number of oxide-ion conductors were evaluated as solid electrolyte to establish a reference point for comparison of other compatible materials for ancillary components in the high-temperature solid-oxide fuel cell. It was concluded that ZrO_2-10 m/o Y_2O_3 is the preferred electrolyte for use in the fuel cell at a temperature of 1000°C, as it has been studied the most extensively for this application and its long-term behavior under fuel cell conditions is defined more completely.

A number of other oxides, such as doped-CeO_2 and substituted perovskites (e.g., aluminates, titanates, and bismuthates) show considerable promise for use as solid electrolytes at temperatures as low as 700°C. Additional research is needed, however, before these mixed conductors can equal Y_2O_3-stabilized ZrO_2 in electrochemical performance. At such time, the MHD literature can be re-evaluated to identify materials compatible for use with these improved oxides.

B. Interconnector

A variety of MHD-electrode materials were examined for possible use as interconnectors in the solid-electrolyte fuel cell. The carbides, nitrides, silicides, and borides are not suitable because of their poor oxidation resistance at the air side of the interconnector.

The bulk of the spinels examined are mixed conductors and exhibit a strong P_{O_2} dependence in electrical conductivity, which makes them

unsuitable for interconnector use. Only $CoCr_2O_4$ has been studied as an interconnector, and its performance was not entirely satisfactory. The electrical properties of ZrO_2-based oxides also do not meet the interconnector requirements. Of the perovskites, Mg- and Sr-doped $LaCr_{1-x}Al_xO_3$ have the best overall physical properties for use as interconnectors. Westinghouse presently is using the composition $La_{0.95}Mg_{0.05}Cr_{0.75}Al_{0.25}O_3$ as the interconnector in their thin-film solid-electrolyte battery, because its coefficient of thermal expansion is compatible with that of the Y_2O_3-stabilized ZrO_2 electrolyte and its electrical properties are not significantly temperature and P_{O_2} dependent.

C. Cathode

As was noted for the interconnector, carbides, nitrides, silicides, and borides are not suitable for use as cathodes because of the incompatible oxidizing environment. However, a number of the rare-earth nickelates, cobaltates, and manganates, have been operated successfully as air electrodes in solid-electrolyte fuel cells. These materials have adequate electrical conductivity, but their thermal expansion properties do not match those of Y_2O_3-stabilized ZrO_2. These perovskite mixed-conductors are best used in the solid-electrolyte fuel cell by incorporation into the air electrode to increase oxygen ion mobility and thus reduce cathode polarization.

Sr-doped, Cr-substituted $YFeO_3$ has electrical and thermal-expansion properties which appear promising as a potential cathode material. The expected high mobility of iron, however, may pose chemical compatibility problems with the electrolyte of the fuel cell

over long periods of operation.

None of the spirels and ZrO_2-based oxides examined appear suitable for use as cathodes when compared to the current choice of Sn-doped In_2O_3.

D. Anode

Metals and non-oxide ceramics appear to have the best promise for use in the solid-electrolyte fuel cell as anodes.

1. Metals

Of the metals used for MHD electrodes, nickel and cobalt and perhaps some of their alloys would be suitable for use as anodes in the solid-electrolyte fuel cell. These materials are being used already for this application in the form of ZrO_2-metal cermets.

2. Non-Oxide Ceramics

Table 35 lists the best non-oxide ceramics in each category for key materials properties (electrical conductivity, thermal expansion, and thermodynamic stability toward oxidation) for consideration as anode components in the solid-electrolyte fuel cell. No single compound in each category meets all of the key materials properties requirements necessary for optimum anode use The non-oxide ceramics have the best potential for utilization in the form of composites or mixtures with other ceramics or metals (e.g., nickel). These materials optimally would be used to replace a portion of the ZrO_2 in the Ni-ZrO_2 cermet anode currently used in order to increase the electrical conductivity. The silicides offer the most promise, as they are generally better con-

TABLE 35.--Possible non-oxide ceramics for anode use in the solid electrolyte fuel cell as related to key materials properties

Highest Electrical Conductivity	Coefficient of Thermal Expansion Compatible with ZrO_2 Electrolyte	Thermodynamically Stable Toward Formation of Highest Oxide at 1300 K	Thermodynamically Stable Toward Formation of Lowest Stable Suboxide at 1300 K
WC, TaC	Cr_3C_2	None (high-CO_2 gas)* VC, WC (low-CO_2 gas)+	None (high-CO_2 gas) NbC, WC (low-CO_2 gas)
Mo_2N, TiN	TiN, VN. NbN, Cr_2N	VN, V_2N	None
$NbSi_2$, $TaSi_2$, WSi_2, $TiSi_2$	Ti_5Si_3, TiSi, $TiSi_2$, V_5Si_3, VSi_2, $NbSi_2$, $TaSi_2$, Cr_3Si	V_2Si, Mo_5Si, Mo_3Si, Mo_3Si, W_5Si_3, Fe_3Si, Ni_3Si, Ni_2Si	None
ZrB, ZrB_2, HfB, HfB_2	ScB_2, CrB_2	Mo_2B, W_2B, WB	Mo_2B, W_2B, WB

* Lurgi gasifier (See Table 10).

\+ Combustion engineering gasifier (see Table 10).

ductors and a larger number meet the other two key anode requirements.

3. Oxide Ceramics

The oxide ceramics are not considered competitive with the non-oxide ceramics for anode use because their electrical resistivities are orders of magnitude greater.

II. MOLTEN-CARBONATE FUEL CELL

A. Cathode

The air electrode in the molten-carbonate fuel cell is excessively oxidizing for the possible use of carbides, nitrides, silicides, and borides. Perovskites, such as the rare-earth nickelates, cobaltates, and manganates offer promise in this area, however. Corrosion studies of these materials in molten carbonates first are necessary to ascertain chemical compatibility. Reduction in the ionic component of electrical conductivity by modification of the chemical composition then would be merited for the more promising materials. None of the spinels or ZrO_2-based oxides evaluated have suitable electrical properties for use as cathodes.

B. Anode

Metals and non-oxide ceramics appear to have the best promise for use in the molten-carbonate fuel cell as anodes.

1. Metals

Of the metals used for MHD electrodes, nickel and cobalt and perhaps some of their alloys would be suitable for use as anodes in the solid-electrolyte fuel cell, and are in use already for

this application.

2. Non-Oxide Ceramics

Except for the thermal-expansion data, the properties listed in Table 35 would be applicable equally for evaluating non-oxide ceramics for anode use in the molten-carbonate fuel cell, except that the temperature would be 900K instead of 1300K. The thermodynamic stability of non-oxide ceramics toward oxidation is increased at 900K, so more materials can be considered suitable for anode use. There is some question, however, as to the chemical compatibility of these materials with the molten carbonate. The carbides are supposedly soluble under vacuum and the nitrides, silicides, and borides also are said to be reactive, but perhaps only under oxidizing conditions. Corrosion information is needed under a fuel-gas environment before final conclusions can be drawn regarding the overall suitability of the non-oxide ceramics as anodes or anode constituents in molten-carbonate fuel cells.

3. Oxide Ceramics

The oxide ceramics are not considered likely candidates for anodes in the molten-carbonate fuel cell because of high electrical resistivities, relative to more suitable alternate materials (e.g., nickel), and chemical-compatibility problems with the electrolyte.

C. Electrolyte Support

The materials utilized as MHD interelectrode insulators are best suited at electrolyte-support tiles in the molten-carbonate fuel cell. Nitrides such as BN and Si_3N_4 suffer from low resistance to water

vapor, while SiO_2-rich materials are reactive with the electrolyte. MgO has been used already as tile material but has an unacceptable solubility in the molten carbonate. Materials which appear promising for screening as tile materials include: alkaline-earth hafnates and zirconates, lithium and alkaline-earth tantalates, and rare-earth aluminates. The corresponding titanates and niobates are less promising candidates.

III. FUTURE RESEARCH

To evaluate properly the many promising MHD materials delineated in this report for utilization in high-temperature fuel cells will require an experimental research effort to verify the predicted suitability or nonsuitability.

A. Basic Information

There are major discrepancies in the published literature for resistivity data for many of the non-oxide ceramics. In a number of cases, there is little reliable information regarding electrical properties at elevated temperatures. It is felt that this is due, in large part, to poor characterization (e.g., analysis) of the samples.

Reliable data on the electrical resistivities of non-oxide ceramics at temperatures of 700° to 1000°C would be helpful in confirming the projected suitability of these materials for use in high-temperature fuel cells, based on presently available information. Factors which must be considered in such research are method of preparation (e.g., chemical synthesis, CVD, r-f sputtering), and stoichiometry, and purity of the prepared material. Such research could

serve to resolve existing discrepancies in published values of resistivity and would aid in the formulation of better candidate materials for use in high-temperature fuel cells.

B. Stability Toward Oxidation

Kinetic factors can prevent predicted oxidation reactions from occurring at significant or measurable rates. Reliable data are needed for the kinetics of oxidation and the stable products formed during oxidation under typical fuel-gas conditions of anode materials such as carbides, nitrides, silicides, borides, and their composites. A temperature range of 700° to 1000°C would be representative of both the molten-carbonate and solid-oxide high-temperature fuel cells.

C. Chemical and Electrochemical Compatibility

Any new promising material considered for incorporation into components of the high-temperature fuel cells must pass a chemical compatibility test. This is especially important for non-oxide ceramic cermets considered for anodes. At the anode, the possibility of alloy and intermetallic-compound formation should be examined as a function of composition, temperature, time, and the gas environment. The effect of such interaction upon the electrical and thermal properties of the cermet should be determined.

In the solid-oxide fuel cell, the main area of concern will be interaction of anode candidates at interfaces with other cell components. This interaction should also be studied under the influence of an applied d-c field, as electrotransport processes will be promoted under these conditions.

In the molten-carbonate fuel cell, the main area of concern will be the chemical reaction of anode and tile materials with the molten carbonate. Corrosion rate of candidate non-oxide ceramics (considered for anode use) under typical fuel cell conditions would be desirable, both in the absence and the presence of an applied emf. Similar information is needed for potential candidates based on oxyanion compounds (e.g., zirconates).

REFERENCES

1. John B. Wachtman, Jr., Samuel J. Schneider, Alan B. Franklin, "The Role of Ceramics in Energy Systems," Proceedings of the Energy Research and Development Administration and National Science Foundation Workshop on Ceramics for Energy Applications, CONF-751194, November 24-25, 1975, Columbus, Ohio.

2. Open Cycle Coal Burning MHD Power Generation: An Assessment and a Plan for Action, Research and Development Report No. 71, 1971, The Massachusetts Institute of Technology, Cambridge, MA.

3. E. F. Sverdrup, C. J. Warde, and A. D. Glasser, "A Fuel Power System for Central Station Power Generation Using Coal as a Fuel," Scientific Paper No. 71-9E6-FCELA-PI, June 7, 1971, Westinghouse Research Laboratories, Pittsburgh, PA.

4. W. Feduska, A. O. Isenberg, J. E. Bauerle, W. J. Biter, Y. Ichikawa, J. L. Iskol, P. J. Nalepa, R. J. Ruka, and L. M. Yannopoulos, Thin Film Battery/Fuel Cell Power Generating System, Task E3, First Annual Report, April 14, 1977, Westinghouse Electric Corporation, Research and Development Center, Pittsburgh, PA.

5. J. B. Heywood and G. J. Womack, Eds., Open Cycle MHD Power Generation, Pergaman Press, Oxford, England, 1969.

6. H. K. Bowen, "Electrical Stabilization," Second U.S.-U.S.S.R. Colloquim on Magnetohydrodynamic Electrical Power Generation, June 5-6, 1975, Washington, D.C.

7. E. T. Etsell and S. N. Flengas, "The Electrical Properties of Solid Oxide Electrolytes," Chem. Rev. 70(3), 339-76 (1970).

8. V. S. Stubican, R. C. Hink, and S. P. Ray, "Phase Equilibria and Ordering in the System ZrO_2-Y_2O_3," J. Amer. Ceram. Soc. 61(1-2), 17-21 (1978).

9. V. S. Stubican and S. P. Ray, "Phase Equilibria and Ordering in the System ZrO_2-CaO," J. Amer. Ceram. Soc. 60(11-12), 534-40 (1977).

10. Z. S. Volchenkova and S. F. Pal'guev, "Electrical Conductivity of Solid Oxides in the Systems ZrO_2-BeO, ZrO_2-CaO, ZrO_2-MgO, ZrO_2-SrO, ZrO_2-BaO," Tr. Inst. Elektrokhim., Akad. Nauk SSSR, Ural. Filial 1961 (2), 173-83, Chem. Abstr. 59: 8170c (1963).

11. J. M. Dixon, L. D. LaGrange, U. Merten, C. F. Miller, and J. T. Porter, "Electrical Resistivity of Stabilized Zirconia at Elevated Temperatures," J. Electrochem. Soc. 110, 276-280 (1963).

12. D. W. Strickler and W. G. Carlson, "Electrical Conductivity in the ZrO_2-Rich Region of Several M_2O_3-ZrO_2 Systems," J. Amer. Ceram. Soc. 48, 286-289 (1965).

13. J. E. Bauerle and J. Hrizo, "Interpretation of the Resistivity Temperature Dependence of High Purity $(ZrO_2)_{0.90}(Y_2O_3)_{0.10}$," J. Phys. Chem. Solids 30, 565-570 (1969).

14. D. T. Bray and U. Merten, "Transport Numbers in Stabilized Zirconia," J. Electrochem. Soc. 111, 447-452 (1964).

15. D. W. Strickler and W. G. Carlson, "Ionic Conductivity of Solid Solutions in the System CaO-Y_2O_3-ZrO_2," J. Amer. Ceram. Soc. 47, 122-127 (1964).

16. H. Tannenberger, H. Schachner, and P. Kovacs, "Solid Zirconium Oxide-Based Electrolyte for Fuel Cells," Rev. Energ. Primaire 2(1), 19-26 (1966).

17. J. W. Patterson, E. C. Bogren and R. A. Rapp, "Mixed Conduction in $Zr_{0.85}Ca_{0.15}O_{1.85}$ and $Th_{0.85}Y_{0.15}O_{1.925}$ Solid Electrolyte," J. Electrochem. Soc. 114, 752-758 (1967).

18. R. E. Carter and W. L. Roth, "Conductivity and Structure in Calcia-Stabilized Zirconia," Electromotive Force Measurements in High-Temperature Systems, C. B. Alcock, Ed., Institution of Mining and Metallurgy, London, England, p. 125, 1968.

19. J. Weissbart and R. Ruka, "Ionic Conduction in $(ZrO_2)_{.85}(CaO)_{.15}$," (Abstract No. 44, Detroit Meeting of the Electrochem. Society), J. Electrochem. Soc. 108, 167C (1961).

20. C. F. Grain, "Phase Relations in the ZrO_2-MgO System," J. Amer. Ceram. Soc. 50(6), 288-290 (1967).

21. Z. S. Volchenkova, "Ionic and Electronic Conductivity of Zirconium Oxide-$PrO_{1.83}$ Systems," Khim. Vysokotemp. Mater., Tr. Vses. Soveshch., 2nd 1965, 65-69 (Publ. 1967); Chem. Abst. 68: 108453t (1963).

22. H.- H. Moebius, H. Witzmann, and G. Proeve, "Oxygen-Ion Conducting Solid Electrolytes and Their Application Possibilities. VI. Systematic Conductivity Measurements of Oxygen - Conductivity Measurements of Oxygen - Conduction Solid Electrolytes of Zirconium Dioxide and Rare-Earths," Z. Chem. 4(5), 195-196 (1964).

23. M. Guillou, "High Temperature Electrochemistry. III. Use of Electrochemical Methods for Studies on MHD Electrodes," Rev. Gen. Elect. 76(1), 58-68 (1967).

24. F. Trombe and M. Foëx, "Ceramics Composed of Zirconia and Lanthanum Oxide," C. R. Acad. Sci., Paris 233, 254-256 (1951).

25. R. S. Roth, "Pyrochlore-Type Compounds Containing Double Oxides of Trivalent and Tetravalent Ions," J. Res. Nat. Bur. Stand. 56(1), 17-26 (1956).

26. B. C. H. Steele and C. B. Alcock, "Factors Influencing the Performance of Solid Oxide Electrolytes in High-Temperature Thermodynamic Measurements," Trans. Met. Soc. AIME 233,1359-1367(1965).

27. M. F. Lasker and R. A. Rapp, "Mixed Conduction in ThO_2 and ThO_2-Y_2O_3 Solutions," Z. Physik. Chem. (Frankfurt am Main) 49(3-5), 198-221 (1966).

28. F. Hund, "The Abnormal Lattice Distrubances and Electrical Resistance in the System ThO_2-La_2O_3," Z. Anorg. Allg. Chem. 274, 105-113 (1953).

29. A. D. Neuimin and S. F. Pal'guev, "Methods of Investigating the Nature of Conductivity of Solid Oxides," Silikaty Okisly Khim. Vys. Temp., Akad. Nauk. SSSR, Inst. Khim. Silikatov, Vses. Khim. Obshch. im D. I. Mendeleeva, 253-268 (1963); Chem. Abst. 62: 15536e (1965).

30. H. L. Tuller and A. S. Nowick, "Doped Ceria as a Solid Electrolyte," J. Electrochem. Soc. 122(2), 255-259 (1975).

31. R. N. Blumenthal, F. S. Brugner, and J. E. Garnier, "The Electrical Conductivity of CaO-Doped Nonstoichiometric Cerium Dioxide from 700° to 1500°C," Ibid., 120(9), 1230-1237 (1973).

32. T. Kudo and H. Obayashi, "Oxygen Ion Conduction of the Flourite-Type $Ce_{1-x}Ln_xO_{2-x/2}$ (Ln = Lanthanoid Element)," Ibid., 122(1), 142-147 (1975).

33. T. Takahashi, K. Ito, and H. Iwahara, "Fuel Cells With a New Type Solid Electrolyte," Rev. Energ. Primaire 2, 42-48 (1966).

34. T. Takahashi, K. Ito and H. Iwahara, "Fuel Cell XV. Characteristics of the Fuel Cell With a CeO_2-La_2O_3 Solid Electrolyte," Denki Kagaku 34, 205-209 (1966).

35. A. D. Neuimin, S. F. Pal'guev, and V. C. Chebotin, "Reduction of Cerium Dioxide in a Mixture of Oxides of the System CeO_2-La_2O_3 and Electrical Conductance of Mixtures," Tr. Inst. Elektrokhim. Akad. Nauk SSSR, Ural'sk. Filial 4, 97-110 (1963); Chem. Abstr. 60: 11457h (1964).

36. P. N. Ross, Jr. and T. J. Benjamin, "Thermal Efficiency of Solid Electrolyte Fuel Cells with Electronic Conduction," Proceedings of the Workshop on High-Temperature Solid Oxide Fuel Cells, May 5-6, 1977, Brookhaven National Laboratory, Upton, N. Y., pp. 195-213.

37. T. Takahashi, H. Iwahara, and Y. Nagai, "High Oxide-Ion Conduction in Sintered Bismuth Oxide Containing Strontium Oxide, Calcium Oxide, or Lanthanium Oxide," J. Appl. Electrochem. 2(2), 97-104 (1972); Chem. Abstr. 77: 53618d (1972).

38. T. Takahashi and H. Iwahara, "Perovskite-Type Oxide Solid-Electrolyte High-Temperature Fuel Cells," Toyoda Kenkyu Hokoku 25, 39-47 (1972); Chem. Abstr. 77: 134196s (1972).

39. H. Iwahara and T. Takahashi, "Ionic Conduction in Sintered Oxides. V. Ionic Conduction in Sintered Oxides Based on Calcium Titanium Trioxide or Strontium Titantium Trioxide," Denki Kagaku Kogyo Butsuri Kagaku 39(5), 400-405 (1971); Chem. Abstr. 75: 134377k (1971).

40. T. Takahashi and H. Iwahara, "Ionic Conduction in Perovskite-Type Oxide Solid Solution and Its Application to the Solid Electrolyte Fuel Cell," Energy Convers. 11(3), 105-111 (1971); Chem. Abstr. 75: 147022r(1971).

41. T. Takahashi, H. Iwahara, and T. Ichimura, "Ionic Conduction of Sintered Oxides. 3. Ionic Conduction in Solid Solutions of $CaTi_{1-x}Al_xO_{3-\alpha}$," Denki Kagaku Oyobi Kogyo Butsuri Kagaku 37(12), 857-862 (1969); Chem. Abstr. 73: 19476p (1970).

42. T. Takahashi, H. Iwahara, T. Ichimura, and H. Aoyama, "Solid Electrolytes and Their Applications. 2. Ionic Conduction in Perovskite-Type Oxide Solid Solutions," Asahi Garasu Kogyo Gijutsu Shoreika Kenkyu Hokoku 15, 239-253 (1969); Chem. Abstr. 73: 81810w (1970).

43. T. Takahashi, K. Ito, and H. Iwahara, "The Efficiency of Solid-Electrolyte Fuel Cells," Electrochim. Acta 12, 21-30 (1967).

44. D. S. Tannhauser, "The Theoretical Energy Conversion Efficiency of a High-Temperature Fuel Cell Based on a Mixed Conductor," J. Electrochem. Soc. 125(8), 1277-1282 (1978).

45. D. Russell, H. S. Isaacs, and A. C. C. Tseung, "Studies on Glass Composites and Doped Rutile as Interconnection Materials," op. cit., ref. 36 pp. 96-102.

46. L. H. Bennett, M. I. Cohen, A. L. Dragoo, A. D. Franklin, and A. J. McAlister, Materials for Fuel Cells, NBSIR 76-1091, Quarterly Report for February through April, 1976 (issued August, 1976), National Bureau of Standards, Washington, D.C.

47. H. L. Bennett, M. I. Cohen, A. L. Dragoo, A. D. Franklin, A. J. McAlister, and K. F. Young, Materials for Fuel Cells, Annual Report, January to December, 1976 (issued May, 1977), National Bureau of Standards, Washington, D.C.

48. F. J. Rohr, "High-Temperature Solid Oxide Fuel Cells: Present State and Problems of Development," op. cit., ref. 36, pp. 122-138.

49. J. Schieltz, J. W. Patterson, and D. R. Wilder, "Electrolytic Behavior of Yttria," J. Electrochem. Soc. 118(7), 1140-1144 (1971).

50. A. Feduska, A. O. Isenberg, J. L. Iskoe, R. J. Ruka, P. Nalepa, and A. Noreika, Thin Film Battery/Fuel Cell Power Generating System, Task E-2, Project Status Report for July to September, 1976 (issued October 8, 1976), Westinghouse Research Laboratory, Pittsburgh, PA.

51. "Incoloy Alloys," Huntington Alloy Products Division, INCO, Huntington, W.V.

52. Phase I. Improvement of Fuel Cell Technology Base, Final Report, Contract No. EY-76-C-03-1169, January 19, 1976 to March 31, 1977, Power Systems Division, United Technologies Corporation, South Windsor, CT.

53. F. A. Cotton and G. Wilkinson, Advanced Inorganic Chemistry, Interscience Publishers, New York, 1962, pp. 219-222.

54. Yu. B. Paderno, I. G. Barantseva, and V. L. Yupko, "Measurement of Thermal Conductivity and Electrical Resistance of Zirconium Carbide, Hafnium Carbide, Niobium Carbide, and TaC at High Temperatures," Vysokotemp. Neorgan. Soedin., Akad. Nauk Ukr. SSR, Inst. Probl. Materialoved. 1965, 199-204; Chem. Abstr. 64: 13495c (1966).

55. S. M. L'vov, V. F. Nemchenko, T. Ya. Kosolapova, and G. V. Samsonov, "Effect of Carbon on the Physical Properties of Titanium Carbide in Homogeneous Regions," ibid., 1965, 237-242; Chem. Abstr. 64: 16758f (1966).

56. H. E. Pattee, R. M. Evans, and R. E. Monroe, Joining Ceramics and Graphite to Other Materials, NASA Report SP-5052, 1968, p.8.

57. J. F. Lynch, C. G. Ruderer, and W. H. Duckworth, Engineering Properties of Selected Ceramic Materials, American Ceramic Society, Columbus, OH, 1966.

58. J. H. Westbrook, and E. R. Stover,"Carbides for High-Temperature Materials and Technology," I. E. Campbell and E. M. Sherwood, Eds., John Wiley and Sons, Inc., N.Y., 1967, pp. 312-348.

59. H. J. Goldschmidt, Interstitial Alloys, Plenum Press, N.Y., 1967

60. P. Schwarzkopf and R. Kieffer, Refractory Hard Metals (Borides, Carbides, Nitrides, and Silicides), The MacMillan Company, N.Y., 1953.

61. D. R. Stull and H. Prophet, Eds., JANAF Thermochemical Tables, 2nd ed., U.S. Department of Commerce, National Bureau of Standards, NSRDS-NBS 37, June, 1971.

62. C. E. Wicks and F. E. Block, "Thermodynamic Properties of 65 Elements - Their Oxides, Halides, Carbides, and Nitrides," U.S. Bureau of Mines Bulletin 605, 1963.

63. M. W. Chase, J. L. Curnutt, H. Prophet, R. A. McDonald, and A. N. Syverud, "JANAF Thermochemical Tables, 1975 Supplement," J. Phys. Chem. Ref. Data 4(1), 1-175 (1975).

64. Development of Molten Carbonate Fuel Cells for Power Generation, SRD-78-045, Six-month Progress Report, August 15, 1977 through February 15, 1977 (issued March 1978), General Electric Company, Corporate Research and Development, Schenectady, N.Y.

65. A. Feduska, A. O. Isenberg, J. E. Bauerle, W. J. Biter, Y. Ishikawa, R. J. Ruka, and L. N. Yannopoulos, Thin Film Battery/Fuel Cell Power Generating System, Task E2, Project Status Report for the period July 1977 to September 1977 (issued October 7, 1977), Westinghouse Electric Corporation Research and Development Center, Pittsburgh, PA.

66. R. Hultgren, P. D. Desai, D. T. Hawkins, M. Gleiser, and K. K. Kelley, Selected Values of the Thermodynamic Properties of Binary Alloys, American Society for Metals, Metals Park, OH, 1973.

67. J. C. Passefort, F. Anselin, and D. Calais, "Reactions Between Nickel and the Carbides and Nitrides of Uranium," Sci. Ceramics 4, 421-457 (1968).

68. R. C. Weast, Handbook of Chemistry and Physics, 51st ed., The Chemical Rubber Company, Cleveland, OH, 1970-1971, p. F-140.

69. H. C. Maru, A. Pigeaud, E. Ong, J. R. Selman, V. Sampath, L. G. Marianowski, and K. F. Blurton, Fuel Cell Research on Second Generation Molten-Carbonate Systems. Volume II. Characteristics of Carbonate Melts, Project 8984, Quarterly Status Report for the period July 1 through September 30, 1976, Institute of Gas Technology, Chicago, IL.

70. J. L. Margrave and G. Mamantov, "High-Temperature Reactions," op. cit., ref. 58, pp. 78-127.

71. M. C. Ball, D. S. Brown, D. Page and R. R. Thurman, "The Action of Alkali on Transition-Metal Carbides," Trans. Brit. Ceram. Soc. 66(71), 307-313 (1967).

72. R. A. Perkins and H. H. Lavendel, Reactions of Silicon Carbide with Fused Coal Ash, Lockheed Missiles and Space Company, Inc., Palo Alto, CA, EPRI AF-294, Final Report, November 1976.

73. Op. cit., ref. 53, pp. 219-222.

74. J. M. Blocher, Jr., "Nitrides," in ref. 58, op. cit., pp. 379-398.

75. T. S. Verkhoglyadova, "The Technology of Preparation and Some Properties of the Nitrides of Rare Metals," Redk. Redkozem. Elem. Tekh. 1964, 104-113.

76. R. A. Guidotti, G. B. Atkinson, and D. G. Kesterke, "Nitride Intermediates in the Preparation of Columbium, Vanadium, and Tantalum Metals. Part 2. Thermal Decomposition of the Nitrides," U.S. Bureau of Mines Rept. of Invest. 8103, 1976.

77. H. L. Schick, Thermodynamics of Certain Refractory Compounds, Vol. 2: Thermodynamic Tables, Bibliography, and Property File, Academic Press, N.Y., 1966.

78. Ya. I. Gerasimov and V. I. Larentev, "Tantalum: Physiochemical Properties of Its Compounds and Alloys," At. Energy Rev. 1972, (Spec. Iss. 3), 7-39; Chem. Abstr. 79: 117579t (1973).

79. J. H. Swisher and M. H. Read, "Thermodynamic Properties and Electrical Conductivity of Ta_3N_5 and TaON," Met. Trans. 3, 489-494 (1972).

80. High-Temperature Fuel Cell Research and Development, Technical Status Report No. 12, for the period April through June 1978 (issued July 18, 1978), Montana Energy and MHD Research and Development Institute, Butte, Montana.

81. R. Wehrmann, "Silicides," op. cit., in ref. 58, pp. 399-430.

82. B. S. Rabinovich, I. Z. Rodovskii, F. N. Kozlov, F. A. Sidorenko and P. V. Gel'd, "Electrical and Magnetic Properties of Titanium Monosilicide and Titanium Disilicide," Izv. Akad. Nauk SSSR, Neorg. Mater. 6(12), 2202-4 (1970); Chem. Abstr. 74: 58271h (1971).

83. G. I. Kalishevich, P. V. Gel'd, and R. P. Krentsis, "Specific Heat, Enthalpy, and Entropy of Cr_5Si_3 and $CrSi_2$," Teplofiz Vys. Temp. 4(5), 653-659 (1966); Chem. Abstr. 66: 22856y (1967)

84. R. C. Marshall, "Growth and Characterization of a Transition Metal Silicide," J. Cryst. Growth 3-4, 295-299 (1968); Chem. Abstr. 70: 51543g (1969).

85. "Kanthal Super and Its Use in Furnaces," The Kanthal Corporation, Bethel, CT, 1966.

86. O. Kubaschewski, L. L. Evans, and C. B. Alcock, Metallurgical Thermochemistry, 4th ed., Pergamon Press, N.Y., 1967, pp. 202-237.

87. V. P. Bondarenko, L. A. Dvorina, N. P. Slyusar, and E. N. Fomichev, "Enthalpy of Niobium Silicides Nb_4Si and Nb_5Si_3 within the Temperature Range 1200-2200K," ibid., pp. 48-51; Chem. Abstr. 76: 77386g (1972).

88. V. P. Bondarenko, V. I. Zmii, and E. N. Fomichev, "Thermodynamic Properties of Tungsten Silicides at 1200-2200K," Porosh. Met. 2, 59-62 (1972); Chem. Abstr. 76: 132385h (1972).

89. V. N. Eremenko, G. M. Lukashenko, and V. R. Sidorko, "Thermodynamic Properties of Vanadium, Chromium, and Manganese Silicides," Rev. Int. Hautes Temp. Refract. 12(3), 237-240 (1975); Chem. Abstr. 84: 36045s (1975).

90. V. P. Bondarenko, L. A. Dvorina, V. I. Zmii, E. N. Fomichev, N. P. Slyusar, and A. D. Krivorotenko, "Enthalpy and Heat Capacity of Titanium and Vanadium Disilicides above 1200K," Porosh. Met. 11, 47-49 (1973); Chem. Abstr. 80: 52995z (1974).

91. M. Golutvin and E. G. Maslennikova, "Thermochemistry of a Zirconium-Silicon System," Izv. Akad. Nauk SSSR, Metal 1968(2), 193-207; Chem. Abstr. 69: 13519a (1968).

92. A. Kalashnik and N. P. Slyusar, "Determination of the Enthalpy and Specific Heat of Tantalum and Niobium Disilicides at 1200-2100K," Teplofiz. Vys. Temp. 8(4), 910-912 (1970); Chem. Abstr. 73: 124260m (1970).

93. S. R. Levine and M. Kolodney, "Free Energy of Formation of Tantalum Silicides Using Solid Oxide Electrolyte," J. Electrochem. Soc. 116(10), 1420-1424 (1968).

94. V. N. Eremenko, G. M. Lukashenko, and V. R. Sidorko, "Thermodynamic Properties of the Chromium Silicides $CrSi_2$ and CrSi," Zh. Fiz. Khim. 48(5), 1996-1998 (1971); Chem. Abstr. 75:123060a (1971).

95. C. F. Powell, "Borides," in ref. 58 , op. cit., pp. 349-378.

96. F. G. Keihn and E. J. Keplin, "High-Temperature Thermal Expansion of Certain Group IV and Group V Diborides," J. Amer. Ceram. Soc. 50(2), 81-84 (1967).

97. G. V. Samsonov, B. A. Kovenskaya, B. A. Serebryakova, and E. Ya. Tel'nikov, "Thermal Expansion of Diborides of Group IV and V Transition Metals," Teplofiz. Vys. Temp. 9(1), 195-197 (1971); Chem. Abstr. 74: 116183u (1971).

98. G. V. Samsonov, A. S. Bolgar, E. A. Guseva, L. A. Klochkov, B. A. Kovenskaya, T. I. Serebreyakova, and I. I. Timofeeva, "Thermophysical Properties of Transition Metal Carbides and Diborides," High-Temp. - High Pressures 5(1), 29-33 (1973).

99. S. N. L'vov and F. I. Nemchenko, "Possible Application of the Single-Zone Representation to the Diborides of the Group IV Transition Metals," Izv. Vyssh. Ucheb. Zaved., Fiz. 11(1), 59-62 (1967); Chem. Abstr. 68: 108889q (1968).

100. V. Mandorf, J. Hartung, and E. J. Seldin, "High-Temperature Properties of TiB_2," Met. Soc. Conf. 18 455-67 (1961) (Publ. 1963)

101. E. N. Severyanina, E. M. Dudnik, and Yu. B. Paderno, "Thermal Expansion of Tetraborides of Some Rare Earth Metals," Porosh. Met. 12, 72-74 (1973); Chem. Abstr. 80: 137312z (1974).

102. G. K. Johnson, E. Greenberg, J. L. Margrave, and W. N. Hubbard, "Flourine Bomb Calorimetry: Enthalpies of Formation of the Diborides of Zirconium and Hafnium," J. Chem. Eng. Data 12(1), 133-135 (1967).

103. G. L. Gal'chenko, D. A. Gedakyan, B. I. Timofeev, S. M. Skuratov, T. I. Serebryakova, and G. V. Samsonov, "Standard Heat of Formation of Tantalum Diboride and Tantalum Pentachloride," Dokl. Akad. Nauk SSSR 170(1), 132-134 (1966); Chem. Abstr. 66: 49785n (1967).

104. I. D. Baehren and D. Vollath, "Determination of the Thermodynamic Data of Molybdenum Boride (Mo_2B), Tungsten Boride (W_2B), and Rhenium Boride (Re_2B)," Planseeber. Pulvermet. 17(3), 180-183 (1969); Chem. Abstr. 72: 36584u (1970).

105. V. Ya. Leonidov, O. M. Gaisinskaya, and V. S. Pervov, "Enthalpies of Formation of Tungsten Borides by the Method of Flourine Bomb Calorimetry," Conf. Int. Thermodyn. Chem., (C.R.), 4th, 1, 48-53 (1975); Chem. Abstr. 84: 127408d (1976).

106. S. Omori and Y. Hashimoto, "Studies on Thermodynamic Properties of Cobalt Borides (Co_3B and Co_2B) by EMF Measurements," Nippon Kinzoku Gakkaishi 40(6), 601-605 (1976); Chem. Abstr. 85: 52590s (1976).

107. S. P. Gordienko, E. A. Guseva, and V. V. Fesenko, "Thermodynamic Properties of Lanthanum Hexaboride," Teplofiz. Vys. Temp. 6(5), 821-825 (1968); Chem. Abstr. 70: 61844v (1969).

108. N. W. Chase, J. L. Curnutt, A. T. Hu, H. Prophet, A. N. Syverud and L. C. Walker, "JANAF Thermochemical Tables, 1974 Supplement," J. Phys. Chem. Ref. Data 3(2), 311-480 (1974).

109. T. Manabe and T. Gejo, "Syntheses of Zirconium Diboride by Chemical Vapor Deposition," Yogyo Kyokai Shi 76(877), 324-330 (1968); Chem. Abstr. 70: 80535m (1969).

110. N. V. Philip's Gloeilampenfabrieken, "Applying Metal Boride Layers on a Substrate," Neth. Appl. 6,607,850, Dec. 12, 1966; Chem. Abstr. 66: 89543n (1967).

111. C. Urban, G. Provost, and G. Bentz, "Plasma-Gun Spraying of Borides and Nitrides II. Properties of the Samples Obtained," Bull. Soc. Fr. Ceram. 79, 1-16 (1968); Chem. Abstr. 70: 31366y (1969).

112. L. Lecrivain and G. Provost, "Properties of Plasma-Sprayed Borides and Nitrides," Ber. Deut. Keram. Ges. 45(7) 347-351 (1968); Chem. Abstr. 69: 99056g (1968).

113. S. S. Kiparisov, O. A. Nikiforov, and Yu. K. Kuz'mina, "Possible Sintering of Tungsten Boride with Nickel," Izv. Vyssh. Ucheb. Zaved., Tsvet. Met. 13(5), 93-95 (1970); Chem. Abstr. 74: 102385z (1971).

114. H. Stadelmaier, "The Ternary System Nickel-Vanadium-Boron," Metall (Berlin) 21(7), 691-692 (1967).

115. H. K. Bowen, "MHD Channel Materials Development Goals," Proceedings of NSF-OCR Engineering Workshop on MHD Materials, November 20-22, 1974, Massachusetts Institute of Technology, Cambridge, MA, pp. 85-112.

116. W. W. Rummel, "Materials for MHD Ducts," Proceedings of Symposium on MHD Electrical Power Generation, Paris, 1964, pp. 1119-1126.

117. H. K. Bowen and B. R. Rossing, "Materials Problems in Open Cycle Magnetohydrodynamics," op. cit., ref. 1, pp. 107-130.

118. A. Taylor and N. J. Doyle, "Thermal Expansion of Titanium, Vanadium, and Niobium Monoxides," J. Appl. Crystallogr. 4(2), 103-109 (1971).

119. V. G. Grebenkina and E. N. Denbnovetskaya, "Temperature Coefficient of the Electrical Resistivity of Some Refractory Compounds and Their Solid Solutions," Izv. Akad. Nauk SSSR, Neorg. Mater. 4(12), 2196-2197 (1968); Chem. Abstr. 70: 70796h (1969).

120. Yu. G. Zainulin, S. I. Alyamovskii, G. P. Shveikin, and P. V. Gel'd, "Coefficients of Thermal Expansion of Cubic (Sodium Chloride Type) Oxycarbides and Oxynitrides of Zirconium and Hafnium," Teplofiz. Vys. Temp. 9(3) 546-549 (1971); Chem. Abstr. 75: 134063e (1971).

121. Yu. G. Zainulin, S. I. Alyamovskii, and G. P. Shveikin, "Thermal Expansion Coefficients and Characteristics of Interatomic Interactions in Cubic (Sodium Chloride Type) Titanium Oxycarbides," ibid., 14(4), 900-903 (1976); Chem. Abstr. 85: 200751n (1976).

122. G. A. Geach and I. O. Jones, "Interactions in Mixtures of Hard Metals," Plansee. Proc. 1955, 80-91 (Publ. 1956); Chem. Abstr. 50: 11908c (1956).

123. V. Mandorf, Jr., "Container for Vaporization of Aluminum," Brit 943,698, December 4, 1963; Chem. Abstr. 60: 5171c (1964).

124. M. A. Roche, Jr. and J. C. Fisher, Jr., "Improving the Resistance of Mixed Titanium Diboride and Boron Nitride Refractories to Moisture and Thermal Cracking," Brit. 999,415, July 28, 1965; Chem. Abstr. 63: 9628g (1965).

125. General Electric Company, "Catalyst Electrodes for Fuel Cells," Brit. 1,194,642, June 10, 1970; Chem. Abstr. 73: 83265w (1970).

126. E. L. Simons and E. J. Cairns, "Effect of Hot Cesium Carbonate on Fuel Cell Components," Mater. Prot. 6(9), 51 (1967); Chem. Abstr. 67: 104505t (1967).

127. N. I. Voronin, N. K. Krasotkina, V. V. Levchuk, L. N. Klyukvina, R. V. Svoboda, I. M. Mal'tseva, M. L. Blyushtein, D. I. Amel'kovich, and A. B. Gluz, "Testing of New Materials for Conduction of Current to the Cathode of an Electrolytic Aluminum Cell," Tsvet. Metal. 40(4) 63-66 (1967); Chem. Abstr. 66: 49823t (1967).

128. J. M. Diller, "Activation of Cryolite-Alumina Compositions," U.S. 3,392,092, July 9, 1968; Chem. Abstr. 69: 48730q (1968).

129. C. E. Ransley, "Refractory Carbides and Borides for Aluminum Reduction Cells," J. Metals 14, 129-135 (1962).

130. Fuel Cell Research on Second Generation Molten Carbonate Systems, Project 9105 Quarterly Technical Progress Report for the period January 1 through March 31, 1978, Institute of Gas Technology, Chicago, IL.

131. J. Faber, Jr., M. H. Mueller, W. L. Procarione, A. T. Aldred, H. W. Knott, and H. U. Anderson, "Structural and Physical Properties of the $La_{1-x}Sr_xCrO_3$ Systems," Proceedings of the Conference on High Temperature Sciences Related to Open Cycle Coal-Fired MHD Systems, April 4-6, 1977, Argonne, IL, pp. 154-159.

132. D. B. Meadowcraft, "Some Properties of Strontium-Doped Lanthanum Chromite," Brit. J. Appl. Phys. (J. Phys. D) 2(2), 1225-1233 (1969).

133. J. L. Henry and G. G. Thompson, "Thermal Expansion Match Between Molybdenum (TZM Alloy) and Oxides of the Perovskite and Spinel Types," Ceram. Bull. 55(3), 281-284 (1976).

134. W. Feduska, A. O. Isenberg, J. E. Bauerle, W. J. Biter, W. Ichikawa, P. J. Nalepa, R. J. Ruka, L. N. Yannopoulos, and S. A. Zeitman, Thin Film Battery/Fuel Cell Power Generating System, Final Report, Task 4, for the period April 1976 to April 1978 (issued March 31, 1978), Westinghouse Research and Development Center, Pittsburgh, PA.

135. G. P. Telegin, A. I. Romanov, E. G. Spiridonov, Ya. P. Gokhshtein, and F. A. Akopov, "Research and Development of Refractory Materials for the MHD Generator Channel," Proceedings of the Third U.S.-U.S.S.R. Colloquim on Magnetohydrodynamic Electrical Power Generation, October 20-21, 1976, Moscow, U.S.S.R., pp. 413-431.

136. E. K. Keler, "Development of Physical and Chemical Bases for MHD Generator Oxide Electrode Materials," op. cit., ref. 135, pp. 405-412.

137. S. J. Schneider, W. Capps, H. P. R. Frederilkse, W. R. Hosler, D. A. Kauffman, C. L. McDaniel, T. Negas, and E. R. Plante, High Temperature MHD Materials, NBSIR 74-543, Interim Report for the period July 1, 1972 through June 30, 1974 (issued August 1974), National Bureau of Standards, Washington, D.C.

138. G. Rudins, U.S. and U.S.S.R. MHD Electrode Materials Development Report No R-1656-ARPA, December, 1974, Rand Corporation, Santa Monica, CA.

139. L. Bates. L. R. Bunnell, J. L. Daniel, D. D. Marchant, and G. B. Mellinger, Development, Characterization and Evaluation of Materials for Open Cycle MHD BNWL-2004-5, Quarterly Report for the period October through December, 1976 (issued July 1977), Battelle Pacific Northwest Laboratories, Richland, WA.

140. H. P. R. Frederikse, T. Negas, and S. J. Schneider, Development Testing, and Evaluation of MHD Materials, E-(49-1)-3800-5, Quarterly Report for the period July through September, 1976 (issued September 30, 1976), National Bureau of Standards, Washington, D.C.

141. G. Rudins, S. J. Schneider, T. Negas, B. R. Rossing, J. L. Bates, G. P. Telegin, T. I. Borodina, Yu. L. Dolinsky, and V. Zalkind, "The Second Joint Test of a U.S. Electrode System in the U.S.S.R. U-02 Facility," Proceedings of the 16th Symposium, Engineering Aspects of Magnetohydrodynamics, May 16-18, 1977, Pittsburgh, PA, pp. IV.1.1 - IV.1.12.

142. H. U. Anderson, R. Murphy, S. Semachaibovorn, B. Rossing, A. Aldred, W. L. Procarione, and R. J. Ackerman , "Electrical Conductivity, Volatilization, and Preparation of $LaCrO_3$-Based Oxides," op. cit., ref. 131, pp. 142-147.

143. J. W. Sadler, W. E. Young, L. H. Cadoff, J. A. Dilmore, E. L. Kochka, J. A. Kuszyk, J. Lempert, B. R. Rossing, S. J. Schneider, and A. B. Turner, Development, Testing, and Evaluation of MHD Materials and Component Designs, Quarterly Report, April 1 through June 30, 1977 (issued December 1977), Westinghouse Electric Corporation, Pittsburgh, PA.

144. P. E. D. Morgan, "Highly Conducting Oxide Materials," op. cit., ref. 36, pp. 54-55.

145. J. F. Louis, Critical Contributions in MHD-Power Generation, Annual Report, June 1, 1976 through May 31, 1977 (issued June 1977), Massachusetts Institute of Technology, Cambridge, MA.

146. J. F. Louis, Critical Contributions in MHD-Power Generation, Quarterly Technical Report for the period September 1 through November 30, 1977 (issued December 1977), Massachusetts Institute of Technology, Cambridge, MA.

147. L. P. Domingues, T. Negas, A. J. Armstrong, and W. R. Hosler, "Development of a Potential Electrode Material for MHD: Yttrium Orthoferrite," Proceedings of the 17th Symposium, Engineering Aspects of Magnetohydrodynamics, March 27-29, 1978, Stanford, CA, pp. G.6.1-G.6.5.

148. H. U. Anderson, "Fabrication and Property Control of $LaCrO_3$-Based Oxides," Proceedings of Crystalline Ceramics, November 1977, North Carolina State University, Raleigh, NC, Plenum Press, New York (in press).

149. H. U. Anderson, University of Missouri, Rolla, MO, private communication, August 10, 1978.

150. M. Berberian, R. W. Ure, and I. B. Cutler, "The Preparation, Electrical Resistivity and Chemical Stability of Doped $LaCrO_3$ Compounds," Proceedings of the Sixth International Conference on Magnetohydrodynamic Electrical Power Generation, June 9-13, 1975, Washington, D.C., pp. 219-231.

151. P. Kofstad, Nonstoichiometry, Diffusion, and Electrical Conductivity in Binary Metal Oxides, Wiley-Interscience, New York, 1972, pp. 227-242.

152. E. F. Sverdrup, D. H. Archer, and A. D. Glasser, "Stannic Oxide and Indium Oxide Films as Air Electrodes for High-Temperature Coal Reacting Fuel Cells," Adv. in Chem. Ser. 90, 301-314 (1969).

153. T. Vojnovich and R. J. Bratton, "Impurity Effects on Sintering and Electrical Resistivity of Indium Oxide," Ceram. Bull. 54(2) 216-217 (1975).

154. P. J. Meschter, "Mechanisms of Electrode Polarization in High-Temperature Solid Electrolyte Systems," op. cit., ref. 144, pp. 83-84.

155. T. H. Etsell, "Performance of Solid Oxide Fuel Cell Electrodes," op. cit., ref. 144, pp. 66-83.

156. C. C. Sun, E. W. Hawk, and E. F. Sverdrup, "Electrical Evaluation of Doped and Undoped Cobalt Chromite as the Interconnector Material for High-Temperature, Zirconia-Electrolyte, Fuel Cell Batteries," J. Electrochem. Soc. 119(11), 1433-1438 (1972).

157. H. P. R. Frederikse, T. Negas, and S. J. Schneider, Development, Testing, and Evaluation of MHD Materials, E-(49-1)-3800-7, Quarterly Report for the period January through March 1977 (issued March 31, 1977), National Bureau of Standards, Washington, D.C.

158. T. K. Bowen, T. O. Mason, R. L. Prober, M. Yoshimura, and T. Pollack, "The Spinel Electrode Module," op. cit., ref. 135, pp. 343-356.

159. J. F. Louis, Critical Contributions in MHD Power Generation, Quarterly Technical Report for June 1 through August 31, 1977 (issued October 1977), Massachusetts Institute of Technology, Cambridge, MA.

160. H. P. R. Frederikse, W. R. Hosler, A. J. Armstrong, and T. Negas, "Spinels for MHD Electrodes," Development, Testing, and Evaluation of MHD Materials, E-(49-1)-3800-4, Quarterly Report for the period April through June 1976 (issued June 30, 1976), National Bureau of Standards, Washington, D.C., pp. II.2.1 - II.2.4.

161. H. P. R. Frederikse, T. Negas, and S. J. Schneider, Development, Testing, and Evaluation of MHD Materials, FE-1230-3, Quarterly Report for the period January through March 1976 (issued March 31, 1976), National Bureau of Standards, Washington, D.C.

162. W. E. Young, J. A. Dilmore, J. Lempert, B. R. Rossing, S. J. Schneider, A. B. Turner, R. J. Wright, and S. Way, Magnetohydrodynamics Investigation of Coal-Fired Open Cycle Systems, Progress Report for December 1975 (issued January 15, 1976), Westinghouse Research Laboratories, Pittsburgh, PA.

163. H. P. R.Frederikse, T. Negas, and S. J. Schneider, Development, Testing, and Evaluation of MHD Materials, E-(49-1)-3800-6, Quarterly Report for the period October through December 1976 (issued December 31, 1976), National Bureau of Standards, Washington, D.C.

164. H. P. R. Frederikse, T. Negas, and S. J. Schneider, Development, Testing, and Evaluation of MHD Materials, EA-77-A-01-6010-8, Quarterly Report for the period April through August 1977 (issued June 30, 1977), National Bureau of Standards, Washington, D.C.

165. W. R. Hosler, ed., Joint U.S.-U.S.S.R. Test of U.S. MHD Electrode Systems in U.S.S.R. U-02 MHD Facility (Phase I), Final Report, Energy Research and Development Administration Report ERDA-76/154, 1976.

166. Excerpts from the 1975 Annual Report of the U.S.S.R. Institute of High Temperatures, Moscow, Energy Research and Development Administration translation ERDA-tr-264.

167. G. R. Telegin, A. I. Romanov, F. A. Akopov, Ya. P. Gokhstein, E. K. Keler, T. I. Borodina, V. A. Bakunov, S. Schneider, B. Rossing, T. Negas, J. L. Bates, and W. Hosler, "Studies of Zirconia-Ceria Base Ceramics for MHD Channel Electrodes," op. cit., ref. 135, pp. 357-377.

168. H. P. R. Frederikse and W. R. Hosler, "Electrodes and Insulators: Design and Materials Considerations," op. cit., ref. 141, pp. IV.4.22 - IV.4.28.

169. A. Solbes, S. Petty, I. Sadovnik, and R. Kessler, "Mark VI MHD Generator Studies," op. cit., ref. 141, pp. I.2.11 - I.2.18.

170. H. P. R. Frederikse, T. Negas, and S. J. Schneider, Development, Testing, and Evaluation of MHD Materials, E-77-A-01-6010-9, Quarterly Report for the period July through September 1977 (issued September 30, 1977), National Bureau of Standards, Washington, D.C.

171. Refractory Materials for Coal-Fired MHD Power Generation, UTEC 75-133, Progress Report No. 7, January 1 through June 30, 1975 (issued October 1975), University of Utah, Salt Lake City, UT.

172. H. K. Bowen, R. L. Pober, J. Cordero, M. Yoshimura, J. L. Nash-Webber, J. F. Louis, and W. R. Cannon, "Design and Performance of High-Temperature Ceramic Electrode Modules," op. cit., ref. 141, pp. IV.6.35 - IV.6.40.

173. T. O. Mason, W. T. Petuskey, W. W. Liang, J. W. Halloran, F. Yen, T. M. Pollak, J. F. Elliott, and H. K. Bowen, "Properties and Thermochemical Stability of Ceramics and Metals in an Open-Cycle, Coal-Fired MHD System," Proceedings of the Sixth International Conference on Magnetohydrodynamic Electrical Power Generation, Vol. II-Open Cycle Components and Materials, CONF-7506001-P2, June 9-13, 1975, Washington, D.C.

174. J. W. Hafstrom and J. T. Dusek, "Fabrication and Testing of MHD Electrodes Containing an Integral Leadout/Attachment System," op. cit., ref. 138, pp. G.4.1 - G.4.6.

175. J. W. Sadler, W. E. Young, L. H. Cadoff, J. A. Dilmore, E. L. Kochka, J. A. Kuszyk, J. Lempert, B. R. Rossing, S. J. Schneider, A. B. Turner, and S. Way, Development, Testing, and Evaluation of MHD Materials, Quarterly Report for the period January 1 through March 31, 1974 (issued April 1977), Westinghouse Electric Corporation, Pittsburgh, PA.

176. H. Yamada and G. R. Miller, "Point Defects in Reduced Strontium Titanate," J. Sol. State Chem. 6, 169-177 (1973).

177. J. C. Trocciola, United Technologies Corporation, S. Windsor, CT, private communication, June 5, 1978.

178. J. L. Bates, D. D. Marchant, J. L. Daniel and C. W. Griffin, Development, Characterization, and Evaluation of Materials for Open Cycle MHD, PNL-20047, Quarterly Report for the period ending September 1977 (iussued April 1978), Battelle Pacific Northwest Laboratory, Richland, WA.

APPENDIX A

BIBLIOGRAPHY OF ADDITIONAL REFERENCES FOR PHYSICAL AND CHEMICAL PROPERTIES OF CARBIDES RELATED TO HIGH-TEMPERATURE FUEL CELL NEEDS

1. G. V. Samsonov, L. A. Klochkov, and I. I. Timofeeva, "Thermal Expansion of Titanium Carbide, Zirconium Carbide, and Niobium Carbide in Their Homogeneity Regions," Vysokotemperatur. Karbidy 1975 46-8; Chem. Abstr. 83:171346 (1975).

2. G. V. Samsonov, I. I. Timofeeva, V. Ya. Naumenko, L. N. Bazhenova and B. M. Rud, "Properties of Niobium Carbide (Nb_2C) and Vanadium Carbide (V_2C) in the Homogeneity Region," Izv. Akad. Nauk SSSR, Neorg. Mater. 11(1), 62-5 (1975); Chem. Abstr. 82: 178614j 1975.

3. A. A. Boiko, B. N. Kodess, and V. Sh. Shekhtman, "Abnormal Trends in the Temperature Dependence of Coefficients of Thermal Expansion of Superconducting Niobium and Tantalum Carbides," Kristallografiya 17(3), 683-4 (1972); Chem. Abstr. 77: 80651r (1972).

4. V. G. Bukatov, G. A. Rymashevskii, and V. B. Fedorov, "Thermal Expansion of Nonstoichiometric Zirconium Carbides," Izv. Akad. Nauk SSSR, Neorg. Mater. 7(3), 519-20 (1971); Chem. Abstr. 75: 10473u (1971).

5. G. V. Samsonov, V. Ya. Naumenko, and L. N. Okhremchuck, "Preparation and Properties of Transition Metal Carbides in Their Homogeneity Ranges," Phys. Status Solidi A 6(1), 201-11 (1971); Chem. Abstr. 75: 92114o (1971).

6. A. L. Bowman, G. P. Arnold, and N. H. Krikorian, "Anisotropic Thermal Expansion of Refractory Carbides by High-Temperature Neutron Diffraction," J. Appl. Phys. 41(13), 5080-1 (1970); Chem. Abstr. 74: 25219u (1971).

7. G. V. Samsonov and V. Ya. Naumenko, "Thermal Expansion of Groups IV-V Transition Metal Carbides in the Regions of Their Homogeneity," Teplofiz. Vys. Temp. 9(5), 1093-5 (1970); Chem. Abstr. 74: 6126v (1971).

8. E. Rudy, Ternary Phase Equilibria in Transition Metal-Boron-Carbon-Silicon Systems II. Ternary Systems 8. Tantalum-Tungsten Carbon System, U.S. Clearinghouse Fed. Sci. Tech. Inform., AD 1966, AD-487622; Chem. Abstr. 70: 81393a (1969).

9. G. V. Samsonov and G. Sh. Upodkhaya, "Properties of Niobium and Tantalum Carbide Alloys in Their Homogeneous Region," Porosh. Met. 8(9) 70-4 (1968); Chem. Abstr. 70: 14117a (1969).

10. O. A. Golikova, E. O. Dzhafarov, A. I. Augustinik, L. V. Kudryashova, and S. S. Ordan'yan, "Electrical Properties of Solid Solutions of Carbides of Group IV and V Transition Metals," Fiz. Tverd. Tela 9(5), 1557-8 (1967); Chem. Abstr. 67: 77085x (1967).

11. O. A. Golikova, A. I. Avgustinnik, G. M. Klimashin, and L. V. Kozlovskii, "Electrical Properties of Titanium Carbide," Fiz. Tverd. Tela 7(9), 2860-2 (1965); Chem. Abstr. 64: 101a (1966).

12. Yu. B. Paderno, I. G. Barantseva, and Y. L. Yupko, "Measurement of Thermal Conductivity and Electrical Resistance of ZrC, HfC, NbC, and TaC at High Temperatures," Vysokotemp. Neorgan. Soedin., Akad. Nauk Ukr. SSR, Inst. Probl. Materialoved., 1965, 199-204; Chem. Abstr. 64: 13495c (1966).

13. T. Tsuchida, Y. Nokamura, M. Mekata, J. Sokurai, and H. Takaki, "Hall Effect in the Carbides of Transition Metals," J. Phys. Soc. Japan 16, 2453-6 (1961); Chem. Abstr. 57: 254i (1962).

14. S. N. L'vov, V. F. Nemchenko, and G. V. Samsonov, "Electrical Properties of Chromium Carbides," Fiz. Metal. Metalloved., Akad. Nauk SSSR 11(1), 143-5 (1961); Chem. Abstr. 55: 11231c (1961).

APPENDIX B

BIBLIOGRAPHY OF ADDITIONAL REFERENCES FOR PHYSICAL AND CHEMICAL PROPERTIES OF NITRIDES RELATED TO HIGH-TEMPERATURE FUEL CELL NEEDS

1. V. F. Nemchenko, G. V. Samsonov, and T. S. Verkhoglyadova, "Semiconductor Conductivity of Refractory Nitrides," Ukr. Fiz. Zh. 8(12), 1372-7 (1963); Chem. Abstr. 60: 7558h (1964).

APPENDIX C

BIBLIOGRAPHY OF ADDITIONAL REFERENCES FOR PHYSICAL AND CHEMICAL PROPERTIES OF SILICIDES RELATED TO HIGH-TEMPERATURE FUEL CELL NEEDS

1. T. G. Chart, "Thermodynamic Properties of the Tungsten-Silicon and Chromium-Silicon Systems," Met. Sci. 9(11), 504-9 (1975).

2. V. N. Eremenko, G. M. Lukashenko, and V. R. Sidorko, "Thermodynamic Properties of Vanadium, Chromium, and Manganese Silicides at Elevated Temperatures," Rev. Int. Hautes Temp. Refract. 12(3), 237-40 (1975); Chem. Abstr. 84: 36045s (1976).

3. V. I. Lazorenko, B. M. Rud, Yu. B. Paderno, L. A. Klochkov, and I. I. Timofeeva, "Thermal Expansion and Nature of Interatomic Interaction in Lanthanide Silicides," Dopov. Akad. Nauk Ukr. RSR, Ser. A, 36(9), 850-2 (1974); Chem. Abstr. 81: 178199g (1974).

4. R. P. Krentsis, G. I. Kalishevich, P. V. Gel'd, and L. P. Andreeva, "Thermal Expansion of Chromium, Manganese, Iron, and Cobalt Monosilicides," Izv. Vyssh. Ucheb. Zaved., Fiz. 15(1), 153-5 (1972); Chem. Abstr. 76: 145177s (1972).

5. E. Fitzer and K. Reinmuth, "Reaction of High-Melting Silicides with Nitrogen and Oxygen," Sixth High Temp. Mater. Pap. Plansee Semin., 1968, (Publ. 1969), 767-802, F. Benesovsky, Ed.; Chem. Abstr. 72: 74267a (1970).

6. G. I. Kalishevich, P. V. Gel'd and Yu. V. Putintsen, "Heat Capacity, Enthalpy, and Entropy of Chromium and Nickel Monosilicides," Tr. Ural. Politekh. Inst. 167, 152-4 (1968); Chem. Abstr. 70: 513332n (1969).

7. E. Nikitin, V. I. Tarasov, and P. V. Tamarin, "Thermal And Electrical Properties of the Higher Manganese Silicide from 4.2° to 3000° and Its Structure," Fiz. Tverd. Tela 11(1), 234-6 (1969); Chem. Abstr. 70: 81895r (1969).

8. B. S. Rabinovich, I. Z. Radovskii, and P. V. Gel'd, "Coefficients of Thermal Expansion of Chromium Disilicide and Its Solid Solutions with $TiSi_2$ and VSi_2," Porosh. Met. 8(11), 49-55 (1968); Chem. Abstr. 70: 91051b (1969).

9. G. I. Kalishevich, P. V. Gel'd, and Yu. V. Putintsev, "High-Temperature Enthalpy Changes of the High Silicides of V, Co, and Ni," Topelofiz. Vys. Temp. 6(6), 1003-6 (1968); Chem. Abstr. 70: 81695a (1969).

10. G. I. Kalishevich, P. V. Gel'd, and R. P. Krentsis, "Heat Capacity of the High Silicides of V, Co, and Ni at 60° to 300°," Zh. Fiz. Khim. 42(5), 1288-9 (1968); Chem. Abstr. 69: 30818q (1968).

11. B. K. Voronov, L. D. Dudkin, and N. N. Trusova, "Anisotropy of Thermoelectric Properties in Single Crystals of Chromium Disilicide and Higher Manganese Silicide," Kristollografiya 12(3), 519-21 (1967); Chem. Abstr. 67: 77269K (1967).

12. F. A. Sidorenko, I. Z. Radovskii, L. P. Zelenin, and P. V. Gel'd "Electric and Magnetic Properties of Solid Solutions of Vanadium and Titanium Disilicides in Chromium Disilicide," Porosh. Met. 6(9), 67-74 (1966); Chem. Abstr. 66: 32742x (1967).

13. L. P. Andreeva, F. A. Sidorenko, and P. V. Gel'd, "Valence of Atoms in Monosilicides of Some 3d-Transition Metals at Low Temperatures," Fiz. Metal. i Metalloved 19(5), 784-6 (1965); Chem. Abstr. 63: 14059a (1965).

14. G. V. Samsonov, V. S. Neshpor, and Yu. B. Paderno, "Preparation and Properties of Some Rare-Earth Silicides," Redkozem. Elementy, Akad. Nauk SSSR, Inst. Geokhim. i Analit. Khim. 1963, 22-35; Chem. Abstr. 61: 3893a (1964).

15. G. V. Samsonov, V. S. Neshpor, and V. A. Ermakova, "Properties of Alloys of the Niobium-Silicon System," Zhur. Neorg. Khim. 3, 868-78 (1958); Chem. Abstr. 52: 16165i (1958).

APPENDIX D

BIBLIOGRAPHY OF ADDITIONAL REFERENCES FOR PHYSICAL AND CHEMICAL PROPERTIES OF BORIDES RELATED TO HIGH-TEMPERATURE FUEL CELL NEEDS

1. R. Favre and F. Thevenot, "Preparation and Study of Titanium, Zirconium, and Hafnium Diborides," Bull. Soc. Chem. Fr. 11, 3911-16 (1971).

2. Yu. B. Paderno, V. V. Odintsov, I. I. Timofeeva, and L. A. Klochkov, "Thermal Expansion of Metal Dodecaborides," Teplofiz. Vys. Temp. 9(1), 200-2 (1971); Chem. Abstr. 74: 130646a (1971).

3. E. S. Garf and V. I. Shcherbina, "Electrophysical Properties of Rare-Earth Hexaborides at Low Temperatures," Teplofiz. Vys. Temp. 9(1), 110-16 (1971).

4. G. V. Samsonov, B. A. Kovenskaya, and T. I. Serebryakova, "Physical Characteristics of Group IV and V Transition Metal Diborides," Izv. Vyssh. Ucheb. Zaved., Fiz. 14(1), 19-23 (1971); Chem. Abstr. 74: 117318v (1971).

5. B. A. Kovenskaya, "Electrophysical Properties of Titanium, Zirconium, and Hafnium Diborides," Dopov. Akad. Nauk Ukr. RSR, Ser. A, 32(7), 661-3 (1970); Chem. Abstr. 74: 58250a (1971).

6. B. A. Kovenskaya and T. I. Lerebryakova, "Physical Properties of Boride Phases of Niobium," Porosh. Met. 10(5), 79-82 (1970); Chem. Abstr. 73: 70948w (1970).

7. I. N. Frantsevich and A. L. Lyashchenko, "Characteristic Temperature, Young's Modulus, and Root-Mean-Square Atomic Displacement in Lattices of Titanium, Vanadium, Chromium, Iron, Cobalt, and Zirconium Borides," Dopov. Akad. Nauk Ukr. RSR, Ser. A, 31(1), 64-6 (1969); Chem. Abstr. 71: 6274e (1969).

8. Yu. Paderno, V. I. Novikov, and E. S. Garf, "Electrical Properties of Alkaline-Earth and Rare-Earth-Metal Hexaborides at Low Temperatures," Porosh. Met. 9(11), 70-3 (1969); Chem. Abstr. 72: 36879u (1970).

9. V. P. Bondarenko and B. A. Kovenskaya, Electrophysical Properties of Cerium Hexaboride with Transition Metals I.," Izv. Vyssh. Ucheb Zaved. Fiz. 11(6), 66-70 (1968); Chem. Abstr. 69: 62611h (1968).

10. V. P. Bondarenko and B. A. Kovenskaya, "Temperature Dependence of the Electrophysical Properties of CeB_6 Alloys with Transition Metals II.," Izv. Vyssh. Ucheb. Zaved. Fiz. 11(6), 97-100 (1968); Chem. Abstr. 69: 62612j (1968).

11. G. V. Samsonov, L. A. Sorin, M. V. Vlasova, and V. I. Shcherbina "Some Electrophysical Properties of Rare-Earth Hexaborides," Dokl. Akad. Nauk SSSR 178(6), 1346-7 (1968); Chem. Abstr. 69: 13782 b (1968).

12. M. Konoshita, S. Kose, and Y. Hamano, "Hot-Pressing of Zirconium Diboride with Binder Metals," Yogyo Kyokai Shi 75(859), 84-90 (1967); Chem. Abstr. 69: 69432j (1968).

13. P. Peshev. "Thermodynamic Study on Some Reactions Used for the Preparation of Borides of Group II-VI Metals, "Rev. Int. Hautes Temp. Refract. 4(4), 289-96 (1967); Chem. Abstr. 69: 5740a (1968).

14. A. Y. Chang, Ternary Phase Equilibria in Transition Metal-Boron-Carbon-Silicon Systems. II. Ternary Systems. 5. Titanium-Hafnium-Boron System, U. S. Clearinghouse Fed. Sci. Tech. Inform., AD 1966, AD-482359, 64 pp.; Chem. Abstr. 70: 81392z (1969).

15. D. P. Harmon, Ternary Phase Equilibria in Transition Metal-Boron Carbon-Silicon Systems. II. Ternary Systems. 11. Hafnium-Molybdenum-Boron and Hafnium-Tungsten-Boron Systems, U.S. Clearinghouse Fed. Sci. Tech. Inform., AD 1966, AD- 800389, 54 pp.; Chem. Abstr. 70: 81396d (1969).

16. T. E. Eckert, Ternary Phase Equilibria in Transition Metal-Boron Carbon-Silicon Systems. II. Ternary Systems. 12. Ti-Zr-B Systems, Pseudobinary Systems ZrB_2-NbB_2, ZrB_2-TaB_2, and HfB_2-NbB_2, U. S. Clearinghouse Fed. Sci. Tech. Inform., AD 1966, AD-803913, 61 pp.; Chem. Abstr. 70: 81397e (1969).

17. C. E. Brukl and E. Rudy, Ternary Phase Equilibria in Transition Metal-Boron-Carbon-Silicon Systems. II. Ternary Systems. 14. Hf-Ir-B Systems, U. S. Clearinghouse Fed. Sci. Tech. Inform. AD 1966, AD-820649, 67 pp.; Chem. Abstr. 70: 81399g (1969).

18. G. L. Gal'chenko, D. A. Gedakyan, B. T. Timofeev, S. M. Skuratov, T. I. Serebryakova, and G. V. Samsonov, "Standard Heats of Formation of TaB_2 and $TaCl_5$," Dokl. Akad. Nauk SSSR 170(1), 132-4 (1966); Chem. Abstr. 66: 49785m (1967).

19. T. I. Serebryakova and B. A. Kovenskaya, "Physical Properties of Chromium Boride Phases," Izv. Akad. Nauk SSSR, Neorg. Mater. 2(12), 2134-8 (1966); Chem. Abstr. 67: 1513a (1967).

20. L. Kaufman and E. V. Clougherty, "Investigation of Boride Compounds for High-Temperature Applications," Fifth Plansee Proc., Seminar, Reutte/Tyrol, 1964 (Publ. 1965), 722-58; Chem. Abstr. 64: 17226e (1966).

21. T. I. Serebryakova, "The Nature of the Chemical Bond in Boron-Transition Metal Compounds," Izv. Akad. Nauk SSSR, Neorgan. Materialy 1(10), 1811-15 (1965); Chem. Abstr. 64: 7803b (1966).

22. M. T. Milliken and J. E. Senkin, Some Kinetic and Thermodynamic Properties of the Refractory Metal Borides and Nitrides. An Annotated Bibliography, U. S. At. Energy Comm. UCRL-7559, 1963, 341 pp.; Chem. Abstr. 60: 12992d (1964).

23. R. Mezaki, E. W. Tilleux, D. W. Barnes, and J. L. Margrave, "High-Temperature Thermodynamic Properties of Some Refractory Borides," Thermodyn. Nucl. Mater. Proc. Symp., Vienna, 1962, (Publ. 1963), 775-88; Chem. Abstr. 63: 332d (1965).

24. B. Post, Refractory Metal Borides, USAEC NP-12652, 1962, 67 pp.; Chem. Abstr. 61: 14325c (1964).

25. P. W. Gilles, "High-Temperature Chemistry of Binary Compounds of Boron," Advances in Chem. Ser. 32, 53-9 (1961).

APPENDIX E

BIBLIOGRAPHY OF ADDITIONAL REFERENCES FOR PHYSICAL AND CHEMICAL PROPERTIES OF GENERAL REFRACTORY COMPOUNDS RELATED TO HIGH-TEMPERATURE FUEL CELL NEEDS

1. S. M. L'vov, V. F. Nemchenko, and G. V. Samsonov, "Physical Properties of Borides, Carbides, Nitrides, and Silicides of Chromium," Izv. Vyssh. Ucheb. Zaved., Fiz. 5, 21-6 (1963); Chem. Abstr. 60: 7558h (1964).

2. J. Piper, Electrical Properties of Some Transition-Metal Carbides and Nitrides, NASA Accession No. N64-19548, Rept. No. AD-435624; Chem. Abstr. 62: 92h (1965).

3. S. M. L'vov and V. F. Nemchenko, "Temperature Relation of Thermal EMF and Specific Electrical Resistance of Titanium, Vanadium, and Chromium, and Their Borides, Carbides, and Nitrides," Vysokotemp. Neorgan. Soedin., Akad. Nauk Ukr. SSR, Inst. Probl. Materieloved. 1965, 100-71; Chem. Abstr. 64: 13495f (1966).

4. V. V. Fesenko, A. L. Bolgar, and S. P. Gordienko, "Vaporization Rate, Vapor Pressure, Composition Discontinuity, and Certain Thermodynamic Properties of Refractory Compounds at Temperatures Up to 3000°C," Rev. Int. Hautes Temp. Refract. 3(13), 261-71 (1966); Chem. Abstr. 66: 13737h (1967).

5. H. Bernstein and L. Kaufman, Development and Application of Methods of Predicting the Temperature-Composition Stability of Refractory Compounds, U.S.A.F. Systems Command, Res. Technol. Div., A.F. Mater. Lab. Tech. Rep. AFML TR-66-193, 1966, 157 pp.; Chem. Abstr. 66: 5442z (1967).

6. C. E. Brukl and D. P. Harmon, Ternary Phase Equilibria in Transition Metal-Boron-Carbon-Silicon Systems. II. Ternary Systems. 4. Titanium-Zirconium-Carbon, Titanium-Hafnium-Carbon, and Zirconium-Hafnium-Carbon, U. S. Clearinghouse Fed. Sci. Tech. Inform.,AD 1966, AD-480801, 92 pp.; Chem. Abstr. 70: 81391y (1969).

7. A. Y. Chang, Ternary Phase Equilibria in Transition Metal-Boron-Carbon-Silicaon Systems. II. Ternary Systems. 9. Zirconium-Carbon-Boron Systems and the Pseudobinary System Tantalum Diboride-Hafnium Diboride, U. S. Clearinghouse, Fed. Sci. Tech. Inform., AD 1966, AD-489140, 37 pp.; Chem. Abstr. 70: 81394b (1969).

8. C. E. Brukl, Ternary Phase Equilibria in Transition Metal-Boron Carbon-Silicon Systems. II. Ternary Systems. 10. Zirconium-Silicon-Carbon Systems and Hafnium-Silicon-Carbon, Zirconium-Silicon-Boron, and Hafnium-Silicon-Boron Systems, U. S. Clearinghouse, Fed. Sci. Tech. Inform., AD 1966, AD-489752, 109 pp.; Chem. Abstr. 70: 81395c (1969).

9. E. Rudy, Ternary Phase Equilibria in Transition Metal-Boron-Carbon-Silicon Systems. II. Ternary Systems. 13. Phase Diagrams of the Systems Ti-B-C, Zr-B-C, and Hf-B-C, U. S. Clearinghouse, Fed. Sci. Tech. Inform., AD 1966, AD-803270, 234 pp. Chem. Abstr. 70: 81398f (1969).

10. A. Nagahiro, M. Shiota, T. Fukui, Y. Amemiya, T. Hosoda, T. Mataba, S. Iida, and S. Takahashi, "Preparation and Testing of MHD-Duct-Wall and Electrode Materials," Elec. MHD Proc. Symp., Salzburg, Austria 3, 349-63 (1966); Chem. Abstr. 67: 58674x (1967).

11. V. S. Neshpor, Yu. N. Vilk, and I. N. Danisina, "Change in the Electro- and Thermophysical Properties in Pseudobinary Alloys along the Path $ZrC_{0.92}$-$ZrN_{0.85}$ of the Zr-N-C System," Porosh. Met. 7(1), 89-94 (1967); Chem. Abstr. 66: 109309w (1967).

12. R. F. Voitovich and N. J. Shakhanova, "Calculation of Heat Capacity of Refractory Compounds," Porosh. Met. 7(3), 75-9 (1967); Chem. Abstr. 67: 26516f (1967).

13. R. F. Voitvich, "Calculation of the Reduced Thermodynamic Potential of Some Carbides and Nitrides," Porosh. Met. 7(2), 40-3, (1967); Chem. Abstr. 67: 26484u (1967).

14. A. Would, Electrolytic Growth and Preparation of Transition Metal Compound Single Crystals, U. S. Clearinghouse Fed. Sci. Tech. Inform., AD 660615, 1967, 41 pp.; Chem. Abstr. 68: 90511y (1968).

15. V. G. Grebenkina, "Temperature Coefficient of the Electrical Resistivity of Borides, Carbides, Nitrides, and Silicides of Transition Metals," Tr. Nauch. Konf. Aspir. Inst. Probl. Materieloved. Akad. Nauk Ukr. SSR,1st 1967 (Publ. 1968), 144-51 Chem. Asbstr. 72: 16492j (1970).

16. G. V. Samsonov and V. G. Grebenkina, "Temperature Coefficients of the Electrical Resistivity of Some Refractory Compounds," Porosh. Met. 8(2), 35-40 (1968); Chem. Abstr. 69: 31233g (1968).

17. V. O. German, Yu. P. Kukota and G. A. Lyubinov, "Operation of Electrode Material Using Thermal and Chemical Surface Protection," Nop. Tekh. Teplofiz. Mater. Nauch. Konf. Molodykh. Issled., 1st, 1967, 148-54 (Publ. 1968); Chem. Abstr. 74: 17393f (1971).

18. V. G. Grebenkina, "Temperature Coefficient of the Electrical Resistivity of Borides, Carbides, and Silicides of Transition Metal," Tr. Nauch. Konf. Aspir. Inst. Probl. Materieloved. Akad. Nauk Ukr. SSR, 1st, 1967 144-51 (Publ. 1968); Chem. Abstr. 72: 16492j (1970).

19. Yu. G. Zainulin, S. I. Alyamovskii, G. P. Shveikin, and P. V. Gel'd, "Coefficients of Thermal Expansion of Cubic (Sodium Chloride Type) Oxycarbides and Oxynitrides of Zirconium and Hafnium," Teplofiz. Vys. Temp. 9(3), 546-9 (1971); Chem. Abstr. 75: 134063e (1971).

20. S. A. Alyamovskii, Yu. G. Zainulin, V. A. Tskhai, G. P. Shveikin and P. V. Gel'd, "Thermal Expansion of Titanium Oxycarbides and Oxynitrides with Sodium Chloride Type Structure," Izv. Akad. Nauk SSSR, Neorg. Mater. 8(10), 1770-3 (1972); Chem. Abstr. 78: 21158h (1973).

21. F. I. Ajami and R. K. MacCrone, "Thermal Expansion, Debye Temperature, and Gruneisen Constant of Carbides and Nitrides," J. Less-Common Met. 38(2-3), 101-10 (1974); Chem. Abstr. 82: 8325y (1975).

22. C. M. B. Henderson and D. Taylor, "Thermal Expansion of the Nitrides and Oxynitride of Silicon in Relation to Their Structures," Trans. J. Br. Ceram. Soc. 74(2), 49-53, (1975); Chem. Abstr. 83: 19737f (1975).

23. C. Politis, Thermal Lattice Dilation of Some Transition Metal Compounds, Kernforschungszentrum Karlsruhe, (Ber.), (KFK 2168), 1975, 86 pp.; Chem. Abstr. 83: 200480g (1975).

24. I. I. Matveenko, L. B. Dubrovskaya, G. D. Bogomolev, V. G. Zubkov, and P. V. Gel'd, "Electrical Conductivity of Titanium Oxycarbide," Izv. Akad. Nauk SSSR, Neorg. Mater. 6(6), 1190-1 (1970); Chem. Abstr. 73: 70946m (1970).

APPENDIX F

BIBLIPGRAPHY OF ADDITIONAL REFERENCES FOR PHYSICAL AND CHEMICAL PROPERTIES OF OXIDES RELATED TO HIGH-TEMPERATURE FUEL CELL NEEDS

1. S. K. Filatov and V. A. Frank-Kamenetskii, "Anomalous Thermal Expansion of Zirconium Dioxide and Hafnium Dioxide in the 20° to 2000° Range," Kristallografiya 14(5), 804-8, 1969, Chem. Abstr. 72: 25145a (1970).

2. A. M. Gavrish, B. Ya. Sukharevskii, E. I. Zoz, and A. E. Solov'eva, "Axial Thermal Expansion of Solid Solutions in the Zirconium Dioxide-Hafnium Dioxide System," Dokl. Akad. Nauk SSSR 199(4), 880-2, (1971); Chem. Abstr. 75: 123170m (1971).

3. D. M. Shakhtin, E. V. Levintovich, G. G. Eliseeva, A. G. Karaulov, and I. N. Rudyak, "Thermal Expansion of Fully and Partially Stabilized Zirconium Dioxide at 1000° to 2000°," Teplofiz. Svoistva Tverd. Tel Vys. Temp., Tr. Vses. Konf., Ser. 1, 94-8, (1969); Chem. Abstr. 73: 134155v (1970).

4. J. Hatibarua and P. C. Mahanta, "Lattice Expansion Data of the Oxides of Cerium, Praseodymium, and Erbium," Indian J. Pure Appl. Phys. 13(7), 479-980 (1975); Chem. Abstr. 83: 124418a (1975).

5. S. B: Kocheregin, A. K. Kuznetsov, and P. A. Tikhonov, "Anisotropy of Thermal Expansion of Hafnium Titanium Oxide ($HfTiO_4$) and the Solid Solutions of the Oxides," Izv. Akad. Nauk SSSR, Neorg. Mater. 11(2), 380-1 (1975); Chem. Abstr. 83: 36032o (1975).

6. G. Bayer, "Thermal Expansion Anisotropy of Oxide Compounds," Proc. Brit. Ceram. Soc. 22, 39-53 (1973); Chem. Abstr. 80: 30048r (1974).

7. V. I. Aleksandrov, E. E. Lomonova, A. A. Maier, V. V. Osiko, V. M. Tatarintsev, and V. T. Udovenchik, "Physical Properties of Zirconium Dioxide and Hafnium Dioxide Single Crystals," Kratk. Soobshch. Fiz. 11, 3-7 (1972); Chem. Abstr. 79: 97860x.

8. J. Hatibarua and P. C. Mahanta, "Thermal Expansion of the Oxides of Cerium, Praseodymium, and Erbium by the X-Ray Diffraction Method," Indian J. Pure Appl. Phys. 10(8), 599-601 (1972); Chem. Abstr. 78: 76622k (1973).

9. V. P. Elyutin, Yu. A. Pavlov, and A. V. Manukhin, "Relation Between Some Semiconductor and Chemical Properties of Metal Oxides," Sb., Mosk. Inst. Stali Spalvov 49, 46-68 (1968); Chem. Abstr. 70: 32635x (1969).

10. J. Millet, M. Guillou, and S. Palous, "Electrochemistry of Electronic-Ionic Mixed Semiconductor Oxides," Electrochim. Acta 13(6), 1425-40 (1968); Chem. Abstr. 69: 73429f (1968).

APPENDIX B

Fuel Cell - Quarterly Report - October 1, 1978

Harlan Byker, Reed A. Howald, Isaac Eliezer
and Mary Verwolf

Department of Chemistry
Montana State University
Bozeman, Montana 59717

The bulk of our work has been on the thermodynamic analysis of binary oxide subsystems of importance to work on molten carbonate fuel cells. These systems have included relatively simple ones with readily available data such as the potassium carbonate-lithium carbonate pseudo-binary. However most of the efforts have been on difficult and incompletely understood systems such as $KO_{.5}$-O and $KO_{.5}$-CO_2. These systems are sufficiently important that a substantial amount of experimental data exists. However, in part because the data have not been clearly understood, they are often available only in reports and in minor journals. The clearest example of this concerns vaporization data for potassium peroxide where the JANAF tables cite a 1935 IUPAC report (1) and one of the best studies is available only in the form of a thesis (2). Our initial treatment of the $KO_{.5}$-O system was based primarily upon the oxygen pressure data of Leffler and Wiederhorn (3), but as more data have been analyzed it has become increasingly clear that the measurements at high $KO_{.5}$ concentrations are not equilibrium oxygen pressures. Apparently (4) (5) there is appreciable vaporization as KO(g) or $K_2O_2(g)$ and this species reacts with glass walls to form oxygen. At the moment the comment of (6) that "The extensive literature data on the dissociation oxygen pressures over the various oxide phases cannot be reconciled with any reasonable thermodynamic data" is valid. However, we expect a recon-

ciliation to come from our continuing study of this literature with the recognition of $K_2O_2(g)$ as a significant species.

The first system we analyzed was the potassium carbonate-lithium carbonate pseudobinary. Equations were obtained from which the activities of $K(CO_3)_{.5}$ and $Li(CO_3)_{.5}$ can be calculated over a range of temperatures and compositions. The vapor pressures of various gaseous potassium and lithium containing species can be calculated in turn from these activities. This calculation is quite straightforward for gaseous species of known thermodynamic values such as K and KOH. Recent work of T. C. Ehlert (5) (7) has provided good data for $K_2CO_3(g)$ and $K_2O(g)$, and the most important gaseous potassium species for which there are still major uncertainties is probably $K_2O_2(g)$. In the presence of substantial CO_2 pressures, $K_2CO_3(g)$ is the major potassium species. Table 1 shows calculated equilibrium constants over a range of temperatures for the reaction $K_2CO_3(l) = K_2CO_3(g)$. In the presence of substantial pressures of both H_2O and CO_2, as in the anode gas stream in fuel cells, the principal gaseous species of the alkali metals are KOH and LiOH. A typical calculation of the pressures of KOH ignoring the effect of H_2O on the liquid phase activities is shown in Table 2. A similar analysis of lithium-containing gaseous species in equilibrium with lithium carbonate should be undertaken.

The first step in the thermodynamic analysis of binary systems is the selection of thermodynamic values for the pure materials. For purely hypothetical materials such as O(l) and $CO_2(l)$ at high temperatures, the selection of values is not critical because there is no experimental data

in the Raoult's law region for these materials. It has proved to be surprisingly difficult to obtain satisfactory values for liquid potassium oxide, $KO_{.5}$(l). There is an accepted (8) (9) value for the heat of formation of solid $KO_{.5}$ based upon some old heat of solution values (10), but there do not seem to be any definitive recent measurements to support this value. In fact the Leffler and Wiederhorn study (3) indicates that errors of as much as 9 kcal mol^{-1} are possible for potassium oxides. Potassium oxide is so reactive and so corrosive that good experimental data on it are very difficult to obtain, and only estimates are available for such basic properties as the standard entropy, melting point, and heat of fusion. We have been able to analyze potassium oxide systems such as $KO_{.5}$-SiO_2 (11) with a particular set of estimates because none of the experimental data used in the analysis is in a region of high $KO_{.5}$ concentrations. In contrast, Leffler and Wiederhorn (3) report oxygen pressures for the $KO_{.5}$-O system at mole fractions as high as 0.90 for $KO_{.5}$. These data also extend to near the KO_2 composition, X_1=0.40, and excellent thermodynamic values are available for solid and liquid potassium superoxide (6) (9) (12). Surprisingly, the data of Leffler & Wiederhorn (3) do not show a break in the curve of oxygen pressure vs. composition at the peroxide composition. The measured pressures in the peroxide to superoxide region (3) are in reasonable agreement with other measurements (2,13) including some data on the KO_2 liquidus curve (14). Our initial evaluation of these data was to accept them over the whole composition range, even though this requires a change of -5.884 kcal mol^{-1} in the enthalpy of liquid $KO_{.5}$. It was then possible to calculate a reasonable $KO_{.5}$-O phase

diagram using 960K for the melting point of potassium oxide. The results of this calculation are shown in Figure 1. Unfortunately this shift in the enthalpy of $KO_{.5}$ is inconsistent with mass spectrometric data on the vaporization of solid $KO_{.5}$(4). It is clear now that the $KO_{.5}$ liquidus will be much steeper than that shown in Figure 1, and a correct final calculated phase diagram will have a higher melting point for $KO_{.5}$ and a lower temperature for the eutectic between $KO_{.5}$ and K_2O_2. Work will continue in order to resolve the discrepancy.

There is a substantial body of literature (7,15-17) including an NSRDS review (18) on the vaporization of potassium carbonates. The recent work of Ehlert (7) resolves some of the previous discrepancies and gives good thermodynamic values for K_2CO_3(g). It also provides vapor pressure data, and hence activities and activity coefficients for $KO_{.5}$ and CO_2 over a narrow but significant range of compositions and temperatures. We have analyzed these data (4,7) and fitted Redlich-Kister coefficients to them. However, because of the uncertainties remaining in the thermodynamic values for $KO_{.5}$(1) we have been unable to complete these calculations. The definitive reference for the $LiO_{.5}$-CO_2 binary system (19) has been located and obtained on inter-library loan, but these data have not yet been analyzed.

The bulk of our efforts in the last month have been devoted to the $LiO_{.5}$-$AlO_{1.5}$ system. The literature work was initiated early in the contract period, but calculations on this system were deferred while waiting for photocopies of the significant articles. This matter of scheduling of the calculations accounts for the number of systems upon which calculations have started, but are not yet completed.

The $LiO_{.5}$-$AlO_{1.5}$ calculations have now been carried through to the second complete calculated phase diagram, shown here as Figure 2. This phase diagram is substantially more detailed than the best existing literature sketches (20,21) and is supported by quite reliable thermodynamic values for the solids present, and reasonable activity coefficient calculations in the spinel and liquid phases. The quantity of literature analyzed in this system is sufficient that the discussion has been written up separately, and constitutes an appendix to this report.

REFERENCES

1. M. Centnerszwer and M. Blumenthal, IX Congr. IUPAC, 3A 201 (1935).
2. John F. Riley, Diss. Abstr. 30 598B (1969); Ph.D. thesis, Univ. of Rhode Island, (1968).
3. A. J. Leffler and N. M. Wiederhorn, J. Phys. Chem., 68, 2882 (1964).
4. T. C. Ehlert, private communication.
5. T. C. Ehlert, High Temp. Sci., 9, 237 (1977).
6. L. Brewer, Chem. Reviews, 52, 1 (1953).
7. L. L. Simmons, L. F. Lowden, and T. C. Ehlert, J. Phys. Chem., 81 706 (1977).
8. D. D. Wagman, U. S. Nat. Bur. Stand., Circular 500 (1950).
9. JANAF Thermochemical Tables. Nat. Stand. Ref. Data Ser. Nat. Bur. Stand. NSRDS37 (1971).
10. M. E. Rengade, Compt. Rend., 145, 236 (1907); Ann. Chim Phys., 14, 540 (1908).
11. N. Eliezer, R. A. Howald, M. Marinkovic and I. Eliezer, J. Phys. Chem. 82, 1021 (1978).
12. P. W. Gilles and J. L. Margrave, J. Phys. Chem., 60, 1333 (1956).
13. R. deForcrand, Compt. Rend 158, 843, 991 (1914).
14. A. B. Tsentsiper and T. I. Rogozhnikova, Bull. Akad. Nauk, SSR, 189 (1967).
15. J. T. Howarth and W. E. S. Turner, J. Soc. Glass. Tech., 15 360 (1931).
16. T. Kosugi, Bull. Chem. Soc., Japan, 45 15 (1972).
17. C. Kroger and J. Stratmann, Glastechn. Ber., 34 311 (1961).
18. Natl. Stand. Ref. Data. Ser. Natl. Bur. Stand., 30 (1969).
19. M. V. Smirnov and I. Ya. Liubimtseva, Tr. Inst. Electrokhim. Ural Nauchn. Tsentr, Akad. Nauk SSR., 16, 82 (1970).

20. D. W. Strickler and R. Roy, J. Am. Ceramic Soc., 44, 225 (1961).

21. A. M. Lejus and R. Collongues, Compt. Rend. 254, 2005 (1962).

TABLE 1

Equilibrium Constants, KEQ, Calculated for the Reaction

$$K_2CO_3(\ell) \rightarrow K_2CO_3(g)$$

Values of ΔH and ΔG in cal mol^{-1} are also listed.

T, K	KEQ	ΔH, cal/mol	ΔG, cal/mol
900.00K	0.216348E-09	0.680616E 05	0.398005E 05
925.00K	0.603944E-09	0.678000E 05	0.390190E 05
950.00K	0.159099E-08	0.675077E 05	0.382450E 05
975.00K	0.397146E-08	0.671843E 05	0.374791E 05
1000.00K	0.942913E-08	0.668291E 05	0.367219E 05
1025.00K	0.213643E-07	0.664411E 05	0.359739E 05
1050.00K	0.463390E-07	0.660197E 05	0.352358E 05
1075.00K	0.964815E-07	0.655646E 05	0.345081E 05
1100.00K	0.193316E-06	0.650744E 05	0.337915E 05
1125.00K	0.373623E-06	0.645490E 05	0.330864E 05
1150.00K	0.698020E-06	0.639872E 05	0.323934E 05
1175.00K	0.126303E-05	0.633889E 05	0.317130E 05
1200.00K	0.221735E-05	0.627530E 05	0.310456E 05
1225.00K	0.378309E-05	0.620792E 05	0.303920E 05
1250.00K	0.628206E-05	0.613665E 05	0.297525E 05
1275.00K	0.101674E-04	0.606143E 05	0.29.276E 05
1300.00K	0.160597E-04	0.598221E 05	0.285178E 05
1325.00K	0.247847E-04	0.589891E 05	0.279238E 05

Table 7

Calculation of Equilibrium Pressures of KOH(g) in Atmospheres Over $K(CO_3)_{.5}$ - $Li(CO_3)_{.5}$ Liquids at 1000K and 900K with $P(CO_2) = P(H_2O)$

T = 1000K $K = .828727 \times 10^{-5} = P(KOH)P^{\frac{1}{2}}(CO_2)/a_1 P^{\frac{1}{2}}(H_2O)$

X_1	a_1*	P(KOH) atm
.4	.33117	$.27445 \times 10^{-5}$
.5	.45062	$.37344 \times 10^{-5}$
.6	.57121	$.47338 \times 10^{-5}$

T = 900 $K = .346522 \times 10^{-6}$

X_1	a_1	P(KOH) atm
.4	.30767	$.10661 \times 10^{-6}$
.5	.42942	$.14880 \times 10^{-6}$
.6	.55491	$.19229 \times 10^{-6}$

*Activities were calculated using the following Redlich-Kister coefficients for the $K(CO_3)_{.5}$ - $Li(CO_3)_{.5}$ liquid phase.

	A	B
$\log \gamma_{1000}$	-.298561	.117924
enthalpy (cal mol^{-1})	-3972.2	525.

Figure 1. Phase diagram for the $KO_{.5}$-O system based upon the vapor pressure measurements of Leffler and Wiederhorn (3). The calculations are close to correct in the region between K_2O_2 and KO_2, but entirely wrong between $KO_{.5}$ and K_2O_2 where the measured pressures do not correspond to equilibrium oxygen pressures.

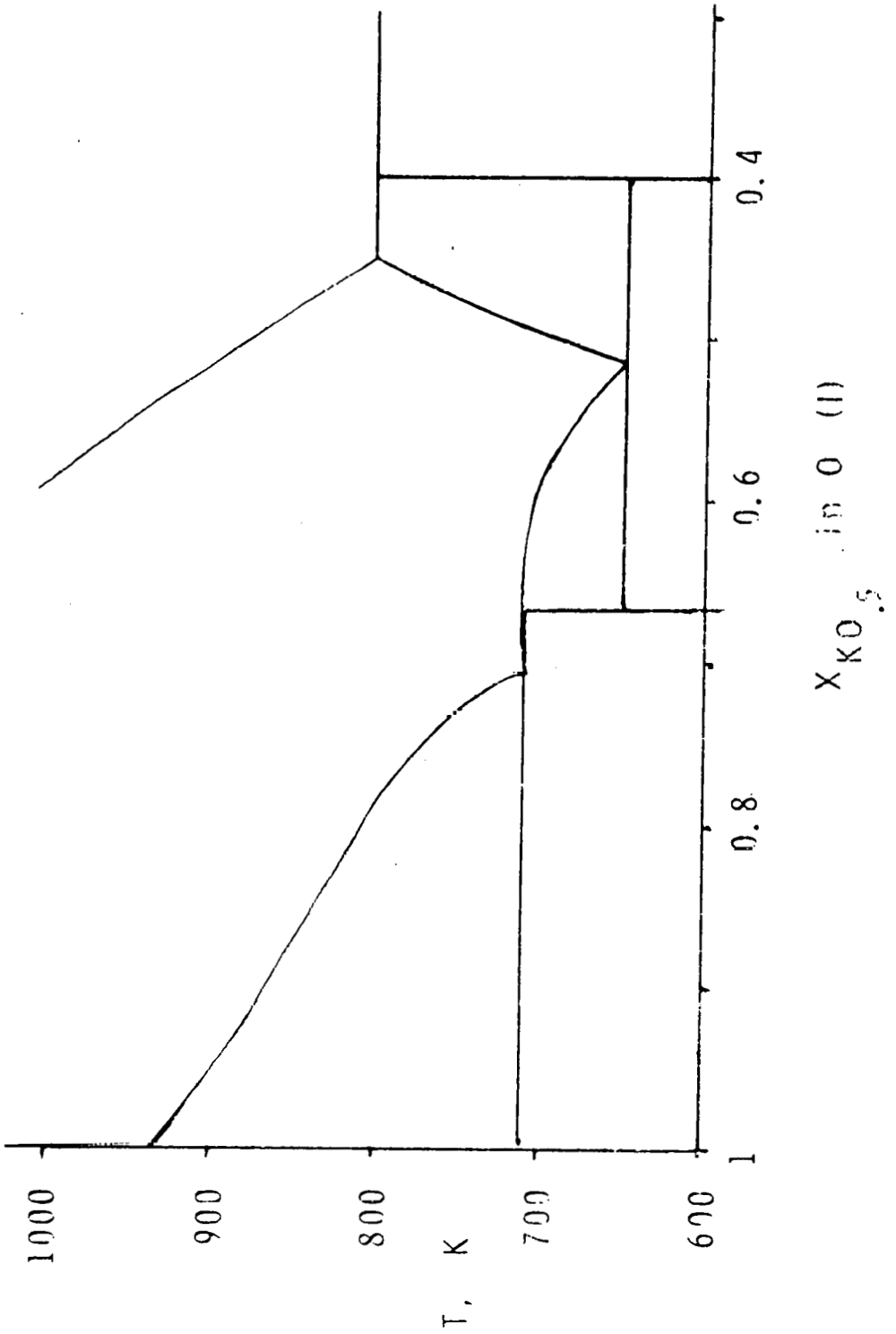

Figure 2. Preliminary calculated phase diagram for the lithium oxide-aluminum oxide system.

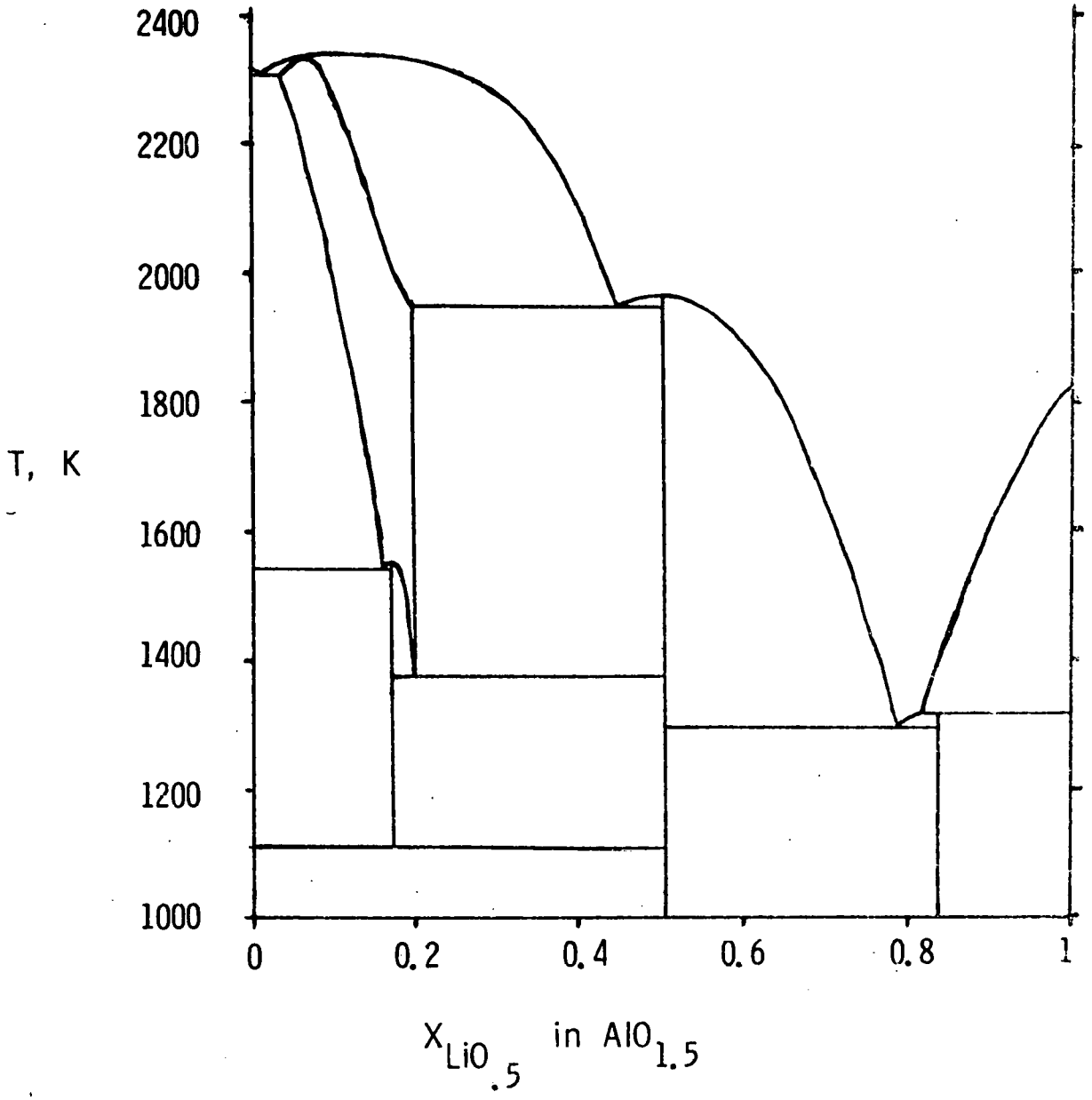

Preliminary calculated phase diagram for the $LiO_{.5}$-$AlO_{1.5}$ system.

THIS PAGE

WAS INTENTIONALLY

LEFT BLANK

Calculation of a Preliminary Phase Diagram for the $LiO_{.5}$-$AlO_{1.5}$ System with A Review on Lithium Aluminum Oxides

Harlan J. Byker, Isaac Eliezer, Naomi Eliezer,
Reed A. Howald, Mary C. Verwolf and Puligandla Viswanadham

Chemistry Department
Montana State University
Bozeman, Montana 59717

THIS PAGE

WAS INTENTIONALLY

LEFT BLANK

Lithium oxide is a strong base, and it forms a whole series of compounds with aluminum oxide, even though aluminum oxide is a weak acid. The best characterized compound is the one-to-one reaction product, $LiAlO_2$. At least three different crystal structures, α, β and γ(1,2) are known for $LiAlO_2$, but it appears that only the gamma form is thermodynamically stable. There is a stable spinel structure on the alumina-rich side of the phase diagram(3,4) which can be formulated as $Li_{.5}Al_{2.5}O_4$, although these crystals are stable over a substantial range of stoichiometry at high temperature(5-6). The compounds at the lithium-rich side of the phase diagram are naturally more highly basic and thus quite reactive, but at least two have been identified and characterized, Li_5AlO_4 and Li_3AlO_3(7). The stoichiometry Li_3AlO_3 is nominally an orthoaluminate, with all the hydrogen atoms of $Al(OH)_3$ replaced with lithium, but it is not exceptionally stable. In fact Li_3AlO_3 disproportionates to $LiAlO_2$ and Li_5AlO_4 on heating above 723 K(7).

The degree of acidity of aluminum oxide is somewhat variable as is the coordination number of aluminum with oxide ions. Alumina tetrahedra readily share corners to form large polymeric anions analogous to SiO_2 and silicates. However, since Al has one less electron than Si, these structures have one net negative charge per Al atom, and the $LiAlO_2$, $NaAlO_2$ and $KAlO_2$ stoichiometries are natural. In aqueous solutions, aluminum ions can adopt six-fold coordination in species such as $Al(H_2O)_6^{3+}$, $Al(H_2O)_5OH^{2+}$ etc. The hydrated aluminum ion is

amphoteric, but even in strong hydroxide solutions the most negatively charged ion produced is $Al(H_2O)_2(OH)_4^-$, with only one negative charge per aluminum atom. In crystal structures, alumina octahedra often share edges or faces. It is common to find OH ions shared between two octahedra, as one H and two Al^{3+} octahedra will completely satisfy the electrostatic valence rule(8) for an oxygen atom. Full layers of such octahedra are found in crystalline $Al(OH)_3$ and there are similar layers in micas and clays. In the corundum crystal structure, each oxygen atom is a part of four Al^{3+} octahedra, which again exactly satisfies the electrostatic valence rule. Thus Al_2O_3 reacts with oxide ions not because of any inherent reactivity of the corundum structure, but simply to help distribute the charge on the oxide ion

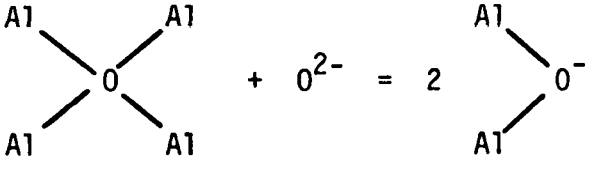

In principle, this type of reaction can proceed to form orthoaluminate ions, AlO_3^{3-}, and this can even form a coordinate covalent bond to another oxide ion giving AlO_4^{5-}. In fact, the reaction with the first oxide ion is only mildly exothermic, and as negative charge builds up per Al atom, the tendency for further reaction rapidly decreases. In most cases it is the meta-aluminate, with only one negative charge per Al atom, which is most stable.

Thus the compounds $NaAlO_2$ and $KAlO_2$ are well known, while Na_3AlO_3 and K_3AlO_3 are prepared only with great difficulty if at all. A higher negative charge on oxygen atoms is stabilized by more highly charged cations, and a large variety of crystalline calcium aluminates are known. CaO is a weak base, so none of the reactions of CaO with Al_2O_3 is very exothermic, but again the most exothermic corresponds to the meta-aluminate composition (9)

$$1/3\ CaO(s) + 1/3\ Al_2O_3(s) = 1/3\ CaAl_2O_4(s),\ \Delta H = -1.2366\ kcal\ mol^{-1}.$$

The stoichiometry for a calcium orthoaluminate is known, but here the heat of reaction is even smaller (9)

$$3/5CaO(s) + 1/5Al_2O_3(s) = 1/5Ca_3Al_2O_6(s),\ \Delta H = -0.326\ kcal\ mol^{-1}.$$

Table 1 summarizes the data compiled by the NBS (9) on the heats of formation of crystalline calcium aluminates at 298.15K

Table 1.

X_{CaO}	formula	heat of formation from elements kcal mol^{-1}	heat of formation from oxides, kcal per mole metal atoms
.20000	$CaO{\cdot}2Al_2O_3$	- 950.7	+ .418
.33333	$CaO{\cdot}Al_2O_3$	- 556.0	-1.2366
.46154	$12CaO{\cdot}7Al_2O_3$	-4644.	- .7315
.50000	$2CaO{\cdot}Al_2O_3$	- 707.	- .73
.60000	$3CaO{\cdot}Al_2O_3$	- 857.5	-.326
.66667	$4CaO{\cdot}Al_2O_3$	-1008.	- .0567

The formation of sodium meta-aluminate is considerably more exothermic (10)

$1/4Na_2O(s) + 1/4Al_2O_3(s) = 1/2\ NaAlO_2 \qquad \Delta H = -10.32\ kcal\ mol^{-1}$

but even here we do not expect the reaction with additional sodium oxide to be very exothermic.

The reactions of Li_2O should be intermediate between those of Na_2O and CaO, and, as expected, the reaction

$1/4Li_2O(s) + 1/4Al_2O_3(5) = 1/2LiAlO_2 \qquad \Delta H = -6.2025\ kcal\ mol^{-1}$

is moderately exothermic (10-12) using the best current data for $Li_2O(s)$, $\Delta H^o_{f298} = -142.89$ (10,12).

La Ginestra et. al (7) have reported differential thermal analysis results for the heats of reaction

$3Li_2O(s) + Al_2O_3(c,\gamma) = 2Li_3AlO_3(s) \qquad \Delta H_{673} = -16.5 \pm 2kcal\ mol^{-1}$

and

$5Li_2O(s) + Al_2O_3(c,\gamma) = 2Li_5AlO_4(s) \qquad \Delta H_{743} = -13.5 \pm .8\ kcal\ mol^{-1}$

We have selected and published values for the thermodynamic properties of gamma alumina (13) from which we can calculate ΔH for the reaction

$LiO_{.5}(s) + AlO_{1.5}(c,\gamma) = LiAlO_2(s) \qquad \Delta H_{700} = -15.02\ kcal\ mol^{-1}$

with only a slight variation with temperature. Combining this with the reactions of La Ginestra et al. (7) gives

$LiAlO_2(s) + 4LiO_{.5}(s) = Li_5AlO_4(s) \qquad \Delta H = +8.27\ kcal\ mol^{-1}.$

and

$LiAlO_2(s) + 2LiO_{.5}(s) = Li_3AlO_3(s) \qquad \Delta H = +6.77\ kcal\ mol^{-1}$

We assume that ΔC_p is zero for these reactions, so these ΔH values are valid at the temperatures of measurement and at 298.15K. Thus we can calculate the heats of formation at 298.15K as -420.22 kcal mol^{-1} for Li_3AlO_3 and -561.61 for Li_5AlO_4. These values are significantly different from the heats of formation at higher temperatures given in the abstract of the experimental work (7) primarily because the melting point of lithium comes below the experimental reaction temperatures.

These values can be used to calculate the heat for the disproportionation of Li_3AlO_3 to Li_5AlO_4 and $LiAlO_2$

$$1/4Li_3AlO_3 = 1/8Li_5AlO_4 + 1/8LiAlO_2 \qquad \Delta H = -.66 \text{ kcal mol}^{-1}.$$

Since this reaction occurs when Li_3AlO_3 is heated (1), we know that if this reaction is exothermic, Li_3AlO_3 is thermodynamically unstable at all temperatures. The formation of Li_3AlO_3 at 673K from Li_2O_2 plus gamma alumina does not establish that Li_3AlO_3 is thermodynamically stable at this temperature, and we have chosen to omit Li_3AlO_3 from the equilibrium phase diagram. However the range reported for the enthalpy of Li_3AlO_3(7), ± 2 kcal mol^{-1}, is almost wide enough to admit a slight endothermicity for the reaction. Li_3AlO_3 could have a heat of formation of -423 kcal mol^{-1} and be a thermodynamically stable phase at 298K.

Li_5AlO_4(c) is a thermodynamically stable phase, but since its formation from $LiAlO_2$ and $LiO_{.5}$ is endothermic, it is stabilized by entropy of mixing on the cationic sites rather than by enthalpy. This is further evidence that meta-aluminates are not very acidic. Thus we are on quite safe grounds in assuming that the minimum excess enthalpy

of mixing for $LiO_{.5}(\ell)$ and $AlO_{1.5}(\ell)$ occurs at a mole fraction near .5, and certainly not at the orthoaluminate composition $X_1 = .75$. There are essentially no heat data for lithium aluminate liquids. Even the heat of fusion of $LiAlO_2$ is only an estimate in the JANAF tables which give T_m = 1883K, ΔH_m = 6 kcal mol^{-1} in 1961 (10) and T_m = 1883K, ΔH_m = .21 kcal mol^{-1} in 1973 (14). The data in support of the melting point at 1883 K (3,15) are somewhat shaky since the same paper shows a sample only partially fused after a considerable time at 1973K. On the other hand there is a substantial body of data for a melting point near 1975K (16) or 1973 ±15K (17), and this value has been accepted in the phase diagram of Lejus and Collongues (6).

The thermodynamic properties of solid gamma (tetragonal) $LiAlO_2$ are quite well established (14) including three independent enthalpy values (18,20), low temperature heat capacity data (21) and drop calorimetric values to 1795K (22). We have fitted the heat capacity values (10,14,22) from 800 to 1800K to the power series $C_p = 24.35106 + .0040882(T-1000) - .83333 \times 10^{-6}(T-1000)^2$ to facilitate the calculation of enthalpy values and equilibrium constants at any temperature desired. Table 2 is a computer calculation of the thermodynamic properties of $LiAlO_2$ at a selected set of temperatures. Table 3 summarizes the input parameters for this calculation together with similar values for the other principal solids and liquids in this system. The choices for alpha and liquid $AlO_{1.5}$ are discussed in connection with the $AlO_{1.5}$-SiO_2 system (13),

and the $LiO_{.5}$ values are chosen to match the JANAF values (10). With these values the enthalpy of $LiAlO_2$(c) is -243333 cal mol^{-1} at 1973K. If the heat of fusion is 21 kcal mol^{-1}, the enthalpy of the liquid is -222333 cal mol^{-1}, 9911 calories more negative than the sum of one mole of each of the pure liquids at this temperature. Thus the excess enthalpy of mixing is -4955 calories mol^{-1}, and can be represented by the Redlich-Kister (23) coefficients.

A(H) = -19821, B(H) = 0, and C(H) = +11256.

The equilibrium constant for $LiAlO_2 \rightarrow LiO_{.5}(\ell) + AlO_{1.5}(\ell)$ is .0117542 at 1973 K. If this is accepted as the correct melting point, it gives log $\gamma_1\gamma_2$ = -1.3278 at 1973 K, which can be corrected using the enthalpy terms to log $\gamma_1\gamma_2$ = -1.34470 for X = .500 at 1943, the eutectic temperature. A similar calculation for the eutectic composition, X = .45 at 1943K (4), gives log $\gamma_1\gamma_2$ = -1.37619.

We can get both γ_1 and γ_2 at this composition if we have good thermodynamic values for the solid spinel present in this equilibrium. Venero and Westrum (24) have measured the heat capacity of solid $LiAl_5O_8$ from 7.4 to 541K, which gives the value S^o_{298} = 35.798 cal mol^{-1} K^{-1}. We can assume with very little error that the heat capacity at higher temperature is given as the sum $C_p(LiO_{.5}) + 5[C_p(AlO_{1.5})]$. Using this in conjunction with the heat of formation at 968 K (25) reported in ref. 24 gives a full set of thermodynamic values for the spinel. However these values cannot be

completely correct, since they indicate disproportionation of $LiAl_5O_8$ to $LiAlO_2$ and corundum at all temperatures. There is evidence that the spinel is stable (3) even below the order-disorder transition near 1563K (6,26). Preventing this disproportionation requires an entropy of mixing of at least 3.3 cal mol^{-1} K^{-1} even in the "ordered" form. Complete randomization of Li and Al in both tetrahedral and octahedral sites will give 5.4 cal mol^{-1} K^{-1} entropy of mixing, part of which should be shown in the third law entropy value. For the high temperature form of $LiAl_5O_8$ in Table 3 we have added the full 5.4 cal mol^{-1} K^{-1} to the entropy at 298.15 and to the free energy function at 1000K. The enthalpy measured at 968K must apply to a more ordered material and to calculate the enthalpy of the high temperature form we assumed that the transition at 1563K involves ΔH = +1563 cal mol^{-1} and ΔS = +1.0 cal mol^{-1} K^{-1}. Later it was necessary to increase ΔH to 2563 cal mol^{-1} to get a better phase diagram. This gives reasonable values for the enthalpy and entropy of the high temperature form of $LiAl_5O_8$ which are shown in Table 3. The equilibrium constant at 1943K calculated from these values for the reaction

$$LiAl_5O_8(c) \rightarrow LiO_{.5}(\ell) + 5AlO_{1.5}(\ell)$$

is $.6062 \times 10^{-3}$. This corresponds to $\log \gamma_1\gamma_2^5 = -1.572$, which goes well with $\log \gamma_1\gamma_2 = -1.376$ for the same temperature and eutectic composition. From these values we can calculate $\log \gamma_2 = -.049$, $\gamma_2 = .893$ and

an activity of a_2 = .491 for liquid alumina at the eutectic. We have used these values. However, it is possible that $LiAl_5O_8$ is more stable than this, and that $AlO_{1.5}$ has an activity coefficient substantially smaller than .89 at a mole fraction of .55.

There is in fact good evidence for an enthalpy for $LiAl_5O_8(c)$ substantially more negative than the value $H^o_{298.15}$ = -1080.4 kcal mol^{-1} which corresponds to γ_2 = .89 at the eutectic. Guggi, Ihle, and Neubert (20) have studied the vaporization of lithium oxide and lithium aluminates, providing both second and third law enthalpy values for these compounds. The values for $LiAlO_2$ (20) are in excellent agreement, within 0.2 kcal mol^{-1}, with the other studies on gamma $LiAlO_2$(18,19). Guggi et al. report an enthalpy of -568 ± 3 kcal mol^{-1} for Li_5AlO_4, in fair agreement with the value -561.6 calculated here from the data of La Ginestra et al. (7). Unfortunately, the measurements (20) for $LiAlO_2$ + $LiAl_5O_8$ and for $LiAl_5O_8$ + Al_2O_3 are not in agreement, giving values of $H^o_{298.15}$ for $LiAl_5O_8$ of -1096 ± 3 and -1091 kcal mol^{-1}. Both of these values are substantially more negative than the value -1080 kcal mol^{-1} which we obtained from the heat of solution of Gross (24). Guggi et al. (20) also cite a value around -1093 kcal mol^{-1} from an unreferenced report (27).

With the direct experimental data on enthalpy covering this wide a range, it is reasonable to turn to the phase diagram for guidance. The melting point of $LiAl_5O_8$ is reported as 1950°C or 2123K with a

question mark(6). Presumably $LiAl_5O_8$ melts over a range of temperatures as the compositions of both liquid and solid vary, but we can expect that pure solid $LiAl_5O_8$ would be in equilibrium with liquid of the same composition somewhere in the range 2100 ± 200K. At 1973K at X = .5 for $LiO_{.5}$ - $AlO_{1.5}$ liquid we have log γ_e = -.664. The value will increase as the temperature is raised to about log γ_e = -.63 at 2100K and X = .5. We can then estimate log γ^e at X = .166667 as -.21, and the equilibrium constant for the reaction

$$LiAl_5O_8(c) \rightarrow LiO_{.5}(\ell) + 5\ AlO_{1.5}(\ell)$$

should be approximately K = .0037 at the melting point. This value for the equilibrium constant is reached at about 2175K for H^o_{298} = -1080.4 kcal mol^{-1}. Even for the next lower value, H^o = -1091 kcal mol^{-1}, this calculation gives a melting point above 2450K. Thus the information available on the melting point of $LiAl_5O_8$ provides excellent support for the -1080 kcal mol^{-1} value for the enthalpy (24,25), and this value has been selected for Table 3.

With these values selected for the two solids, we can calculate the activities of both components in the eutectic liquid, a_1 = .0211876 and a_2 = .491249. The value for a_2 is only about 10% less than the mole fraction. Thus the Raoult's law region for $AlO_{1.5}$ extends out to a mole fraction of nearly 0.45 for $LiO_{.5}$. This behavior with a break at X = 0.50 is approximated by a set of three Redlich-Kister coefficients proportional to those selected for the enthalpy. To give log $\gamma_1\gamma_2$ = -1.34470 at X = .500 one can use the set A(log γ) = -2.6894, B(log γ) = 0, and C(log γ) = 1.52724 at 1943K. This set was tested in the

calculation but it gives a eutectic for $LiAlO_2$ - $LiAl_5O_8$ substantially below 1943K. A much better phase diagram is obtained using only two Redlich-Kister coefficients at 1943K, with the B value selected to give log γ_2 = -.0628 at X = .45. Thus the Redlich-Kister coefficients at 1943K are -2.6894, -1.9826, and 0.0. The Redlich-Kister coefficients at 1000K can be calculated from these, using the enthalpy coefficients given above. The three values at 1000K are -4.7918, -1.9826 and 1.1939. They are listed in Table 4. With these values we can calculate the liquidus curve for $LiAlO_2$ shown in Figure 1. This curve shows a significant solubility of gamma $LiAlO_2$ ($X_{AlO_{1.5}} = X_2 = .24$) in liquid lithium oxide at 1400K. The related solubility in carbonate electrolytes with excess lithium oxide present may be a significant feature in fuel cell longevity, and it is important to extend this work to the calculation of $LiO_{.5}$ and $AlO_{1.5}$ activity coefficients in three and four component systems.

The $LiAlO_2$ liquidus curve in Figure 1 gives a melting point of 1973K and a good fit at the eutectic with $LiAl_5O_8$ because these data were used in the curve fitting process. However the curve on the $LiO_{.5}$ rich side also looks quite reasonable. Even the calculated temperature for the $LiAlO_2$ - Li_5AlO_4 eutectic in Figure 1 is reasonably close to the temperature, 1320 ± 10K, reported (20) for the melting point of Li_5AlO_4(c).

The crystal structure of the compound Li_5AlO_4 is a distorted form of the Li_2O lattice with Al^{3+} ions substituted for Li^+ and cation vacancies (28,29). This has interesting consequences for the ionic conductivity of this material (30,31). For the phase diagram, it suggests that both

cubic Li_2O and orthorhombic Li_5AlO_4 will exist over a substantial range of compositions. It would be valuable to include this in a calculated phase diagram. However, this would require more data than are available on the various solubility relationships at high temperatures. The general features of the liquidus curves are indicated by calculations for equilibria with stoichiometric $LiO_{.5}$ and Li_5AlO_4, and this is what is shown in Figure 1. The heat capacity used for Li_5AlO_4 is estimated as the sum of those for $LiAlO_2$ and $4LiO_{.5}$, and the free energy function at 1000K listed in Table 3 was selected to give Li_5AlO_4 a congruent melting point in one of the preliminary calculations. With the final values used for the liquid phase, Li_5AlO_4 must melt incongruently unless the melting point is 1400K or higher.

At the other side of the phase diagram, we have a substantial amount of data for the spinel phase. The thermodynamic values in Table 3 for the stoichiometric form, $LiAl_5O_8$, correspond to an excess enthalpy of formation from $LiO_{.5}(c)$ and $AlO_{1.5}(c,\gamma)$ of $3.97 \pm .20$ kcal mol^{-1}. The value for $\log \gamma^e$ depends upon the free energy of pure solid gamma alumina, which is alumina with a spinel structure. The value selected in our work on the $AlO_{1.5}$-SiO_2 system corresponded to equilibrium between α and γ alumina at 2342K. This low value was necessary for a good fit of the highest temperature point of Aksay and Pask (32). The latest (6/30/75) JANAF estimates (33) give 2420K for this temperature. The solubilities of $AlO_{1.5}$ in $LiAl_5O_8$ reported by Lejus and Collongues extrapolate to 3465K for pure alumina, which is much too high. The JANAF value (33) is a

reasonable compromise, so we have used it for the calculations here and for the gamma alumina values in Table 3.

With the JANAF values (33) selected for the standard state of pure gamma alumina we can calculate log γ values for the points where we have experimental data. At 1673K we get log γ^e = -.314074 at X = .166667 from the properties of stoichiometric $LiAl_5O_8$ and log γ_2 = -.07287 from the composition reported by Lejus and Collongues (6), X_2 = .85714, for saturation with corundum. It is possible to fit these two values with two Redlich-Kister coefficients. However, we have chosen to use a set of four coefficients which give more curvature at X = .16667. The final set of coefficients used for the calculations of the lithium aluminate spinel phase boundaries in Figure 1 are listed in Table 5.

The liquidus and solidus curves for the melting of lithium aluminate spinel consist of two lines intersecting at the melting point of gamma alumina, 2284 K. In this particular calculation, the two lines are tangent at a maximum melting point. However for most compositions a spinel will melt over a range of temperatures. Both published phase diagrams (4,6) show a melting point of 2223K for $LiAl_5O_8$, which is inside the range of 2030 to 2340 shown in figure 1 for melting of this composition.

The maximum melting point for $LiAl_5O_8$ at X = .065 is one of the most striking features of Figure 1. A melting point above that for pure gamma alumina (2284K) implies that the addition of $LiO_{.5}$ stabilizes the spinel more than it stabilizes the liquid phase. This is not at all unreasonable; in fact, the behavior is shown for MgO in the $MgO-AlO_{1.5}$

phase diagram (34). However, the solubility data for corundum in lithium alumina spinel (6) indicate positive deviations from ideality, while the liquid phase is close to Raoult's law. It is thus likely that the maximum is an artifact of the calculation. It could easily be eliminated by the use of an additional Redlich-Kister coefficient for the liquid phase.

The shape of the left hand edge of the spinel region is pretty much determined by the temperature used for equilibrium between gamma alumina and corundum, and the point of Lejus and Collongues (6) at X = .14286 and 1673K. They also report a value of X = .103 at 2173K, which is in only fair agreement with our calculated value of X = .085 at this temperature. An experimental reexamination of the range of equilibrium spinel compositions would be very valuable. This could be done quite easily with diffusion couple techniques.

There are a number of other questions concerning the equilibrium behavior of the $LiO_{.5}$-$AlO_{1.5}$ system which are not answered by the preliminary phase diagram in Figure 1. The most important of these questions are considered in the following sections of this report together with pertinent literature references and suggestions for further work which might provide further clarification.

The stability of alpha $LiAlO_2$. Hexagonal crystals of alpha $LiAlO_2$ are readily prepared in a variety of reactions (1,2,35,36-38). On heating, the alpha crystals are converted to gamma (tetragonal) crystals (35,6,38 - 41), but different samples appear to undergo the transformation somewhat

differently. It has been observed as low as 873K (35) but samples have been held at 983K for 3 days without reaction (2). The dilatometric results of Lejus and Collongues (6) clearly show an irreversible transformation at about 1173K. At these temperatures, the γ phase is clearly the stable form at one atmosphere pressure. There are claims that the α phase is stable at lower temperatures (6), but it is also likely that it is not thermodynamically stable even at 298K (35). The reverse transformation is observed at higher pressures, 35 kbar at 1123K (35). Since the volume change on reaction is known (5,35,36), this gives us an approximate value for ΔG of the transition, 4.56 kcal mol^{-1}, if the equilibrium pressure is 30 kbar. The enthalpy and entropy for the α form could be independently established either by studies of the equilibrium pressure at two temperatures or by careful enthalpy measurements of heats of solution or of heats of transformation by differential thermal analysis. The gamma form has tetrahedra sharing edges, so it is likely that the alpha form can have greater disorder of the cations and a higher entropy. Thus it is likely that the alpha to gamma transition at high temperature is exothermic, but not enough to make the alpha form stable at 1 atm before the melting point is reached. The transitions between the crystal forms are slow and it is difficult to measure the enthalpy of transition by differential thermal analysis (42). However, at temperatures around 1200K, the alpha to gamma transition has been shown to be endothermic (38). It cannot be highly endothermic or the alpha form would not transform to the gamma form at this temperature (38) at 1 atm pressure. This is sufficient

information combined with reasonable entropy estimates to estimate the phase boundary between the alpha and gamma forms of $LiAlO_2$ in a temperature-pressure plot. If ΔG is positive at 1200K for the reaction

$$LiAlO_2(c,\gamma) \rightarrow LiAlO_2(c,\alpha)$$

but ΔH is negative (the reverse reaction is endothermic), there must be a negative ΔS in the equation

$$\Delta G = \Delta H - T\Delta S$$

It is reasonable to expect that the lower density gamma form has a higher thermal entropy, and 1200K could be below the expected order-disorder transition for the alpha crystals. ΔS could be as low as -2 cal $mol^{-1}K$. With this value for ΔS, the minimum possible value for ΔH is -2.4 kcal mol^{-1}, and it is reasonable to expect it to be in the range -1 ± 1. ΔG at 1123K is thus probably 1.2 ± 1 kcal mol^{-1}. This is considerably less than the +4.56 kcal mol^{-1} value for equilibrium at 30 kbar, but it is possible that the equilibrium pressure is as low as 8 kbar.

Alpha $LiAlO_2$ has both cations in octahedral positions, and considerable cation disorder should be possible at high temperatures. Complete cation randomization would give an entropy of $2(4.5756 \log 2) = 2.7$ cal $mol^{-1}K^{-1}$. We can expect an order-disorder transition in alpha $LiAlO_2$. We have estimated a transition at 1400K with $\Delta S = +2$ cal $mol^{-1}K^{-1}$ and $\Delta H = +2.8$ kcal mol^{-1}. These estimates together with an assumed value of $\Delta C_p = 0$ give the estimated temperature pressure phase diagram in figure 2. This is certainly not an accurate calculation, but it is a very useful starting point in interpreting experimental data. It indicates for example that the very slow gamma to alpha transition reported by Lejus and Collongues (6) at about 370K may be correct.

The liquid region in Figure 2 is sketched assuming that the liquid at 1 atm is less dense than even the gamma crystals, but that the liquid is quite compressible.

Stability of the beta form of $LiAlO_2$. Beta $LiAlO_2$ (1,2) has both tetrahedral and octahedral cations and a density close to that of the gamma form (43). It can be prepared at one atmosphere pressure (1.43) although high pressure (2) was used in the initial preparations. Work is needed here to determine both the equilibrium pressure and the heat of transition. There is no reason to believe that beta $LiAlO_2$ is thermodynamically stable at one atmosphere pressure and high temperatures, so we expect beta $LiAlO_2$ to convert to the gamma form on heating. It is not clear at what temperature we can expect this to occur. However, a recent paper cites 1173K (43). The range of transition temperatures observed for the alpha to gamma transition is an indication that these transformations can be catalyzed, and they should be studied both in the presence and absence of a molten carbonate liquid phase. Alpha and beta $LiAlO_2$ have cations in octahedral sites, so they should be stabilized by the presence of larger ions such as Mg^{2+} and Ga^{3+}. The transitions and, if possible, the equilibria in the presence of up to 10% doping with additional ions should be studied. Even a rough estimate of the region of T and P in which beta $LiAlO_2$ is stable would assist in the interpretation of the available data on beta $LiAlO_2$. If the density is as low as 2.61 g cm^{-3} (43) it has roughly the same molar volume as gamma $LiAlO_2$ and probably is not thermodynamically stable at any temperature and pressure.

Thermodynamics of the spinel phase. Early work with gamma $LiAlO_2$ (44) reported a reversible transition in the range 1473 to 1573K. This has not been confirmed in later work (4) and was probably the result of the order-disorder transition (6,45) in some $LiAl_5O_8$ crystals which may have been present. The calculated phase diagram in Figure 1 indicates that this transition starts at a lower temperature for $LiAl_5O_8$ saturated with $LiAlO_2$ than for the stoichiometric composition.

In any case it is clear that $LiAl_5O_8$ can be present in equilibrium with solid $LiAlO_2$ from a high temperature eutectic down to a temperature below 1200K where the equilibrium favors disproportionation to corundum and gamma $LiAlO_2$. The equilibrium disproportionation temperature was found at 1110K in the calculations for figure 1. Unfortunately neither of these equilibria are well established, and the stability of $LiAl_5O_8$ is somewhat uncertain. However any substantial change from the values used in Figure 1 will be inconsistent with the high temperature data (3,4). In any case it is desirable to check the heat capacity, enthalpy and entropy of $LiAl_5O_8$ in as many ways as possible.

Choosing a lower enthalpy for $LiAl_5O_8$ would tend to increase the area for this phase in the phase diagram, including increased solubilities of corundum in the spinel. The line in Figure 1 is constrained to go through the value reported by Lejus and Collongues (6) at 1673K, X_1 = .14286. It is questionable whether this could be maintained with the spinel almost 8 times as stable as suggested by the enthalpy data of Guggi et al. (20).

It is also desirable to test the activity coefficient equations used in calculating Figure 1. The temperatures for liquids in the high alumina side of the phase diagram are rather high for vapor pressure measurements, and probably the best check that can be obtained here is by careful measurements on the Li_5AlO_4 - $LiAlO_2$ eutectic. An experimental check for the spinel phase will be even more difficult, but a detailed theoretical study of the spinel in the MgO-$AlO_{1.5}$ system could add to confidence in the $LiO_{.5}$-$AlO_{1.5}$ equations. It should be possible to obtain good activity coefficient equations for spinels in the ternary system $LiO_{.5}$-$AlO_{1.5}$-MgO.

Other features on the alumina rich side of the phase diagram. The maximum in the spinel meting point in figure 1 obscures most of the region where the corundum liquidus curve should lie. The calculated corundum liquidus using activity coefficients for the liquid phase calculated from the numbers in Table 4 is quite flat around 2290K and X = .16 because the calculation gives positive deviations from ideality in this region. This can be adjusted with more Redlich-Kister coefficients for the liquid, but what is really necessary is additional activity coefficient data in this range of compositions and temperatures to evaluate additional coefficients. The experimental problems in working at such high temperatures are severe, but it should be possible to find and measure the liquid in equilibrium with corundum, spinel, or both. Another interesting possible feature of the phase diagram

in this region which should be checked by additional experiments and calculations is the possible equilibrium presence of delta alumina (46).

Vaporization Studies of Lithium Aluminates. Lithium compounds are of interest as possible blanket materials in a fusion reactor, where the lithium serves as a source of tritium by nuclear reactions (20,47-49). Lithium aluminates are of special interest because the reactions of Al and O with neutrons do not cause serious additional problems. Thus Guggi et al. (20, 50-51) and others (52) have undertaken studies of the vaporization behavior of the lithium aluminates. Lithium oxide vaporizes (53-59) primarily as Li atoms and O_2 and as $Li_2O(g)$ Other gaseous lithium oxides including LiO(g) and $Li_2O_2(g)$ are present to a minor extent. The thermodynamics of the gaseous lithium oxides are quite well established (10), but work is still proceeding to refine the values (60). If there is any water present, LiOH(g) is a major high temperature species (10,61-64) and mixed oxide species such as LiOK(g) and LiONa (10) may be significant. Compounds with stable small anions may sublime without decomposition to some extent, giving species like $Li_2CO_3(g)$ and $Li_2SO_4(g)$ although this does not occur with lithium compounds to the extent found for the heavier alkali metals. In any case, gaseous lithium aluminates should not be significant, and the interpretation of their vaporization data should be straightforward. Thus the agreement of the data for $LiAlO_2(s)$ (20) with values of the enthalpy from other methods (16,19) is to be expected. The value for Li_5AlO_4

from vaporization data (20) may be more accurate than the differential thermal analysis value (7), but this difference will not make a major change in the calculated phase diagram. The reason for the discrepancy observed for $LiAl_5O_8$ is unclear, and must await more detailed publication of the vapor pressure values. It is possible that the difficulty lies in the range of compositions possible for the spinel as shown in Figure 1.

Other areas of active current work on lithium aluminates. We have not attempted to cite all the procedures reported in the literature for the formation of lithium aluminates. It is true that the changes observed for different starting materials, temperatures, and pressures may give significant data on relative stabilities, and a detailed study could be valuable. Annopol'skii and coworkers have several recent papers (65-56) summarizing their observations with various alkali hydroxides and carbonates. Studies on ternary systems such as MgO-$LiAlO_2$(67) and $LiAlO_2$-$LiGaO_2$ (68) may prove very valuable when data become available on the effects of substitution on the alpha-gamma equilibrium.

The substitution of Al^{3+} for Fe^{3+} in lithium ferrites is covered in such a wide range of papers that only a few leading references can be included here (24,69). The literature on lithium aluminum silicates is even more voluminous, but almost all of it is in the region of over 40% SiO_2, quite far from regions of possible interest in fuel cells.

One of the significant uses of $LiAl_5O_8$ is as a host lattice for the luminescence of transition metals. This literature includes significant

information on preparing both ordered and disordered forms, and the spectra provide further information on cation positions. Thus a substantial but not exhaustive listing of the references is in order here (70-75). The spinel structure exists at even lower $LiO_{.5}$ concentrations, and recent papers describe the structure (76), phase transitions (77), and e.s.r (78) of these solid solutions.

On the lithium-rich side of the phase diagram, there is additional IR data for both α and β Li_5AlO_4 (79) and a calculated Madelung energy (80) for the observed crystal structure (80). The value calculated for $5LiO_{.5}(c) + AlO_{1.5}(c,\alpha) \rightarrow Li_5AlO_4$ is $\Delta H = -6.8$ kcal mol^{-1}. This is a good compromise between the value $\Delta H = -4.14$ kcal mol^{-1} calculated from table 3 and $\Delta H = -10.5$ from the heat of formation of Guggi et al. (20).

There is also one important paper on fuel cell work which covers equilibria between molten alkali carbonates and $LiAlO_2$ (81).

REFERENCES

1. K. Kinoshita, J. W. Sim, and J. Ackerman, Mat. Res. Bull., 13, 445 (1978).

2. C. H. Chang and J. L. Margrave, J. Am. Chem. Soc., 90, 2020 (1968).

3. F. A. Hummel, B. S. R. Sastry, and D. Wotring, J. Am. Ceramic Soc., 41, 88 (1958).

4. D. W. Strickler and R. Roy, J. Am. Ceramic Soc., 44, 225 (1961).

5. P. Bassoul, A. Lefebvre and J. C. Gilles, Mat. Res. Bull., 11, 11 (1976).

6. A. M. Lejus and R. Collongues, Compt, Rend., 254, 2005 (1962).

7. A. La Ginestra, M. Lo Jacono, and P. Porta, Journal of Thermal Analysis, 4, 5 (1972).

8. L. Pauling, The Nature of the Chemical Bond, Cornell Univ, Press

9. D. D. Wayman, W. H. Evans, V. B. Parker, I. Halow, S. M. Bailey, & R. H. Schumm, National Bureau of Standards, Technical Note 270-3, 270-4, 270-5 and 270-6 (1968-76).

10. JANAF Thermochemical Tables, Natl. Stand. Ref. Data Ser., Natl. Bur. Stand. NSRDS-NBS 37 (1971).

11. P. A. G. O'Hare, M. Ader, W. N. Hubbard, G. K. Johnson, and J. L. Settle, Proc. 4th Symp. Therm. Nuclear Materials, Vol. II, p. 439 (1975).

12. J. F. Smith and Z. Moser, J. Nuclear Materials, 59, 158 (1976).

13. R. A. Howald and I. Eliezer, J. Phys. Chem., 82, October (1978).

14. JANAF Thermochemical Tables, 1974 Supplement, J. Phys. Chem. Ref Data, 3,311 (1974).

15. K. H. Kim and F. A. Hummel, J. Am. Ceramic Soc., 43, 611 (1960).

16. H. Prophet, private communication, cited in JANAF (10).

17. D. W. Strickler and R. Roy, J. Am. Ceramic Soc., 44, 225 (1961).

18. J. P. Coughlin, J. Am. Chem. Soc., 79, 2397 (1957).

19. P. Gross, J. Christie and C. Hayman, Fulmer Research Inst. Report R. 163/SR16 (June 1970).

20. D. Guggi, H. R. Ihle, and A. Neubert, Proc. 9th Symp. on Fusion Technology, pp. 635-543, Pergamon Press, Oxford, U.K., (1976).

21. E. G. King, J. Am. Chem. Soc., 77 3189 (1955).

22. A. U. Christensen, K. C. Conway, and K. K. Kelley, U.S. Bur. Mines Rept. Invest. 5565 (1960).

23. O. Redlich, A. T. Kister and C. E. Turnquist, Chem. Eng. Programs, Symposium Series, 48, 49 (1952).

24. A. F. Venero and E. F. Westrum, Jr., J. Chem. Thermodynamics, 7, 693 (1975).

25. P. Gross, personal communication cited in reference 24.

26. P. Tarte, Compt. Rend, 254, 2008 (1962).

27. N. D. Potter, M. H. Boyer, F. Ju, D. L. Hildenbrand, E. Murad, and W. F. Hall, Final Technical Report, Thermodynamic Properties of Propellant Combustion Products, AD 6/5.567 (1970).

28. F. Stewner and R. Hoppe, Z. Anorg. Allgem. Chem., 381, 149 (1971); 380, 241 (1971).

29. H. A. Lehman and H. Hasselbarth, Z. Anorg. Allgem. Chem., 315, 15 (1962).

30. R. T. Johnson, Jr., R. M. Biefeld and J. D. Keck. Mat. Res. Bull., 12, 577 (1977).

31. I. D. Raistruck, C. Ho and R. A. Huggins, Mat. Res. Bull, 11, 953 (1976).

32. I. A. Aksay and J. O. Pask, J. Am. Ceramic Soc., 58, 507 (1975).

33. JANAF Thermochemical Tables, 1975 Supplement, J. Phys. Chem. Ref. Data 4, 1 (1974).

34. D. M. Roy, R. Roy & E. F. Osborn, Am. J. Sci., 251, 337 (1953).

35. M. Marezio and J. P. Remeika, J. Chem. Phys., 44, 3143 (1966).

36. M. Marezio, Acta. Cryst. 19, 396 (1965).

37. T. A. Lokotosh and S. S. Lisnyak, Izv. Vyssh Vichebn. Zaved., Khim. Khim. Technol, 20 (9), 1278 (1977).

38. S. Gol, K. Tomor, E. Pungor, G. Sooki-Toth and P. Horvath, Journal of Thermal Analysis, 9, 241 (1976).

39. H. A. Lehman and H. Hesselbarth, Z. Anorg. Allgem. Chem., 313, 117 (1961).

40. N. N. Semenov, Izv. Sit. Òtd., Akad. Nauk. SSSR Ser. Khim, 2 156 (1967).

41. G. Sooki-Toth, P. Horvath, S. Gal, and K. Lomor, 5th Conf. Ceramics for Electronics, Liblice (CSSR) 22 (1974).

42. J. Ackerman, private communication.

43. A. K. Fischer, Inorg. Chem., 16 974 (1977).

44. F. A. Hummel, J. Am. Ceramic Soc., 34, 235 (1951).

45. R. K. Datta & R. Roy, J. Am. Ceramic Soc., 46 388 (1963).

46. A.-M. Lejus and R. Collongues, Compt. Rend., 254, 2780 (1962).

47. K. Sako, M. Ohta, Y. Seki, H. Yamoto, T. Hiraoka, K. Tanaka, N. Asami and S. Mori Report, JAERI-M 5102 (Dec. 1973).

48. J. R. Powell, F. T. Miles, A. Aronson, W. E. Winsche. Report BNL-18236 (1973).

49. B. Badger, R. W. Conn, G. L. Kulcinsky, M. A. Abon, R. Aronstern, H. I. Avci, R. W. Boom, T. E. Cheng, J. Davis, J. M. Donhowe, G. H. Emnest, Y. Eyssa, N. M. Ghoniam, S. Ghose, W. Houlberg, J. Kessner, W. Lue, C. W. Maynard, A. Mense, N. Mohare, H. A. Peterson, T. Y. Sung, I. Sviatoslavsky D. K. Sye, R. Weaterman, J. L. Wittenberg, T. F. Yang, J. Young and W. D. Young. Report UW FDM-112 (Oct. 1975).

50. D. Guggi, A. Neubert & K F. Zm bov, Proc. 4th Int. Conf. on Chemical Thermodynamics, 124 (1975).

51. D. Guggi, H. Ihle, A. Neubert and R. Woelfle, Radcat: Eff. Tritium Technol. Fusion React. Proc. Int. Con., 3, 416 (1976).

52. O. S. Popkov, and G. A. Semenov, Zhur. Fiz. Khim., 45, 476 (1971).

53. J. Berkowitz, W. A. Chupka, G. D. Blue and J. L. Margrave, J. Phys. Chem., 63, 644 (1959).

54. D. White, R. S. Seshadri and D. F. Dever, D. E. Mann and M. J. Linevsky, J. Chem. Phys., 39, 2463 (1963).

55. D. L. Hildenbrand, W. F. Hall & N. D. Potter, J. Chem. Phys. 39, 296 (1963).

56. L. P. Firsova and A. N. Nesmayanov, Russ. J. Phys. Chem., 34 1232 (1960).

57. L. Brewer, Chem. Reviews, 52 1 (1953).

58. A. Buechler, J. L. Stauffer, W. Klemperer, and L. Wharton, J. Chem. Phys., 39 2299 (1963).

59. L. Brewer & J. L. Margrave, J. Chem. Phys., 59 421 (1955).

60. E. L. Wagner, Theor. Chim. Acta, 32, 295 (1974).

61. J. M. King, Report EPRI, EM-576, Project 114-2 (1977).

62. D. E. Jensen and P. J. Padley, Trans Farad. Soc., 62 2132 (1966).

63. D. H. Cotton and D. R. Jenkins, Trans. Farad. Soc., 65, 1537 (1969).

64. M. J. McEwan and L. F. Phillips, Combustion and Flame, 9, 457 (1960).

65. E. K. Belyaev and V. F. Annopol'skii, Zh. Neorg. Khim, 17, 2072 (1972).

66. V. F. Annopol'skii, E. K. Belyaev, and I. P. Knigovko, Zh. Neorg. Khim., 20, 298 (1975).

67. R. C. Doman and R. N. McNally, J. Mater. Sci., 8, 189 (1973).

68. H. Schwarzer and H. Neels, Krist. Tech, 6, 639 (1971).

69. N. N. Efimova and Yu. A. Mamalui, Ukr. Fiz. Zh., 20, 1201 (1975).

70. P. M. Jaffe, J. Electrochem. Soc., 115, 1203 (1968).

71. G. T. Pott and B. D. McNichol, Chem. Phys. Letters, 12, 52 (1971); J. Solid State Chem., 7, 132 (1973); J. Chem. Phys., 56, 5246 (1972); J. Luminescence, 6, 320 (1973).

72. M. N. Baranov and E. F. Kustov, Opt. Spektrosk., 34, 726 (1973).

73. W. H. J. Stork and G. T. Pott, J. Phys. Chem., 78, 2496 (1974).

74. W. P. Petrov, H. Szymczak, R. Wades, and W. Wardzynski, J. Phys. (Paris), 32, Suppl. 847 (1971).

75. H. P. Fritzer, E. Sliuc, and K. Torkar, Monatsh. Chem., 104 172 (1973).

76. A. Fruma, D. Ciomartan, J. Brasoveanu and I. V. Nicolescu, Rev. Roum. Chim. 18, 803 (1973).

77. N. F. Ermolenko, M. D. Efror and A. V. Oboturov Absorbenty. Ikh. Poluch., Svoistva Primen. Tr. Vses. Soveshch. Adsorbentam, 3rd 1969, 83 (1971).

78. R. T. Cox, Solid State Commun., 9 1989 (1971).

79. V. A. Kolesova, Zh. Neorg. Khim., 19 2898 (1974)

80. R. Happe and H. Koenig, Z. Anorg. Allg. Chem., 430, 211 (1977).

81. G. H. J. Broers and H. J. J. Van Ballegoy, Journees Int. Etude Piles Combust, C. R. 3rd 1969 77 (1969).

Table 2. Thermodynamic Values for Gamma $LiAlO_2$. ΔH_T^o in cal mol^{-1}, the free energy function in cal $mol^{-1}K^{-1}$, and C_p in cal $mol^{-1}K^{-1}$.

T,K	ΔH_T^o	ϕ	C_p
1000.000	-268706.00000	23.006989	24.35106
900.000	-271120.43750	21.435760	23.93391
925.000	-270520.68750	21.834457	24.03976
950.000	-269918.37500	22.229279	24.14456
975.000	-269313.50000	22.620132	24.24834
1000.000	-268706.00000	23.006989	24.35106
1025.000	-268095.93750	23.389816	24.45274
1050.000	-267483.37500	23.768631	24.55338
1075.000	-266868.31250	24.143417	24.65298
1100.000	-266250.68750	24.514221	24.75154
1125.000	-265630.75000	24.881012	24.84908
1150.000	-265008.31250	25.243866	24.94554
1175.000	-264383.43750	25.602829	25.04097
1200.000	-263756.25000	25.957932	25.13536
1225.000	-263126.68750	26.309235	25.22871
1250.000	-262494.81250	26.656754	25.32103
1275.000	-261860.62500	27.000595	25.41229
1300.000	-261224.18750	27.340805	25.50252
1325.000	-260585.56250	27.677429	25.59169
1350.000	-259944.68750	28.010529	25.67984

Table 3. Thermodynamic Properties of the Pure Materials in the $LiO_{.5}$-$AlO_{1.5}$ System

Substance	S^o_{298} cal $mol^{-1}K^{-1}$	Φ^o_{1000} cal $mol^{-1}K^{-1}$	H^o_{298} kcal mol^{-1}	H^o_{1000} kcal mol^{-1}	Cp equation A	$Bx10^3$	$Cx10^6$	$Dx10^9$	$Ex10^6$
$LiAlO_2$ (c,γ)	12.75	23.007	-284.1	-268.706	24.35106	4.0882	-.83333		
$AlO_{1.5}$ (c,corundum)	6.087	12.2175	-200.25	-190.933	14.908	2.3471	-1.2717	.34615	
$AlO_{1.5}$(c,γ)	6.25	12.668	-198.000	-188.245	15.5835	1.40191	-.12140	0	-.53590
$AlO_{1.5}$ (ℓ,<2000K)	9.27	16.5551	-190.358	-182.152	17.312				
$AlO_{1.5}$ (ℓ,<2000K)	--	(19.1587)	-190.358	(-191.020)	27.66	-2.96			
$LiO_{.5}$(c)	4.528	8.6045	-71.445	-65.222	10.3127	3.1535	-1.5276		
$LiO_{.5}$(ℓ)	6.58	12.5897	-64.2084	-57.9674	9.84	2.7			
$LiAl_5O_8$ (c,spinel,high temp form)	41.198	75.90	-1080.437	-1027.637	84.5049	9.84839	-2.1074	0	-2.5592
$LiAl_5O_8$ (c,ordered spinel,low T)	40.198	74.399	-1082.8	-1030.0	84.5049	9.84839	-2.1074	0	-2.5592
Li_5AlO_4(c)	27.83	64.8742	-561.61	-521.324	65.6019	16.702	-6.9437		
Li_3AlO_3(c)	22.	44.	-420.22	-392.60	40.9765	10.3952	-3.8895		

Table 4

Redlich-Kister Coefficients for the Liquid Phase in the $LiO_{.5}$ - $AlO_{1.5}$ System

	A	B	C
log γ_{1000}	-4.7918	-1.9826	1.1939
enthalpy kcal mol^{-1}	-19.821	0.0	11.256

Table 5

Redlich-Kister Coefficients for the Solid Spinel Phase in the $LiO_{.5}$ - $AlO_{1.5}$ System Referred to $LiO_{.5}(c)$ and $AlO_{1.5}(c,\gamma)$ as Standard States.

	A	B	C	D
log γ_{1000}	-3.971271	.847024	-.578040	-.068274
enthalpy kcal mol^{-1}	-23.7622	5.0690	-3.4593	-0.4086

Figure 1

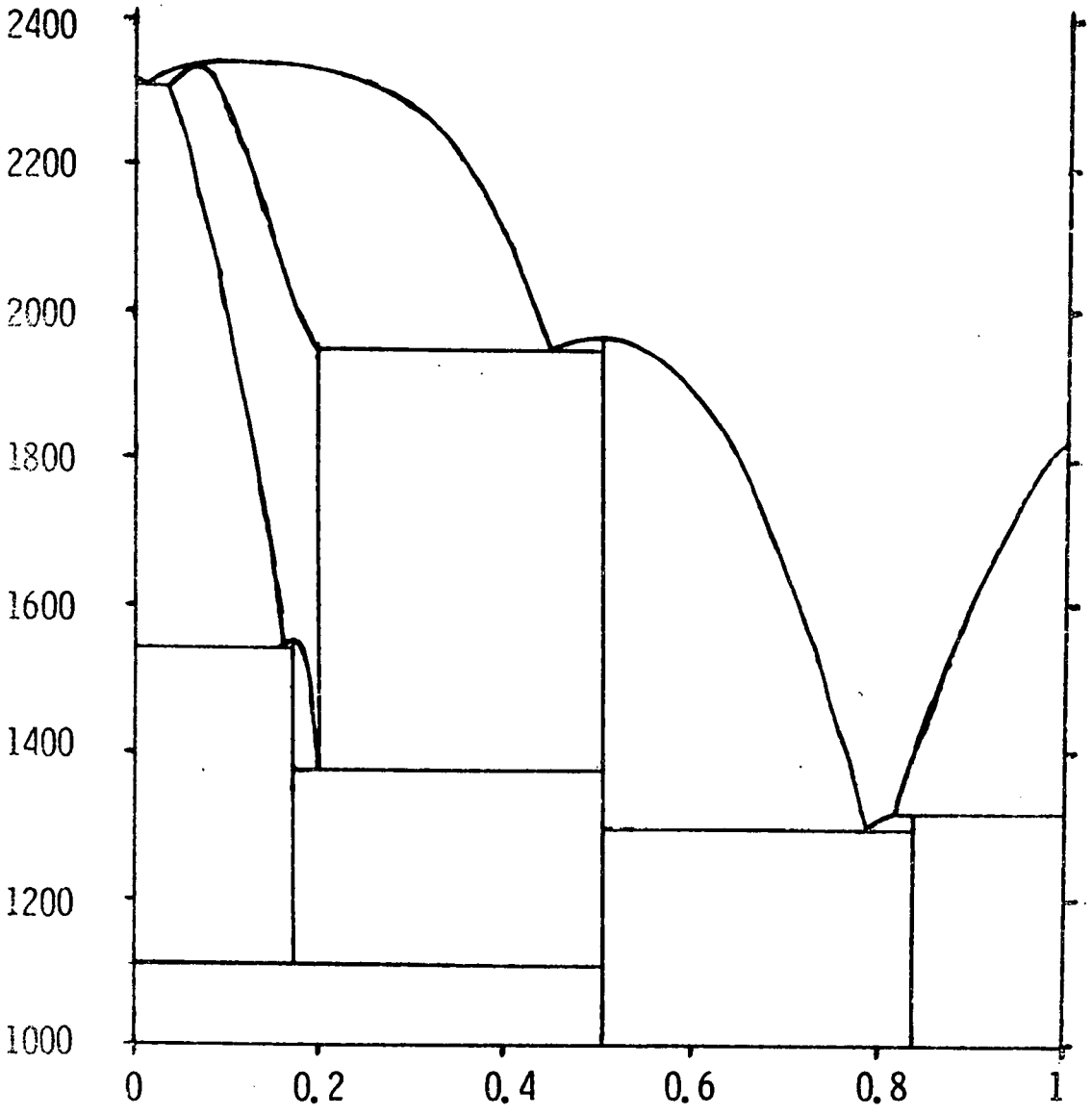

Preliminary calculated phase diagram for the $LiO_{.5}$-$AlO_{1.5}$ system.

Figure 2

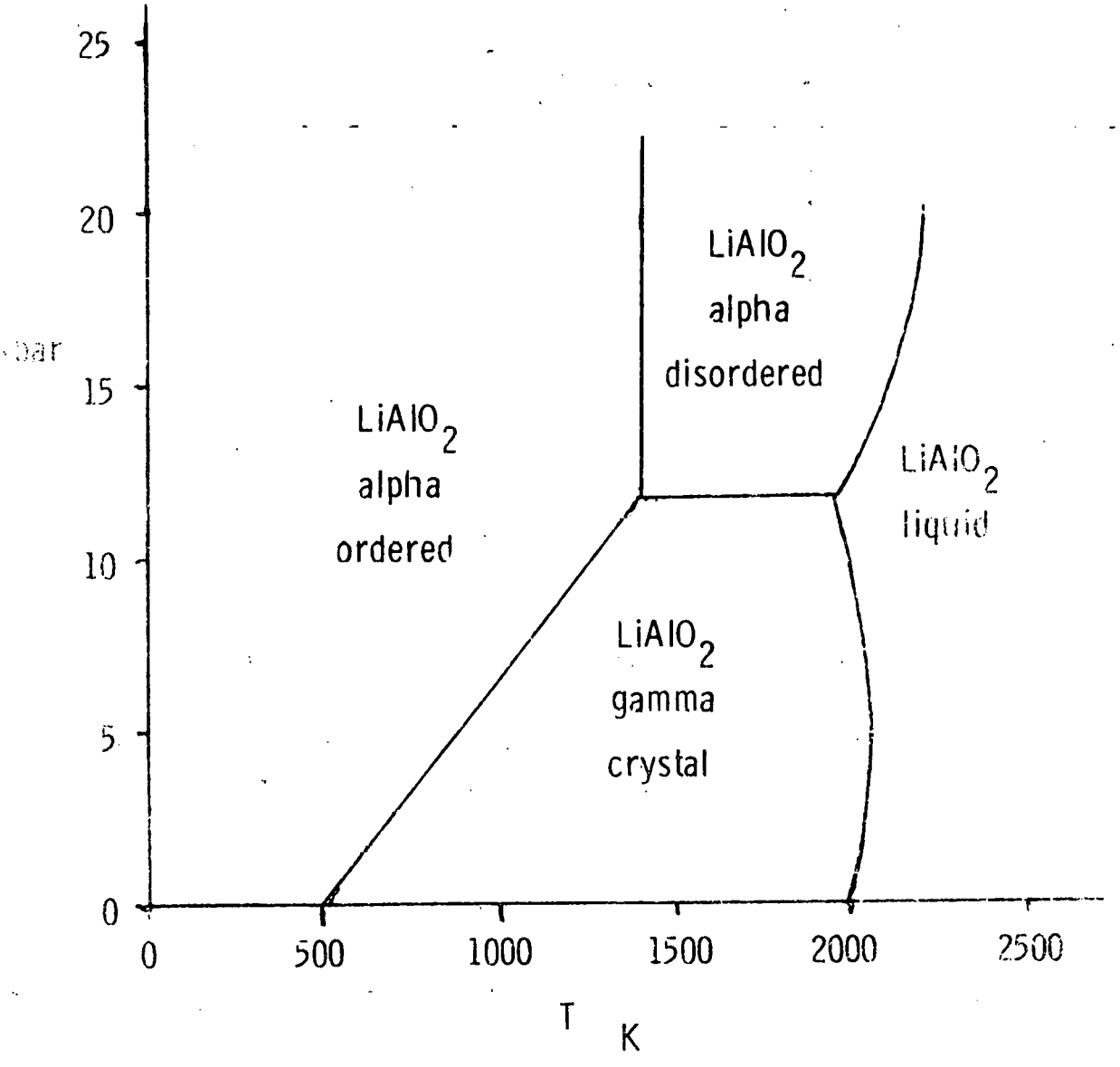

Estimated temperature pressure phase diagram for $LiAlO_2$

U.S. GOVERNMENT PRINTING OFFICE: 1980—640-258/1554